The protein corona of polymeric nanocarriers: characterisation and impact on cellular uptake

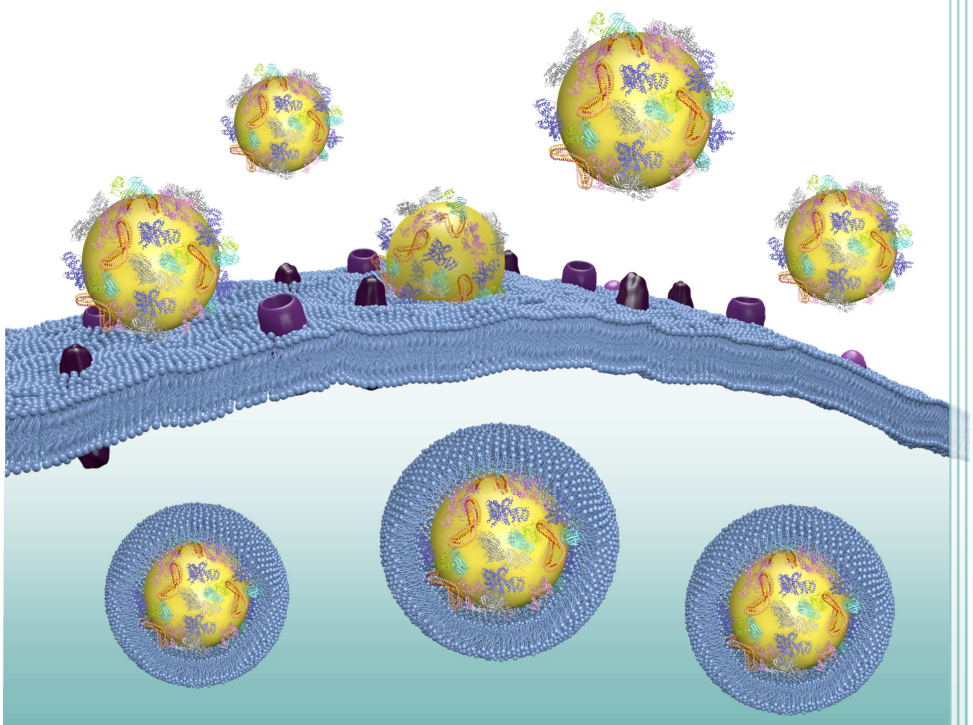

JOHANNES GUTENBERG UNIVERSITÄT MAINZ

The protein corona of polymeric nanocarriers: characterisation and impact on cellular uptake

Dissertation in fulfilment of the requirements for the degree of

Doktor rerum naturalium (Dr. rer. nat.)

Submitted to

THE FACULTY OF BIOLOGY

JOHANNES GUTENBERG UNIVERSITY, MAINZ

The doctoral thesis has been carried out at the

MAX-PLANCK INSTITUTE FOR POLYMER RESEARCH, MAINZ

Susanne Schöttler

Born in Lörrach, Germany

Date of Submission: 12.06.2015

Date of Defence: 24.07.2015

MAX PLANCK INSTITUTE FOR POLYMER RESEARCH

1. Reviewer:

2. Reviewer:

Dean:

LIST OF FIGURES

LIST OF TABLES

1 ABSTRACT

In the recent decade, the interest in polymeric nanocarriers for medical applications has gradually increased and accordingly a plethora of different nanoparticles has been fabricated. In particular when used as drug vectors in targeted delivery, nanocarriers could overcome many obstacles of cancer therapy. Nevertheless, their application is still impeded by insufficient knowledge about interactions of nanocarriers with their biological environment.

The rapid coverage of intravenously injected nanocarriers with blood proteins complicates any prediction of cell interaction, biodistribution and toxicity. The formation of this complex protein corona is highly dependent on the nanoparticles´ surface characteristics as well as on the biological environment and it dramatically alters the nanoparticles´ properties.

The present study unravels the protein corona composition of various polymeric nanocarriers by label-free quantitative liquid chromatography mass spectrometry. By correlating the relative abundances of identified proteins with cellular uptake of nanoparticles, key proteins are determined. The role played by apolipoproteins, one of the most abundant classes of proteins identified on nanoparticles, is partially disclosed. Coating polystyrene nanoparticles with single proteins reveals a strong influence on cell interactions. Apolipoproteins A4 and C3 are identified to decrease cellular uptake while APOH increases cell internalisation.

So far, all attempts to completely prevent protein adsorption by introducing protein repelling modifications as poly(ethylene glycol) (PEG) have failed. With hydroxyethyl starch (HES) and poly(ethylene ethyl phosphate) (PEEP) innovative, biodegradable stealth materials are introduced and analysed regarding their protein adsorption behaviour and ability to evade cell internalisation. The stealth effect provoked by PEG and PEEP is shown to be dependent on protein adsorption and clusterin is identified to play a crucial role in this mechanism.

Furthermore, two different techniques for protein corona preparation are compared and the reliability of the convenient magnetic separation as an alternative to centrifugation is

verified. The evolution of the corona during the preparation process is monitored with specific proteins being enriched and others depleted with each washing step.

Finally, the importance of the protein source used for *in vitro* protein corona analysis is emphasised. Major differences in protein composition are determined for coronas formed in serum and plasma. A strong influence of heparin, which is used as an anticoagulant for plasma generation, is detected. While heparin enhances the uptake into macrophages, it prevents internalisation into HeLa cells. The strong impact of the protein source on corona formation and the consequence for interaction with different cell types are factors which are often neglected, but should be taken into account for a meaningful analysis.

2 INTRODUCTION *

In recent years, nanotechnology has gained great importance in research and industry. With decreasing size a material´s surface properties play an increasingly important role compared to the bulk material. The significantly different characteristics of materials in the nanoscale range offer great potential for a variety of research areas. As a matter of fact, nano-based products are already used in medicine, biotechnology, electronics, in the cosmetic and food industry, or for surface coatings of everyday commodities as clothing or cars.

2.1 NANOMEDICINE

The application of nanoscale materials for therapeutic purposes is probably the most exciting field of nanotechnology. Engineered nanoparticles (NPs) are a promising tool and are currently under investigation for application in drug delivery, diagnostics, imaging and medical products such as implants. Their small size of typically 10-100 nm[1] allows crossing various biological barriers and enhanced permeation into organs and tissues. It opens the potential for size-dependent interaction with cells, cell organelles, proteins or DNA. As these opportunities also bear risks, health and safety issues of nanoparticles need to be thoroughly assessed.

Nanotechnology enables a specific design of materials according to application requirements. Particular features of nanoparticles can be manipulated in order to gain unique physical, chemical and biological properties and ultimately design multifunctional nanoparticle platforms. Nanoparticles can be made from various materials including inorganic materials as gold, iron oxide or silica, organic polymers such as polystyrene (PS), polylactic acid (PLA), or poly(lactic-co-glycolic acid) (PLGA) or biopolymers such as proteins, lipids, or carbohydrates.

2.1.1 NANOCARRIERS AS DRUG DELIVERY VEHICLES

Most applications in nanomedicine are currently dedicated to targeted delivery of drugs within the body.[2] Encapsulation of pharmaceuticals in nanoparticles or nanocapsules has the potential to circumvent many problems especially in cancer therapy. Due to their cytotoxicity, chemotherapeutic drugs cause serious side effects which could potentially be

* Parts of this introduction will be published as a focus review in CHEMNANOMAT.

minimised by using nanocarriers as drug delivery systems. A localised treatment enabled by site-specific drug delivery could improve therapy efficiency. Furthermore, the encapsulated pharmaceuticals are protected from degradation and the solubility of water-soluble drugs can be improved.

In addition to the classical small molecule substances, the class of biopharmaceuticals such as proteins or nucleic acids are innovative drugs which could be used to treat a variety of medical conditions. They are extremely specific and potent but their high molecular mass and instability limit their administration. Integration of biopharmaceuticals into nanosized carriers could overcome these challenges and improve their pharmacokinetic characteristics.[3]

Passive targeting of tumours is achieved as a consequence of the enhanced permeability and retention (EPR) effect which has been exploited by several research groups.[4] The EPR effect is a consequence of the defective vasculature surrounding cancer tissue leading to enhanced uptake of nanoparticles. Nevertheless, attachment of high-affinity ligands can further improve targeting of tumours. Furthermore, in this manner, other targets such as cells of the immune system can be addressed, which can be exploited for an immune cell based therapy approach. Conjugation of targeting moieties usually employs antibodies or ligands specific for cell receptors.

One of the most frequently employed targeting ligands is folic acid. It has been coupled to the surface of nanoparticles to target cancer cells overexpressing a specific folic acid receptor.[5] Another tumour marker overexpressed on cancer cell surfaces and commonly used as target for directed therapy is the EGFR-2 (HER2). Improved internalisation has been reported for anti-HER2 and folic acid coated nanoparticles intended for tumour targeting.[6] Anti-CD8 antibodies have been applied for targeting of PLGA nanoparticles to CD8 cells.[7]

Until today only very few nanocarrier drug systems are on the market, including albumin nanoparticles containing paclitaxel (Abraxane, Celgene)[8] and doxorubicin liposomes (Doxil, Janssen)[9] both applied in cancer treatment. In contrast to the vast number of novel nanoscale systems produced, the low number of FDA approved nanocarrier systems illustrates the complexity of their application.

2.2 THE PROTEIN CORONA

Despite all the advantages nanomedicine offers, the application of nanocarriers is still restricted by insufficient knowledge of their interaction with the biological environment. Thorough assessment of biological responses evoked by nanocarriers is essential. One major challenge is the formation of a protein corona. Upon contact with physiological fluids, nanomaterials are immediately covered with proteins.[10-12] This rapidly forming protein corona dramatically alters the nanocarriers´ physicochemical properties including hydrodynamic size, surface charge and aggregation behaviour. The original identity of the bare nanoparticle is lost. Furthermore, the interaction with cell membranes and the mechanism of cellular uptake is controlled by the adsorbed proteins. Therefore, the corona defines the biological identity of nanoparticles, influencing cytotoxicity, body distribution and endocytosis into specific cells.[13,14] As it is often stated, when nanocarriers are introduced into the body, what the cells actually see is the protein corona.[10] Thus, prediction of nanocarrier cell interactions are only possible if the protein corona is taken into account.

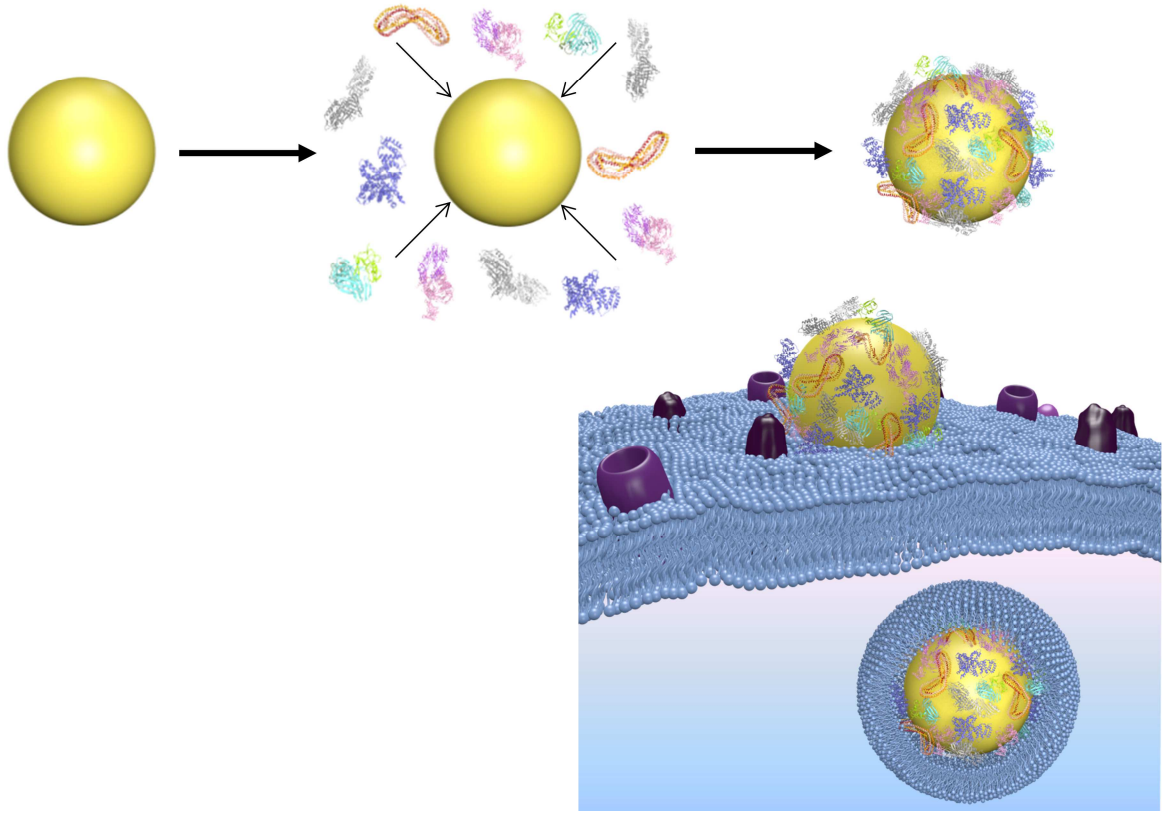

Figure 2-1: The formation of the protein corona on the naocarrier´s surface can influence the interaction with the cell membrane.

Studies analysing the protein corona have determined two layers of adsorbing proteins: an inner layer of irreversibly attached proteins known as the hard corona and an outer layer of loosely bound and continuously interchanging proteins forming the soft corona.[11,15] The allocation is defined by the proteins´ affinity for the nanocarriers´ surface.

It has been hypothesised that proteins of the hard corona interact directly with the nanocarriers' surface while proteins belonging to the soft corona interact with already bound proteins by weak protein-protein interactions.[13] As the hard corona remains bound to the surface for a longer time and can survive processes as endocytosis and translocation to different physiological environment it is thought to play a more important role in biological responses as the soft corona.[13]

Protein corona formation is a general observation and has been described for various nanoparticle materials as polystyrene,[10,12,15,16] silica,[12,16,17] metal,[18,19] or lipid.[20] A universal consequence of protein adsorption for nanoparticles is an increase in size and the creation of a negative surface charge due to the anionic character of most blood proteins.[20]

2.2.1 COMPOSITION OF THE PROTEIN CORONA

Knowledge of the protein corona composition is a prerequisite to understand the physiological reactions triggered by nanocarriers *in vivo*. Nanocarriers designed for biomedical applications are often administered intravenously and thus exposed to blood proteins. Hence, the protein corona composition is determined by the over 3700 proteins present in plasma with concentrations varying from 50 mg/ml for albumin to 5 pg/ml for interleukin 6.[21,22]

Because of the longer residence time and higher affinity, proteins of the hard corona are more easily isolated and thus investigated in most studies dealing with the protein corona.[11,15,23] Several studies have proven that the composition of the protein corona does not merely reflect the abundance of proteins in blood.[20,24]

Furthermore, it was shown that there is no universal protein corona for all nanocarriers but complex varying composites.[13] Independent of the bulk material and surface functionalities highly abundant blood proteins as albumin, immunoglobulin G (IgG) and

fibrinogen are associated with a wide range of NPs.[11,18,24] Albumin was for example determined as the main protein on gold nanoparticles[18] and also detected on silica or polystyrene NPs[12,24] or liposomes.[25]

But these highly abundant proteins often display higher rates of association and dissociation compared to e.g. apolipoproteins which are frequently identified as strongly adsorbing proteins on the vast majority of investigated nanoparticles.[13,26,27] The high affinity of apolipoproteins for many nanoparticle types was suggested to be based on hydrophobic interactions and could additionally be driven by size-dependent interactions.[27] Together with phospholipids, apolipoproteins assemble lipoproteins such as high density lipoprotein (HDL) or low density lipoprotein (LDL) which also have sizes in the nanoscale range. These transport vehicles carry phospholipids and cholesterol through the bloodstream. Apolipoproteins participating in building up HDL such as APOA1, A2, A4, C1, C3, D, E or J were found on the surface of various nanoparticles consisting of distinct material.[12,15,23,24,28] Additionally, phospholipids have been identified in the corona of copolymer NPs indicating that intact HDL particles might interact with the particles´ surface.[14,29]

A second group of proteins often identified on NPs are the complement factors.[24] As part of the innate immunity the complement system helps to remove foreign substances from the body. Upon a trigger, normally a pathogen, the complement cascade consisting of over 30 proteins is activated. Their main task is to tag a pathogen´s surface for identification by phagocytes. Complement C3 is a widely observed example in the protein corona of gold,[30] lipid-coated[31] and polymeric nanoparticles.[32]

2.2.2 EVOLUTION OF THE PROTEIN CORONA

Already in 1962, Leo Vroman postulated a dynamic adsorption process of blood proteins on surfaces. Studying protein attachment on flat surfaces, he showed a high adsorption of fibrinogen at an intermediate incubation time and assumed a subsequent replacement of fibrinogen by other proteins.[33,34] This phenomenon of sequential competitive adsorption known as the Vroman effect has been applied for other proteins and other surfaces.

For nanocarriers it is assumed that highly abundant and motile blood proteins as albumin, IgG, and fibrinogen adhere to the surface initially, but are later displaced by proteins with lower abundance but higher affinity such as apolipoproteins or coagulation factors.[13,35] Such a sequential binding pattern of plasma proteins was confirmed for several polymeric model nanoparticles[23,35] and solid lipid NPs.[36] Additionally, an increase of rather large proteins with molecular weights over 200 kDa during incubation time has been reported.[20] Eventually a time point is reached at which the continuous exchange of proteins does not affect the protein corona composition any further and equilibrium is established.[29] A rapid formation of the hard corona was reported already after one minute[20] and it is generally recognised that after one hour a stable composition is achieved.[10]

Recently, an extensive study on polystyrene and silica nanoparticles revealed that protein fingerprints were already determined at the earliest exposure time point of 0.5 min and did not significantly change qualitatively on prolonged plasma exposure.[12] Interestingly, also for iron oxide nanoparticles,[37] oil-in-water nanoemulsions[38] and gold nanoparticles[39] no competitive protein displacement over time was observed. One has to take into account that Vroman suggested that displacement takes place within seconds. An investigation of the protein corona at such a short incubation time is difficult to implement. Thus, in most studies analysing adsorption kinetics, 0.5 to 5 minutes are used as the earliest time point.[12,39] Other studies - especially those confirming the Vroman effect - have used different dilutions of plasma instead, to simulate early stages of protein adsorption.[23,35,36]

A dynamic variation of the protein corona composition does not only occur over time but also during a nanocarrier´s way through the body. Nanocarriers entering through the lung will be covered by proteins differing from proteins present on a nanocarrier´s surface administered intravenously and the composition evolves with the changing environment. This characteristic protein pattern could possibly be employed to trace the transport of nanoparticles throughout the body or even within a cell. Lundqvist *et al.* analysed the corona composition on polystyrene nanoparticles transferred from plasma to cytosolic fluid.[40] They reported that while some proteins as apolipoprotein A1 (APOA1) are replaced by cytosolic proteins a fingerprint from plasma is also retained. Furthermore, the protein corona enables monitoring intracellular trafficking pathways employed by nanoparticles.[41]

The time dependency of protein adsorption is of special relevance since nanocarrier interactions with the environment in biomedical applications take place on different time scales. Protein attachment within the bloodstream may be a question of minutes but interaction with cells of distant organs may be relevant after hours or days after exposure.[2]

2.2.3 PARAMETERS AFFECTING THE PROTEIN CORONA

Several studies attempted to connect nanoparticles´ physicochemical properties as material size, shape, charge and chemical functionalities with the corona composition. But due to the high tunability, a wide range of distinct NPs have been synthesized, which makes reliable predictions of nanoparticle protein interaction even more difficult.

Regarding NP size no universal conclusions can be drawn. Variation of particle size resulted in a primarily quantitative influence on protein composition for some polymeric nanoparticles.[23,24] On the other hand, a size-dependent qualitative influence on the protein pattern has also been reported for gold[42] and polystyrene nanoparticles.[15] In their study on polystyrene nanoparticles, Lundqvist and colleagues assigned both NP size and surface properties an important role in determining protein adsorption.[15]

Many interactions contribute to protein attachment such as van der Waals interactions, electrostatic interactions, hydrophobic interactions and hydrogen bonding.[43,44] Although all these forces might be relevant in driving protein adsorption, and factors such as electrostatic interactions between functionalised nanoparticles and charged side chains of proteins play a role in protein binding, it is now understood that adsorption is mainly driven by hydrophobic interactions.[24,45]

A correlation of NP hydrophobicity and protein association has been demonstrated with an enhanced adsorption of proteins on hydrophobic compared to hydrophilic surfaces.[2,46] Furthermore, it has been suggested that a negative surface charge of NPs correlates with a reduced protein adsorption as most serum proteins also have a negative charge.[47,48] However, despite their surface charge, anionic NPs are equally covered by proteins.[49,50] Modulating the surface charge of nanoparticles significantly influences the corona composition.[11,51] Preferential binding of negatively charged proteins to positively charged

NPs and vice versa has been reported for some nanocarriers,[18,52] but it does not appear to be a general rule. Protein binding affinities have in contrast been shown to be independent of the NP charge and not dictated by the isoelectric point of proteins.[24,53]

Although the particle material can also influence protein adsorption, surface characteristics as hydrophobicity and charge seem to play a more important role in determining the protein corona.[51]

Apart from the nanocarrier surface properties, the protein corona composition is highly dependent on the protein source. If the corona is determined after incubation in blood plasma, proteins of the coagulation system are often identified.[15,24,54] In contrast, serum is depleted of coagulation factors. The group of Mahmoudi has reported significant variations in the protein pattern of the NP corona formed in foetal bovine serum (FBS) or human plasma.[55] In a second study they compared protein adsorption in human plasma samples obtained from patients with distinct diseases which also significantly affected protein composition indicating the existence of personalised protein coronas.[56] Additionally, parameters as concentration[57] or temperature[58] of the protein source are important factors in protein interactions.

2.2.4 STEALTH MATERIALS

As all foreign substances, nanocarriers are cleared from the bloodstream by cells of the mononuclear phagocyte system (MPS) - also known as reticuloendothelial system (RES). This part of the immune system consists of phagocytes such as monocytes and macrophages which are mainly located in liver, spleen, lungs and lymph nodes. Phagocytosis of nanocarriers is promoted by opsonising proteins such as IgG and complement proteins which label the nanoparticles as foreign material. The rapid removal of circulating nanocarriers is a major problem, as it prevents the nanocarriers from reaching their destination within the body. Hence, nanocarriers have been equipped with protein repellent surfaces to reduce protein attachment and extend a carrier´s circulation time in the body. Resulting stealth nanocarriers are promising tools to avoid immune system activation and allow successful drug delivery.

Due to the higher degree of opsonisation, hydrophobic nanoparticles have a shorter circulation half-life. Hence, nanoparticles have been coated with hydrophilic molecules to protect them from opsonisation and recognition by cells of the MPS.[59] Covalent attachment of polyethylene glycol (PEG), also known as PEGylation, is the standard approach and has been used to increase circulation time of a variety of polypeptides,[60,61] polymeric NPs[62-64] and liposomes.[65,66]

Despite intensive research, the mechanism behind the protein resistance of PEGylated surfaces is not fully understood, yet. It is assumed, that the protein repellent properties of PEG coated surfaces are due to steric repulsion caused by adsorbed water molecules via hydrogen bonding. The nature of PEG derivates including chain length, conformation and surface density play important roles in the effectiveness of protein resistance.[67] Walkey *et al.* demonstrated that PEG grafting leads to a decreased total protein adsorption on gold nanoparticles which is reduced continuously with increasing density of the PEG coating.[30] The protein amount could also be reduced by increasing molecular weight of PEG grafted on gold nanoparticles from 2 to 20 kDa.[39] Different conformations of PEG are formed dependent on the grafting density. A mushroom-like configuration is formed if the surface coverage of PEG is rather low, while densely packed PEG on the nanoparticle surface results in a brush-like structure. A high steric protection has predominantly been shown for brush conformations and mushroom/brush intermediates.[68]

Although modifying nanocarriers with PEG reduces unspecific protein adsorption,[62,69] and extends blood residence time,[70] it cannot completely prevent protein corona formation.[28,30,62]

Despite the widespread use of PEG for medicinal applications, drawbacks have been recognised. For example PEG is not biodegradable and may thus accumulate in the body. Additionally, the development of PEG-antibodies[71,72] and severe hypersensitivity reactions has been reported.[73] Antibody formation can lead to an accelerated blood clearance in repeated systemic adminsitrations.[74] These factors give rise to search for PEG-alternatives. Zwitterionic molecules as polybetaines or polysaccharides can also generate hydrophilic shells when coupled to nanoparticles and are discussed as PEG alternatives.[59] The

biodegradability of polysaccharides makes them especially interesting for medical applications.

2.2.5 IMPACT OF THE PROTEIN CORONA ON PHYSIOLOGICAL RESPONSES

The interaction of nanocarriers with cells including immunological response and internalisation pathways is dominated by adsorbing proteins. These effects can be disadvantageous as for example described above for the unspecific phagocytosis of opsonised NPs. Two further aspects of protein adsorption have raised concerns. Firstly, adsorption of proteins can trigger conformational changes in the protein structure.[75,76] Structural changes give rise to functionality loss of proteins[77] and exposure of cryptic epitopes could trigger an inappropriate immune response.[78,79] Secondly, proteins adhering to nanocarriers equipped with antibodies or ligands can impair the targeting ability by masking the ligand and thus provoking a loss of recognition by its specific cell receptor.[80,81]

On the other hand, protein adsorption can also be beneficial. A general reduction of unspecific cellular uptake by the presence of a protein corona was described for several NPs,[82-87] which additionally results in a lower toxicity of the nanocarriers.[88] The prevented random internalisation is probably triggered by a reduced interaction of nanoparticles with the cell membrane via a shielding effect of adsorbed proteins. Proteins which evoke this effect for phagocytic cells are called dysopsonins. Albumin and apolipoproteins have been described as proteins with dysopsonising character which prolong blood half-life of nanocarriers,[16,20,51] and indeed coating of polymeric nanoparticles with human serum albumin (HSA) has been shown to increase their blood circulation.[89]

Originally protein corona studies were driven by the search for protein repellent surface modifications and the need to increase blood circulation times. But recently the perception of the protein corona is changing. Since protein corona formation is inevitable, the concept of its exploitation for targeted delivery is emerging. In contrast to the aforementioned unspecific interaction of proteins and cells, a specific uptake of nanocarriers could be promoted if receptor specific proteins reside in the protein corona.[88]

Several blood proteins have known cellular binding sites as the transferrin receptor present on a variety of cells.[90] Endothelial cells express an albumin-binding glycoprotein,[91] and multiple receptors for apolipoprotein complexes have been described.[92] The best known receptor for lipoproteins is the scavenger receptor class B type 1 (SR-B1) expressed in brain, liver and intestines but also on endothelial cells and macrophages.[20] It is responsible for the bidirectional lipid transfer between LDL, HDL and cells.[93] Thus, nanoparticles covered with apolipoproteins could mimic HDL and interact with scavenger receptors. A prostate carcinoma cell line expressing high levels of scavenger receptors was already successfully targeted with lipid NPs having a protein corona rich in apolipoproteins.[20]

The decoration of nanocarriers with single proteins has been exploited for targeting of specific organs. For example, apolipoproteins APOE, APOA1 and APOB-100 promote transport into the central nervous system.[94-96] APOE attached to the surface of nanoparticles has been proposed to facilitate transport of NPs across the blood-brain barrier, probably by interacting with lipoprotein receptors on the brain capillary endothelial cell membranes.[97,98] Apart from the opportunities to develop new innovative neurotherapies via this approach, these findings are also very important considering neurotoxicity.[27] Additionally, apolipoproteins could also be used to selectively target hepatocytes of the liver,[99,100] and also fetuin was shown to be involved in NP uptake into hepatic macrophages via scavenger receptors.[101]

So far, the biological impact has only been defined for few corona proteins. Understanding which proteins determine the fate of nanocarriers is crucial to ensure the success of designed targeted nanocarriers. Optimising the properties of nanocarriers in order to exploit the protein corona for specific biomedical applications is of high interest.[102-104]

2.3 ANALYTICAL METHODS FOR PROTEIN CORONA CHARACTERISATION

Given the importance of the protein corona on nanomaterials designed for medical applications, the search and development of analytical methods for its characterisation is essential. Different techniques have been used in order to analyse the various parameters of the protein corona.

Binding affinities of single proteins or protein mixtures can be analysed by fluorescence spectroscopy,[105-107] isothermal titration calorimetry (ITC)[108,109] or surface plasmon resonance (SPR).[110,111] Cedervall *et al.* were the first to utilise ITC and SPR for protein corona analysis.[11] ITC monitors the change in heat that results from protein adsorption onto nanomaterials and can provide information on protein binding affinities and stoichiometry.

With differential centrifugal sedimentation (DCS)[112] and dynamic light scattering (DLS)[10,113,114] the protein corona thickness can be determined. DLS uses the light scattering from particles in solution to determine the size distribution profile. Thereby changes in the hydrodynamic radius are detected which provides information on particle size increase and protein-induced NP aggregation. In DCS particle size distributions are measured using a spinning disc with a defined viscous sucrose gradient. The primary information is the time taken by the particles to travel from the centre of the disk through the gradient to a detector placed at the outer side.[16] DLS and DCS are some of the few methods applicable *in situ*.[13]

Several techniques for monitoring conformational changes of proteins attaching to the NP surface are available. With circular dichroism (CD)[106,115,116] protein secondary structures can be determined but the technique is limited to single proteins and cannot be applied in complex protein mixtures. Further techniques to follow structural changes are Fourier transform infrared (FTIR)[106,117,118] or Raman spectroscopy[119-121] which will not be further discussed here.

In order to obtain indications on the effect of the protein corona on cellular uptake, aggregation, bio-distribution, clearance and toxicity it is necessary to provide protein identification. Thus, the present study focuses on the identification of associating

proteins. For this purpose, the hard corona needs to be purified and proteins separated by polyacrylamide electrophoresis or chromatography. The identification is then realised by mass spectrometry (MS). These techniques are discussed in more detail in the following sections.

2.3.1 PREPARATION OF THE HARD CORONA

In most studies analysing the protein corona of nanocarriers initially incubation in plasma or serum is performed. An excess of proteins to the particle surface area is normally applied as this ratio is more representative of the actual *in vivo* situation.[122] The subsequent isolation of NP-protein complexes from the surrounding medium is a central challenge of PC investigation as it may disrupt the interaction of particles and proteins.[11] The most commonly used method for protein isolation is centrifugation which exploits the differences of size and density of nanoparticles relative to free proteins.

With an acceleration of 15 to 20,000 g nanocarriers with associated proteins are sedimented. False positive identification of large proteins or protein aggregates sedimenting during centrifugation is possible and should be reduced by aggregate removal in advance to NP incubation. Several washing cycles ensure the purification of strongly attached proteins and removal of loosely and unspecifically bound proteins. The intensity of resuspension, the type and volume of the washing solution, and the number and duration of washing steps may influence the affinity of attached proteins.

Size exclusion chromatography (SEC), also known as gel filtration, has been proposed as an alternative to centrifugation for separation of NP-protein complexes from the bulk of unbound proteins.[11] In SEC free proteins enter the pores of the stationary phase while NPs are too big and hence pass through the column much faster. Although the method was described as less perturbing of protein-particle complexes than centrifugation, until now it has not been widely used for protein corona preparation.[123] For nanoparticles with magnetic properties a separation from incubation medium with a strong magnet is possible and has been applied for PC purification.[53,124-126]

After separation from weakly associated proteins, proteins of the hard corona need to be detached from the nanoparticles for further analysis. Treatment of NP-protein complexes

with anionic detergents as urea, thiourea or SDS causes protein repulsion and denaturation and hence detachment of the proteins from the NP surface. Alternatively, attached proteins can be set free by dissolving the particle material.[127,128]

2.3.2 GEL ELECTROPHORESIS

Once the protein-NP complexes have been isolated from excess plasma and the adhering proteins removed from the NP surface, they need to be separated for further identification. The most common method for protein separation is sodium dodecyl sulphate polyacrylamide gel electrophoresis (SDS-PAGE).

For an accurate separation of proteins based on their molecular weight, they need to be denatured to eradicate structural effects on mobility. SDS anions adhere to hydrophobic region of the proteins and thus destroy the native structure. Additionally the SDS covers the charge of the protein and gives them an anionic character, whereby the overall negative charge is proportional to the molecular weight of the protein. For reduction of disulphide bonds dithiothreitol (DTT) is added. Electrophoresis is carried out in a polyacrylamide gel in which the negatively charged SDS-protein complexes migrate towards the anode under an applied electric field. The porous gel acts as a molecular sieve in which smaller molecules move faster resulting in the separation of proteins according to molecular weight.

Although SDS-PAGE is a very convenient and fast method to separate proteins, it suffers from co-migration of several proteins with similar molecular weights in the same gel band if the protein mixture is too complex. For a more effective separation of complex protein samples two-dimensional gel electrophoresis (2D-GE) additionally employs the charge of proteins as a second parameter. Isoelectric focusing (IEF) separates the proteins along a pH gradient where they will accumulate at their isoelectric point, the point at which the overall charge of a protein is zero. Separation according to molecular weight is performed subsequently in the same way as described for the 1D-PAGE resulting in a separation in two dimensions.

The separated proteins in one and two dimensional SDS-PAGE need to be visualised within the gel by a staining procedure. Coomassie brilliant blue (CBB) is the most commonly used

dye for staining proteins after gel electrophoresis. In the protonated state, the triphenylmethane dyes (R-250 and the dimethylated derivative G-250) primarily bind through electrostatic interactions to basic amino acid residues. The original procedure requires a destaining step to remove the background. Exploiting the relatively low solubility of CBB in acidic solutions, a staining method using colloidal dye particles was developed.[129] In this way entry of dye molecules into the gel is prevented and background-free staining occurs by localised solvation of the dye into protein bands.[130] The limit of detection for conventional and colloidal CBB staining is around 100 and 10 ng, respectively.[131,132]

In comparison, the procedure of silver staining allows detection of approximately 1 ng protein per band.[131,132] The silver straining technique is based upon saturating the gel with silver ions, washing loosely bound ions out and subsequently reducing protein-bound ions to metallic silver. The soluble silver ions bind to proteins by electrostatic interaction with sulfhydryl or carboxyl moieties. Due to the more complex procedure with several washing and incubation steps, the reproducibility is lower than for coomassie staining. In addition, most silver staining protocols use aldehyde-based fixatives which covalently modify proteins and prevent subsequent analysis by mass spectrometry. In contrast, CBB is completely compatible with mass spectrometric protein identification.

Gel electrophoresis is normally used for comparative purposes to provide qualitative information about the differences in protein adsorption to distinct NPs. Spots on a 2D gel can be identified by comparison with a reference plasma proteome map. In this way, Gessner *et al.* have for example analysed changes in plasma adsorption patterns on polystyrene nanoparticles influenced by either hydrophobicity,[46] surface charge density,[133] or functional groups.[52]

Unfortunately, a definite assignment of protein spots is not always possible, thus N-terminal sequencing[62,134] or mass spectrometric approaches on individual excised protein spots have been applied. The combination of SDS-PAGE and mass spectrometry has been applied in the majority of studies analysing protein corona composition.[11,15,16,23,28,40,135] Recently, 2D-PAGE gives way to liquid chromatography directly coupled to mass spectrometry.[12,24,30]

2.3.3 LIQUID CHROMATOGRAPHY

A second common method for protein separation is chromatography which exploits the affinity of peptides for a specific column matrix. The widely used technique of high-performance liquid chromatography (HPLC) operates on the principle of hydrophobic interactions. Proteins or peptides are dissolved in a mobile phase which carries them through the stationary phase of a column. Depending on the amino acid sequence, the peptides interact differently with the solid adsorbent material causing distinct flow rates and resulting in separation of the sample components.

The stationary phase consists of a granular material made of solid particles. A commonly used column material for peptide separation is made of silica beads which have been modified with linear octadecane groups (C18). This functionalisation gives the silica a hydrophobic character. The mobile phase is usually a combination of water and organic solvents as acetonitrile or methanol.

A mobile phase gradient with increasing percentage of the organic solvent can be used for an effective separation of peptides according to their hydrophobicity. Polar peptides with a low affinity for the hydrophobised silica have a short retention time, while more hydrophobic peptides are eluted from the column with increasing acetonitrile concentration.

Originally, the mobile phase in HPLC was non-polar and the technique based upon the interaction of analyte molecules with a hydrophilic matrix. Therefore, the protein separation with a polar solvent as mobile phase is called reversed-phase liquid chromatography (RPLC). Figure 2-2 illustrates the basic principles of RPLC. The peptides eluting from the column can be visualised graphically by a detector in form of a chromatogram.

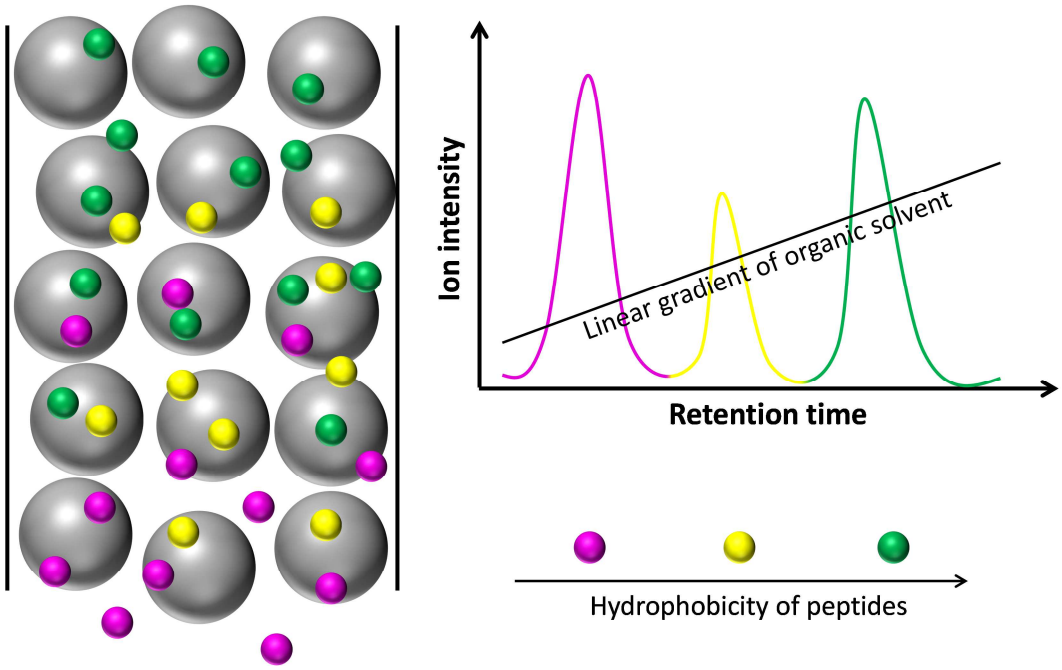

Figure 2-2: Schematic illustration of the principles of reversed-phase liquid chromatography (RPLC). During RPLC peptides are separated according to their polarity based on their specific interaction with porous hydrophobised silica particles (grey spheres).

The acronym HPLC was initially used to indicate that high pressure was applied to generate the flow required to pass the liquid through the packed column. With continuous improvements in performance including development of columns with smaller particles and greater selectivity the name was changed to high-performance liquid chromatography with the acronym remaining the same. Today particle sizes of 1.7 µm and instrumentation with specialised capabilities designed to deliver mobile phase at up to 1,000 bar are available. The term ultra-performance liquid chromatography (UPLC) is often used to refer to these advances in resolution, speed and sensitivity in liquid chromatography, although the name is original a trademark of the Waters Corporation.

2.3.4 MASS SPECTROMETRY FOR PROTEMIC ANALYSIS

In general, mass spectrometry can provide both qualitative and quantitative information of an analyte. It is used for mass determination for a wide variety of applications including identification of unknown compounds, determining the structure or isotopic composition of a molecule or quantifying the composition of the analyte. All MS techniques available have two basic principles in common: a mass spectrometer can measure the mass of a molecule only after it is converted to a gas-phase ion and the actual measured value is the mass to charge ratio (m/z) which is affected by the ion movement in an electric field.

In proteomics the coupling of liquid chromatography to mass spectrometry (LC-MS) has become the standard method. Before the chromatographic separation, proteins need to be digested into smaller fragments. This is usually performed by the enzyme trypsin which cleaves proteins C-terminal to lysine and arginine residues into peptides of an average length of 14 amino acids.[136] The proteolytic digestion of proteins prior to mass spectrometric analysis is commonly referred to as bottom-up approach and is the basis of shotgun proteomics, in which proteins are identified in complex mixtures using LC-MS. In contrast to the direct in-solution digestion of the crude protein extract, in-gel tryptic digestion is applied after 1/2D-SDS-PAGE. For PC analysis both, gel-free and gel-based, methods have been widely used.

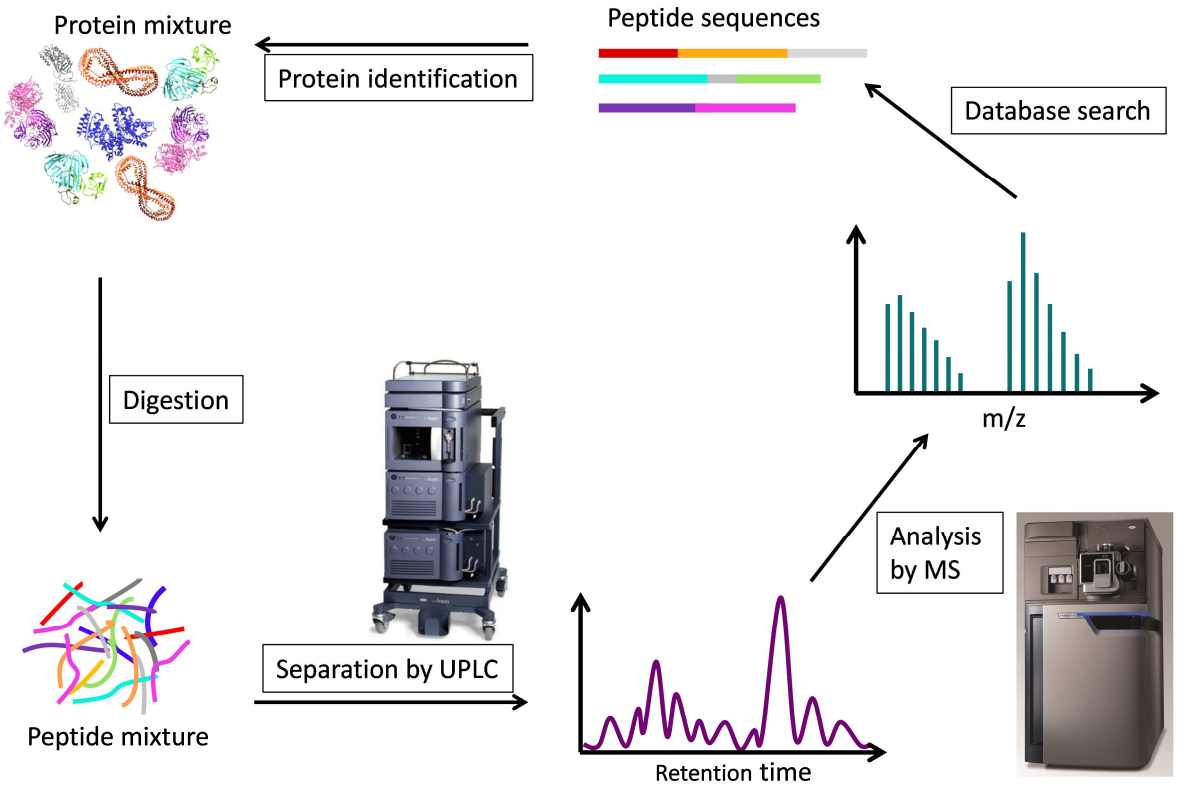

Figure 2-3: Liquid chromatography-mass spectrometry based proteomics.

A typical workflow of a shotgun proteomics experiments as used in this study is displayed in Figure 2-3. Initially, the protein mixture is digested by trypsin into short peptides. The resulting peptides are then separated according to their hydrophobicity by liquid chromatography before they are ionised and separated according to their mass-to-charge ratio by the mass spectrometer. The resulting mass spectra are used for a search against a

protein sequence database for protein identification. The individual steps will be further addressed in this chapter.

IONISATION

While generally, many mass spectrometers work in either positive or negative ion mode, proteins and peptides are usually analysed under positive ionisation conditions. For the initial generation of gas-phase peptides two main ionisation sources are utilised. Matrix-assisted laser desorption ionisation (MALDI) is used for analysis of large organic molecules as biopolymers, which tend to be fragile. In MALDI the analyte is embedded in a matrix material typically consisting of acidic molecules such as alpha-cyano-4-hydroxycinnamic acid used for intact proteins. A high energy laser fires at the matrix which strongly adsorbs the laser energy. This causes mainly ionisation of the matrix molecules followed by energy and proton transfer to the analyte molecules. The explosive release of energy enables the transition of matrix and analyte molecules from solid to gas phase.

Mass spectrometers coupled to HPLC are normally equipped with an electrospray ionisation (ESI) source. In ESI peptides in solution are sprayed through a small capillary emitter which has a pulled-tip with a diameter of 1-10 µm. A voltage is applied at the end of the capillary (+1.5 to + 4 kV for positive ion mode) creating an electric field between the capillary and the counter electrode. As a consequence the analyte solution is pulled towards the counter electrode, which results in the formation of a so-called Taylor cone at the capillary tip (see Figure 2-4). Due to the repulsion of the ions small droplets are dissolved from the Taylor cone and exit the capillary in form of a fine aerosol. As solvent evaporates from the charged droplets, the surface tension in the shrinking droplets increases and the ions are pushed closer. Once the electrostatic repulsion of the ions exceeds the surface tension holding the droplet together (Rayleigh limit) the droplets break up into smaller fragments. This process is called Coulomb fission and the smaller more stable droplets undergo subsequently further Coulomb fissions once more solvent has evaporated. Finally, solvent free positively charged gas-phase ions are ejected and enter the mass spectrometer through a cone induced by a combined effect of electrostatic attraction and vacuum. In ESI an acid (e.g. formic acid) is often added to solvents to facilitate ionisation by providing a proton source.

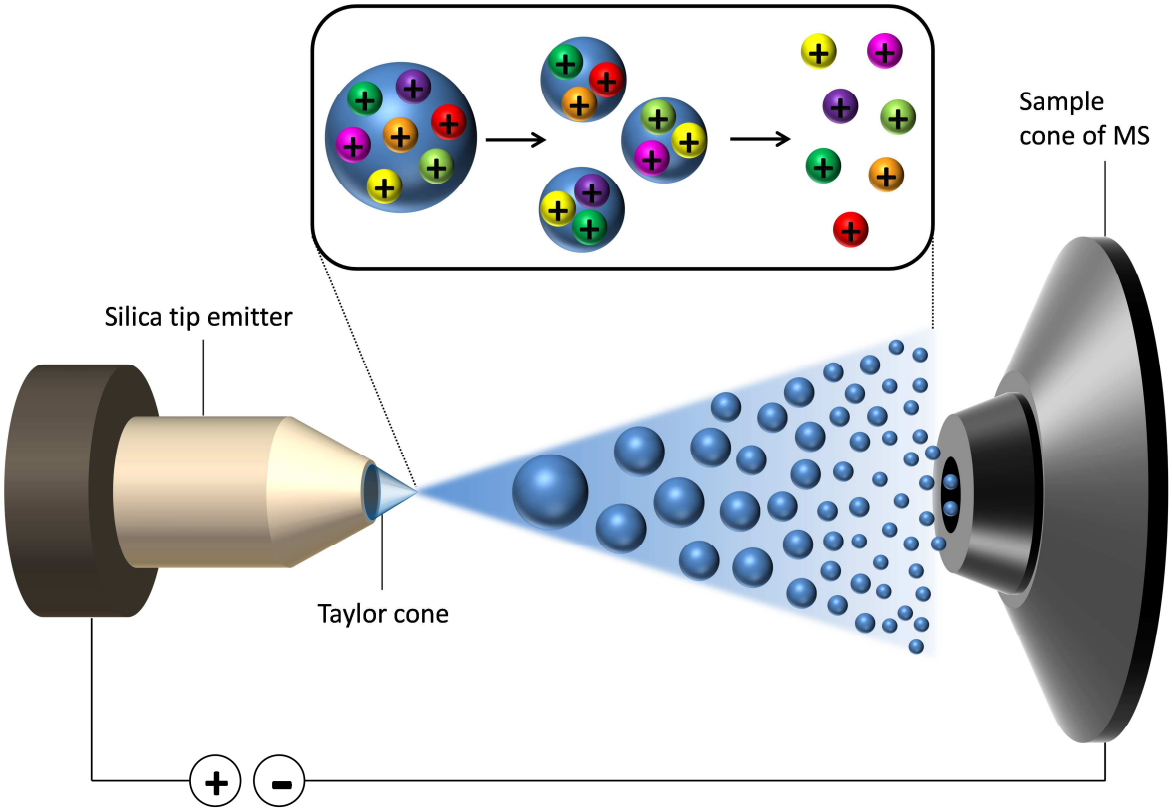

Figure 2-4: Schematic illustration of electrospray ionisation (ESI) in positive ion mode.

In new devices the ions are sprayed in an angle towards the insert cone of the mass spectrometer. In this way a higher sensitivity is achieved by reducing the amount of neutral and other polluting molecules entering the mass spectrometer. Another significant development is based on decreasing sample consumption and flow rates down to 20 nl/min - a technology referred to as nano-spray.[137]

ANALYSER

Once an ion is created it must be detected with appropriate sensitivity. The principle of ion detection in MS is based upon the separation of ions according to their mass to charge ratio (*m/z*), which is accomplished by the mass analyser. Several mass analysers are used, the most well-known of which include quadrupoles, ion traps and time-of-flight (TOF) analysers.

In a time of flight (TOF) analyser, ions are accelerated by a uniform electromagnetic field resulting in all ions with the same charge also sharing identical kinetic energies. The

velocity is thus only dependant on the ion mass with lighter ions reaching a detector plate at known distance sooner than heavy ions. The time ions need to reach the detector provides an accurate *m/z* measurement. A reflectron used as an ion mirror additionally increases the length of the flight path allowing a larger temporal distribution between ions of similar *m/z*. The combination of a TOF analyser and a MALDI source (MALDI-TOF) is often used for the analysis of large molecules or bio-polymers such as single proteins excised from 2D-gels.

A quadrupole consists of four parallel rod electrodes kept at equal distance (see Figure 2-5). Two opposing rods have a positive constant direct current (DC) voltage and the other two a negative DC voltage. Additionally, a superimposed high frequency alternating current (AC) voltage is applied. Positive ions entering the quadrupole are accelerated and forced to a particular oscillating trajectory between the rods by the applied electric field. If the trajectory is unstable the ion is non-resonant and collides with one of the rods. The molecule is then removed in the vacuum and will not be detected.

Only ions of a particular *m/z* ratio exhibiting oscillations of constant amplitude can travel through the quadrupole and reach the detector. Varying the parameters with specific combinations of the potentials and the AC frequency allows filtering ions with different *m/z* ratios which builds up a mass spectrum. In the end the ion current is measured by a detector, plotting it versus *m/z* producing the mass spectrum.

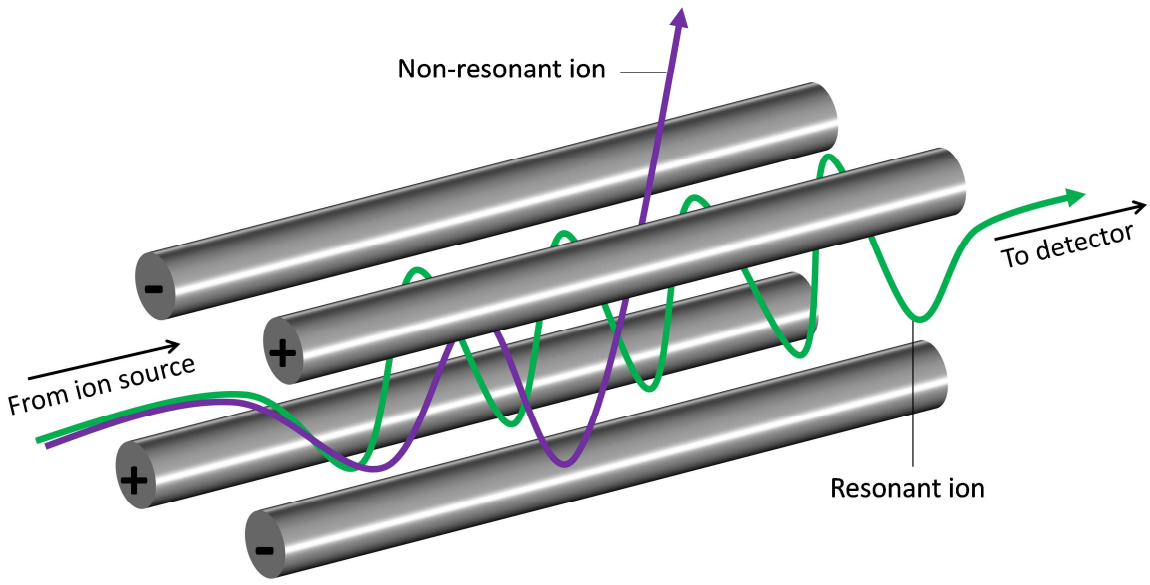

Figure 2-5: Schematic illustration of the operating principle of a quadrupole mass analyser.

Ions travel from the ionisation source through the four metal rods, where their motion is dictated by the applied electric fields. Non resonant ions are filtered out; only resonant ions with specific *m/z* values can reach the detector.

A quadrupole operates as a mass selective filter and is thus similar to an ion trap instrument. In contrast to the quadrupole which filters streaming ions, an ion trap stores ions of a specific *m/z* ratio for subsequent analysis.

A common variant of this analyser is the triple quadrupole, with three quadrupoles set up in line. As only the first and the third function as actual mass analysers this technique is also known as tandem mass spectrometry or MS/MS.

Initially, ions are mass-selected in the first quadrupole as described above. These precursor or parent ions are then fragmented in a second chamber known as the collision cell. This is usually done by colliding the accelerated ions with a neutral gas (e.g. argon) in a process called collision induced dissociation (CID). The fragmented product or daughter ions are then analysed in the third quadrupole, which only transmits specific fragment ions to the detector. The controlled fragmentation of the analyte molecule provides further structural information.

Instead of the third quadrupole a TOF analyser can be used to generate the mass spectrum of the resulting product ions. This hybrid instrument is then described as a Q-TOF mass spectrometer.

The MS/MS described above is also referred to as tandem-in-space MS/MS as opposed to the tandem-in-time MS/MS analysis performed on an ion trap mass spectrometer. Instead of having separate mass analysers as described for the triple quadrupole, an ion trap mass spectrometer performs the functions of precursor ion selection, CID and product ion mass analysis at different time points. Stored ions can be ejected according to their *m/z* value or further fragmented to produce structural information. Multiple separation steps including ion fragmentation, fragment selection and successive fragmentation of daughter ions is also referred to as MS^n.

A further development of MS^n technology continuously recording all precursor and product ions is known as MS^e. Without preselection of precursor ions the TOF mass

spectrometer continuously switches between two rapidly alternating MS functions. With low collision energy no fragmentation occurs and all precursor ions are transmitted from the source through the collision cell to the mass analyser. In the second function ramped collision energy generates information on fragment ions.

Another technology which has recently been coupled to LC-MS is the ion mobility spectrometry (IMS). Ion mobility differentiates between ions with equal mass and charge and separates them according to their three-dimensional conformation, which allows separation of isomers. The Synpat-G2-Si mass spectrometer used in this study combines the IMS technology with a Q-TOF with a dual stage reflectron (Figure 2-6).

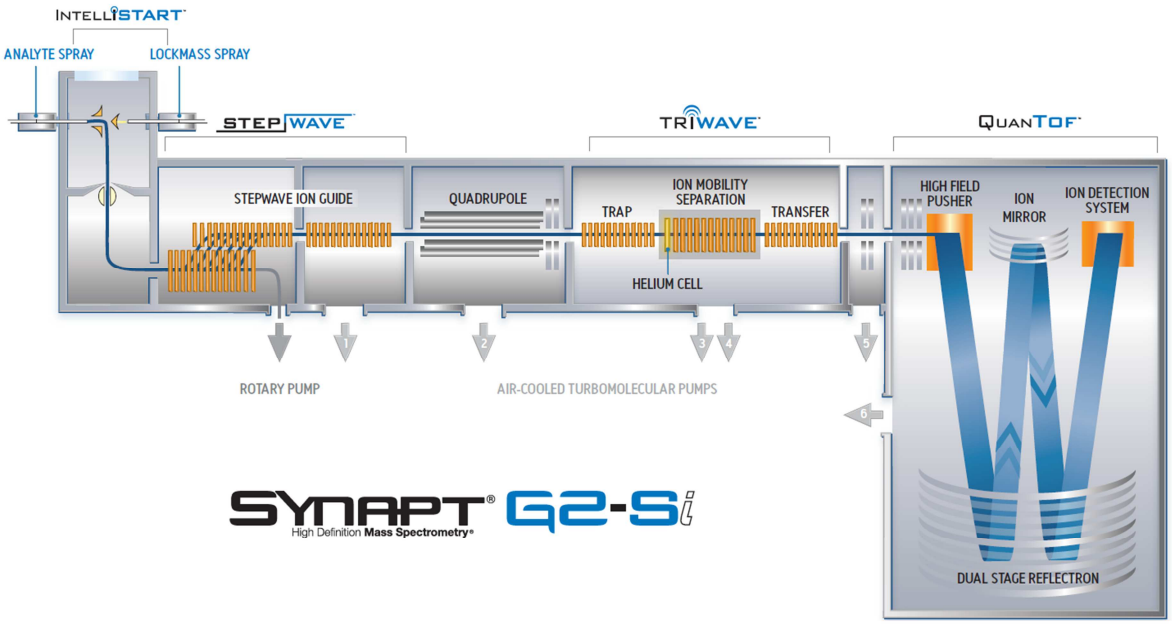

Figure 2-6: Schematic of SYNAPT G2-Si system.[138]

IDENTIFICATION AND QUANTIFICATION

Having generated tandem mass spectra from all ions detected, the original proteins need to be identified. A chromatographic run of a complex protein mixture can take up to several hours and thousands of MS/MS spectra representing the peptides are collected during the run. Fortunately, peptides fragmented by CID are cleaved into characteristic ion series as they tend to fragment along the backbone. The generated N- and C terminal peptides reveal the peptide's primary structure, its amino-acid sequence. Hence, protein identification in bottom-up proteomics is based upon protein sequencing. The assignment to the original proteins is performed by specific software which matches the mass spectra

with protein sequences from a database. A species specific database used in the experiment (e.g. human) can be obtained from uniprot.org to eliminate false-positives from closely related species.

The identification rate of proteins attached to nanoparticles has increased enormously. While in first studies using 2D-PAGE only 10-20 proteins could be detected, nowadays up to 500 proteins can be identified.[12] To determine the relative or absolute amount of a protein in a sample several quantitation methods are available all based on tandem mass spectrometry.

In contrast to labelling approaches, which use isotope tagging of peptides, label-free quantitative proteomics is more reliable for complex protein mixtures and allows comparison of multiple samples.[139] Two main label-free quantification approaches have been used. Spectral counting simply counts the number of MS/MS spectra acquired for all identified peptides from a particular protein as an indicator for the respective amount in the original sample.

In the second approach the intensities of the precursor ions are measured and the abundance of each protein is calculated from the integrated peak areas of all its constituent peptide ions.[140] The label-free TOP3 (or Hi3) method used in this study, is based on the assumption that the original amount of a protein infused in the mass spectrometer correlates with the averaged abundance of its three most efficiently ionised peptides. Using a spiked calibrant protein as reference the absolute amount of every protein can be calculated.[141]

2.4 AIMS

This study aims to shed some light on protein adsorption to polymeric nanocarriers and its influence on internalisation of nanocarriers into cells. Parallel analysis of the protein corona composition and the uptake into cells allows drawing conclusions on crucial roles played by individual proteins. The primary goal was the identification of key players in the protein corona determining cell interaction, aggregation or biodistribution. Furthermore, novel stealth materials were investigated regarding their protein adsorption and cell

interaction. The influence of distinct protein sources on protein corona formation and subsequent uptake by distinct cells was another focus of this study.

3 MATERIALS AND METHODS

3.1 MATERIALS

3.1.1 NANOCARRIERS

In Table 3-1 all nanoparticles and nanocapsules used in this study are listed with their respective properties and characteristics. The synthesis and characterisation procedure of each nanocarrier is described elsewhere (see reference in the respective results section).

Table 3-1. Nanoparticles and nanocapsules.

Name	Polymer	Co-Monomer	Functionalisation	Surfactant	Diameter [nm]	ζ-potential [mV]
PS-COOH	PS	3% AA	COOH	LAT50	102	-27
PS-NH_2	PS	3% AEMH	NH_2	LAT50	100	+8
PS-SO_3	PS	3% SSNa	SO_2OH	LAT50	119	-33
PS-PO_3	PS	C12-PET	$PO(OH)_2$	-	104	-60
PS-PO_3-Lut	PS	C12-PET	$PO(OH)_2$	LAT50	109	-50
PS-PO_3-SDS	PS	C12-PET	$PO(OH)_2$	SDS	104	-61
PS-LUT	PS	-	-	LAT50	192	-9
PS-LUT-COOH	PS	2% AA	COOH	LAT50	162	-29
PS-LUT-NH_2	PS	2% AEMH	NH_2	LAT50	178	+4
PS-SDS	PS	-	-	SDS	340	-37
PS-NH_2	PS	2% AEMH	NH_2	CTMA-Cl	106	+46
PS-PEG-44	PS	2% AEMH	PEG_{44}	CTMA-Cl	117	+15
PS-PEG-110	PS	2% AEMH	PEG_{110}	CTMA-Cl	119	+8
PS-PEEP-49	PS	2% AEMH	$PEEP_{49}$	CTMA-Cl	117	-9
PS-PEEP-92	PS	2% AEMH	$PEEP_{92}$	CTMA-Cl	122	-10
HES	HES	TDI	-	SDS	155	-7
HES-PEG	HES	TDI	PEG	SDS	152	-2
HES-PEG-Gal	HES	TDI	Gal	SDS	159	-
HES-PEG-Man	HES	TDI	Man	SDS	153	-
HES-PEG-DEC-205	HES	TDI	DEC-205	SDS	160	-
SPION	PS	SSNa	FeO	SDS	130	-67

3.1.2 EQUIPMENT

Table 3-2. List of equipment

Instrument	Supplier
Automated cell counter TC10	Bio-Rad, USA
Cell culture flow c-(Max Pro)3-130	Berner, DE
Cell culture incubator C200	Labotec, DE
Centrifuge 5810R	Eppendorf, DE
CLSM Leica SP5 II with CW-STED	Leica, DE
Flow cytometer CyFlow ML	Partec, DE
Freezer -20 °C	Liebherr, DE
Freezer -80 °C Hera Freeze Top	Thermo Fisher Scientific, DE
Microscale AE100	Mettler Toledo, CH
nanoACQUITY UPLC	Waters, USA
Nitrogen tank LS6000	Taylor-Wharton, DE
Pipettes	Eppendorf, DE
Pipetting aid Accujet Pro	Brand, DE
Plate Reader Infinite M1000	Tecan, DE
Power Supply	Bio-Rad, USA
SDS-PAGE chamber Mini Gel Tank	Life Technologies, USA
Synapt G2-Si mass spectrometer	Waters, USA
Vacuum pump Vacusafe comfort	IBS Integra Bioscience, DE
Vortexer Reax Control	Heidolph, DE

Table 3-3. List of software

Software	Supplier/Source
Blender 2.7	www.blender.org
FCS Express 4	DeNovo Software, USA
FlowMax 3	Partec, DE
Gimp 2.8	www.gimp.org
GraphPad Prism 5	GraphPad software Inc., USA

i-control 1.6.19.0	Tecan, DE
ImageJ (Fiji)	www.fiji.sc
LAS AF 2.6.0.7266	Leica, DE
MassLynx MS Software	Waters, USA
MS Office 2010	Microsoft, USA
Progenesis QI for proteomics	Nonlinear Dynamics, Waters, USA
TransOmics Informatics Software	Nonlinear Dynamics, Waters, USA

3.1.3 CHEMICALS

Table 3-4. List of chemicals

Chemical	Supplier
[Glu1]-Fibrinopeptide B human	Sigma Aldrich, USA
2-Propanol	Sigma Aldrich, USA
2-Propanol LC-MS	Biosolve, NL
2-Propanol LC-MS	Biosolve, NL
7-Aminoactinomycin D	Sigma Aldrich, USA
Acetic acid	Sigma Aldrich, USA
Acetonitrile ULC/MS	Biosolve, NL
Ammonium bicarbonate	Sigma Aldrich, USA
Ammonium sulphate	Applichem, Illinois Tool Works Inc, USA
Antithrombin III, human	CSL Behring, DE
Apolipoprotein A-I, human	Biopur AG, CH
Apolipoprotein A-IV, human	Alpha Diagnostic International, USA
Apolipoprotein C-III, human	Alpha Diagnostic International, USA
B2-Glycoprotein I (ApoH), human	Thermo Fisher Scientific, USA
BSA	Sigma Aldrich, USA
CellMaskOrange	Life Technologies, Thermo Fisher Scientific, USA
CHAPS	Serva Electrophoresis, DE
Clusterin, human	Active Bioscience, DE
Coomassie Brilliant Blue G250	Serva Electrophoresis, DE

DMEM	Life Technologies, Thermo Fisher Scientific, USA
DMSO	Sigma Aldrich, USA
DPBS	Life Technologies, Thermo Fisher Scientific, USA
DTT	Sigma Aldrich, USA
Ethanol	Sigma Aldrich, USA
FBS	Life Technologies, Thermo Fisher Scientific, USA
Formic acid LC-MS Grade	Thermo Fisher Scientific, USA
Glutamine	Sigma Aldrich, USA
GMCSF	Leukine sargramostim, Sanofi, FR
HCl	Sigma Aldrich, USA
Heparin	Rotexmedica, DE
Hi3 Ecoli Standard	Waters, USA
HSA	Sigma Aldrich, USA
Human Serum	Lonza AG, CH
IAA	Sigma Aldrich, USA
IL-4	Promocell, DE
Immersion oil	Leica, DE
Leucine Enkephalin acetate salt hydrate	Sigma Aldrich, USA
Lymphocyte Medium LSM 1077	PAA, GE Healthcare, USA
MassPREP Digestion Standard Mix 1	Waters, USA
MassPREP Digestion Standard Mix 2	Waters, USA
MassPREP E. Coli Digest Standard	Waters, USA
MassPREP Enolase Digestion Standard	Waters, USA
Methanol	VWR International, USA
Methanol absolute LC-MS	Biosolve, NL
NuPAGE® LDS Sample buffer	Novex, Thermo Fisher Scientific, USA
NuPAGE® Reducing agent	Novex, Thermo Fisher Scientific, USA
Penicillin/Streptomycin	Life Technologies, Thermo Fisher Scientific, USA
Penicillin/Streptomycin 100x	Life Technologies, Thermo Fisher Scientific, USA
Phosphoric acid	Sigma Aldrich, USA
Pierce 660nm Protein Assay Reagent	Thermo Fisher Scientific, USA
Pierce Silver Stain Kit	Thermo Fisher Scientific, USA

ProteoExtract protein precipitation kit	Merck Millipore, USA
Prothrombin, human	Oxford Biomedical Research, USA
RapiGest SF Powder	Waters, USA
RPMI-1640	Sigma Aldrich, USA
SeeBlue® Plus2 prestained standard	Life Technologies, Thermo Fisher Scientific, USA
Sequencing Grade Modified Trypsin	Promega, USA
Sheath Fluid for flow systems	Life Technologies, Thermo Fisher Scientific, USA
SimplyBlue SafeStain	Life Technologies, Thermo Fisher Scientific, USA
Sodium pyruvate	Sigma Aldrich, USA
Thiourea	Sigma Aldrich, USA
Trypsin	Life Technologies, Thermo Fisher Scientific, USA
Urea	Sigma Aldrich, USA
Water ULC/MS	Biosolve, NL
α-MEM	Lonza Group AG, CH

3.1.4 CONSUMABLES

Table 3-5. List of consumables

Name of product	Supplier
ACQUITY UPLC PST C18 nanoACQUITY Column 10K psi	Waters, USA
ACQUITY UPLC PST C18 nanoACQUITY Trap 10K psi	Waters, USA
Cell counting slides	Bio-Rad Laboratories Inc., USA
Cell culture plates (6-well)	Greiner Bio-One, DE
Cell strainer (70 µm)	Becton Dickinson, USA
Cryo tubes	Greiner Bio-One, DE
Disposable scalpel	Feather, JP
Eppendorf Safe-Lock Tubes (1.5 and 2 ml)	Eppendorf AG, DE
FACS tubes	Partec, DE
Falcon tubes (15 and 50 ml)	Greiner Bio-One, DE
Fused Silica Tube 375µm x 75µm x 3m	Waters, USA
Fused Silica Tube, 25-micron ID, 1m	Waters, USA

LCMS Certified Clear Glass Max Recovery Vial	Waters, USA
Multiwell plates (96-well)	Corning Inc., USA
NuPAGE 10% Bis-Tris Protein Gels	Life Technologies, Thermo Fisher Scientific, USA
One-Piece PEEK Knurled Fitting	Waters, USA
Parafilm	Pechiney Plastic Packaging, USA
Pasteur pipettes	Brand, DE
PEEK Fitting, One Piece, short	Waters, USA
Pin Plug Depth Gauge	Waters, USA
Pipette tips (10, 20, 200 and 1000 µl)	Greiner Bio-One, DE
Pre-Cut SilicaTip Emitters	NewObjective, USA
Pre-Cut TaperTip Emitters	NewObjective, USA
Protein LoBind Tubes 1.5 ml	Eppendorf AG, DE
Serological Pipettes (5, 10, 25, 50 ml)	Greiner Bio-One, DE
Tissue culture flasks (175 cm^2)	Greiner Bio-One, DE
Union, Capillary	Waters, USA
µ-dish 35mm, low, ibiTreat	IBIDI, DE

3.2 METHODS

3.2.1 HUMAN BLOOD AND SERUM SAMPLES

Whole blood was taken at the Department of Transfusion Medicine Mainz from healthy donors after physical examination and after obtaining informed consent in accordance with the Declaration of Helsinki. For human serum generation, blood was clotted overnight according to standard procedure and serum from seven volunteers was pooled into one batch. Plasma was generated by addition of either citrate or lithium-heparin as anticoagulants and subsequent centrifugation. Human heparin plasma from ten donors was pooled into one batch and all samples were stored at -80 °C. With Pierce 660nm protein assay a protein concentration of 69 mg/ml was determined for human serum, 66 mg/ml for human heparin plasma and citrate plasma. To remove any aggregated proteins the samples were centrifuged for 1 h at 20,000 g before usage.

3.2.2 PROTEIN CORONA PREPARATION

To ensure reproducibility the ratio of total particle surface area to plasma concentration was kept at 20 ml/m² for all nanoparticles unless otherwise stated. The nanoparticle dispersions were diluted with ultrapure water to a constant particle surface concentration (0.05 m² in 300 µL) and this dispersion was incubated with 1 ml human plasma for 1 h at 37 °C with constant agitation. The incubation time was chosen because previous reports confirmed that the protein corona is formed in a relatively stable manner over a period of 1 h.[10] The particles were separated from the supernatant by centrifugation at 20,000 g for 1 h. The particle pellet was resuspended in PBS and washed by three centrifugation steps at 20,000 g for 1 h and subsequent redispersion in PBS. Before the last washing step, the dispersion was transferred into a fresh protein lobind tube. Proteins were eluted from the particles by dissolving the particle-protein pellet in 300 µl urea-thiourea buffer (7 M urea, 2 M thiourea, 4% CHAPS). Protein concentrations were determined using Pierce 660nm protein Assay according to manufacturer's instructions with BSA as a standard.

3.2.3 SDS-PAGE

For SDS PAGE 16.25 µl of the protein sample was mixed with 6.25 µl NuPAGE LDS Sample Buffer and 2.5 µl NuPAGE Sample Reducing Agent and loaded onto a NuPAGE 10% Bis-Tris

Protein Gel. The electrophoresis was carried out in NuPAGE MES SDS Running Buffer at 150 V for 1.5 h with SeeBlue Plus2 Pre-Stained Standard as a molecular marker. Proteins were fixed in 10% acetic acid and 40% ethanol for 1 h and subsequently visualised by staining with 0.1% colloidal coomassie brilliant blue G-250 in 10% ammonium sulphate, 2% Phosphoric acid and 25% Methanol for 24 h. Alternatively, gels were stained using SimplyBlue SafeStain or the Pierce Silver Stain Kit according to the instruction manual.

3.2.4 PROTEIN IN-SOLUTION DIGESTION

Proteins were digested following the protocol of Tenzer *et al*.[24] with few modifications. Briefly, 25 µg of each protein sample were precipitated using the ProteoExtract protein precipitation kit according to the supplier's manual. The protein pellet was resuspended in 100 µl 0.1% RapiGest SF in 50 mM ammonium bicarbonate and incubated for 15 min at 80 °C. dithiothreitol was added to a final concentration of 5 mM before the sample was incubated at 56 °C for 45 min. Iodacetamide was added to a final concentration of 15 mM and the samples were kept for 1 h in the dark. Proteins were digested overnight at 37 °C using trypsin with an enzyme to protein ratio of 1:50 ratio. To stop the enzymatic digestions and to degrade RapiGest SF 2 µl hydrochloric acid were added and the sample was incubated for 45 min at 37 °C. To remove water immiscible degradation products of RapiGest SF, the sample was centrifuged at 13 000 g, for 15 min. For LC-MS analysis the samples were diluted 10-fold with aqueous 0.1% formic acid and spiked with 50 fmol/µl Hi3 EColi Standard (Waters Corporation) for absolute quantification.

3.2.5 LIQUID-CHROMATOGRAPHY MASS-SPECTROMETRY (LC-MS) ANALYSIS

Quantitative analysis of protein samples was performed using a nanoACQUITY UPLC system coupled with a Synapt G2-Si mass spectrometer. Tryptic peptides were separated on the nanoACQUITY system equipped with a C18 analytical reversed-phase column (1.7 µm, 75 µm x 150 mm) and a C18 nanoACQUITY Trap Column (5 µm, 180 µm x 20 mm,). Samples were processed with mobile phase A consisting of 0.1% (v/v) formic acid in water and mobile phase B consisting of acetonitrile with 0.1% (v/v) formic acid. The separation was performed at a sample flow rate of 0.3 µl/min, using a gradient of 2-37% mobile phase B over 70 min. As a reference compound 150 fmol/µl Glu-Fibrinopeptide was infused at a flow rate of 0.5 µl/min.

Data-independent acquisition (MS^E) experiments were performed on the Synapt G2-Si operated in resolution mode. Electrospray ionisation (ESI) was performed in positive ion mode using a NanoLockSpray source. Data was acquired over a range of *m/z* 50-2000 Da with a scan time of 1 s, ramped trap collision energy from 20 to 40 V with a total acquisition time of 90 min. All samples were analysed in triplicates. Data acquisition and processing was carried out using MassLynx 4.1.

3.2.6 DATA PROCESSING AND PROTEIN IDENTIFICATION

TansOmics Informatics software or Progenesis QI for Proteomics was used to process data and identify peptides. Continuum LC-MS data were post acquisition lock mass corrected. Noise reduction thresholds for low energy, high energy and peptide intensity were fixed at 120, 25, and 750 counts, respectively. During database searches, the protein false discovery rate was set at 4%. The generated peptide masses were searched against a reviewed human protein sequence database downloaded from Uniprot. For samples originating from FBS a reviewed bovine database was used. Sequence information of Hi3 Ecoli standard (Chaperone protein ClpB) was added to the database to conduct absolute quantification.[142,143] The following criteria were used for the search: one missed cleavage, maximum protein mass 600 kDa, fixed carbamidomethyl modification for cysteine and variable oxidation for methionine. For identification a peptide was required to have at least three assigned fragments and a protein was required to have at least two assigned peptides and five assigned fragments. Identified peptides with score parameters less than 4 were generally rejected. Quantitative data were generated based on the TOP3/Hi3 approach, providing the amount of each protein in fmol.[141]

3.2.7 CELL CULTURE

Human mesenchymal stem cells (hMSCs) isolated from bone marrow were cultured in α-MEM, supplemented with 20% foetal bovine serum (FBS), 1% sodium-pyruvate, 100 U/ml penicillin and 100 mg/ml streptomycin. Human cervix carcinoma cells (HeLa) and the murine macrophage cell line RAW264.7 were cultured in Dulbecco´s modified eagle medium (DMEM), supplemented with 10% FCS, 100 U/ml penicillin, 100 mg/ml streptomycin and 2 mM glutamine.

Human immature dendritic cells (DCs) were generated from adherent peripheral blood mononuclear cells (PBMCs) from buffy coats to a standard procedure.[144] Briefly, buffy coats from healthy blood donors were subjected to Ficoll density gradient centrifugation to harvest PBMCs. The monocytes were then allowed to adhere for 1 h in order to separate them from non-adherent leukocytes. Immature dendritic cells were generated by culturing adherent blood monocytes in RPMI medium in the presence of granulocyte macrophage colony-stimulating factor (GM-CSF) and interleukin-4 (IL-4) for 7 days. DCs were cultured in RPMI-1640 supplemented with 2% human serum, 100 U/ml penicillin and 100 mg/ml streptomycin. All cells were grown in a humidified incubator at 37 °C and 5% CO_2.

3.2.8 NANOPARTICLE TREATMENT OF CELLS

For the uptake experiments, the cells were seeded at a density of 20,000 cells/cm^2. For the analysis of nanoparticle internalisation in serum-free conditions, the cells were washed 3 times with PBS and incubated in fresh serum-free medium for 2 h. Nanoparticle dispersions were added at a concentration of 75 µg/ml to the cells in respective medium and incubated for the indicated period of time. Before the cells were analysed by flow cytometry or laser scanning microscopy, they were washed to remove free nanoparticles.

For the nanoparticle uptake after single protein adsorption nanoparticle dispersions were incubated with the respective protein (human apolipoprotein A-IV, human apolipoprotein C-III, human prothrombin, human antithrombin III, human serum albumin or human clusterin) for 1 h at 37 °C with constant agitation. To ensure comparability, the ratio of protein concentration to total nanoparticle surface area was kept constant at 1 mg/m² for all proteins. Nanoparticles coated with protein were then added to the cells at a concentration of 75 µg/ml in fresh serum-free medium.

3.2.9 FLOW CYTOMETRY

For the quantitative analysis of nanoparticle uptake into cells flow cytometry measurements were conducted. After the indicated incubation time, adherent cells were washed with DPBS and subsequently detached from the culture vessel with 2.5% trypsin. Flow cytometry measurements were performed on a CyFlow ML cytometer with a 488 nm

laser for excitation of Bodipy-1 and a 527 nm band pass filter for emission detection. For cell viability measurements, the cells were stained with 28.6 mg/ml 7-aminoactinomycin D (7-AAD). Excitation of 7-AAD was conducted at 562 nm and emission measured at 682 nm. Data analysis was performed using FCS Express V4 software by selecting the cells on a forward/sideward scatter plot, thereby excluding cell debris. These gated events were further analysed by the amount of fluorescent signal expressed as median intensity. Median intensity of a negative control was subtracted the obtained values. Mean values and standard deviation were determined from triplicates.

3.2.10 CONFOCAL LASER SCANNING MICROSCOPY (CLSM)

In order to demonstrate the intracellular localisation of nanoparticles live cell images were taken. A LSM SP5 STED Leica Laser Scanning Confocal Microscope consisting of an inverse fluorescence microscope DMI 6000 CS equipped with a multi-laser combination and five detectors operating in the range of 400 - 800 nm. An HCX PL APO CS 63 x 1.4 oil objective was used. Fluorescent nanoparticles labelled with BODIPY-I were excited with an argon laser (20 mW, λ = 514 nm), detected at 530 - 545 nm and pseudo-coloured in green. The cell membrane was stained with CellMaskOrange (2.5 mg/ml), excited with a DPSS 561 nm (≈ 1.3 mW), detected at 570 - 640 nm and pseudo-coloured in red. Images were evaluated with LAS AF 3000 software.

4 RESULTS AND DISCUSSION

The results section is divided into six parts. In the first two sections the protein corona of polystyrene nanoparticles was investigated. Single proteins influencing uptake were identified in the first part, whereas in the second chapter the influence on the aggregation behaviour of particles was analysed. In the next two sections different types of "stealthing" nanocarriers were examined. HES and PEEP are introduced as biodegradable polymers with stealth properties. Furthermore, the influence of different protein sources on protein corona composition and cell interaction is discussed and in the end a comparison of different corona preparation methods is presented.

4.1 IDENTIFICATION OF SINGLE PROTEINS INFLUENCING CELLULAR UPTAKE BY AN UNBIASED, QUANTITATIVE APPROACH

In the first part, the composition of the hard protein corona of six differently functionalised polystyrene nanoparticles after incubation in human serum was analysed quantitatively, employing liquid chromatography mass spectrometry. The obtained protein binding profiles were then correlated with the cellular uptake of the nanoparticles in order to identify candidate proteins involved in cellular uptake and their function was further validated. The results presented in this section were partially published as: "*The Protein Corona of Nanoparticles: Distinct Proteins Regulate the Cellular Uptake.*" Reprinted (adapted) with permission from Ritz *et al.*, Biomacromolecules, 2015, 16(4), 1311.[128] (Copyright (2015) American Chemical Society).

4.1.1 NANOPARTICLES

A defined set of four polystyrene nanoparticles (PS-NPs) with average diameters of approximately 100 nm was employed for this study (Figure 4-1). Although PS-NPs are not biodegradable they have been used extensively as a model system and their biocompatibility, wide range of possible sizes and functionalisations makes them a useful tool to study the effects of surface characteristics on various biological parameters.[145] PS-NPs were synthesised by A. Musyanovych and K. Klein using free-radical miniemulsion polymerisation.[146] Surface functionalities were introduced by co-polymerisation of monomers containing either carboxy (PS-COOH), amino (PS-NH_2), sulfonate (PS-SO_3) or phosphonate groups (PS-PO_3). Additionally, non-covalent functionalisations were achieved

by sodium dodecyl sulphate (SDS) and Lutensol AT50 (LAT50) on a surfactant-free NP (PS-PO_3) to control the effect of detergents used for dispersing the NPs in aqueous solution. To follow cellular uptake, the nanoparticles were fluorescently labelled by employing a methaycrylated BODIPY derivate with an adsorption maximum at 523 and emission maximum at 536 nm.

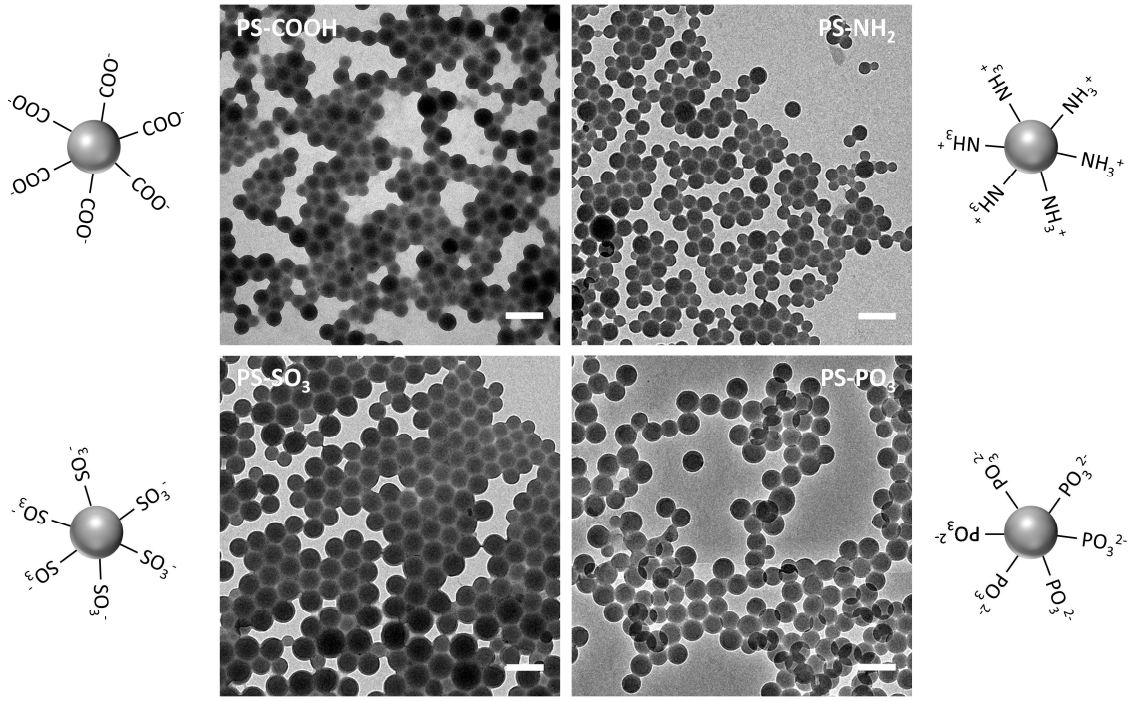

Figure 4-1: TEM images of the functionalised polystyrene nanoparticles.
TEM imaging was performed after drop casting the nanoparticle dispersion onto a carbon coated copper grid. Scale bars: 200 nm. (TEM images were taken by A. Musyanovych) Reprinted (adapted) with permission from Ritz *et al.*[128]

4.1.2 INFLUENCE OF SERUM INCUBATION ON NANOPARTICLE SIZE AND CHARGE

To test the influence of protein adsorption on the physicochemical characteristics of the PS-NPs, the size and charge was determined before and after serum incubation (Figure 4-2). Figure 4-2a depicts the NP diameter, characterised by dynamic light scattering (DLS). As expected, corona formation in serum leads to a slight increase of size for all NPs. Furthermore, it results in a moderately negative zeta potential for all particles (-20 mV to -30 mV) independent of the original surface charge (Figure 4-2b). This is in agreement with previous studies, reflecting the negative charge of most serum proteins at physiological conditions.[16,147]

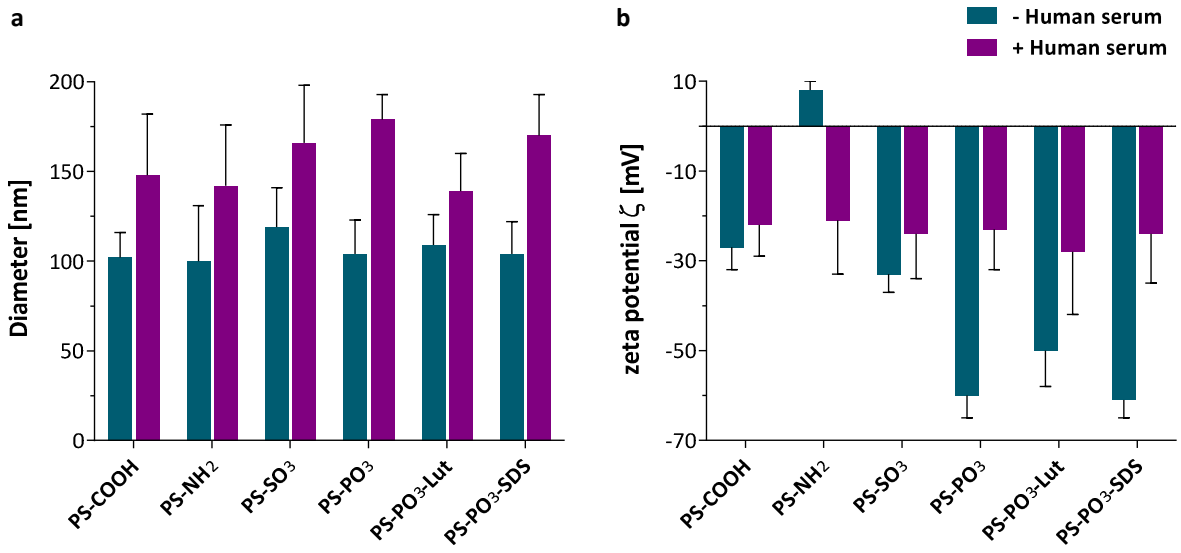

Figure 4-2: PS-NP charactersitics before and after serum incubation.
(a) NP diameter characterised by dynamic light scattering (DLS). (b) Zeta potential ζ determined with a particle charge detector in 1 mM KCl solution at pH 7.2. (Measurements were performed by G. Baier)

4.1.3 IDENTIFICATION OF SERUM PROTEINS ADSORBED TO PS-NPS

In order to get a better understanding of the role of individual proteins adsorbing to the nanoparticles´ surface, it is necessary to analyse the composition of the protein corona. Therefore, the nanoparticles were incubated with human serum for 1 h to form a stable corona. Studying non-crosslinked polystyrene particles offers the advantage of a full recovery of adsorbed proteins through dissolving the particles according to Wessel and Flügge.[148] This procedure also precipitates the proteins, which were then analysed employing a quantitative liquid chromatography mass spectrometry approach (LC-MS TOP3).[141] The protein corona preparation was performed by N. Kotman as described in his dissertation.[127]

In total 169 different proteins were identified. The complete list of identified proteins can be found in Table 7-2 in the appendix. These proteins can be classified by their function into seven groups: acute phase proteins, coagulation proteins, complement factors, immunoglobulins, lipoproteins, other proteins and proteins resulting from tissue leakage. Figure 4-3a displays a general distribution of protein classes and compares it to the protein distribution of human serum. Overall, a strong enrichment of apolipoproteins on all six PS-NPs was observed. Proteins belonging to the family of complement factors were also enriched on most polystyrene particles, while coagulation factors were only enriched

on the surface of the carboxy and phosphonate functionalised PS-NPs, but depleted on the amino and sulfonate functionalised PS-NPs, emphasising the role of surface functionalisation for the formation of an individual protein corona. On the other hand albumin, the most abundant protein in serum belonging to the group of other proteins, and immunoglobulins were consistently depleted.

In Figure 4-3b the identified proteins are grouped according to their isoelectric points. This approach allows evaluation of a potential influence of electrostatic interactions on protein adsorption. All six nanoparticles are mainly covered by proteins with an isoelectric point between 5 and 6, which are also the most abundant proteins in human serum. Further division of this group shows that proteins with isoelectric points between 5 and 5.5 were enriched on all six nanoparticles.

If electrostatic forces played a major role in protein nanoparticle interactions, proteins with low isoelectric points would be expected to predominantly bind to nanoparticles with a basic surface. But acidic proteins were not enriched on the amino functionalised particle. The only correlation between the isoelectric point of the proteins and the surface charge of the PS-NPs was observed for the phosphonate particles PS-PO_3 and PS-PO_3-SDS. These particles with the most negative zeta potentials bound significantly more proteins with an isoelectric point above 6. Overall, the analysis suggests that protein adsorption is not mainly dependent on electrostatic interactions.

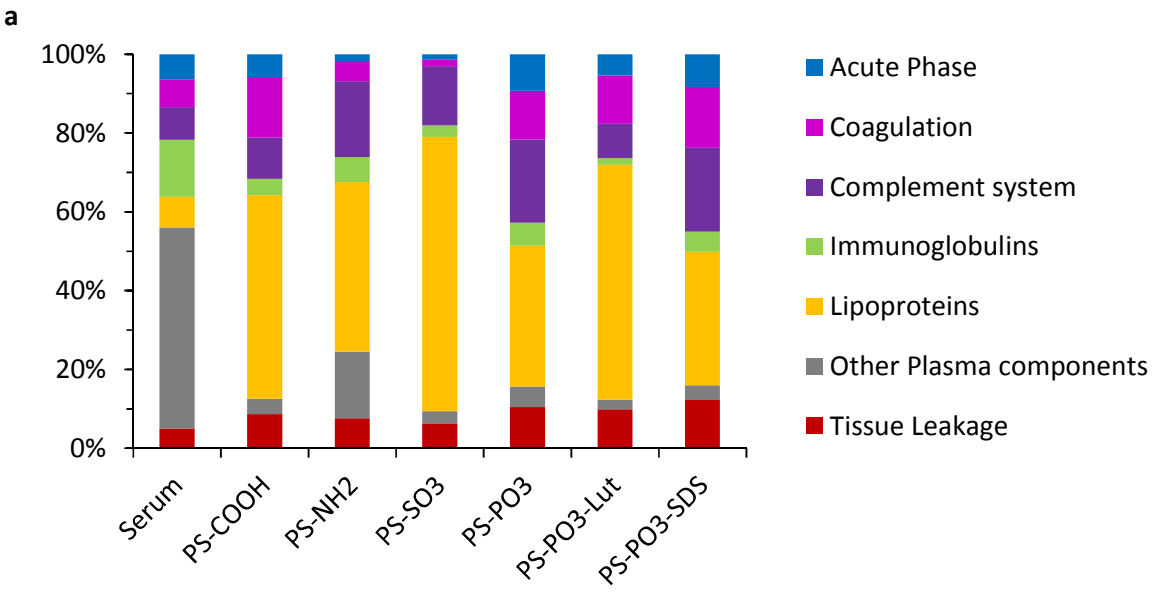

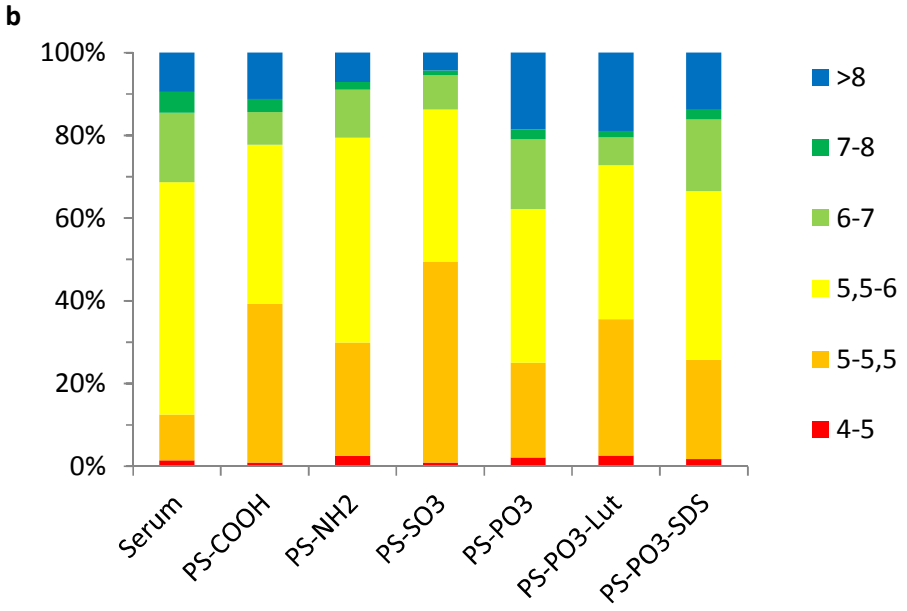

Figure 4-3: Analysis of the protein corona on PS-NPs in dependence of NP functionalisation measured by LC-MS.

Relative percentages of the adsorbed proteins were calculated from the averaged ppm values. Proteins are either classified according to their biological function (a) or according to their isoelectric point (b). (LC-MS measurements were performed by S. Tenzer) Reprinted (adapted) with permission from Ritz *et al*.[128]

Figure 4-4 highlights the 20 most abundant proteins on the individual functionalised PS-NPs. The spot size represents the relative mass per particle and the colour codes for the respective protein class. Most obvious is the high enrichment of the lipoproteins apolipoprotein A-I (APOA1) and clusterin (CLUS, also known as apolipoprotein J) on all six NPs, which make up the majority of the protein corona. Having a closer look, one can identify more interesting candidate proteins which differ strongly in their adsorption behaviour as for example ANT3, APOA4, APOH or ITIH4.

In order to confirm the preferred binding of the most abundant protein APOA1, a consecutive adsorption experiment was conducted. APOA1 and human serum albumin (HSA) were incubated at the same concentration with PS-COOH for 1 h at 37 °C. After three washing steps with PBS, the strongly adsorbing proteins were desorbed using LDS sample buffer and subjected to SDS-PAGE. Furthermore, NPs incubated with APOA1 were subsequently incubated with HSA to test the influence of the pre-coating.

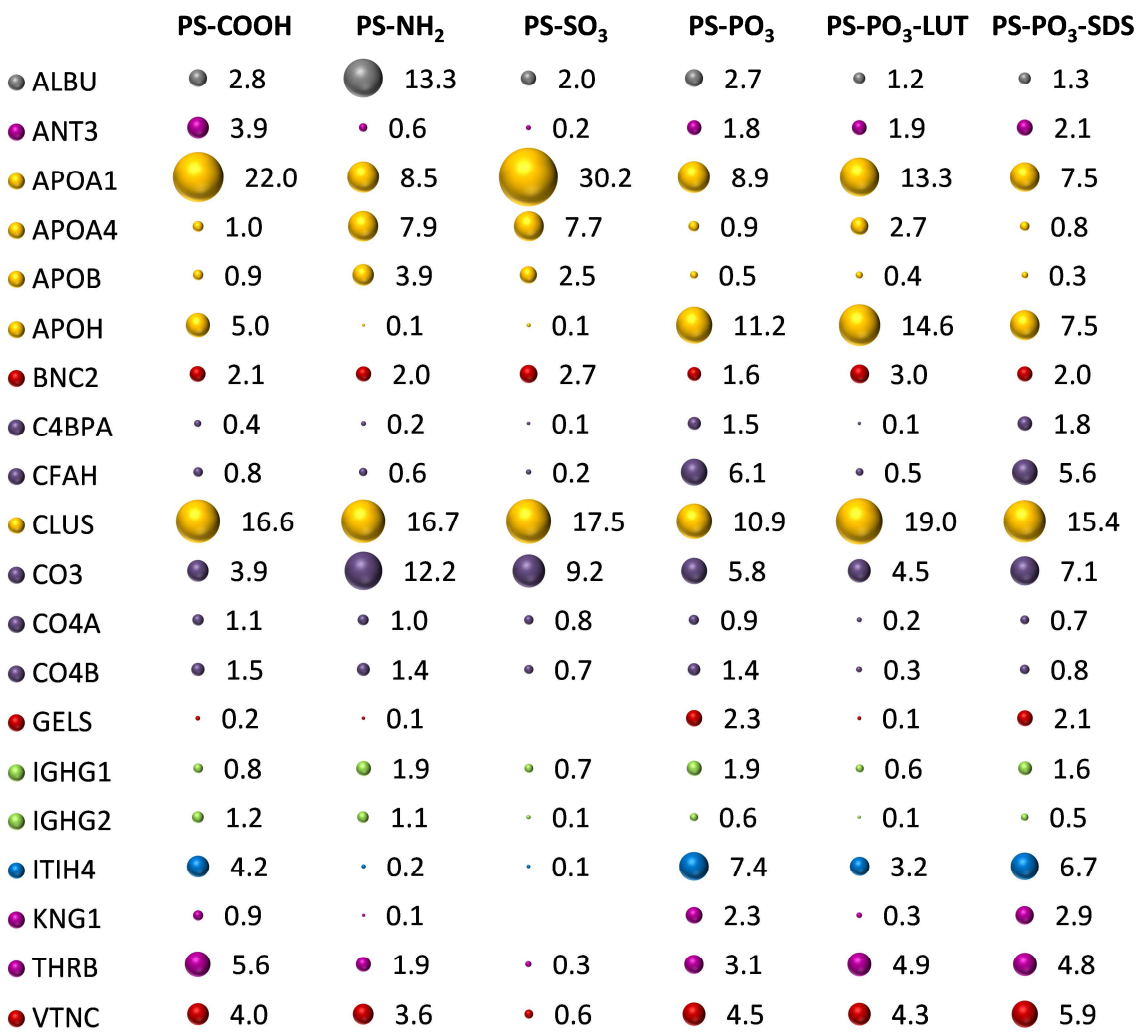

Figure 4-4: Ranking of "TOP20" proteins measured by LC-MS.
Only proteins with the highest mean protein adsorption on the indicated functionalised PS-NPs are shown. Proteins are ordered alphabetically. Colour code indicates the protein family and the spot size represents the mass fraction (%) of the total protein corona. Values calculated from the molar masses of each protein are given in decimal numbers. Reprinted (adapted) with permission from Ritz *et al*.[128]

In Figure 4-5 an intense band at 28 kDa after coating of PS-COOH NPs with APOA1 proves once more the strong adsorption of this protein to the polystyrene nanocarriers. Furthermore, when incubated alone, HSA can be recovered from the NPs. After consecutive adsorption of APOA1 and albumin, almost no HSA is visible on the gel, but again a pronounced APO1 band is detected. This clearly shows that pre-coating the NPs with the strong adhering APOA1 strongly reduces a subsequent interaction with albumin.

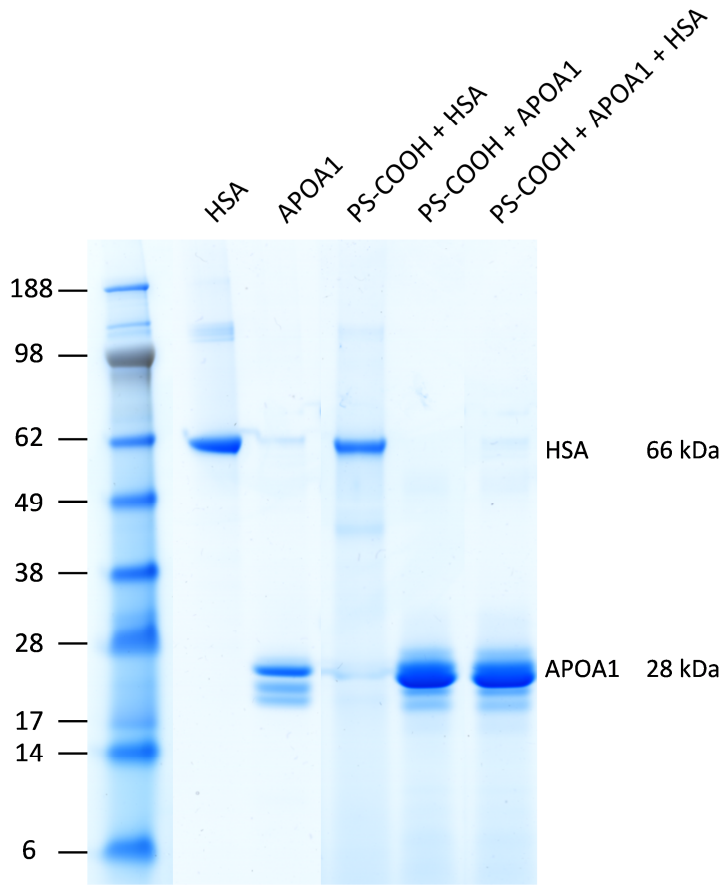

Figure 4-5: SDS-PAGE analysis of HSA and APOA1 adsorbed to PS-COOH.
NPs were incubated with proteins for 1 h at 37 °C (50 µg protein/0.05 m² NP). One sample of APOA1 coated NPs was subsequently incubated with HSA. After three washing steps with PBS, the proteins were desorbed from the NPs using LDS sample buffer. As a control 1 µg of single proteins was also applied on the gel (two lanes on the left).

4.1.4 DIFFERENT BINDING PATTERNS OF APOLIPOPROTEINS

While there is lacking information of the protein corona for the wide variety of nanocarriers produced so far, several studies investigating the protein corona of e.g. polystyrene and lipid nanoparticles have identified apolipoproteins as the dominant protein group in their corona.[12,23,40] Therefore, the enrichment and depletion of specific apolipoproteins in relation to human serum was further analysed (Figure 4-6).

PS-NH_2 and PS-SO_3 NPs displayed an enrichment of almost all identified apolipoproteins, whereas on PS-COOH and PS-PO_3 NPs some lipoproteins were also depleted. Comparing the most abundant proteins with a weight fraction higher than 5%, the lipoproteins clusterin and APOA1 showed the highest prevalence on all PS-NPs. Additionally, APOA4, APOC1, APOC3 and APOE were always enriched, forming an apolipoprotein background on the particle surface independent of surface functionalisation.

Interestingly, some apolipoproteins show a very distinct binding profile. For example APOH was selectively enriched on the PS-COOH and PS-PO_3 NPs, whereas APOA2 and APOB were selectively enriched on the PS-NH_2 and PS-SO_3 NPs. The strong enrichment of APOA1, as well as the adsorption of other HDL apolipoproteins as APOA2, APOC, APOA4 and APOE could indicate a binding of complete HDL complexes[14] suggesting that they may physiologically interact with receptors for the VLDL/LDL/HDL pathway.

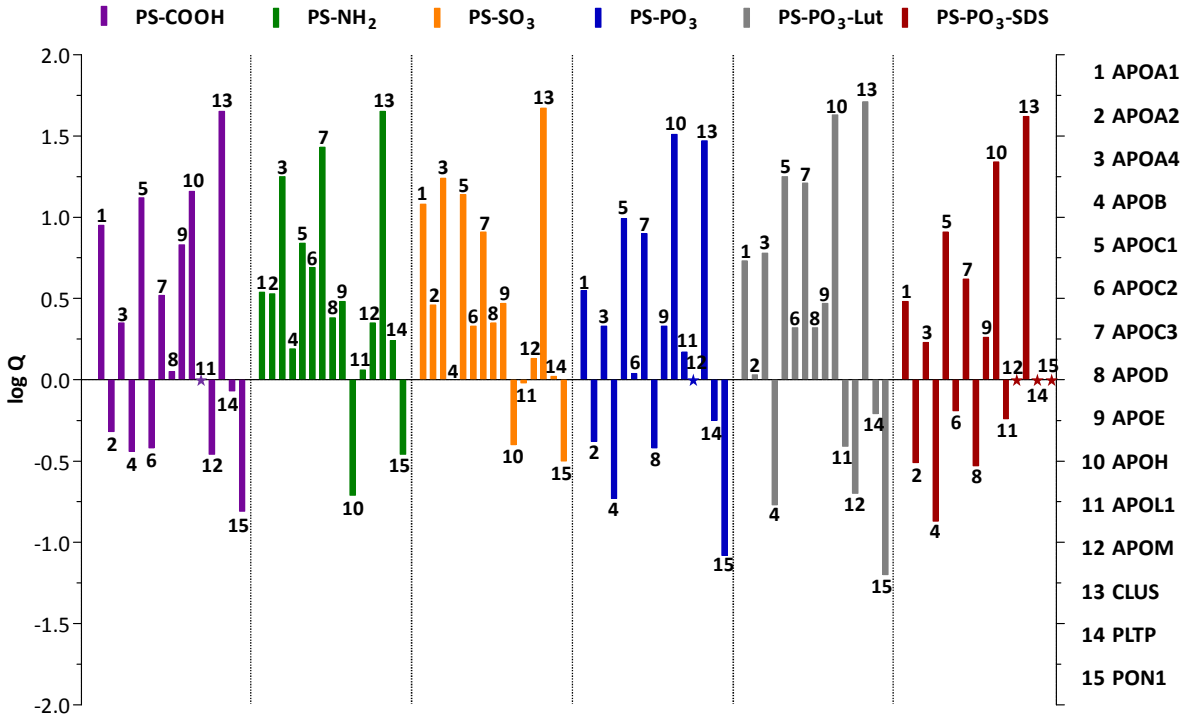

Figure 4-6: Enrichment and depletion of apolipoproteins on PS-NPs.
Logarithm of ratio Q (Q = mass fraction protein x on particle/ mass fraction protein x in serum) illustrates a specific enrichment (log Q > 1) or depletion (log Q < 1) of single apolipoproteins on the different NPs in comparison to serum concentration. Asterisk symbolizes a serum protein which was not detected on the respective particle. Reprinted (adapted) with permission from Ritz *et al.*[128]

4.1.5 CORRELATION OF PROTEIN BINDING PROFILE WITH CELLULAR UPTAKE INTO HMSCS

Next, the uptake of serum protein coated nanoparticles into human mesenchymal stem cells (hMSCs) was analysed by fluorescence laser scanning microscopy (Figure 4-7). Interestingly, PS-COOH and PS-PO_3 NPs were efficiently taken up, while PS-NH_2 and PS-SO_3 showed a lower uptake.

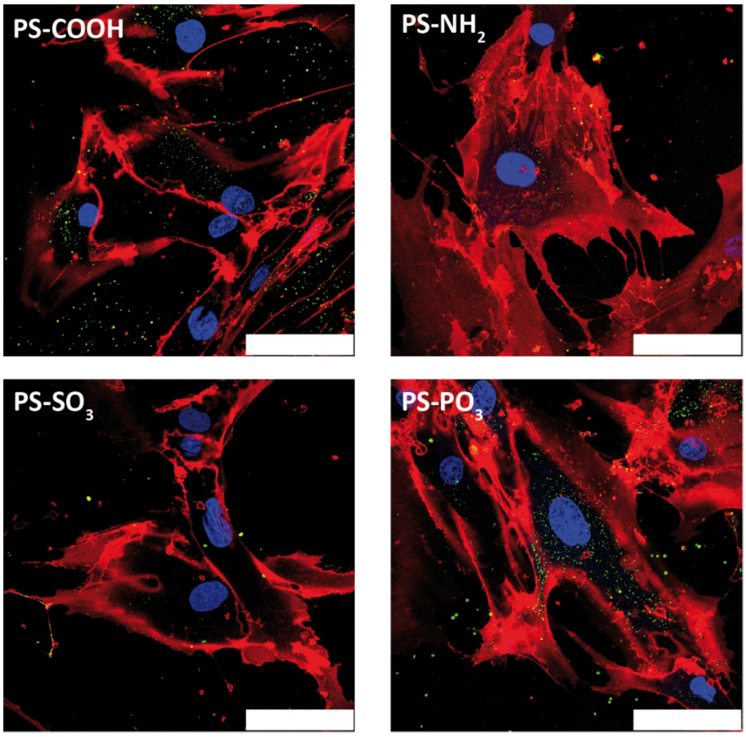

Figure 4-7: Uptake of different functionalised polystyrene nanoparticles in hMSCs.
Confocal microscopy images of cells incubated with 75 µg/ml human serum coated PS-NPs for 24 h. Plasma membrane stained with CellMaskOrange (pseudo-coloured in red), nucleus stained with Draq5 (blue) and nanoparticles labelled with Bodipy-1 (pseudo-coloured in green). Scale bars: 75 µm. (LSM images were taken by S. Ritz) Reprinted (adapted) with permission from Ritz *et al.*[128]

Flow cytometry analysis of hMSCs incubated with the fluorescent NPs supports these results (Figure 4-8a): a high uptake of the carboxylated and phosphonated NPs and a very low internalisation of the amino and sulphonated NPs were detected. Interestingly, this specific uptake pattern is very similar to the adhesion pattern of APOH to the different nanoparticles as seen in Figure 4-6. Here, a strong adsorption of APOH to the surface of PS-COOH and PS-PO_3 was found. Figure 4-8 further illustrates this finding.

As a statistical measurement for the linear association between the amount of each protein identified by LC-MS and the uptake into hMSCs, the Pearson Product-Moment Correlation Coefficient was calculated according to the formula:

$$r = \frac{\sum(x - \bar{x})\,(y - \bar{y})}{\sqrt{\sum(x - \bar{x})^2 \sum(y - \bar{y})^2}}$$

where *x* is the ppm value of each protein and *y* is the relative fluorescence intensity measured by flow cytometry. Values for those proteins which were identified on all six investigated nanoparticles with a percentage of at least 1% on one of the nanoparticles

are shown in Table 4-1. If the value of r is close to +1, this indicates a strong positive correlation, and if r is close to -1, this indicates a strong negative correlation. Calculation of this correlation coefficient enables an identification of single proteins, which are more likely to influence NP uptake.

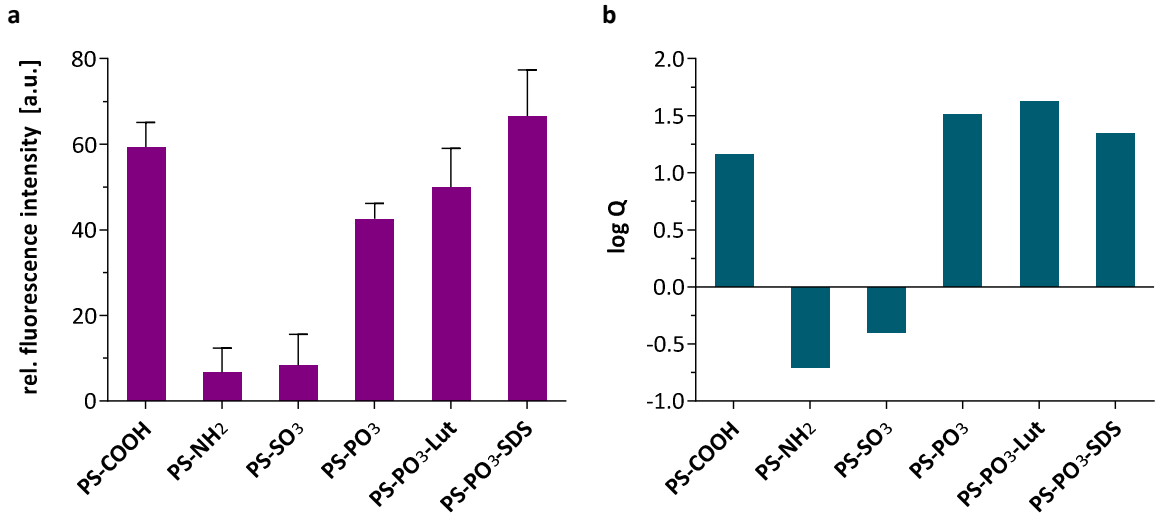

Figure 4-8: Correlation between uptake into hMSCs (a) and abundance of APOH (b) on different PS-NPs. (a) Quantitative assessment of nanoparticle uptake into hMSCs by flow cytometry. Cells treated with 75 µg/ml human serum coated polystyrene nanoparticles for 24 h. (b) Enrichment (log Q > 1) and depletion (log Q < 1) of APOH on PS-NPs expressed as logarithm of ratio Q (Q = mass fraction protein x on particle/ mass fraction protein x in serum). Reprinted (adapted) with permission from Ritz *et al.*[128]

A positive correlation, i.e. a high relative amount of a specific protein on NPs correlating with a high cellular uptake, was observed for the coagulation factors prothrombin (THRB) and antithrombin III (ANT3), vitronectin (VTNC) as well as for inter-alpha-trypsin-inhibitor heavy chain H4 (ITIH4), platelet factor 4 (PLF4) and apolipoprotein H (APOH). A negative correlation was found for apolipoprotein A-IV (APOA4), C-III (APOC3), apolipoprotein B-100 (APOB), for serum albumin (ALBU) and for the complement factor C3 (CO3). Interestingly, no correlation was observed for the most abundant corona proteins APOA1 and clusterin.

Table 4-1: Correlation between cell uptake into hMSCs and mass fraction (ppm) of adsorbed proteins identified by LC-MS.

Values are shown only for those proteins which were identified on all six nanoparticles and constitute for at least 1% of the protein corona on one of the nanocarrier. Table is ordered alphabetically. For a positive correlation coefficient ($r \geq 0.5$) proteins are highlighted in cyan, for a negative correlation in purple. Additionally, average ppm values for the individual nanoparticles are listed. Reprinted (adapted) with permission from Ritz *et al.*[128]

+ correlation: high protein amount/high uptake **- correlation: high protein amount/low uptake**

Protein name	entry	Average ppm of total protein						correlation coeffcient
		PS-COOH	PS-NH_2	PS-SO_3	PS-PO_3	PS-PO_3-Lut	PS-PO_3-SDS	
Antithrombin-III	ANT3	39433	5838	1956	18299	18578	21211	1.0
Apolipoprotein A-I	APOA1	220232	85388	301967	89195	132857	75341	-0.2
Apolipoprotein A-IV	APOA4	9797	78516	76589	9416	26635	7505	-0.9
Apolipoprotein B-100	APOB	9093	39242	25178	4736	4243	3436	-0.8
Apolipoprotein C-III	APOC3	2032	16469	4992	4898	9916	2593	-0.7
Apolipoprotein E	APOE	18354	8195	7964	5822	8024	4952	0.5
Beta-2-glycoprotein 1	APOH	49719	670	1375	112199	146328	75359	0.5
C4b-binding protein alpha chain	C4BPA	4088	2043	1049	15005	908	18082	0.5
Clusterin	CLUS	165887	166996	174579	109050	190072	154368	-0.2
Complement C3	CO3	39212	121983	91584	57796	45163	71400	-0.8
Complement C4 A	CO4A	10967	10098	7502	8867	2003	6551	0.1
Complement C4 B	CO4B	14852	14276	7018	13672	2875	7747	0.2
Complement factor H	CFAH	7714	5908	2369	60793	5084	56342	0.4
IgG-1 chain C region	IGHG1	7531	18609	6564	18811	5538	16057	-0.1
IgG-2 chain C region	IGHG2	11533	11055	1426	5536	930	4689	0.3
Ig mu chain C region	IGHM	5769	10162	5738	5346	2567	5623	-0.4
Inter-alpha-trypsin inhibitor heavy chain H4	ITIH4	42391	1508	1293	73796	32456	66978	0.8
Prothrombin	THRB	56024	19427	3046	31233	49162	47772	0.9
Serum albumin	ALBU	27533	133201	20328	27248	12280	12761	-0.5
Vitronectin	VTNC	40161	36343	6445	44813	42904	59062	0.7
Zinc finger protein basonuclin-2	BNC2	21428	19631	26941	16093	30424	19590	-0.2

4.1.6 IDENTIFICATION OF SINGLE PROTEINS INFLUENCING UPTAKE INTO HMSCS

As the correlation analysis could only demonstrate a coincidence, the physiological impact was validated by single protein coating experiments and uptake studies in hMSCs. Therefore, proteins with a positive ($r \geq 0.5$) or a negative ($r \leq 0.5$) correlation coefficient (Table 4-1) were selected. PS-COOH NPs were pre-coated with individual proteins (50 µg of protein per 0.05 m² particle surface, 1 h, 37 °C), followed by incubation with hMSCs for 6 h in serum-free medium.

It was found, that indeed, coating of PS-COOH with APOH doubled the uptake compared to nanoparticles with a full serum protein corona (Figure 4-9a). In contrast apolipoproteins A4 and C3 reduced the nanoparticle internalisation to a minimum level, which also confirmed the correlation data. Coagulation factors antithrombin III and prothrombin did not show any impact on nanoparticle internalisation, despite the correlation. This clearly demonstrates the need for independent validation of candidate proteins in a cellular system.

These observations were also confirmed by laser scanning microscopy (Figure 4-9b). Again, an increased internalisation of NPs coated with APOH and almost no uptake of NPs coated with APOA4 was observed.

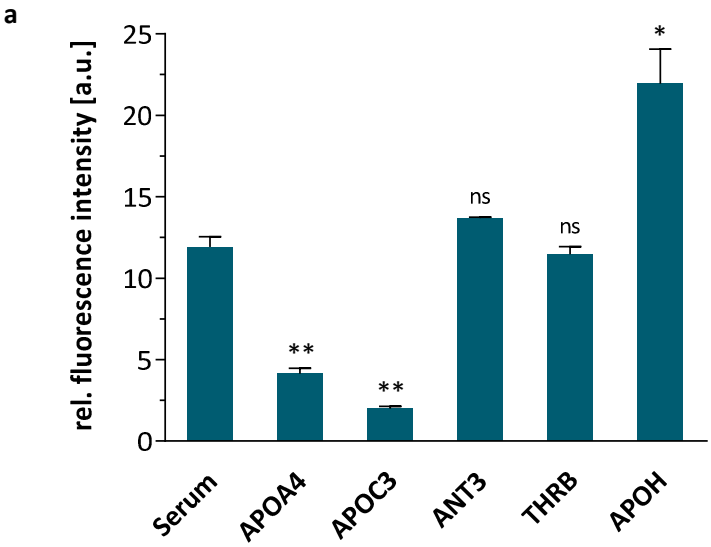

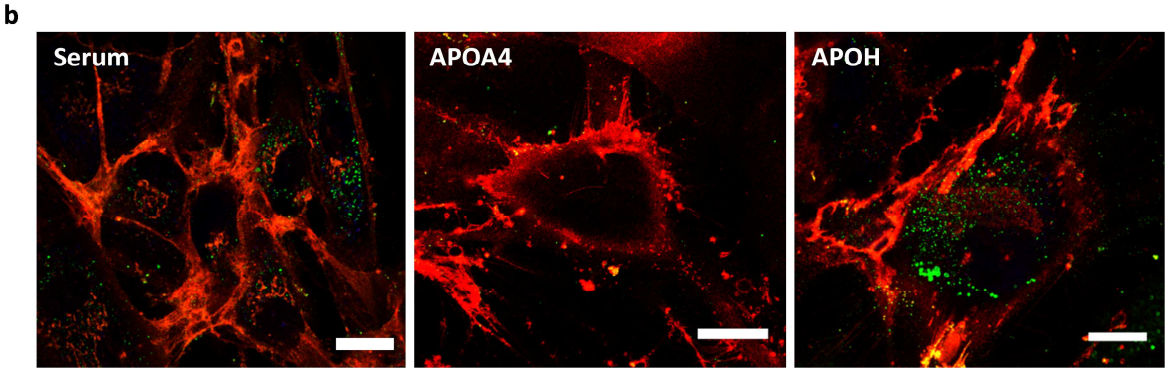

Figure 4-9: Influence of single protein coating on nanoparticle uptake in hMSCs.
(a) The carboxy functionalised polystyrene nanoparticle (PS-COOH) was coated with APOA4, APOC3, ANT3, THRB or APOH (50 µg per 0.05 m², 1 h, 37 °C), respectively, and incubated for 6 h in serum-free medium. Error bars ± SD calculated from two independent experiments with three replicates each. An unpaired student´s t-test was used to determine significance from the control test, significant samples are indicated with an asterisk (*P < 0.05; ** P < 0.01; n = 3). (b) Corresponding confocal microscopy images of living hMSCs treated with APOA4 or APOH coated carboxy functionalised polystyrene nanoparticle. Plasma membrane stained with cell mask orange (red) and nanoparticles labelled with Bodipy-1. Scale bars: 25 µm. (LSM images were taken by S. Ritz) Reprinted (adapted) with permission from Ritz *et al.*[128]

4.1.7 ADSORPTION STRENGTH OF SINGLE PROTEINS TO NANOPARTICLES

All proteins used for the uptake experiments in Figure 4-9 were enriched on PS-COOH and especially the two coagulation factors antithrombin III and prothrombin were rather high abundant on this NP (see Figure 4-4). Yet, here the correlation analysis could not be confirmed by the uptake studies after single protein coating. This could indicate inefficient adsorption of the single proteins.

To investigate how strong the single proteins adhere to the NPs, the particles were again incubated with the individual proteins, washed three times with PBS before the adsorbed proteins were desorbed with LDS sample buffer and analysed on a polyacrylamide gel. Figure 4-10 shows the amount of proteins identified after desorption. For apolipoproteins A4, C3 and H a certain portion of the adsorbed proteins could be made visible indicating a strong to moderate binding to the carboxy PS-NP. For APOA4 several smaller fragments were detected, although these protein fragments are not visible in the pure protein sample (left lane). In the pure sample several bands at higher molecular weights suggest a rather impure sample or aggregation.

More importantly, the SDS-PAGE reveals, that antithrombin III and prothrombin bind only very weakly to PS-COOH. Here, only very faint bands are visible on the gel and almost no

proteins of the actual sizes of 58 (ANT3) and 72 kDa (prothrombin) were identified. This could explain why the two proteins did not influence NP internalisation after single protein incubation (Figure 4-9a). Adsorption of these coagulation factors and other proteins identified in the corona might be dependent on the interaction of several serum proteins. It is conceivable, that only after adsorption of other strong binding proteins as apolipoproteins further proteins can adhere to the nanoparticle-protein complex.

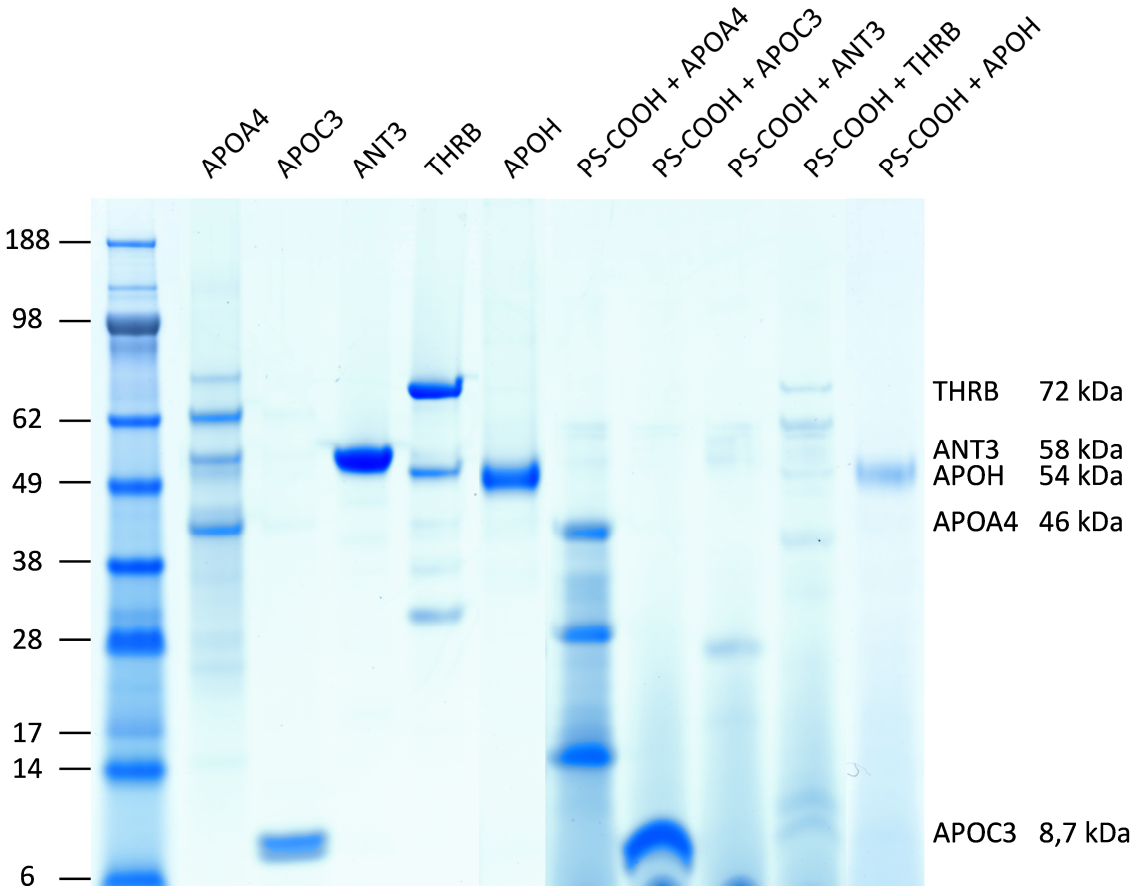

Figure 4-10: SDS-PAGE analysis of single proteins adsorbed to PS-COOH.
NPs were incubated with proteins for 1 h at 37 °C (50 µg protein/0.05 m² NP). After three washing steps, the proteins were desorbed from the NP using LDS sample buffer. As a control 1 µg of single proteins was also applied on the gel.

4.1.8 DISCUSSION

In conclusion, the protein corona on six differently functionalised polystyrene nanoparticles was determined using proteomic mass spectrometry. In general, a high enrichment of apolipoproteins was identified in the protein corona of all six tested polystyrene NPs, which is in agreement with previous studies.[12,13,23,26] Due to their function in lipid transport, hydrophobic regions need to be accessible on the lipoproteins,

which could explain a high adsorption to the particles. Using model polymer particles with decreasing hydrophobicity, Gessner *et al*. have demonstrated that nearly the same apolipoproteins identified here (APOA1, APOA4, APOC3, and CLUS) gradually disappear with decreasing hydrophobicity of the nanoparticle.[46] These results support the hypothesis that hydrophobic interactions between PS nanoparticles with lipid binding domains on the apolipoproteins probably serve as driving force for the adhesion of the proteins.[13]

Furthermore, a methodology to dissect the biological influence of individual proteins on cellular uptake was demonstrated. Correlating the amount of individual proteins with the internalisation into human stem cells revealed that selected proteins are pivotal to reduce or enhance cellular uptake. The results demonstrate that in a mixed protein corona, which is formed as a consequence of the NPs physicochemical properties, specific proteins are more likely to be involved in cell interactions.

Apolipoproteins are commonly referred to as dysopsonins, which promote prolonged circulation in the bloodstream through a reduced uptake by the mononuclear phagocyte system (MPS). Enrichment of almost all apolipoproteins on amino and sulfonate functionalised NPs (Figure 4-6) which are the particles showing the lowest uptake in cells (Figure 4-7), supports the general role of apolipoproteins as dysopsonins. But a more differentiated role of apolipoproteins was revealed by correlating the individual proteins with cellular uptake: most apolipoproteins served as an “apolipoprotein background”, whereas others seem to have a regulative role.

We identified apolipoprotein H (or beta2 glycoprotein-I) as a protein which promotes the internalisation of nanoparticles into human mesenchymal stem cells. Interestingly, APOH is described as an opsonin for the mononuclear phagocyte system[149,150] but not for non-phagocytic uptake. APOH is involved in distinct physiological processes as the blood coagulation cascade, where it demonstrates pro- and anticoagulant activities. By preventing the intrinsic blood coagulation cascade it inhibits agglutination of platelets.[151] It is known to bind to negatively charged compounds, in particular phospholipids.[152] This could explain an increased interaction of the APOH-coated nanoparticles with the cell

membrane, but it still needs to be investigated whether the mechanism is an unspecific interaction between the proteins and the cell membrane or if it is receptor mediated.

In contrast, coating NPs with apolipoproteins A4 and C3 reduced uptake into hMSCs to a minimum level. These results indicate that NP functionalisation with APOA4 or APOC3 could serve as a masking for unspecific cellular uptake and could therefore act as an endogenous alternative to PEG. This function should be further evaluated in studies examining cells of the MPS. Furthermore, organ distribution of nanoparticles *in vivo* needs to be investigated to prove this hypothesis. The following illustration outlines some important results of the study.

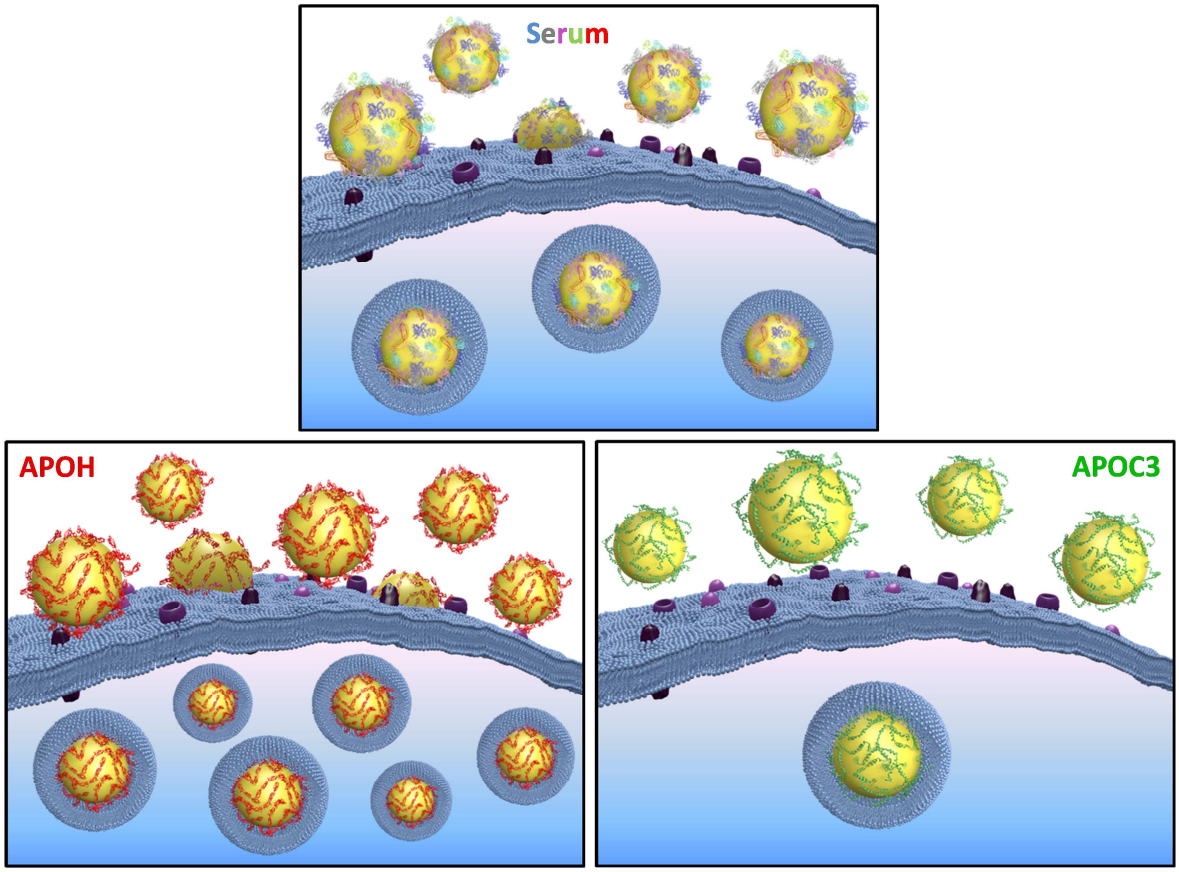

Figure 4-11: Apolipoproteins regulate cellular uptake.
While PS-NPs show an intermediate uptake into hMSCs when incubated with full serum, coating with apolipoprotein H (red) enhances internalisation into the cells. On the other hand, nanocarriers coated with apolipoprotein C3 (green) are barely endocytosed. The pathway of this interaction and whether it is mediated by cell membrane receptors (purple) is not clear yet. Reprinted (adapted) with permission from Ritz *et al*.[128]

4.2 INFLUENCE OF THE PROTEIN CORONA ON THE AGGREGATION BEHAVIOUR OF POLYSTYRENE NANOPARTICLES

In the second study, we analysed how the protein corona can influence nanoparticles´ aggregation behaviour and consequently *in vivo* distribution. The amount and composition of serum proteins adsorbed to different polystyrene nanoparticles was determined and patterns defined. With dynamic light scattering (DLS) the aggregation behaviour of the particles in human serum was investigated. First conclusions regarding the impact of individual proteins on the formation of aggregates can be drawn from this study. Parts of the results shown here are published as *"Aggregation Behavior of Polystyrene-Nanoparticles in Human Blood Serum and its Impact on the in vivo Distribution in Mice." Mohr et al*., Journal of Nanomedicine and Nanotechnology, 2014, 5(2), 193.[153]

4.2.1 NANOPARTICLES

Three differently functionalised polystyrene-based nanoparticles stabilised with the non-ionic surfactant Lutensol AT50 (PS-LUT, PS-LUT-COOH, PS-LUT-NH_2) and one NP stabilised with the anionic surfactant sodium dodecyl sulphate (PS-SDS) were synthesised by G. Baier and K. Klein. The fluorescent dye BODIPY-MA (λ_{ex} = 500 nm, λ_{em} = 540 nm) and the infrared dye IR 780 iodide were covalently coupled to all four NPs. SEM images of the four PS-NPs are shown in Figure 4-12. In aqueous solution the three Lutensol stabilised particles show similar sizes with diameters of 192 nm for PS-LUT, 162 nm for PS-LUT-COOH and 178 nm for PS-LUT-NH_2. Only PS-SDS is larger with a diameter of 340 nm.

4.2.2 PROTEIN ADSORPTION

First, the amount of serum proteins adsorbed to the four polystyrene nanoparticles was quantified by a colorimetric protein assay (Table 4-2). For the present and all following studies, nanoparticles were not dissolved, but proteins were desorbed from the nanoparticles using a urea-thiourea buffer. Two biological replicates of each nanoparticle prove an excellent reproducibility of the method. The total amount of proteins normalised to the particles´ surface area on PS-SDS is almost four times higher than for the other three NPs. The reduced protein adsorption on PS-LUT, PS-LUT-COOH and PS-LUT-NH_2 can be explained by the PEG chains present in Lutensol AT 450 used to stabilise these NPs.

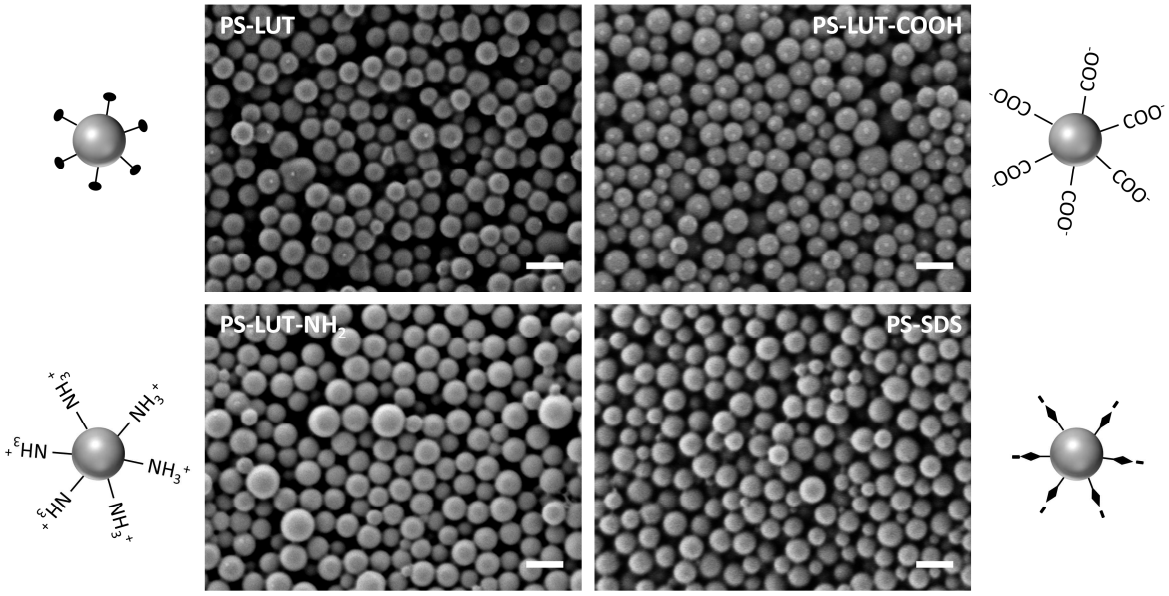

Figure 4-12: SEM images and schematic representation of investigated nanoparticles.
Scale bars: 200 nm. (SEM images were taken by G. Baier)

Next, the protein corona composition was analysed in two technical replicates for both biological replicates by LC-MS. The results are depicted in Figure 4-13. A complete list of all identified proteins and their relative abundances can be found in Table 7-3 in the appendix. As in the previous section, proteins are grouped according to their function into seven different groups for a better overview.

Table 4-2: Quantification of adsorbed serum proteins to the nanoparticles´ surface.
Protein adsorption was quantified with Pierce660nm Assay and is expressed as mg protein per NP surface area (m²).

Protein per NP [mg/m²]	
PS-SDS	4.04
	4.06
PS-LUT	0.99
	1.21
PS-LUT-COOH	1.35
	1.05
PS-LUT-NH_2	0.97
	1.08

Again, the concentration of lipoproteins is highly enriched on all four polystyrene particles compared to serum, followed by a less pronounced enrichment of complement factors.

The concentration of immunoglobulins and albumin - the prominent component of serum listed in the fraction of other proteins - is clearly reduced. Interestingly, significantly more immunoglobulins adsorbed to PS-SDS compared to the other three NPs.

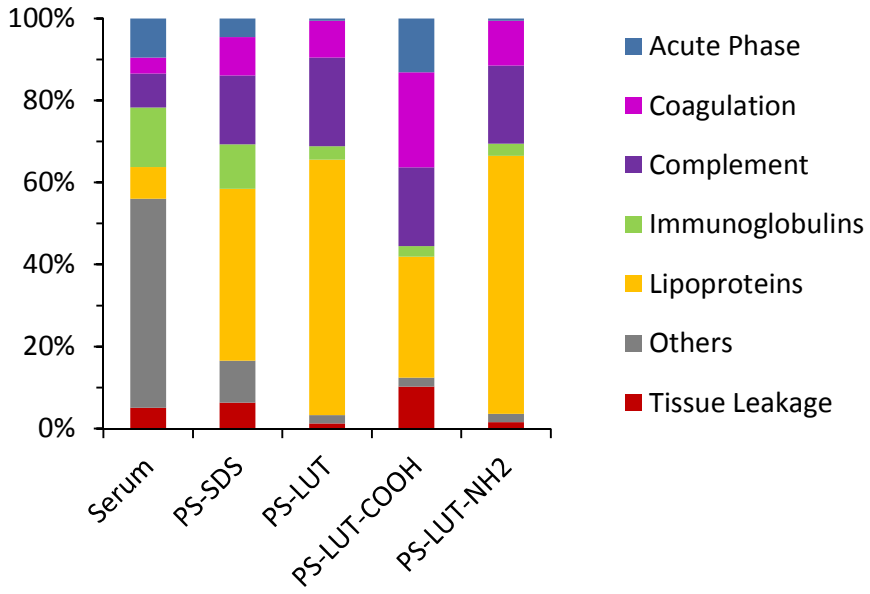

Figure 4-13: Analysis of the protein corona on PS-NPs in dependence of NP functionalisation measured by LC-MS.
Relative percentages of the adsorbed proteins were calculated from the averaged ppm values. Proteins are grouped according to their biological function. Reprinted (adapted) from Mohr *et al.*[153]

The protein corona profile is very similar for PS-LUT and PS-LUT-NH_2 showing the highest lipoprotein content, while acute phase proteins are almost not present in these protein coronas. On PS-LUT-COOH, the coagulation proteins are highly enriched, and also the tissue leakage and acute phase proteins are significantly increased. These differences in the protein corona composition are mainly due to single proteins highly enriched on PS-COOH. Therefore, the most abundant proteins identified on the four PS-NPs are stated in Figure 4-14. The table shows that especially the coagulation protein prothrombin (THRB), which accounts for 10.8% of the whole protein amount on PS-LUT-COOH, vitronectin (VTNC) with 9% and the acute phase protein inter-alpha-trypsin inhibitor heavy chain H4 (ITIH4) are responsible for the significant differences in the corona composition seen in Figure 4-13. With 11.7% ITIH4 is the most abundant protein on PS-LUT-COOH. The other three nanoparticles are mainly covered by apolipoproteins A1 and clusterin. While these proteins are still present in high numbers on PS-LUT-COOH, the NP has a significantly lower amount of APOA1 and clusterin bound to its surface.

	PS-SDS	PS-LUT	PS-LUT-COOH	PS-LUT-NH_2
Antithrombin III	3.08%	7.50%	3.61%	9.42%
Apolipoprotein A I	23.87%	23.00%	11.58%	23.98%
Apolipoprotein A IV	1.15%	1.90%	0.85%	2.55%
Apolipoprotein B 100	0.85%	2.49%	0.98%	2.01%
Apolipoprotein C III	1.10%	0.67%	0.12%	0.55%
Apolipoprotein E	0.81%	1.43%	2.03%	1.39%
Apolipoprotein H	0.90%	0.05%	5.59%	0.06%
C4b binding protein alpha chain	1.42%	0.14%	0.14%	0.12%
Clusterin	12.53%	31.57%	7.69%	31.29%
Coagulation factor V	0.46%	0.39%	1.62%	0.34%
Complement C3	6.30%	13.05%	11.41%	11.15%
Complement C4 A	0.98%	1.25%	0.75%	1.23%
Complement C4 B	2.83%	2.95%	1.98%	2.60%
Complement C5	0.44%	0.72%	1.30%	0.63%
Complement factor H	1.32%	0.30%	1.16%	0.27%
Gelsolin	1.47%	0.03%	0.35%	0.02%
Ig gamma 1 chain C region	5.14%	2.13%	1.29%	1.83%
Ig gamma 2 chain C region	1.27%	0.16%	0.19%	0.16%
Ig kappa chain C region	1.09%	0.05%	0.07%	0.05%
Inter alpha trypsin inhibitor heavy chain H4	3.08%	0.11%	11.72%	0.13%
Kininogen 1	1.38%	0.01%	3.74%	0.01%
Prothrombin	2.05%	0.74%	10.83%	0.82%
Serum albumin	5.97%	0.82%	0.84%	0.90%
Vitronectin	4.34%	0.86%	8.98%	1.10%

Figure 4-14: Most abundant proteins in the protein corona of PS-SDS, PS-LUT, PS-LUT-COOH and PS-LUT-NH_2.

Values were calculated from the molar masses of each protein identified by LC-MS. Shown are only those proteins which constitute for at least 1% of the protein corona on one of the nanocarrier.

Furthermore, Figure 4-14 allows the comparison with the protein corona determined in the previous study. In both studies Lutensol stabilised polystyrene nanoparticles with different surface functionalisations were analysed and many similarities are displayed. The apolipoprotein APOH, for example, which was enriched on the carboxylated and depleted on the amino-functionalised particles in the first study, shows the same pattern here. It constitutes for 5.6% on PS-LUT-COOH and only 0.1% on PS-LUT-NH_2 (first study: PS-COOH: 5.1%, PS-NH_2: 0.1%). The preference of several other proteins for the carboxylated surface were also confirmed, as for example ITIH4 with 11.7% on PS-LUT-COOH (first study: 4.2%)

and 0.1% on PS-LUT-NH_2 (0.2%) or prothrombin (THRB) with 10.8% on PS-LUT-COOH (5.6%) and 0.8% on PS-LUT-NH_2 (1.9%).

Additionally, an enrichment of APOA4 on PS-LUT-NH_2 with 2.6% (7.9%) and only 0.9% (1%) on PS-LUT-COOH was confirmed, too. On the other hand, some binding affinities as the strong adsorption of albumin to PS-NH_2 or of complement C3 to PS-COOH in the first study were not confirmed here. One has to take into account that the procedure of nanoparticle synthesis was not exactly the same resulting in slight changes regarding size or surface charge density. The NPs used for the first study all had a diameter slightly above 100 nm, whereas here they are significantly larger.

For an impression of the specific differences in the protein composition on the four NPs, the proteins which differ between the NPs regarding their enrichment and depletion compared to serum are plotted in Figure 4-15. Once again, in Figure 4-15a the similarity of protein adsorption to PS-LUT and PS-LUT-NH_2 is immediately apparent. For PS-SDS, an enrichment of several individual proteins belonging to the group of coagulation and complement factors is shown, while these proteins are depleted on the other three NPs. Most of these proteins are not included in Figure 4-14 because regarding the overall amount of protein they are not as abundant as other proteins. Nevertheless, relative to the very low concentrations in human serum, these proteins are highly enriched on the NPs.

For a better overview and to further emphasise the differences in the protein patterns, the enrichment score Q is also shown as a heat map in Figure 4-15b. The heat map allows an easier comparison of single protein adsorption between the different NPs and underlines the similarity of the protein corona of PS-LUT and PS LUT-NH_2 on one hand and PS-SDS and PS-LUT-COOH for some protein on the other hand. Furthermore, the specific enrichment of several coagulation proteins as vitamin K dependent protein, coagulation factor XII, plasma protease C1 inhibitor, heparin cofactor 2 and complement factor XIII B on the surface of PS-SDS is pointed out. Additionally, the complement C1 complex, the first component of the human complement system, consisting of subcomponents C1QA, C1Qb, C1QC, C1R and C1S and the C4 binding protein (C4BPA and C4BPB) are enriched only on the SDS stabilised PS-NP. These proteins are highlighted in green in Figure 4-15b.

a

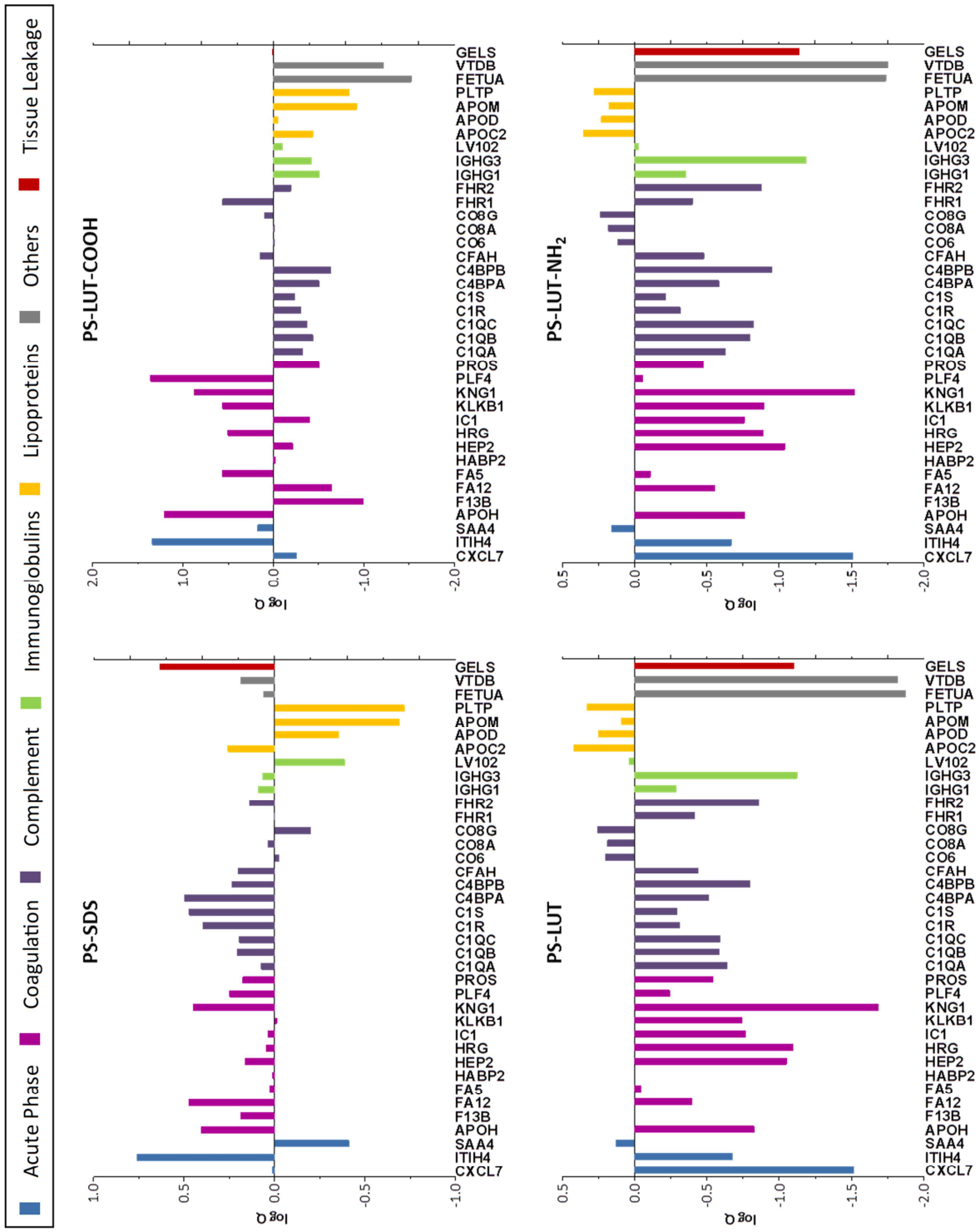

Figure 4-15: Enrichment (log Q > 1) or depletion (log Q < 1) of adsorbed proteins.

Logarithm of ratio Q (Q = mass fraction protein on particle/mass fraction protein in serum) illustrates specific enrichment (log Q > 1) or depletion (log Q < 1) of single proteins on the different NPs. Only proteins which differ between the four NPs regarding their enrichment and depletion are shown. (a) Plotted as bar chart with colour code indicating the respective protein family and (b) as heat map enabling a head-to-head comparison (green indicates enrichment and red stands for depletion). Reprinted (adapted) from Mohr *et al.*[153]

b

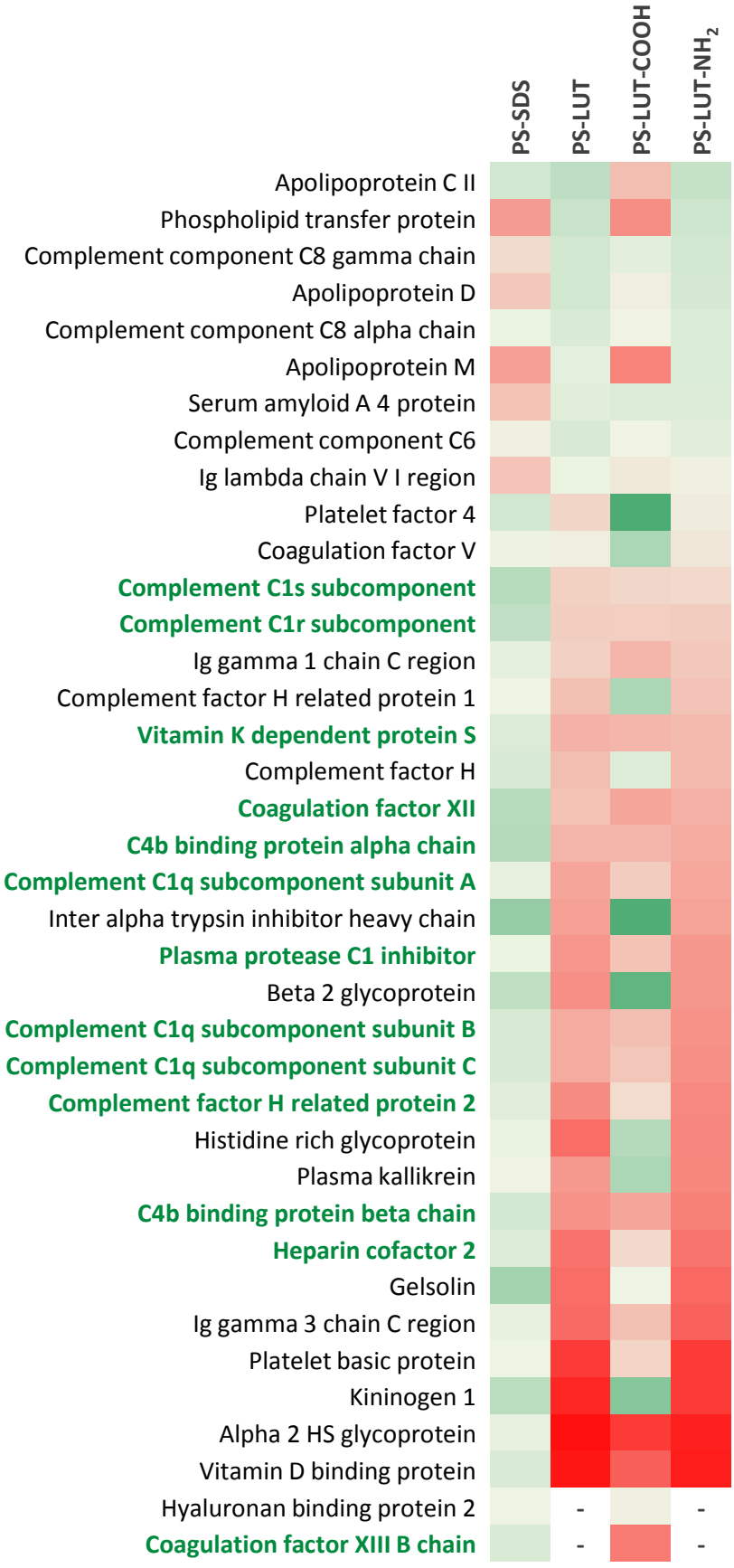
PS-SDS
PS-LUT
PS-LUT-COOH
PS-LUT-NH2
Apolipoprotein C II
Phospholipid transfer protein
Complement component C8 gamma chain
Apolipoprotein D
Complement component C8 alpha chain
Apolipoprotein M
Serum amyloid A 4 protein
Complement component C6
Ig lambda chain V I region
Platelet factor 4
Coagulation factor V
Complement C1s subcomponent
Complement C1r subcomponent
Ig gamma 1 chain C region
Complement factor H related protein 1
Vitamin K dependent protein S
Complement factor H
Coagulation factor XII
C4b binding protein alpha chain
Complement C1q subcomponent subunit A
Inter alpha trypsin inhibitor heavy chain
Plasma protease C1 inhibitor
Beta 2 glycoprotein
Complement C1q subcomponent subunit B
Complement C1q subcomponent subunit C
Complement factor H related protein 2
Histidine rich glycoprotein
Plasma kallikrein
C4b binding protein beta chain
Heparin cofactor 2
Gelsolin
Ig gamma 3 chain C region
Platelet basic protein
Kininogen 1
Alpha 2 HS glycoprotein
Vitamin D binding protein
Hyaluronan binding protein 2
Coagulation factor XIII B chain
-
-
-

4.2.3 AGGREGATION BEHAVIOUR AND IMPACT ON IN VIVO DISTRIBUTION

In order to trace the influence of the protein corona on the nanoparticles' behaviour in human serum, dynamic light scattering measurements were conducted. To this end, nanoparticles were dissolved in undiluted human serum and in serum diluted 10-fold. Aggregation sizes were determined as hydrodynamic radii (R_h), but for a better comparison with nanoparticle sizes they are specified as diameters in Table 4-3.

Table 4-3: Aggregation behaviour of investigated nanoparticles in undiluted and diluted serum.
Aggregate sizes are given as diameters. (DLS measurements were performed by K. Mohr)

Particle	Aggregate size in diluted serum	Aggregate size in serum
PS-SDS	4 µm	Macroscopic precipitation
PS-LUT	400 nm	400 nm
PS-LUT-COOH	No aggregates	500 nm
PS-LUT-NH_2	No aggregates	No aggregates

In diluted serum PS-SDS and PS-LUT clearly showed significant aggregate formation with aggregate sizes of 4 µm and 400 nm, respectively. For PS-SDS macroscopic aggregates were formed when added to undiluted serum. Negligible serum interaction was observed for PS-LUT-NH_2. Here, no aggregation of nanoparticles was detected even in undiluted human serum. A special situation is encountered for PS-LUT-COOH, which showed no aggregates in diluted serum, but detectable aggregation in undiluted serum.

Bio-distribution of nanocarriers is dependent on size, charge, and reactive groups on the surface of nanocarriers.[154] As contact with serum leads to protein corona and potential aggregate formation, we hypothesised that these effects rather than the original NP functionalisation affect *in vivo* distribution. To further study this impact, NPs were injected in the tail vein of mice (Figure 4-16).

All particles partly allocated to the liver region early after injection. In addition, the particles PS-LUT and PS-LUT-NH_2 were also early detected in the lung. Over time, all particles distributed to other body areas to some extent. However, the signals for PS-SDS and PS-LUT-COOH mainly remained in the liver region.

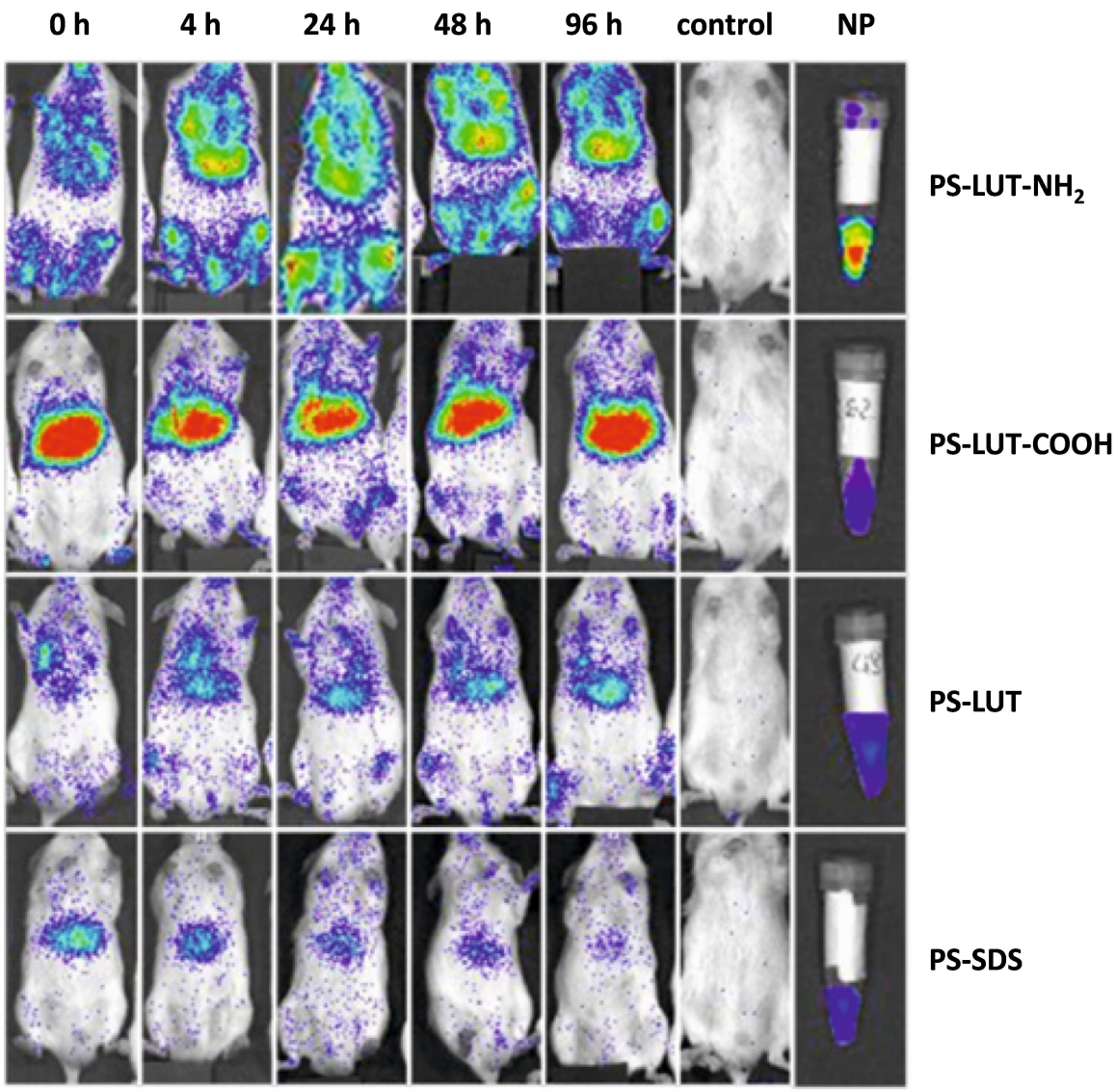

Figure 4-16: Bio-distribution of PS-NPs in NSG mice.[153]
37 µg/ml of each nanoparticle were applied intravenously to the tail vein of the mice. Animals were screened for fluorescence signals by measuring the infrared dye IR 780 iodide. Measurement of fluorescence signals (relative values in relation to liver-fluorescence) are shown for different time points. The control mice on the right side did not receive any nanoparticles. (*In vivo* experiments were conducted by M. Sommer) Reprinted from Mohr *et al*.[153]

4.2.4 DISCUSSION

The LC-MS analysis of the protein corona revealed a strong enrichment of lipoproteins on all four investigated polystyrene nanoparticles. The high percentage of lipoproteins is particularly prominent for the particles PS-LUT and PS-LUT-NH_2. Interestingly, these are the two particles with the strongest enrichment in the lung, in addition to the pronounced liver allocation of all NPs. The high amount of lipoproteins in the formed protein corona might lead to a stronger recognition of those particles by macrophages. Scavenger

receptors expressed on the surface of macrophages show a high affinity for lipoproteins.[155,156] As the largest population of macrophages are located in the liver (Kupffer cells) and the alveolar spaces of the lung (alveolar macrophages)[157] the accumulation of PS-LUT and PS-LUT-NH_2 in these organs could possibly be explained by a scavenger receptor mediated interaction triggered by lipoproteins in the protein corona.[158]

The most promising *in vivo* distribution is exhibited by PS-LUT-NH_2, which spreads most effectively to different body regions and is not cleared as fast as other NPs. DLS analysis shows that only PS-LUT-NH_2 particles do not form any aggregates in diluted as well as in undiluted human serum, which makes a longer and more efficient body distribution more likely.[159]

The SDS stabilised PS-NPs induced the strongest aggregation in human serum resulting in aggregates of a size range between 2 µm in diluted serum and up to macroscopic precipitation in undiluted human serum. The fact that PS-SDS also adsorbs the highest amount of proteins on its surface matches the image of particle aggregation being triggered by inter-particle protein bridging. As shown in Figure 4-15, several proteins belonging to the coagulation and complement system are enriched on PS-SDS while they are depleted on the other three NPs. These proteins are highlighted in green in Figure 4-15b and are potential candidates to participate in the cross-linking of PS-SDS resulting in the very strong aggregation of the NP in serum. In the human body, binding of the complement C1 complex to antigen-bound antibodies (IgM and IgG) initiates the classical pathway of the complement system. Interestingly, in addition to the enrichment of complement C1, PS-SDS is the NP with the highest immunoglobulin share in the protein corona (Figure 4-13). This implies an interaction of immunoglobulins with complement C1 and possibly other complement factors on PS-SDS resulting in the high protein adsorption and possibly NP aggregation.

Moreover, the strong opsonisation of PS-SDS with complement factors and immunoglobulins might lead to rapid clearance from the systemic circulation via different ways of complement activation and receptor-mediated phagocytosis by cells of the mononuclear phagocyte system (MPS).[15,74] In addition to scavenger receptors

macrophages express complement and Fc receptors, mediating receptor specific uptake through recognition of complement factors of the Fc region on antibodies. As Kupffer cells favour the uptake of particles with a diameter between 1-3 µm, the uptake of PS-SDS particles, or rather its higher molecular aggregates in the liver, additionally explain the findings.[160,161] The strong *in vivo* uptake of PS-SDS by the liver and clearance from the bloodstream might result from a fast and size dependent recognition by liver macrophages which have an even higher phagocytic activity compared to lung macrophages. [157]

In addition, the high amount of complement C3 on all NPs could favour an uptake into Kupffer cells. A C3 binding receptor, the complement receptor of the immunoglobulin superfamily (CRig) has been identified on Kupffer cells[162] and is probably involved in efficient phagocytosis of complement C3-opsonised particles.

Particles of sample PS-LUT-COOH induced no aggregate formation in diluted human serum while the particles aggregated to structures with a hydrodynamic radius of 250 nm in undiluted serum. This particle nearly exclusively allocated to the liver *in vivo* and almost completely spared other organs. The investigation of the protein corona revealed a higher enrichment of coagulation factors and acute phase proteins compared to the other particles provoked by a high adsorption of prothrombin and ITIH4. In comparison to the non-functional particles PS-LUT, the protein corona of the carboxy-functionalised particles PS-LUT-COOH illustrated a less pronounced adsorption of lipoproteins which makes the interaction with the scavenger receptors of macrophages less preferable.

The acute phase protein Inter-alpha-trypsin inhibitor heavy chain H4 (ITIH4) was identified as the most abundant protein on PS-LUT-COOH (Figure 4-14). ITIH4 is a plasma glycoprotein that is expressed mainly in the liver. It contains a putative binding site for hyaluronic acid. Circulating hyaluronic acid is rapidly removed from blood circulation by liver endothelial cells and it has been proposed that ITIH4 might be involved in the hepatic clearance of hyaluronic acid.[163] Thus, it is possible, that PS-LUT-COOH is not mainly phagocytised by liver macrophages but interacts with endothelial cells in the liver via hyaluronic acid binding.

Additionally, it is noteworthy that the three proteins which are mainly responsible for the strong difference in the protein corona composition on PS-LUT-COOH, namely ITIH4, prothrombin and vitronectin were all found to have a positive correlation with uptake into hMSCs in the first study. While having a comparable low amount of clusterin and apolipoprotein A1 bound to the surface, PS-COOH-LUT it is the only particle in this study with a remarkable number of APOH molecules in the protein corona (5.6% of total protein amount). As shown in the first study, APOH was able to increase uptake into hMSCs and might also promote internalisation into other non-phagocytic cells as liver endothelial cells.

4.3 THE STEALTH EFFECT OF POLYPHOSPHOESTERS

PEGylation is todays' gold standard for drug delivery vehicles to reduce unspecific cell uptake and establish a "stealth effect". However, disadvantages of PEG are becoming more and more evident: PEG is not biodegradable, has no additional chemical functionality, and recent studies have also reported medical problems with PEG as hypersensitivity reactions or antibody formation. A degradable and chemical versatile stealth polymer is necessary for modern drug delivery as a PEG alternative. Therefore, the stealth behaviour of poly(ethylene ethyl phosphate) (PEEP)-modified model nanocarriers was investigated in terms of protein adsorption, cellular uptake, and protein corona composition and compared to PEGylated nanocarriers. The results presented in this chapter were submitted in an article entitled "*A new definition of the stealth effect: The necessity of protein adsorption for the stealth effect of nanocarriers".*

4.3.1 NANOPARTICLES

Model monodisperse, Bodipy-labelled, amino-functionalised polystyrene nanoparticles with a diameter of 106 nm were prepared by miniemulsion polymerisation. The NPs were then further modified with *N*-hydroxysuccinimide-functionalised PEG (44 and 110 repeat units) and the water-soluble poly(phosphoester) derivative poly(ethyl ethylene phosphate) (PEEP, 49 and 92 repeat units). Figure 4-17 provides schematic representations and SEM images of the different nanoparticles. All nanoparticles used in this study were synthesised by G. Becker as described in her diploma thesis.[164]

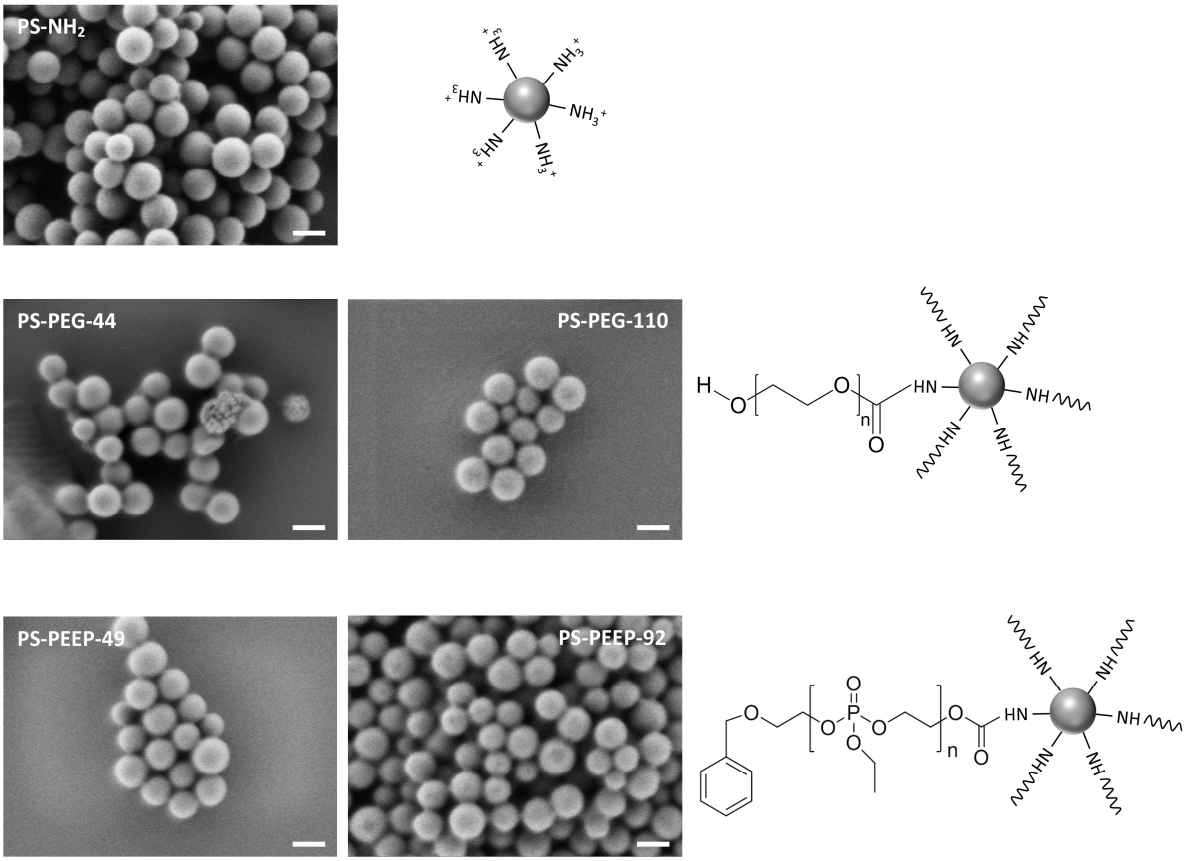

Figure 4-17: SEM images and schematic representation of nanoparticles.
Scale bars: 100 nm. (SEM images were taken by G. Becker)

4.3.2 PEEP REDUCES PROTEIN ADSORPTION TO THE SAME EXTENT AS PEG

In order to investigate the stealth effect of the polymer-modified nanocarriers, the amount of proteins adsorbed after plasma incubation was analysed (Figure 4-18a). The nanocarriers were incubated with human blood plasma for 1 h and separated from unbound proteins by centrifugation and several washing steps. The adsorbed proteins were removed from the surface by treatment with urea and quantified with a colorimetric protein assay. The adsorption of plasma proteins was significantly reduced by the surface functionalisation with PEG and PEEP. A decrease of 79% (PS-PEG-44), 66% (PS-PEG-110), 73% (PS-PEEP-49), and 70% (PS-PEEP-92) was observed compared to the adsorption of proteins onto PS-NH_2 nanocarriers. The reduction of protein adsorption to a similar value as PEG is the first indication for a stealth effect provoked by the polyphosphoesters (PPE).

The adsorbed protein patterns were further visualised via SDS-PAGE (Figure 4-18b). At first glance, a similar protein pattern can be observed for all four “stealth” nanocarriers with a strong enrichment of a protein at the 38 kDa marker band, but several differences

between PEGylated and PPEylated surfaces are also detected. A band slightly below the 28 kDa marker is only seen for PEG-NPs. The molecular weight differences of PEG and PEEP seem not to play a crucial role. The amino-functionalised control nanocarrier is mainly covered by albumin, the most abundant protein in human blood plasma (band at the 62 kDa). Again, the overall stronger protein adsorption to PS-NH_2 is clearly illustrated.

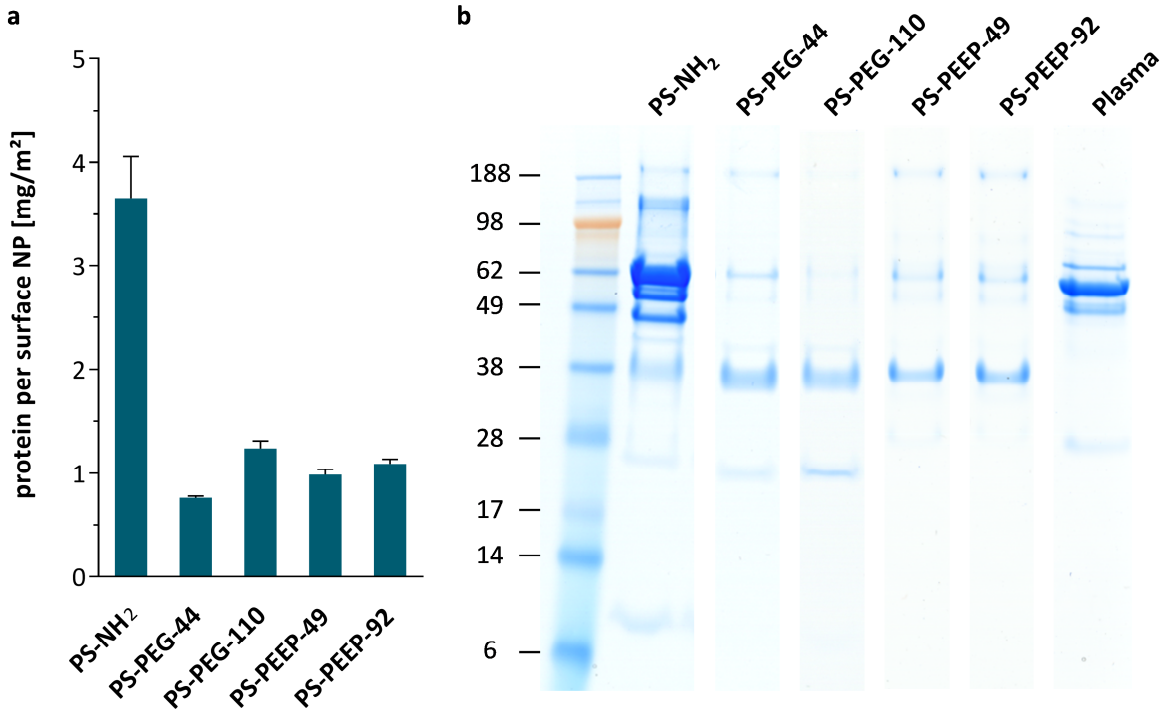

Figure 4-18: Protein adsorption of human plasma proteins to the nanocarriers' surface.
(a) Quantification of adsorbed proteins with Pierce660nm Assay in mg protein per NP surface area (m²). Values are expressed as mean ± SD of triplicates. (b) SDS-PAGE was used to visualise the protein corona composition. The analysis was performed in triplicates - for clarity only one replicate is shown. For comparison human plasma was loaded (right lane).

4.3.3 PEEP INHIBITS UPTAKE INTO MACROPHAGES

The advantage of stealth nanocarriers is their ability to remain in blood circulation for extended periods of time through evading clearance by the immune system. Macrophages are one of the most important components of the immune defence system and play a major role in clearance of foreign molecules in the blood. Only by escaping these phagocytic cells nanocarriers can reach their final destination within the body and fulfil their actual task. Therefore, the internalisation of the described nanocarriers into a murine macrophage-like cell line, namely RAW264.7, was studied.

For this purpose, the nanoparticle dispersions were first incubated in human heparin plasma as described above and separated from residual proteins by centrifugation. The nanocarrier-protein pellet was then resuspended in protein-free medium before the dispersions were added to the macrophages. Flow cytometry analysis revealed that the uptake of the "naked" nanocarrier (PS-NH_2) is inhibited by the attachment of PEEP to the same degree as by PEG, when the nanocarriers are previously incubated with human plasma (Figure 4-19a). Most intriguingly, a high uptake of all nanocarriers in protein-free medium was observed. As these nanocarriers carry no adsorbed blood proteins, this strongly indicates that it is not the reduced amount of proteins alone, which is responsible for the inhibition of cellular internalisation by the stealth polymers. It rather suggests a secondary effect provoked by specific proteins adsorbed to the PEG- and PEEP-functionalised nanocarriers.

Also laser scanning microscopy (Figure 4-19b) shows this effect clearly: strong internalisation of the unmodified (PS-NH_2) and both PEEP-modified nanocarriers into RAW264.7 cells was observed even after only 1 h when the cells were cultured in medium without plasma proteins. In contrast, macrophages cultured with plasma did not internalise PEGylated or PPEylated nanocarriers, while the unmodified nanoparticles were taken up.

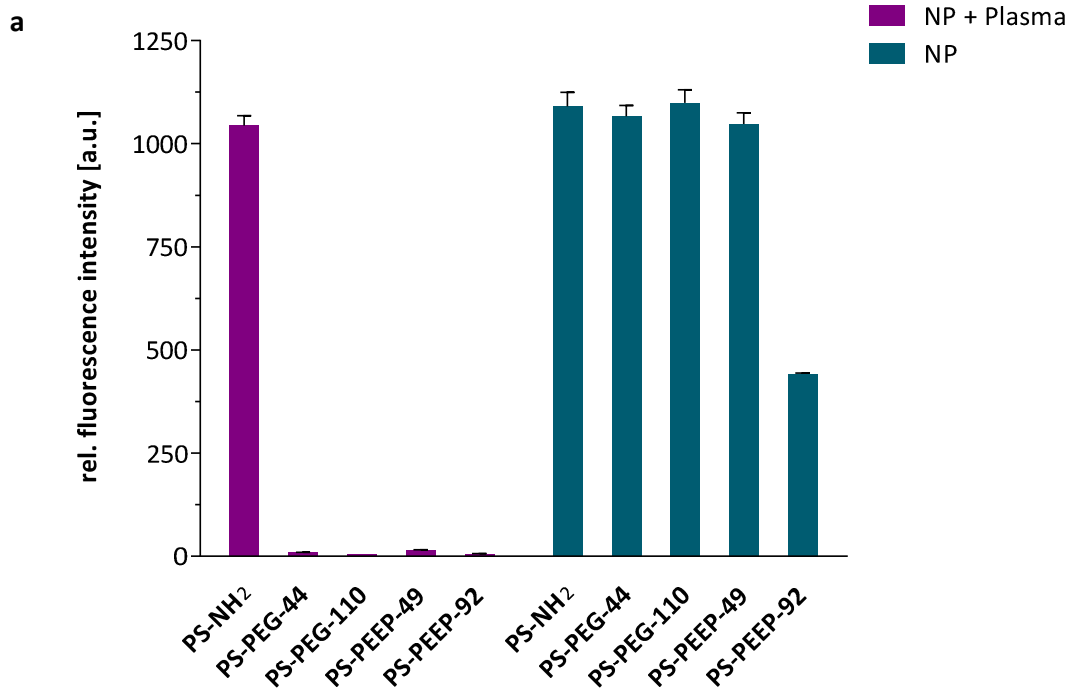

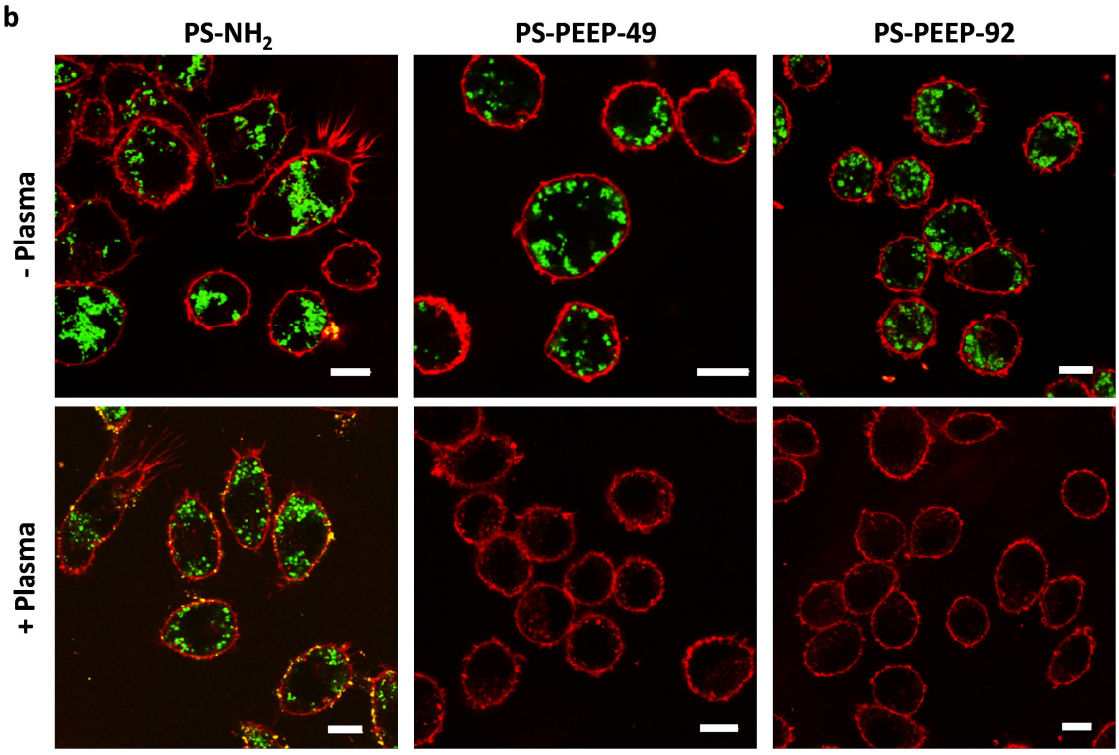

Figure 4-19: Uptake of PEEP and PEG nanoparticles into macrophages.
(a) Flow cytometry analysis of RAW264.7 cells incubated with different nanocarriers for 2h. The nanocarriers were incubated in human plasma or in water for 1 h at 37 °C and separated from residual proteins by centrifugation before they were added to the cells. Values are expressed as mean ± SD of triplicates. (b) CLSM images of RAW264.7 cells incubated with PS-NH_2, PS-PEEP49 and PS-PEEP92 for 1 h in human plasma or DMEM. Scale bars: 10 µm.

4.3.4 EFFECT CAN ALSO BE OBSERVED FOR UPTAKE INTO OTHER CELL LINES

Similar results as for the macrophages were also obtained for the cervical cancer cell line HeLa cultured in medium with or without serum (Figure 4-20a + c). A high uptake when no proteins are present, and no uptake of the PEG and PPEylated nanoparticles when the cells are incubated with 10% FBS was observed by flow cytometry analysis and live cell imaging. Furthermore, human immature dendritic cells, also professional phagocytes in the human body, did not show any significant internalisation of the four stealth nanoparticles (Figure 4-20b).

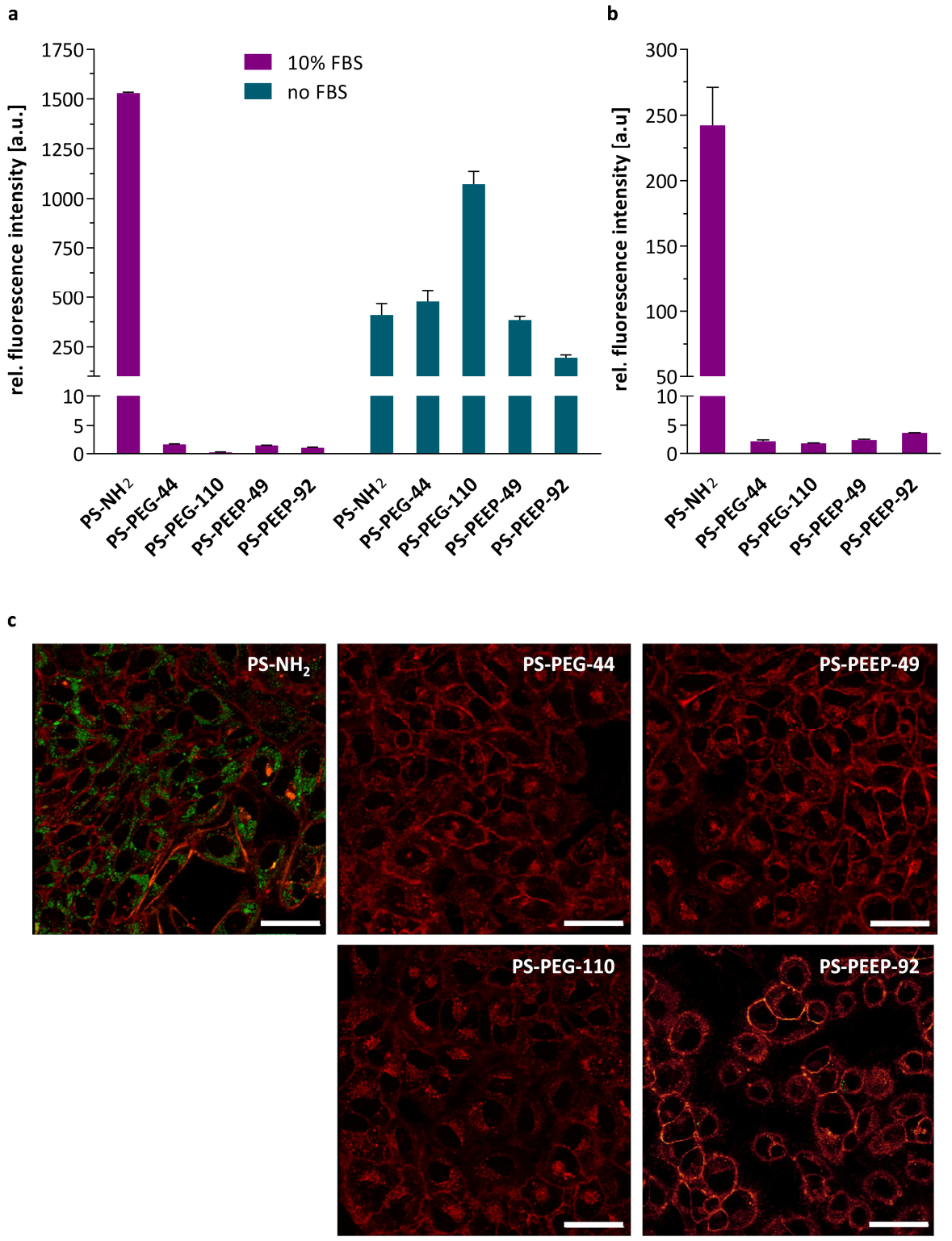

Figure 4-20: Cellular uptake of PEEP and PEG nanoparticles.

(a) Flow cytometry analysis of HeLa cells incubated with the nanocarriers for 4 h in serum-containing and serum-free medium. Values are expressed as mean ± SD of triplicates. In serum-containing medium the uptake of the nanocarriers is inhibited by PEEP to the same extent as by PEG. (b) Flow cytometry analysis of immature dendritic cells incubated with nanocarriers for 24 h in serum-containing medium. Values are expressed as mean ± SD of duplicates. (c) CLSM images of HeLa cells incubated with nanocarriers for 24 h in serum-containing medium. Scale bars: 25 µm.

4.3.5 ANALYSIS OF PROTEIN CORONA COMPOSITION REVEALS A HIGH ABUNDANCE OF CLUSTERIN

From these results fundamental information can be conducted: not only the reduction of the protein adsorption can explain the stealth effect of both PEG- and PEEP-functionalised nanocarriers, more importantly, the type of protein must be highly important. This renders the stealth effect a secondary effect not caused by the polymer itself, but rather by selective protein adsorption.

With LC-MS analysis, in total 171 proteins were identified in the corona of all five nanocarriers (Figure 4-21). Grouping the identified proteins according to their functions shows that while the control nanocarrier is mainly covered by albumin (as already visualised by SDS-PAGE) and proteins involved in coagulation, lipoproteins bind preferentially to the four polymer-modified nanocarriers. Interestingly, for the PEEP-modified nanocarriers lipoproteins constitute for up to 85% of the protein corona.

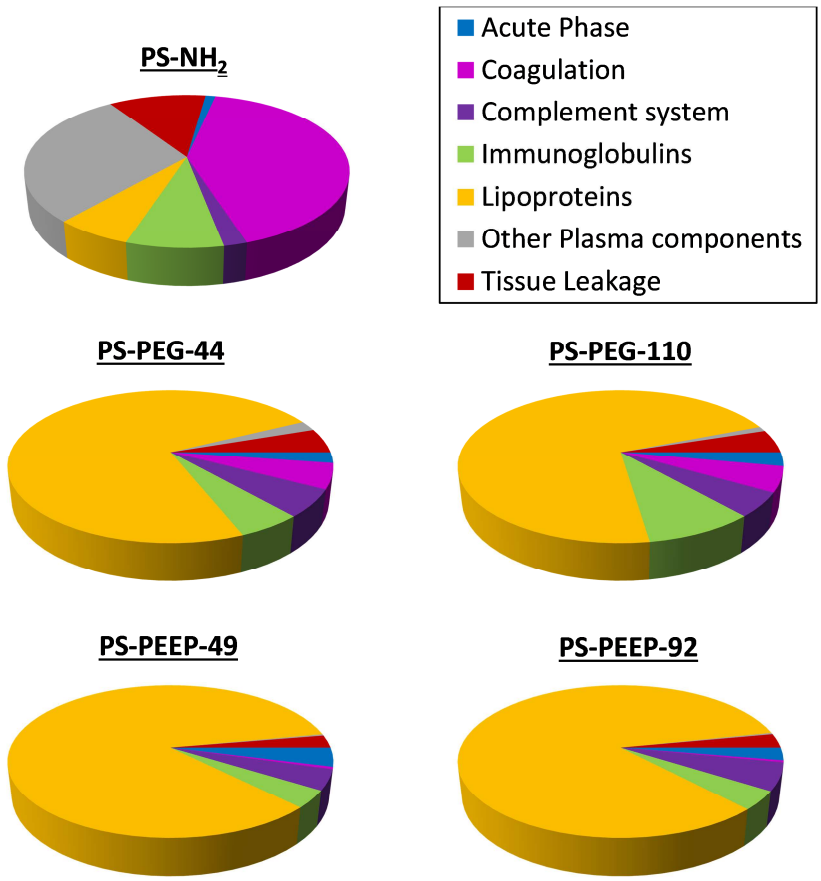

Figure 4-21: Classification of protein corona components identified by quantitative LC-MS.
Identified proteins are grouped according to their function in biological processes and the amount of proteins is summed up.

Figure 4-22 depicts the most abundant proteins identified in the so called “hard corona” of all five nanocarriers (the complete list is provided in Table 7-4 in the appendix). While albumin, fibrinogen and vitronectin are the most prominent proteins on the control nanocarrier (PS-NH_2, >80%), these proteins are strongly depleted on the PEGylated and PPEylated nanocarriers. Here, clusterin is the major protein in the hard corona. Clusterin (or apolipoprotein J) is a glycosylated 75 - 80 kDa disulphide-linked heterodimeric protein. The two dimers of the mature protein appear as an approx. 40 kDa smear on a reducing SDS-PAGE,[165] which can be assigned to the prominent band seen in Figure 4-18b. Additionally, a full-length uncleaved 60 kDa protein can be observed by SDS-PAGE.[165] It makes up for 77% of the protein corona on the PEEP-functionalised nanocarriers, with all other proteins below 2%. This significant enrichment of one single protein is remarkable. To our knowledge, such high abundance for clusterin has not been described before for other nanocarriers. On the PEGylated nanocarriers, besides clusterin, also apolipoprotein A1 is found (ca. 11%) and corresponds to the band at ca. 28 kDa on the SDS-PAGE. The significant enrichment of clusterin on PEG-functionalised nanocarriers and even more on the PEEP-functionalised nanocarriers suggests its important role to their resulting stealth properties.

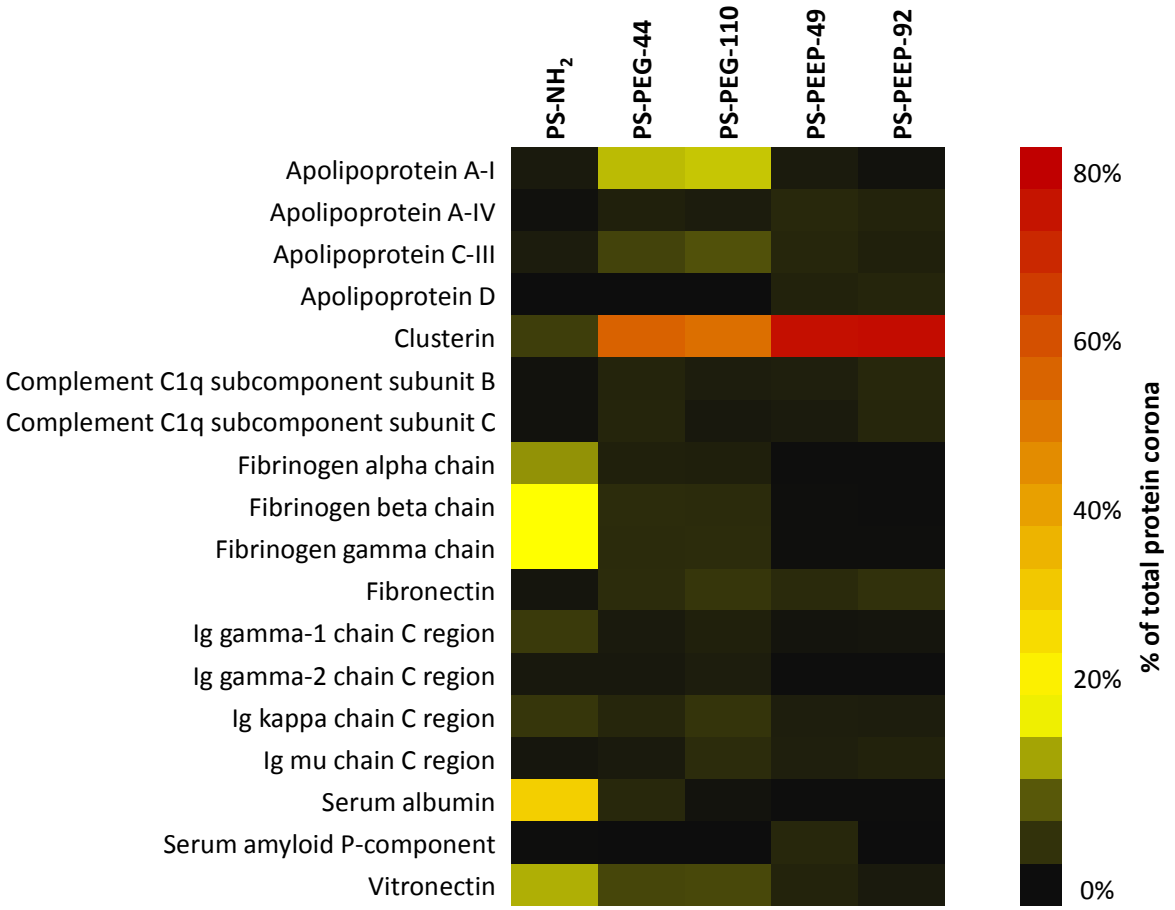

Figure 4-22: Heat map of the most abundant proteins in the protein corona of PS-NH_2, PS-PEG-44, PS-PEG-110, PS-PEEP-49 and PS-PEEP-92 determined by proteomic mass spectrometry.
Values were calculated from the molar masses of each protein identified by LC-MS. Shown are only those proteins which constitute for at least 1% of the protein corona on one of the nanocarrier.

4.3.6 CLUSTERIN INHIBITS UPTAKE OF STEALTH NPS INTO MACROPHAGES

To further analyse the enrichment of clusterin, one of the PPEylated nanocarriers (PS-PEEP-92) was incubated with native clusterin at its physiological concentration[166,167] and the uptake into RAW264.7 cells was studied. Figure 4-23 confirms that incubation with clusterin reduces the uptake of the nanocarriers into macrophages by 75.4% while in the absence of plasma or clusterin a high cellular uptake is detected. To prove, that this effect cannot be provoked by any plasma protein, human serum albumin (HSA) was used as a control. Interestingly, HSA incubation even increased the internalisation by 34%, although albumin is often described as a dysopsonin.[168] Even though pure clusterin does not have the same effect as whole plasma, which decreases the uptake by as much as 99.5%, it shows that clusterin functions as a strong dysopsonin for macrophages and supports the

idea of its predominant participation in the stealth effect of PEG- and PPEylated nanocarriers.

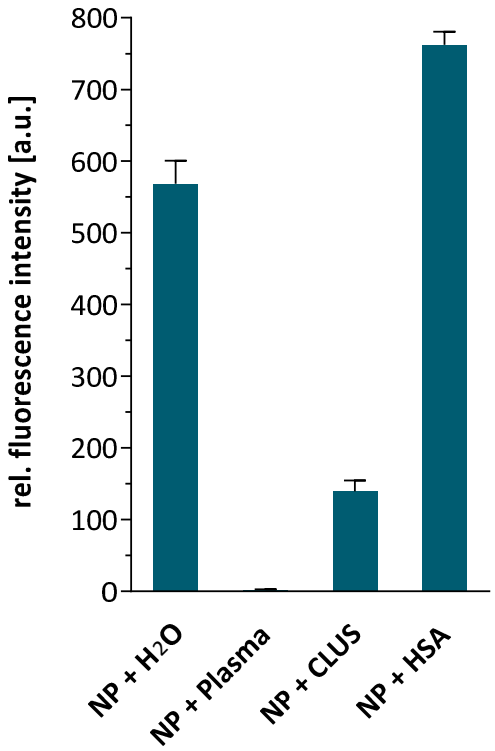

Figure 4-23: Influence of clusterin on macrophage uptake of PPEylated NPs.
PS-PEEP-92 was incubated in water, human plasma, clusterin (66.6 µg/ml) or human serum albumin (HSA, 66.6 µg/ml) for 1 h at 37 °C. The nanocarriers were then added to RAW264.7 cells maintained in DMEM. After 1 h the cells were analysed by flow cytometry. Values are expressed as mean ± SD of triplicates.

4.3.7 DISCUSSION

In summary, the results of this study lead to fundamental insights that should be considered for future nanocarrier design. PEGylated and PPEylated (poly(ethyl ethylene phosphate)-modified) model nanocarriers both show a reduction of protein adsorption after incubation with human plasma in comparison to non-modified nanocarriers. Furthermore, they give rise to a similar but also distinct protein corona composition. These differences in the composition of the protein corona for two different hydrophilic polymers is an additional handle for the future design of novel drug carriers or diagnostic devices, if the molecular structure of the stealth polymer can be tailored in a way to control not only the amount but also the type of plasma protein, for example by copolymerisation or postsynthetic modifications.

The study characterises degradable poly(phosphoester)s as potential PEG-alternatives. The uptake of PEGylated and PPEylated nanocarriers by different cell lines, including a macrophage-like cell line, was completely inhibited. Clusterin was identified as the major protein in the corona of both polymer-modified nanocarriers, with its highest enrichment on PPEylated surfaces. Further, pre-coating of the PPEylated nanocarrier with clusterin reduced the macrophage uptake, providing evidence for a dysopsonising function of clusterin concerning internalisation into macrophages.

In blood, the native glycoprotein clusterin is assembled with other apolipoproteins, like APOA1, into high-density-lipoproteins (HDL). Various physiological functions have been proposed for clusterin: complement attack prevention, promotion of cell aggregation, regulation of apoptosis and lipid transport, but all are mainly based on binding partners.[169] Despite the broad substrate specificity of clusterin no genuine physiological function has been established. Clusterin binds to partly unfolded proteins and thereby prevents stress-induced protein aggregation and is thus described as the first secreted mammalian chaperone.[170] However, no binding to polymeric surfaces of this protein was studies so far.

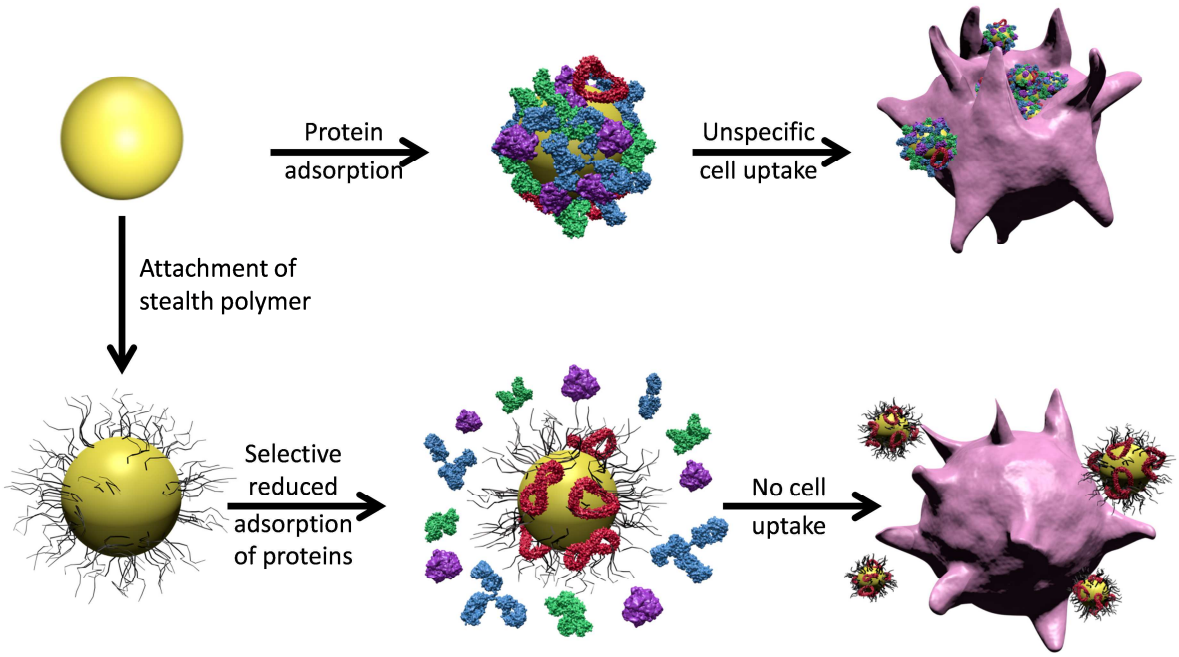

Figure 4-24: New perspective on stealth effect.

It was shown that stealth nanocarriers either functionalised with PEG or PEEP were internalised by macrophages when no proteins are present and therefore opsonisation

cannot have occurred. Although several studies have described the enhanced uptake of nanoparticles in serum-free conditions,[85] the controversy with the generally accepted image of the stealth effect being a polymer property has not been clarified to date. Opsonisation of nanocarriers with plasma proteins is still considered to be the major cause for clearance from the bloodstream. Therefore the image of the stealth effect needs to be revised. Walkey *et al.* have already suggested that PEG does not eliminate serum protein adsorption in total, but selectively suppresses adsorption of specific proteins resulting in a minimised macrophage uptake.[30] We want to go even further and postulate that not only the selective reduction of opsonising proteins as immunoglobulins and complement factors, but in fact the selective enrichment of single proteins as clusterin depending on the polymer structure triggers this (secondary) stealth effect. Figure 4-24 illustrates this alternative perspective of the stealth effect.

4.4 HYDROXYETHYL STARCH (HES) NANOCAPSULES

Due to their high monodispersity, narrow size distribution, and long stability, polystyrene nanoparticles are valuable model nanocarriers. Additionally, the miniemulsion process allows specific surface modifications by inserting functional groups, which makes it possible to covalently couple biomolecules to the nanoparticles.[171] These characteristics were important prerequisites for the comparative analysis of protein adsorption to different surface modifications in the previous chapters.

Nevertheless, for *in vivo* applications, a biodegradable nanocarrier is necessary. Hydroxyethyl starch (HES) has been used to synthesise degradable polymeric nanocarriers.[144,172-174] As a starch derivative HES can be enzymatically hydrolysed by amylases in the body. HES is one of the most frequently used volume expander for treatment of patients suffering from severe blood loss.

Furthermore, protein repellent characteristics have been postulated for HES and prevention of unspecific uptake of HES nanocapsules (HES-NCs) into HeLa cells has been previously demonstrated.[173,175] In a recent study, HES nanocapsules were also shown to have a prolonged circulation time in blood, necessary for a good therapeutic efficacy of encapsulated drugs.[174]

Nanocapsules have the advantage of a hollow core suitable to entrap and protect water soluble substances and they possess the possibility of a targeted release. In addition to the inhibition of unspecific cell uptake, the directed targeting to specific cells is important for a successful application of nanocarriers as drug delivery vehicles. In the present study nanocapsules synthesised from HES were equipped with different targeting molecules to promote uptake into dendritic cells and the protein adsorption properties were further investigated.

This study was published as "*Carbohydrate-Based Nanocarriers Exhibiting Specific Cell Targeting with Minimum Influence from the Protein Corona.*" Reprinted (adapted) with permission from Kang *et al.*[176] (©2015 Wiley-VCH Verlag GmbH & Co. KGaA, Weinheim).

4.4.1 NANOCAPSULES

HES nanocapsules were prepared via the inverse miniemulsion process in aqueous dispersions. The capsules were then PEGylated before the carbohydrates mannose and galactose, and an anti-DEC-205 antibody were coupled to the nanocapsule surface via metal-free click chemistry. Macrophages and dendritic cells express several C-type lectins which function in receptor-mediated endocytosis. The HES capsules were functionalised in order to target three of these C-type lectin receptors: the mannose receptor, the MGL (macrophage galactose/*N*-acetylgalactosamine-specific C-type lectin)[177] and DEC-205.[178] The miniemulsion process allows a precise adjustment of the capsule size which resulted in diameters of 150 to 160 nm for the HES nanocapsules discussed here. The HES nanocapsules used in this study were synthesised by B. Kang as described in detail in Kang *et al*.[176]

4.4.2 PROTEIN ADSORPTION TO FUNCTIONALISED HES NANOCAPSULES

The five HES nanocapsules were initially analysed regarding their protein repellent characteristics. In Figure 4-25 the quantification of hard corona proteins after plasma incubation and three washing steps is shown with the protein amount being normalised to the nanocarriers' surface area. It clearly depicts the reduced protein amount adsorbed to HES nanocapsules in comparison to a polystyrene nanoparticle used as a reference. An 88 to 96% lower protein binding was detected for the HES-NCs supporting the protein repulsive properties of the starch. A second significant outcome is the similarity between the five capsules regarding the protein adsorption strength. This is initial evidence that the functionalisation of the PEGylated HES nanocapsules with mannose, galactose or anti-DEC-205 antibodies does not promote protein adsorption.

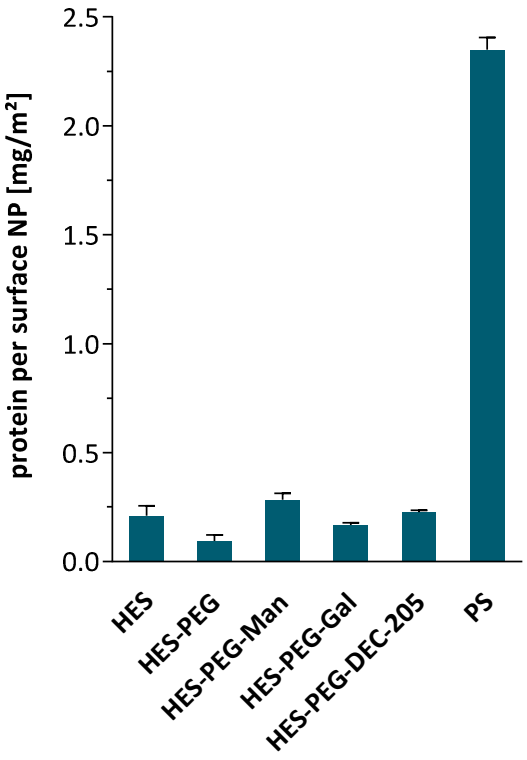

Figure 4-25: Protein adsorption of human plasma proteins to HES capsules in comparison to PS-NPs. Quantification of adsorbed proteins with Pierce660nm Assay in mg protein per NP surface area (m^2). Values are expressed as mean ± SD of triplicates. Reprinted (adapted) with permission from Kang *et al.*[176]

Subsequentely, the plasma proteins desorbed from the HES-NCs were subjecetd to SDS-PAGE analysis (Figure 4-26). For all nanocarriers the same sample volume was applied on the gel. Due to the very low protein amounts determined with the colorimetric protein assay only minimal amounts of 0.5 to 1.5 µg protein are applied on the gel for the HES samples. To ensure detection of even very low abundant proteins in the ng range, two distinct staining techniques were compared. The left polyacrylamide gel was stained with a commercial Silver Stain Kit, whereas the right gel was treated with a self-made colloidal Coomassie Brilliant Blue staining solution.

In general, silver staining is more sensitive (in the low nanogram range) than colloidal Coomassie Blue. Nevertheless, silver staining depends on the reaction of silver with sulfhydryl or carboxyl groups in proteins and is thus not quantitative across different proteins.[179] The comparison proves a better sensitivity of the silver staining especially for some proteins. But more importantly, all proteins detected with the silver staining are also visualised in the gel stained with colloidal Coomassie proving a sufficient sensitivity of the method.

At first sight, the strong decrease of protein binding to all HES capsules and a rather different pattern compared to the reference PS-NP is displayed by the SDS-PAGE. More interestingly, the five different HES-NCs exhibit a very similar protein adsorption pattern with only marginal influence of the capsule surface functionalisation. No differences are detected for the unfunctionalised HES capsule and the capsules functionalised with the monosaccharides mannose and galactose. Only the PEGylated NCs show a slight difference with an overall lower protein adsorption which was also previously determined with the quantification assay (Figure 4-25). The strong enrichment of a protein at about 38 kDa is not as pronounced for the HES-PEG capsules as for the other four NCs. A concentration of this band has been observed before for the stealth nanocarriers analysed in the previous study and is very likely to be caused by clusterin.

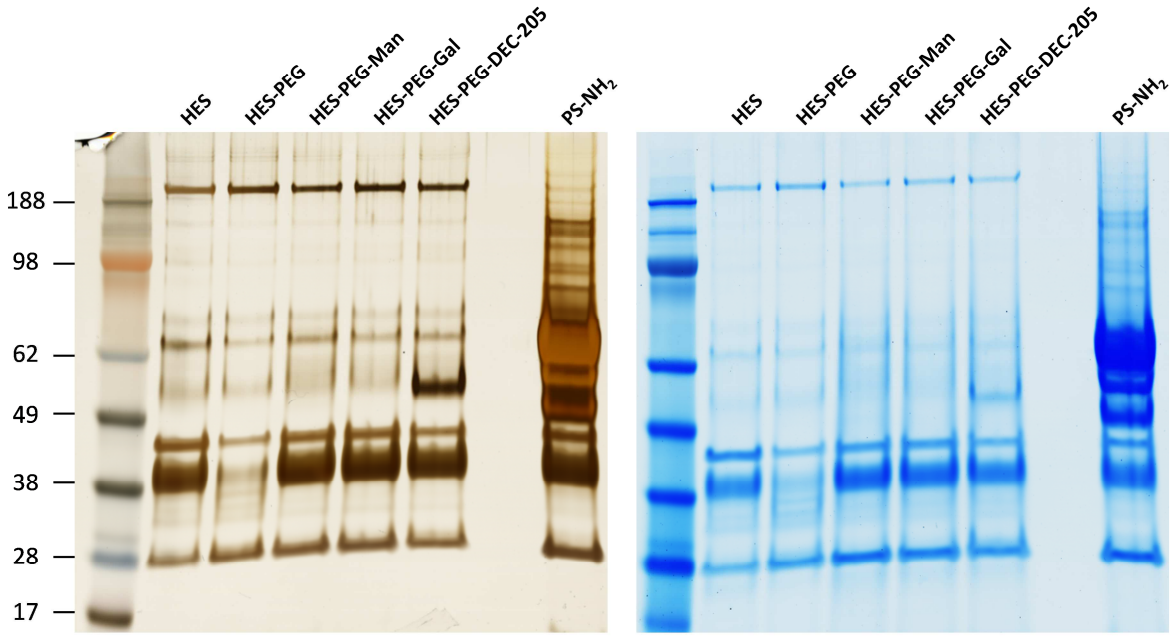

Figure 4-26: SDS-PAGE analysis of plasma proteins adsorbed HES capsules in comparison to PS-NPs.
The same samples were applied on two polyacrylamide gels which were then either stained using the Pierce Silver Stain Kit (left) or Coomassie Brilliant Blue (right). Reprinted (adapted) with permission from Kang *et al.*[176]

In the sample of the HES nanocapsules equipped with anti-DEC-205 an additional prominent band is displayed above 49 kDa which is especially pronounced after silver staining. This band could be provoked by the IgG heavy chain of the coupled antibody indicating either an insufficient covalent binding of anti-DEC-205 or a detachment of the antibody during the protein corona preparation both leading to free antibody molecules in

the sample. Importantly, in all cases the protein adsorption cannot be suppressed completely.

4.4.3 IDENTIFICATION OF PLASMA PROTEINS ADSORBED TO HES-NCS

The previous results are further supported by proteomic mass spectrometry data. A comparable composition of the protein corona was identified on the unmodified HES-NCs and HES-NCs grafted with mannose, galactose or anti-DEC-205. A minor difference is determined for the PEGylated HES capsules. In general, the enrichment of lipoproteins and depletion of albumin and immunoglobulins on all HES-NCs is prominent, as seen for most nanocarriers analysed so far. On HES-PEG nanocapsules the lipoprotein coating is less pronounced, whereas a slightly stronger association of complement factors is detected.

To further examine the specific differences and similarities of proteins detected on the HES-NCs, a heat map with the most abundant proteins is depicted in Figure 4-28. The strong resemblance of the protein pattern between HES, HES-PEG-Man, HES-PEG-Gal and HES-PEG-DEC-205 nanocapsules is immediately evident. A complete list of all identified proteins on the five HES-NCs is provides in Table 7-5 in the appendix.

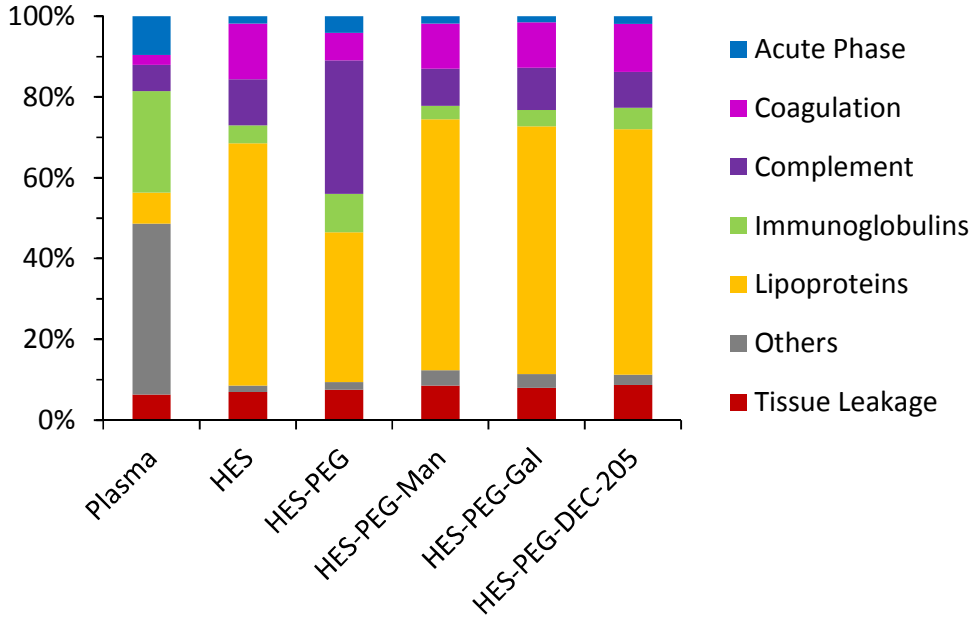

Figure 4-27: Analysis of the protein corona composition on HES-NCs in dependence of functionalisation measured by LC-MS.
Relative percentages of the adsorbed proteins were calculated from the averaged molar masses (fmol) of each protein. Proteins are classified according to their biological function.

As already indicated by the gel electrophoresis analysis, clusterin is the most abundant protein in the corona of all HES-NCs. With a 20% share this enrichment is less pronounced on the PEGylated nanocapsules as on the four other HES-NCs where clusterin accounts for 55 to 56%. Further frequent proteins identified on the HES capsules are APOA1 and APOA4 as well as the complement C1 complex, whereas the enrichment of these three proteins is more pronounced on the PEGylated nanocapsules. APOA1 accounts for 9% of the corona proteins on HES-PEG, whereas on the other four nanocapsules not more than 4% of the proteins were identified as APOA1. 4 to 6% of the protein corona on HES-NCs and the three functionalised nanocapsules is made up of subcomponents of the complement C1 complex, while on the PEGylated NCs they have a 25% share. The higher concentration of complement C1 is mainly accountable for the higher percentage of complement factors in the protein corona of HES-PEG capsules seen in Figure 4-27.

Another protein with a high affinity for the HES nanocapsules is fibulin-1. This protein has not been identified in a significant amount on any of the polystyrene nanoparticles investigated in the previous studies. Therefore, it seems to have a specific affinity for HES. Fibulin-1 is a glycoprotein normally described as an extracellular matrix component with a molecular weight of 90-100 kDa. It has various binding partners including the glycoproteins fibrinogen and fibronectin. The secreted and circulating form of fibulin-1 might have specific functions which are not yet determined.[180]

4.4.4 TARGETING OF DENDRITIC CELLS WITH HES NANOCAPSULES

In her dissertation P. Okwieka analysed the uptake of the HES nanocapsules into mature dendritic cells.[181] As described in Kang *et al.*[176] for mannose-functionalised HES-NCs a receptor-mediated uptake was determined before and after incubation in human plasma. Similar results were also observed for HES-NCs functionalised with galactose and anti-DEC-205, whereas the internalisation of the latter was most efficient.[181] As no difference between the three capsules in the protein corona composition was identified by the methods used herein, it is postulated that the antibody targeting of DEC-205 is more efficient than the ligand binding of galactose and mannose. Further studies analysing the binding efficiency are necessary to confirm this theory.

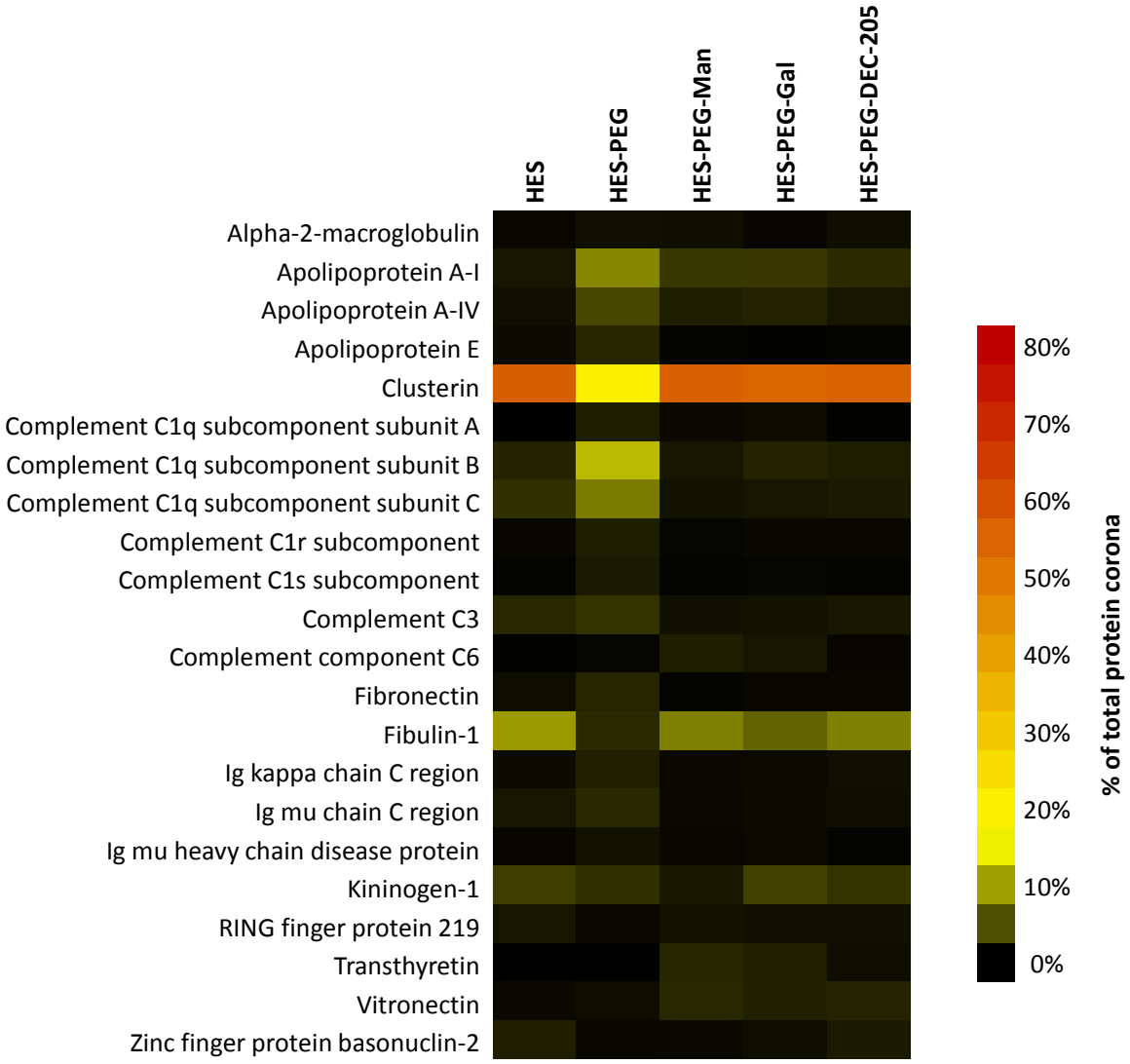

Figure 4-28: Heat map of the most abundant proteins in the protein corona of HES-NCs in dependence of their functionalisation.

Values were calculated from the molar masses (fmol) of each protein identified by proteomic mass spectrometry. Shown are only those proteins which constitute for at least 1% of the protein corona on one of the nanocarrier. Reprinted (adapted) with permission from Kang *et al.*[176]

4.4.5 DISCUSSION

In this study nanocapsules synthesised from hydroxyethyl starch and grafted with PEG were analysed regarding their protein adsorption. The PEGylated nanocarriers were further functionalised with the targeting moieties mannose, galactose and anti-DEC-205 antibodies in order to specifically reach dendritic cells via C-type lectins.

A significant difference between the hydrophobic PS nanoparticles used as a reference and all investigated HES-NCs was demonstrated with respect to protein adsorption. The binding affinity of plasma proteins is strongly decreased for all HES nanocapsules. This

matches the results published previously regarding the low protein affinity of HES[173,175] and renders HES suitable for the application as a PEG substitute.

The results indicate that the attachment of mannose, galactose or anti-DEC-205 to the PEGylated capsules does not cause an increased protein adsorption. Furthermore, the influence of the targeting molecules on the protein corona composition was proven to be minimal. A very similar protein pattern was identified in the hard corona on all HES-NCs with both SDS-PAGE and mass spectrometry.

Interestingly, LC-MS analysis identified clusterin as the most abundant protein on the HES nanocarriers. The high enrichment of clusterin on HES as well as PEEP and PEG - all polymer materials which are claimed to have stealth properties - supports the idea of its function as a dysopsonin for phagocytic cells. In comparison to PEEP and HES the PEGylated carriers show a less pronounced affinity for clusterin. In return, a stronger attachment of apolipoprotein A1 to the PEGylated surface was determined in both studies. Surprisingly, the same strong enrichment of clusterin determined for the unfunctionalised HES-NCs was also found for the capsules further functionalised with targeting molecules on top of PEG. For these four capsules the protein corona composition is almost identical. It seems as a high amount of accessible PEG chains is necessary for the slight alteration of protein adsorption towards more complement C1 and APOA1 and less clusterin on the HES capsules.

The minor influence of the targeting moieties on the protein corona composition indicates a negligible interaction of plasma proteins. This is a promising prerequisite for specific targeting in physiological conditions. Only if protein adsorption does not impair the selective binding of targeting molecules coupled to nanocarriers, targeting of specific cells is possible. Salvati *et al.* demonstrated the importance of this matter.[81] In their study, PEGylated silica nanoparticles functionalised with transferrin lost their targeting specificity for the transferrin receptor expressed on cancer cells (A549 cells) upon exposure to serum. In contrast, the protein corona formed around the HES nanocapsules did not impair recognition by corresponding receptors. Cellular uptake of the NCs by dendritic cells proved that the targeting moieties are active and accessible to the biological receptors after incubation with human plasma.[181]

4.5 INFLUENCE OF PROTEIN SOURCE ON PROTEIN CORONA FORMATION AND CELLULAR UPTAKE

In chapter 4.3 the significant impact of the presence or absence of proteins on the nanoparticles´ cell interaction was already demonstrated. In this section, the influence of the protein source on cell internalisation is further analysed. The concentration of serum necessary to impair cell uptake was determined. Furthermore, the impact of distinct protein sources as serum and plasma containing different anticoagulants was investigated. This is an often overlooked factor in studies examining the protein corona of nanoparticles and its importance is emphasised in this chapter. The results presented in this section will be published as “Protein source and choice of anticoagulant decisively affect nanoparticle protein corona and cellular uptake” in Nanoscale.

4.5.1 INFUENCE OF SERUM CONCENTRATION ON CELLULAR UPTAKE

For the stealth nanoparticles examined in the third section a strong reduction of cell internalisation was detected when proteins were present in cell culture medium. Thus, it was analysed if the absence of proteins has a similar impact on other polystyrene nanoparticles. The uptake of carboxylated and sulphonated PS-NPs into hMSCs cultured in medium with or without 10% human serum (HS) was determined. The two NPs were already introduced in chapter 4.1. Figure 4-29 shows that the uptake of PS-SO_3 NPs into hMSCs cultured in medium containing 10% serum is lower than the uptake of PS-COOH, which supports the result of the first study. On the other hand, in serum-free conditions PS-SO_3 is internalised at a much higher rate than PS-COOH. This correlates with the proteins previously identified in the protein corona of these nanocarriers. Proteins decreasing the uptake as apolipoprotein A4 and C3 adsorbed more to PS-SO_3, while a higher amount of APOH, a protein increasing the uptake into hMSCs, is present in the protein corona of PS-COOH.

Overall, the experiment indicates, that for both particles the cell interaction is inhibited when proteins are present. To investigate which concentration of serum is necessary to decrease the uptake, a dilution series was carried out for PS-SO_3 (Figure 4-30). The cells were cultured in serum-free medium for 2 h before the medium was changed to the indicated human serum concentrations and the particles were added.

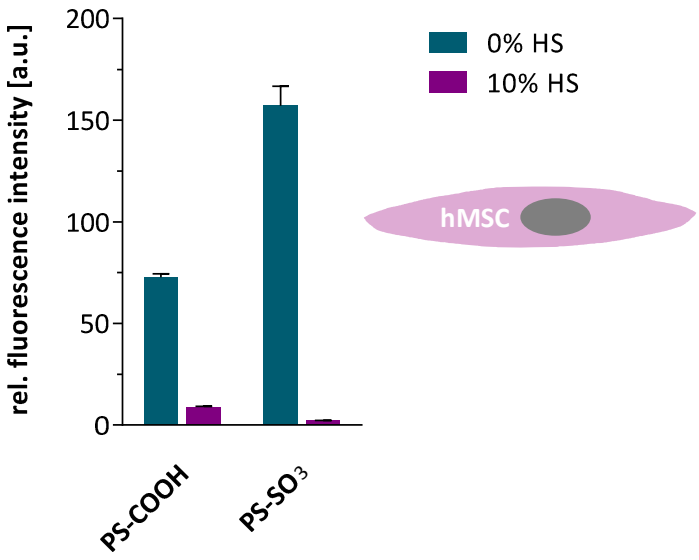

Figure 4-29: Influence of serum on NP uptake into hMSCs.
Uptake of PS-COOH and PS-SO_3 nanoparticles into hMSCs cultured in serum-free medium or medium containing 10% human serum was analysed by flow cytometry after 6 h incubation. Values are expressed as mean values (n=2), error bars (± SD).

The serum dilution series reveals, that uptake of PS-SO_3 is already reduced by 26% with only 0.5% serum present in cell culture medium, and 1% serum decreases the uptake by remarkable 73%. Cells cultured in medium containing 2.5% serum or more did not internalise NPs in a significant amount. Figure 4-30b shows matching cLSM images which confirm the flow cytometry results.

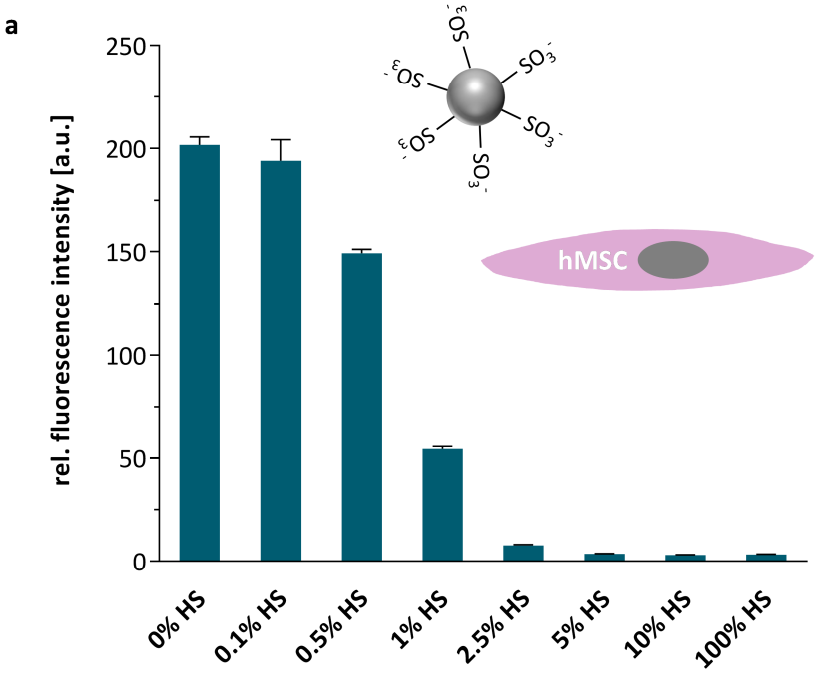

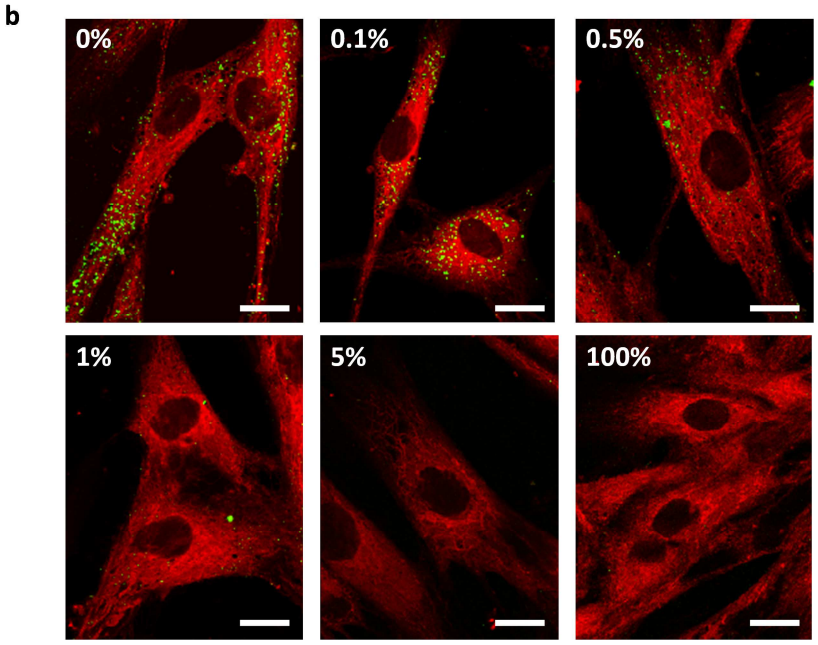

Figure 4-30: Cellular uptake of PS-SO_3 nanoparticles into hMSCs at different serum concentrations.
(a) Flow cytometry analysis of hMSCs cultured in medium containing 0 to 100% human serum after 6 h nanocarrier incubation. Values are expressed as mean values (n=2), error bars (± SD). (b) CLSM images of hMSCs cultured under same conditions. Scale bars: 50 µm.

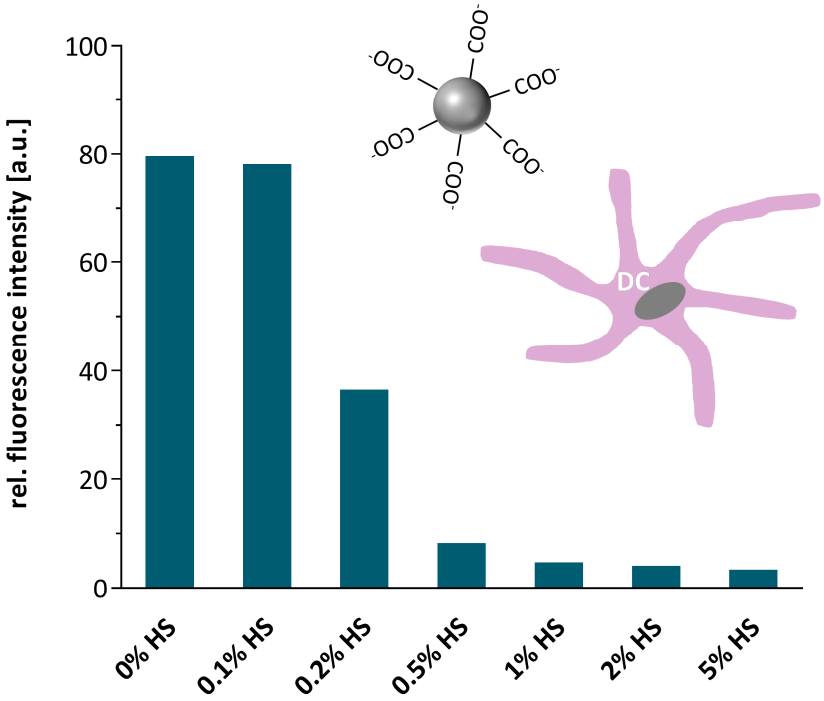

Figure 4-31: Influence of different serum concentrations on uptake of PS-COOH into dendritic cells.
Flow cytometry analysis of DCs cultured in medium containing 0 to 5% human serum after 6 h nanocarrier incubation.

A similar experiment was also conducted for dendritic cells incubated with PS-COOH (Figure 4-31). Here, the impact is even more significant, as 0.2% human serum in the cell culture medium does already decrease the uptake of PS-COOH into DCs by 54%. 0.5% serum is enough to almost completely prevent the uptake.

4.5.2 INFLUENCE OF PROTEIN SOURCE AND CELL TYPE ON NP UPTAKE

Several different types of protein sources are available and many studies analysing the protein corona of nanocarriers, do not further specify the type used or state reasons for their choice. Serum and plasma is often used in an interchangeable manner. The origin of the protein source, i.e. the species from which blood was drawn or the type of anticoagulant used for plasma generation is often neglected. In this section the impact of these different protein sources on NP uptake and protein corona formation was examined.

Initially, the uptake of an amino-functionalised polystyrene nanoparticle into HeLa cells was analysed, comparing interaction of nanoparticles and cells cultured in different concentrations of human serum and heparin plasma (Figure 4-32). For human serum the results are quite similar to the previous study analysing hMSCs and PS-SO_3 NPs in human serum. Cells cultured in medium containing more than 1% serum barely internalise any NPs. For human heparin plasma the effect is even stronger. Only 0.5% plasma is enough to reduce the uptake by 98.8%.

In chapter 4.3 the uptake of the same polystyrene nanoparticle into HeLa cells incubated with 10% FBS (Figure 4-20) on one hand and into macrophages when the NP was incubated with human heparin plasma (Figure 4-19) was found to be rather strong. This significant difference in uptake of the same NP into different cell types cultured in different protein sources is further explored in Figure 4-33. HeLa cells and macrophages were cultured in serum-free medium before the cell medium was exchanged for 100% foetal bovine serum (FBS), the most common protein source in cell culture, human serum (HS), human heparin plasma (HHP) or human citrate plasma (HCP). Then PS-NH_2 particles were added to the cells and uptake was analysed by flow cytometry.

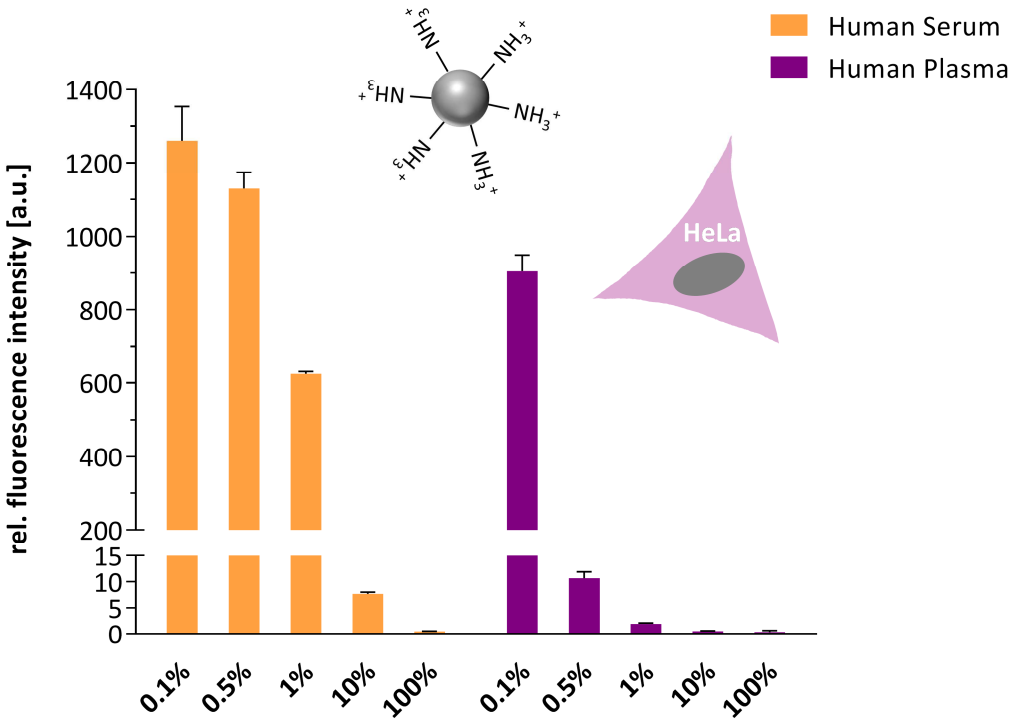

Figure 4-32: Different impact of human serum and plasma on uptake of PS-NH_2 into HeLa cells.
Cellular uptake of PS-NH_2 nanoparticles into HeLa cells cultured in medium containing 0.1 to 100% of either human serum (orange) or human heparin plasma (purple) was analysed by flow cytometry after 2 h incubation. Values are expressed as mean ± SD of triplicates.

In Figure 4-33a uptake into HeLa cells is depicted, showing a significant deviation between the protein sources. A strong uptake of PS-NH_2 into HeLa cells can only be observed when cells are maintained in FBS as described before in Figure 4-20. Human serum, heparin plasma and citrate plasma all strongly reduce the uptake. While for citrate plasma there still is a minimal uptake, heparin plasma and serum completely prevent any cellular uptake. In contrast the uptake into RAW264.7 macrophages (Figure 4-33b) shows a different pattern. Here only human serum and citrate plasma inhibit the uptake, while a quite strong uptake is observed in human heparin plasma, validating the results seen in Figure 4-19.

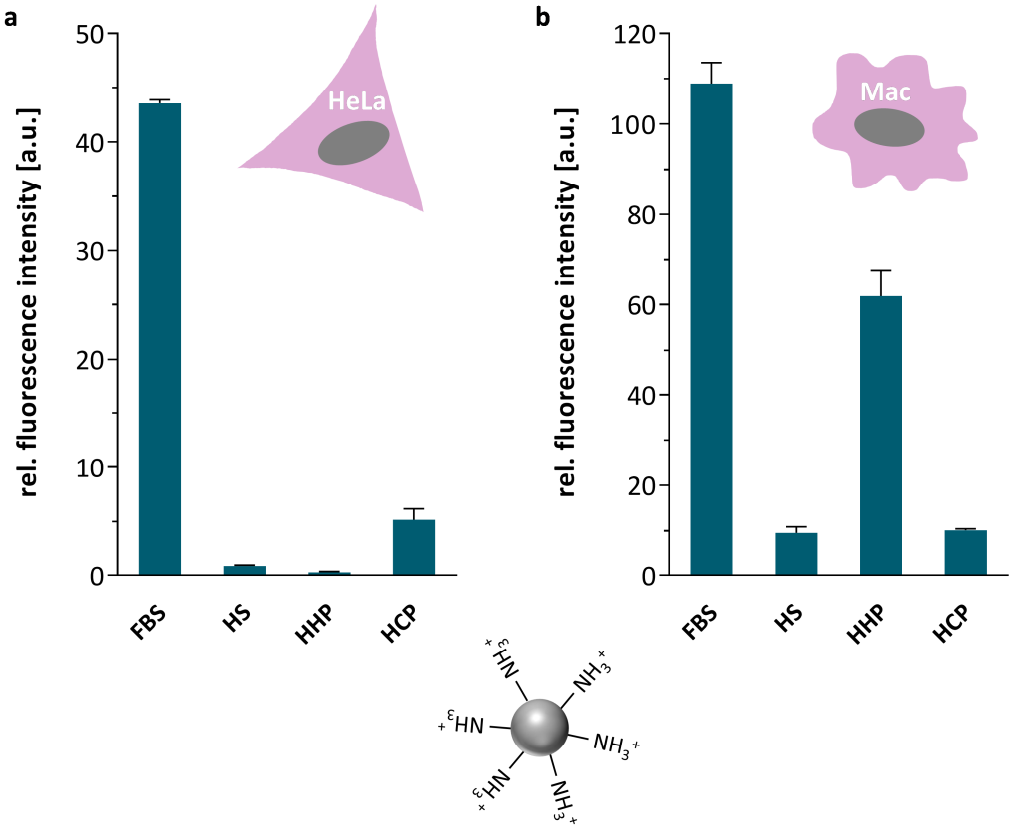

Figure 4-33: Influence of different protein sources on uptake of PS-NH_2 into HeLa cells and macrophages
Uptake of PS-NH_2 into (a) HeLa cells after 4 h incubation and into (b) RAW264.7 macrophages after 2 h incubation analysed by flow cytometry. Cells were cultured in serum-free medium for 2 h before cell medium was changed to 100% foetal bovine serum (FBS), human serum (HS), human heparin plasma (HHP) or human citrate plasma (HCP) directly before NP addition. Values are expressed as mean ± SD of triplicates.

4.5.3 INVESTIGATION OF PROTEIN CORONA COMPOSITION IN DIFFERENT PROTEIN SOURCES

The strong difference in cellular uptake of NPs incubated in various types of protein sources displayed in Figure 4-33 raised the question whether the effect is triggered by a distinct protein adsorption. Thus, the composition of the protein corona was further analysed by SDS-PAGE and quantitative LC-MS.

Comparison of hard corona proteins formed around PS-NH_2 in FBS, HS, HHP and HCP after separation by centrifugation is depicted in Figure 4-34. The amount of adsorbed proteins was quantified by a colorimetric protein assay (Figure 4-34a). The strongest protein adsorption is observed in HCP, followed by HHP and HS. The lowest protein concentration was measured for the FBS samples. The SDS-PAGE in Figure 4-34b shows that the strongest difference in the protein pattern is seen between FBS and the human samples. In addition to the strong albumin band, the plasma samples (HHP and HCP) exhibit bands

for fibrinogen. Fibrinogen consists of three subunits, the alpha, beta and gamma chain, detected at 47, 56, and 63 kDa, respectively.[182]

Furthermore, the high reproducibility of the method is proven by the similarity of the protein pattern between the three replicates for each protein source. Although the difference between the pure protein source on the right side and the protein corona formed in the respective medium is not as pronounced as for other NP samples, the enrichment of several proteins as fibrinogen is still obvious.

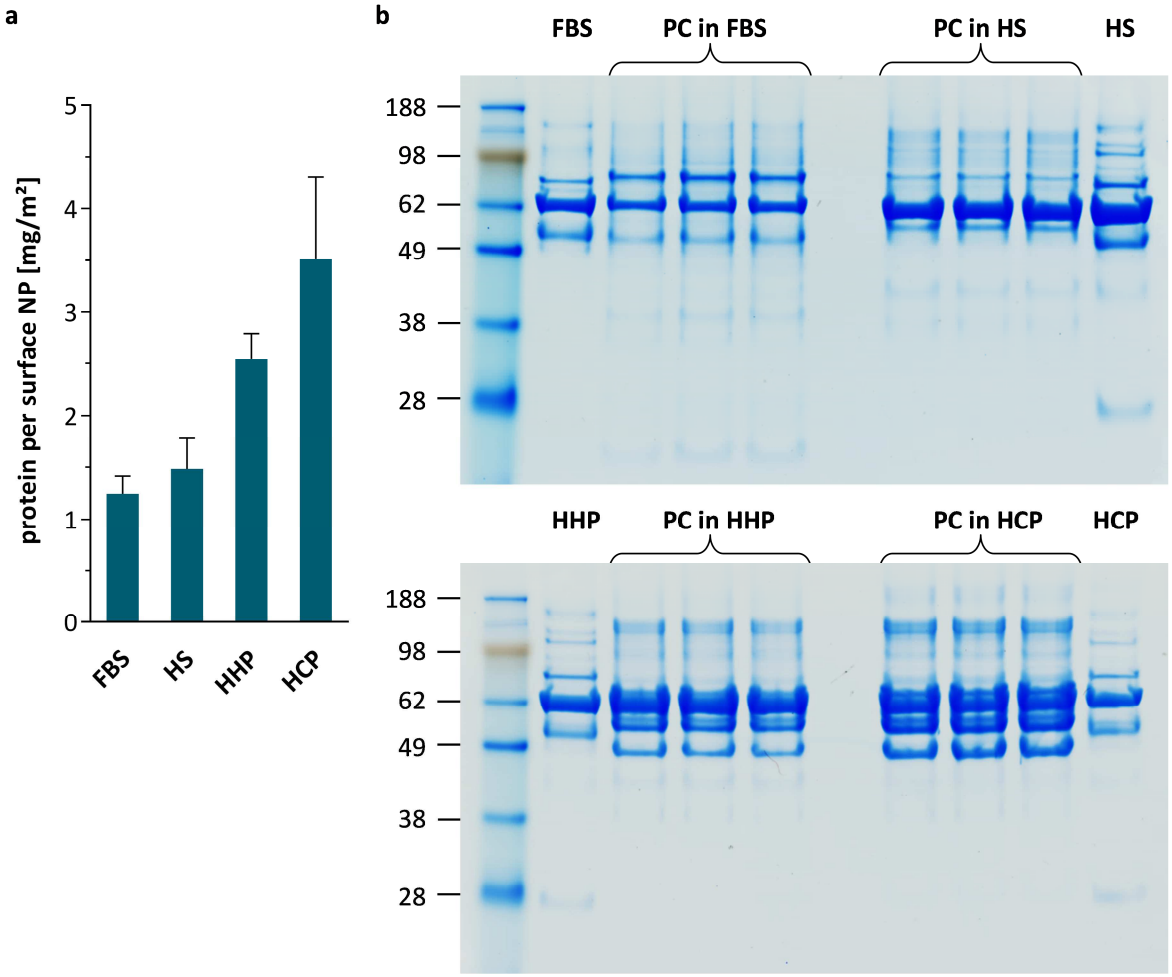

Figure 4-34: Protein adsorption to the surface of PS-NH_2 after incubation in different protein sources.
PS-NH_2 was incubated with FBS, human serum (HS), human heparin plasma (HHP) or human citrate plasma (HCP) for 1h at 37 °C and hard corona proteins were prepared by centrifugation. (a) Quantification of adsorbed proteins with Pierce660nm Assay in mg protein per NP surface area (m^2). Values are expressed as mean ± SD of the three biological replicates. (b) SDS-PAGE was used to visualise the protein corona (PC) composition formed around PS-NH_2 in the different protein sources. To guarantee reproducibility, the analysis was performed in triplicates. For comparison a sample of each protein source was loaded on the gel.

To further analyse the protein corona samples, LC-MS analysis was performed. In total 431 proteins were identified for all samples (4 conditions, 3 biological replicates, 3 technical replicates). The principal component analysis (PCA) in Figure 4-35 shows a low variability between the replicates for the analysis of the protein corona formed around PS-NH_2 in FBS, human serum, human heparin and citrate plasma. The PCA uses protein abundance levels across runs to determine abundance variations. Each colour dot represents one run. The PCA blot is useful in identifying run outliers, as close proximity of runs indicates a similarity of protein composition identified. As expected the bovine samples cluster distant to the human samples and within the human samples the protein corona samples are dislodged from the control samples (pure HS, HHP and HCP). Only one replicate of the protein corona formed in HCP (pink) seems to be far-off and was therefore excluded for further analysis (complete lists of all proteins identified by LC-MS are contained in Table 7-6 and Table 7-7 in the appendix). Figure 4-36 outlines the composition of the different protein coronas around PS-NH_2; the majority of proteins was only identified in very low concentrations and is thus expressed as others.

As already determined by SDS-PAGE, albumin is the major protein in all samples. It accounts for 58% of the protein corona formed in human serum, 46% in the FBS corona and 47% and 39% in the coronas formed in human heparin and citrate plasma, respectively. Additionally, vitronectin and clusterin were identified as abundant proteins on the NPs after incubation in all three human samples. With 19% the highest amount of clusterin was determined for the human serum samples, whereas the same amount of vitronectin adsorbed to the particles in heparin plasma. Furthermore, the plasma samples contain considerable amounts of fibrinogen. Adding up the percentages determined for the three subunits, fibrinogen has a 39% share in the corona formed in citrate plasma. Interestingly, incubation with FBS leads to a strong adsorption of prothrombin and haemoglobin, although these proteins are not very abundant in pure FBS (see Table 7-7).

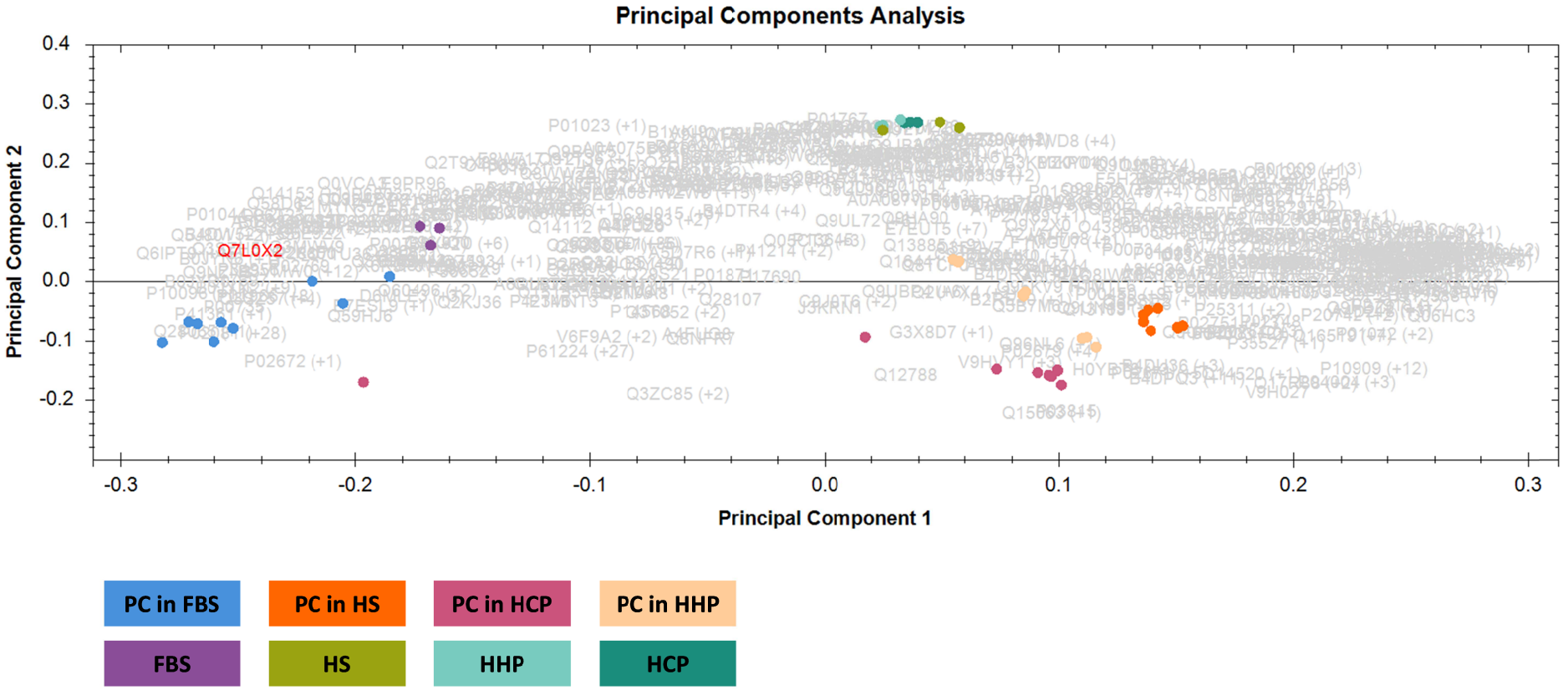

Figure 4-35: Principal component analysis (PCA) of LC-MS runs analysing the protein corona formed around PS-NH_2 after incubation with FBS, HHS, HHP or HCP. For each condition three biological replicates were prepared and each sample was measured in three technical replicates. Additionally the original protein sources were measured in three technical replicates.

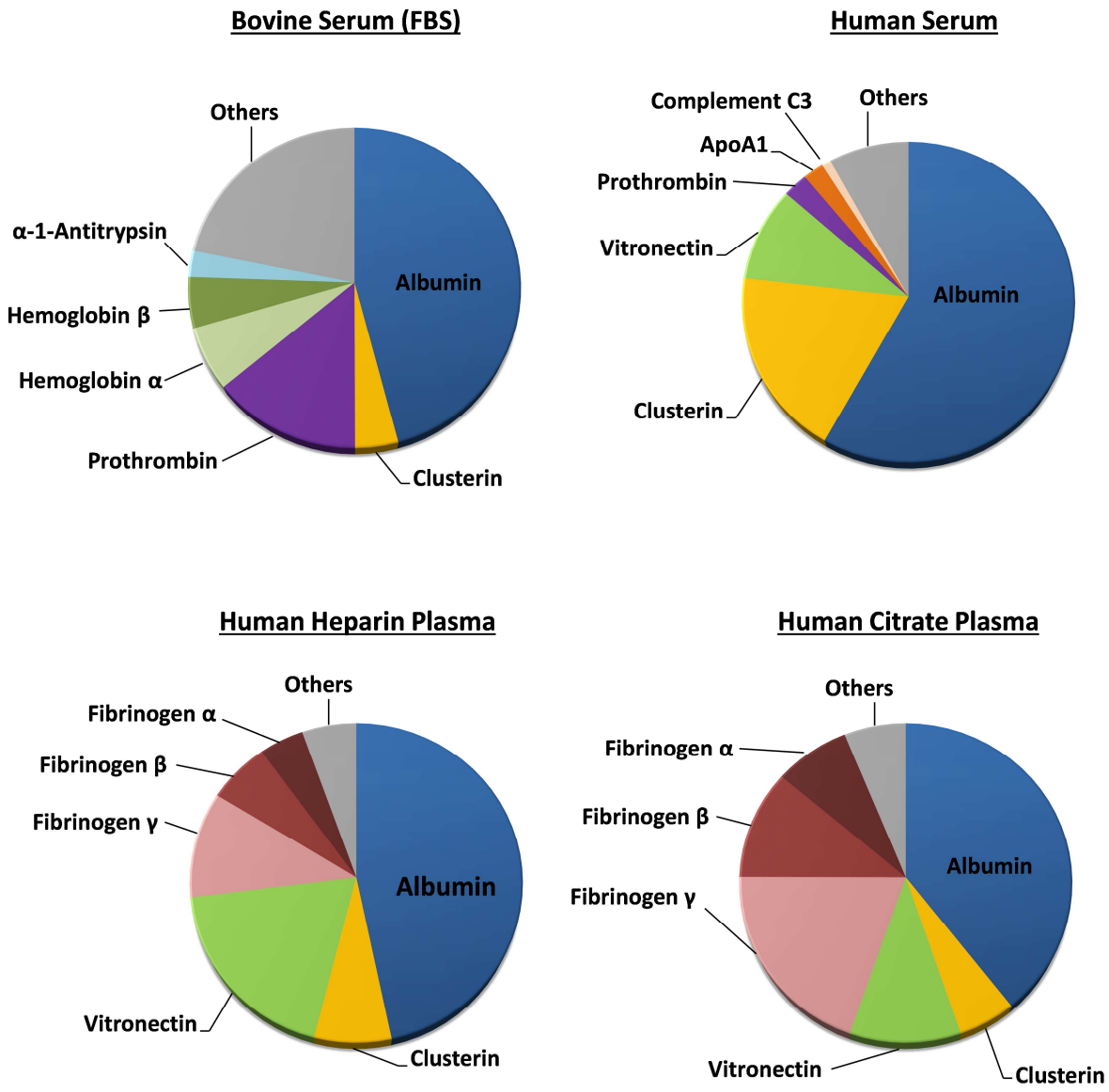

Figure 4-36: Composition of the protein corona of PS-NH_2 after incubation with FBS, HS, HHP or HCP determined by quantitative LC-MS.

Mean values were calculated from the molar masses of each protein for three biological and three technical replicates. Only the six most abundant proteins of each protein corona are shown separately, amount of remaining proteins was summed up as others.

In conclusion, a significant difference between the bovine and human samples was detected. This could explain the increased uptake of PS-NH_2 incubated in FBS for both tested cell types (Figure 4-33), especially as a high abundance of prothrombin on the particle surface has already been linked to an increased cell interaction in chapter 4.1 and 4.2. Additionally, the overall lower protein adsorption in FBS (Figure 4-34a) points towards an enhanced cell uptake. NPs incubated in human serum bound a significantly higher amount of clusterin compared to particles incubated in FBS. This suggests a participation

of clusterin in reducing the uptake of PS-NH_2 incubated in human serum into HeLa cells and macrophages.

Despite these conclusive results, the protein patterns formed around the nanocarrier in citrate and heparin plasma display a high level of similarity. The prominent difference in macrophage uptake of PS-NH_2 incubated in the two plasma types can thus not be explained adequately by protein adsorption. The results suggest that besides protein corona formation the type of anticoagulant used for plasma generation might play a major role in cell interaction and was further examined.

4.5.4 EFFECT OF ANTICOAGULANT HEPARIN

As no strong difference between the compositions of the different protein coronas on PS-NH_2 in the two investigated plasma samples was detected, the part played by the polysaccharide heparin in nanoparticle-cell interaction was explored. The highest uptake of the amino functionalised particle was detected for FBS for both investigated cell lines. Therefore, FBS was used as a reference to monitor the effect of heparin. Figure 4-37 shows the uptake of PS-NH_2 into HeLa cells and macrophages maintained in FBS or heparin plasma as already seen in Figure 4-33, but this time the cells were additionally incubated in FBS supplemented with heparin. Heparin was added at the same concentration (17 IU/ml) as commonly applied in BD Vacutainer® Plasma Tubes for heparin plasma generation.[183]

Strikingly, uptake of PS-NH_2 in FBS containing heparin was almost completely inhibited compared to uptake in pure FBS. The internalisation is reduced to the same extent as by heparin plasma. In contrast, the mixture of FBS and heparin strongly enhances the uptake into macrophages (Figure 4-37b). This is in agreement with the fact that uptake of the particles incubated in heparin plasma is also significantly higher than for particles in human serum or citrate plasma.

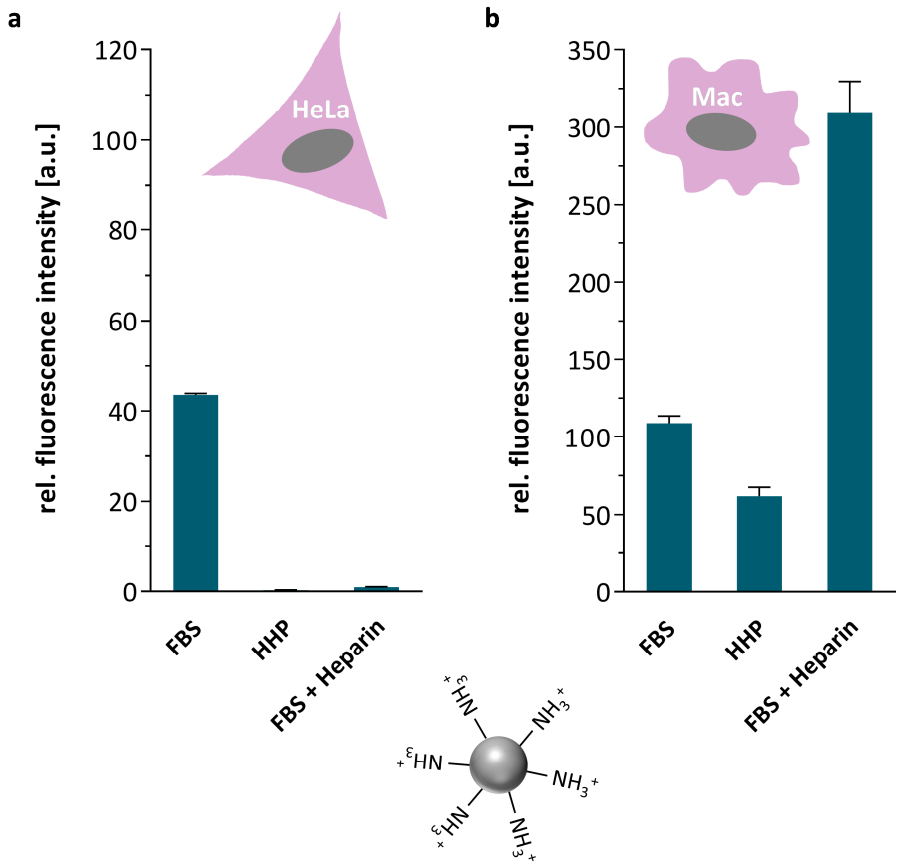

Figure 4-37: Influence of heparin on uptake of PS-NH_2 into HeLa cells and macrophages.
Uptake of PS-NH_2 into (a) HeLa cells after 4 h incubation and into (b) RAW264.7 macrophages after 2 h incubation analysed by flow cytometry. Cells were cultured in serum-free medium for 2 h before cell medium was changed to 100% foetal bovine serum (FBS), human heparin plasma (HHP) or FBS supplemented with heparin (17 IU/ml) directly before NP addition. Values are expressed as mean ± SD of triplicates.

At this point, there are a number of different scenarios for the role played by heparin. For instance, the polysaccharide could either adsorb to the nanoparticles or directly bind to the cells. In order to get closer to a solution, in a next step the particles were either incubated with FBS alone or FBS supplemented with heparin. Unbound proteins and heparin were then removed by centrifugation and the coated NPs were added to HeLa cells. Additionally, the FBS coated particles were added to cells cultured in medium containing heparin (Figure 4-38). It was assumed that in this way a distinction between the interaction of heparin with the particles and an interaction with the cells was possible. Nevertheless, in both cases, uptake of PS-NH_2 was prevented. NPs pre-coated with FBS and subsequently added to cells cultured in medium containing heparin and NPs coated with FBS and heparin were not internalised by HeLa cells.

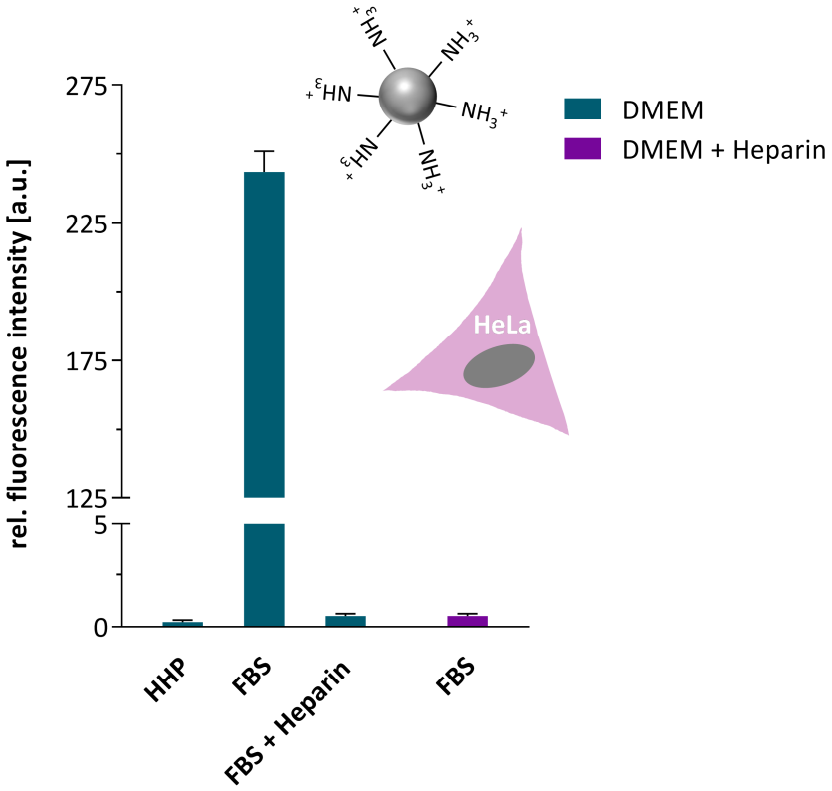

Figure 4-38: Uptake of PS-NH_2 into HeLa cells after incubation with HHP, FBS or FBS and heparin (17 IU/ml) NPs were incubated with protein sources for 1 h at 37 °C and centrifuged to remove residual proteins before NPs were added to cells cultured in pure DMEM (green) or DMEM supplemented with Heparin (17 IU/ml; purple). Uptake was analysed by flow cytometry after 2 h incubation. Values are expressed as mean ± SD of triplicates.

These intriguing results raised further questions. Can heparin alone inhibit particle uptake or are the proteins present in FBS necessary for the effect? Does heparin prevent endocytosis of HeLa cells in general? These questions were addressed in the following experiment depicted in Figure 4-39. First, PS-NH_2 particles were added to HeLa cells cultured in pure DMEM, DMEM containing FBS, DMEM containing heparin or both (Figure 4-39a). The flow cytometry analysis shows that only the combination of FBS and heparin prevents the uptake of particles into HeLa cells. Heparin alone does not have a significant effect on particle internalisation.

Furthermore, the uptake of AF488-Dextran was analysed under the same conditions. Tracing the internalisation of fluorescent Dextran is a standard method to monitor endocytosis. Figure 4-39b illustrates that heparin has no influence on Dextran uptake. Thus heparin does not prevent macropinocytosis of HeLa cells in general but only affects nanoparticles uptake.

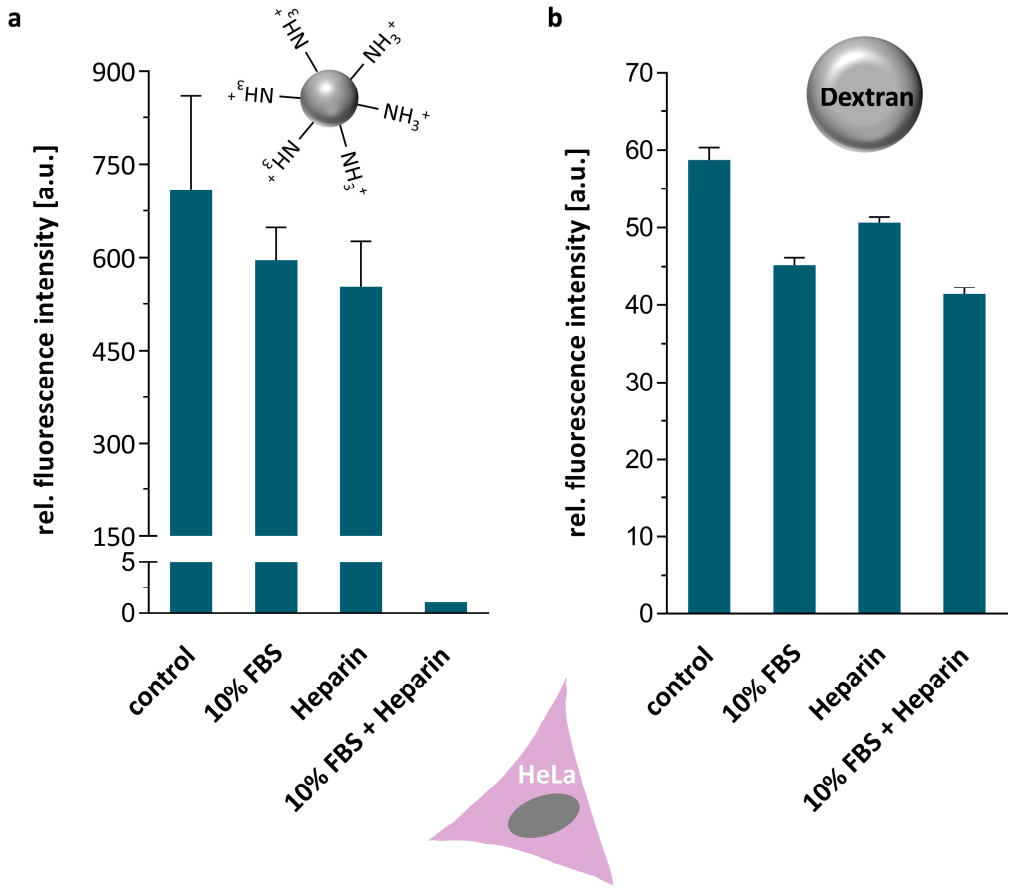

Figure 4-39: Effects of heparin on uptake of PS-NH_2 and Dextran into HeLa cells.
Uptake of (a) PS-NH_2 and (b) AF488-Dextran (100 µg/ml) into HeLa cells was analysed by flow cytometry after 2 h incubation. Cells were cultured in serum-free medium for 2 h before cell medium was changed to pure DMEM (control), DMEM containing either 10% FBS, heparin (17 IU/ml) or both. Values are expressed as mean ± SD of duplicates.

4.5.5 DISCUSSION

This study addresses several parameters which are often neglected when analysing interactions of nanocarriers, proteins and cells, such as protein concentration, protein source and cell type. The results presented in this section indicate that in general proteins attenuate the uptake of polystyrene nanoparticles into cells. Related results have been reported by Lesniak *et al.*, showing a reduced uptake of polystyrene nanoparticles when proteins are present in cell culture medium.[85] In the present study, the effect was tested for different cell types including hMSCs, HeLa and phagocytic cells (DCs, macrophages) and for polystyrene NPs with different surface functionalisations (COOH, SO_3, NH_2).

Furthermore, it was shown that the concentration of the protein source has deep implications on particle uptake. Serum and plasma concentrations as low as 0.5% already have a major impact by strongly reducing nanoparticle internalisation. This should be

considered in all experiments investigating cellular uptake of nanocarriers. In order to adjust *in vitro* experiments to be as close as possible to *in vivo* conditions, 100% of the respective protein source should be used. However, no large discrepancies between 10%, the concentration most commonly used for cell culture experiments, and 100% were observed for particle cell interactions.

Most importantly, it was demonstrated that the choice of protein source is crucial for nanoparticle uptake analysis. Many recent studies of great importance investigating the different aspects of the protein corona of nanocarriers employed different protein sources as FBS[18,85], human serum[30,45], human citrate[12,36] or EDTA plasma[11,16] without further stating reasons for their choice. The results shown here emphasise the necessity of a careful decision concerning the protein source as the outcome of experiments is strongly dependent on it.

Hard corona protein profiles varied significantly between the investigated protein sources FBS, human serum, human heparin and citrate plasma. A strong difference in corona composition was especially prominent between the human and bovine media. As FBS is the most frequently used supplement for many cells cultured *in vitro*, it is also often employed in protein corona studies. But in order to obtain significant improvement in the prediction of the *in vivo* fate of nanoparticles, it is important to test the protein corona formation in the respective medium i.e. the exact protein source of the desired species (e.g. murine or human) before applying nanocarriers *in vivo*.

Furthermore, the distinction between plasma and serum is often neglected. A rather strong adsorption of fibrinogen to nanoparticles from both plasma samples was observed and might affect nanoparticle uptake substantially. Thus the distinction should not be ignored. On the other hand, anticoagulants used for plasma generation can bias the observations significantly. During plasma preparation from whole blood, blood clotting is prevented either by EDTA, citrate or heparin. EDTA and citrate both are effective by calcium complexation and thus deplete the blood of this important cofactor for fibrinogen. Heparin binds to antithrombin III and increases its activity in blocking thrombin and therefore inhibits fibrin clot formation.

In their publication analysing the uptake of polystyrene nanoparticles into different types of white blood cells Baumann *et al.* have already described the influence of EDTA on endocytosis.[184] They report a dramatically reduced uptake of carboxy and amino-functionalised nanoparticles into CD14+ monocytes and CD16+ neutrophil granulocytes when EDTA or citrate was used instead of heparinised blood. Furthermore, they showed that adding heparin to EDTA-blood does not enhance NP uptake but vice versa the addition of EDTA to heparin blood diminishes the uptake substantially. Therefore, it was concluded that EDTA is hindering the uptake by complexing calcium, as calcium is needed as a signalling messenger in phagocytosis, and that heparin should be used for anticoagulation. Although the conclusions are consistent, the present experiments show that heparin does enhance uptake into macrophages and even more strikingly inhibit the uptake of nanoparticles into HeLa cells.

Heparin is a natural glycosaminoglycan composed of repeating disaccharide units (see structure in Figure 4-40). It is most commonly known as an anticoagulant and has been used as a drug since the 1930s. In addition to its well investigated anticoagulant activity, heparin is involved in diverse physiological processes including cell proliferation, differentiation, inflammation, angiogenesis and viral infectivity through interacting with a large range of proteins.[185] It also exerts anticancer activities in the processes of tumour progression and metastasis.[186] Still, usually heparin is stored within the secretory granules of mast cells and released only into the vasculature at sites of tissue injury.[185] With its high content of sulpho and carboxyl groups, heparin has the highest negative charge density of any known biological molecule.[187]

Binding of highly negatively charged heparin to the nanoparticle surface might cause an unfavourable interaction between the particles and the negatively charged cell membrane. Accordingly, numerous studies have shown that surface charge has a significant impact on cellular internalisation of a variety of nanocarriers. Positively charged nanoparticles reveal a high rate of internalisation into HeLa cells, whereas negatively charged NPs exhibit a poor rate of endocytosis.[188-190]

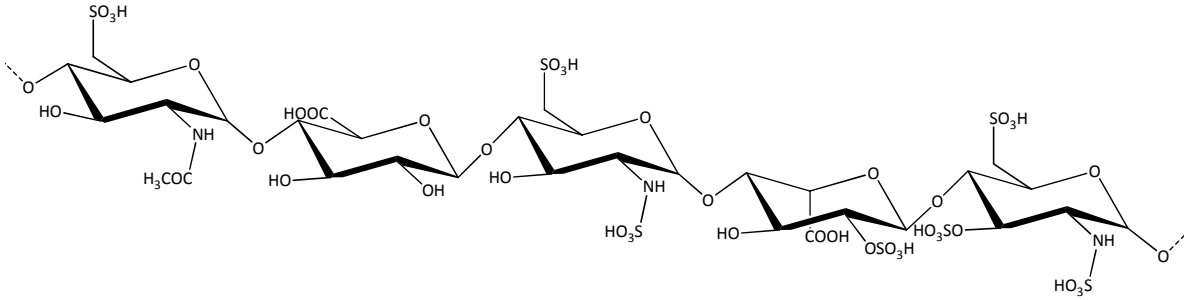

Figure 4-40: Structure of Heparin.
Heparin is built of repeating disaccharide units consisting of an uronic acid (D-glucuronic or L-iduronic acid) and D-glucosamine or N-acetyl-D-glucosamine with various degrees of sulphation on each monosaccharide unit.

Nevertheless, reported effects of heparin on cellular uptake of nanomaterials are quite controversial. As heparin has been shown to inhibit complement activation[191-193] binding of heparin to surfaces has been suggested as an alternative for PEGylation in a biomimetic approach. Heparin immobilised to the surface of nanocarriers can mimic eukaryotic cells that are naturally covered with glycosaminoglycans, thus concealing the unnatural nanoparticles from the immune system. Accordingly, several manuscripts report a prolonged blood circulation of nanoparticles coated with heparin.[194-196] Furthermore, heparin has proved its ability to inhibit the adsorption and the internalisation of nanoparticles by a murine macrophage-like cell line *in vitro*.[197]

On the other hand, a high uptake of heparin-based nanocapsules into different tumour cell lines was described,[198] as well as an enhanced uptake of heparin functionalised PLGA-based nanoparticles into a fibroblast and tumour cell line.[199] Surprisingly, these reports are rather contrary to the results of the study presented here as we have seen an enhanced uptake into macrophages when heparin is present, but an inhibition into the cancer cell line HeLa.

Up to now, the mechanism of this process is unclear. Interestingly, proteins seem to be necessary for this effect as heparin alone does not prevent the uptake of PS-NPs into HeLa cells. Proteins present in FBS are sufficient to provoke the reduced uptake and the high amount of coagulation proteins only present in plasma is not necessary. Furthermore, it was shown that heparin does not impair the internalisation of dextran by HeLa cells

indicating that a specific interaction of heparin and the nanocarriers occurs and endocytosis is not inhibited in general.

The opposing effects of heparin on NP uptake by HeLa cells and macrophages refer to the different mechanisms of entry into various cells. Different ways of endocytosis utilised by non-phagocytic cells as HeLa and phagocytes like macrophages seem to be relevant for the effect provoked by heparin. Further cell types, phagocytic and non-phagocytic, should be employed in future studies to elucidate the exact principle of heparin involvement. Additionally, inhibition assays could help to disclose receptor participation.

Interestingly, attachment and phagocytosis of the intracellular parasite *Chlamydia* into HeLa cells can be inhibited by exogenous heparin.[200-202] A mechanism of host cell interaction in which glycosaminoglycans bound by the pathogen and host cell receptors mediate the adhesion of *Chlamydia* to HeLa cells was proposed.[201] Additionally, heparin-coated polystyrene microspheres bind to HeLa cells, and the specificity of binding was shown by competitive inhibition with exogenous heparin indicating that they compete for the same cell receptor.[203] These publications propose a heparin specific receptor on HeLa cells and a similar mechanism for heparin coated NPs could be envisaged. Nevertheless, our results indicate that the uptake into HeLa is still impaired when there is no excess heparin. Centrifugation of NPs after incubation in FBS supplemented with heparin removes any unbound proteins and heparin molecules, but still the internalisation of these particles was significantly reduced compared to NPs incubated in FBS alone.

Already in 1983, Bleiberg *et al.*[204] postulated heparin receptors on mouse macrophages and evidence for a scavenger mediated uptake into the same macrophage-like cell line used in the present study (RAW264.7) was published by Falcone six years later.[205] Matching *in vivo* data further linked liver uptake of heparin to a scavenger receptor mediated mechanism.[206] Furthermore, Lindstedt *et al.* showed that soluble heparin proteoglycans secreted by stimulated mast cells trigger uptake of LDL by macrophages through scavenger receptor-mediated phagocytosis.[207] All these reports provide evidence that heparin's binding to RAW264.7 cells is mediated by the scavenger receptors and fit

the high uptake of nanoparticles incubated with heparin plasma or FBS supplemented with heparin into macrophages.

It is noteworthy to mention, that for the study investigating the stealth effect of polyphosphoesters (4.3) also heparinised plasma was used. Thus, the possibility of a participation of heparin in triggering the high uptake of the control particle into macrophages exists. Nonetheless, the strong reduction of internalisation into macrophages determined for the stealth nanoparticles incubated in heparin plasma and the high uptake of all particles without plasma indicates that the conclusions drawn are still valid. In particular, the proof of clusterin´s diminishing effect on cell internalisation renders the heparin participation for this study irrelevant.

Laurent *et al.* have already pointed out the key role of the protein source in the formation of the associated protein corona and the impact of the cell "observer" effect.[55] They compared the corona composition formed around superparamagnetic nanoparticles (SPIONs) in FBS and human plasma (the anticoagulant was not further specified) with SDS-PAGE and determined significant differences. Furthermore, cell uptake and toxicity were probed for various cell lines and the results indicate that each cell type responds differently to the nanoparticles. Nevertheless, they did not analyse the combined effect of distinct protein sources and cell types. The results presented here, prove that the same protein source can have a different impact on distinct cell types and that the influence of the employed anticoagulant is of utmost importance and a factor which should be taken into account. For best results, it should be considered analysing the protein adsorption patterns obtained after incubation in both plasma and serum. In a strict sense, only investigations using blood can provide expressive answers with regard to adsorption of plasma proteins onto surfaces *in vivo*.

4.6 INFLUENCE OF SAMPLE PREPARATION ON PROTEIN CORONA COMPOSITION

Until now, investigation of corona proteins associated with nanocarriers directly in the incubation medium is unfortunately only possible with regard to size increase or adsorption strength. But for the analysis of the protein corona composition NP-protein complexes need to be separated from the surrounding medium. This last chapter addresses the influence of preparation methods necessary for the isolation. Magnetic nanoparticles were used in a comparison of two preparation techniques: centrifugation and magnetic separation. Furthermore, the development of the hard corona during the preparation process which includes several washing cycles was monitored concerning the protein composition.

4.6.1 NANOPARTICLES

Superparamagnetic iron oxide nanoparticles (SPIONs) consist of cores made of iron oxides which can be embedded in a polymer matrix. Owing to their superparamagnetic properties, attractive forces between the magnetic particles are only present when an external magnetic field is applied.[208] This feature makes SPIONs interesting for various biomedical applications for example as contrast agents for magnetic resonance imaging (MRI),[209] in cell separation,[210] organelle isolation[41] or for magnetic drug targeting in tumour therapy.[211] The various potential applications imply the necessity of an examination of their interactions with blood proteins in order to assess both potential benefits and side effects. Additionally, the magnetic feature enables a protein corona preparation without centrifugation required.

Therefore, SPIONs were employed as model polymer nanoparticles for the preparation of the protein corona. The nanoparticles used in this study are polystyrene particles with encapsulated magnetite and an average diameter of 130 nm (Figure 4-41). A high negative surface charge of -67 mV is provoked by the charged co-monomer styrene sulfonate which was added during polymerisation and additionally improves NP stabilisation by electrostatic repulsion. The SPIONs were synthesised by D. Estupinan according to the procedure described in Bannwarth *et al.*[208]

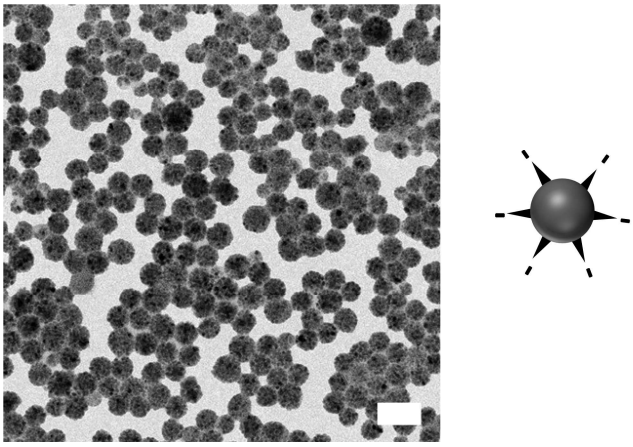

Figure 4-41: TEM images and schematic representation of SPIONs.
Scale bar: 200 nm (TEM images were taken by D. Estupinan)

4.6.2 DIFFERENT HARD CORONA PREPARATION TECHNIQUES LEAD TO SAME PROTEIN COMPOSITION

In order to analyse the protein corona formed around nanoparticles, the adsorbed proteins need to be separated from free proteins in the incubation medium. In all previous chapters the hard corona was prepared by centrifugation of the NP-protein complexes including several washing cycles. Although this is the commonly used method, it might not be the optimal way because long centrifugation steps are necessary to spin down all particles leading to aggregate formation which might affect the outcome. After centrifugation, extensive resuspension is required to ensure an adequate washing of the particles. Separation of nanoparticles from the surrounding medium by a strong magnet is less harsh and less time consuming. In this study the two methods were compared with regard to protein adsorption.

After incubation of SPIONs with human heparin plasma, the samples were either centrifuged or a strong magnet was placed in close vicinity to the sample tube. This enables removal of the supernatant while the SPION-protein complexes are fixed at one side of the tube. For both preparation methods three washing steps with PBS were performed to remove loosely attached proteins. For magnetic separation the magnet was removed for each washing step to assure washing off unbound proteins trapped between the NPs. The hard corona proteins were then desorbed in a urea-thiourea buffer. To ascertain reproducibility the procedure was performed in triplicates for both techniques.

Figure 4-42 displays the hard corona formed around SPIONs in human plasma prepared by either magnetic separation or separation by centrifugation. Both preparation methods resulted in a similar amount of proteins being desorbed from the SPIONs with no significant difference in protein concentration (Figure 4-42a). For the centrifugation a slightly higher variation between the three replicates was measured. The protein patterns produced by the two separation methods bear a strong resemblance. Almost no differences between the samples are detectable in the SDS-PAGE analysis (Figure 4-42b) and additionally the good reproducibility is demonstrated by the identical protein profiles for the triplicates.

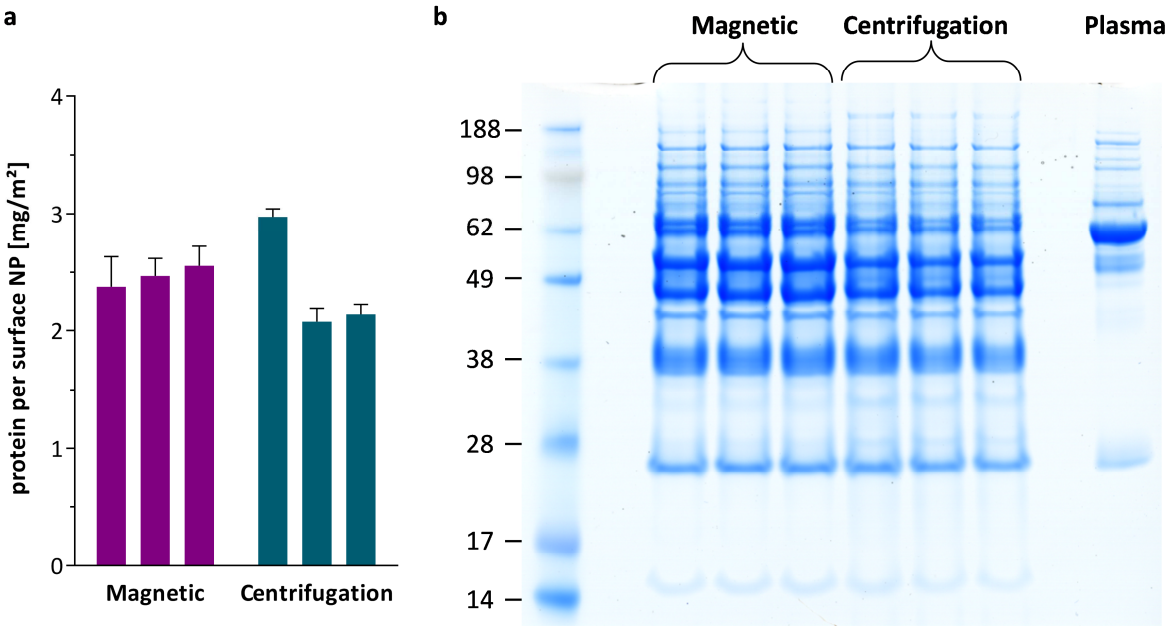

Figure 4-42: Comparison of protein corona preparation techniques.
SPIONs were incubated with human heparin plasma (0.05 m²/ml) for 1 h at 37 °C. The NP-protein complexes were then separated from the plasma by either a strong magnet or centrifugation at 20 000 g for 1 h (each done in triplicates). For both separation methods three washing steps with PBS were performed to remove loosely bound proteins. Proteins were desorbed with 7 M urea, 2 M thiourea and 4% CHAPS. (a) Quantification of adsorbed proteins with Pierce660nm Assay in mg protein per NP surface area (m²) Values are expressed as mean ± SD of triplicates. (b) SDS-PAGE analysis visualises protein corona composition. For comparison human plasma was loaded (right lane).

With LC-MS analysis 183 proteins were identified, but for a better overview Table 4-4 only contains those proteins for which a share of at least 1% in the protein corona was ascertained. The very similar protein profiles already detected by gel electrophoresis were validated by mass spectrometry analysis. The colour code used in the table enables an immediate optical recognition of this analogy. Furthermore, the strong distinction in protein quantities identified in human plasma is visualised. For both preparation methods

fibrinogen and clusterin are the most abundant proteins. This shows that the more convenient method of magnetic separation is just as reliable as the time-consuming procedure of centrifugation.

Table 4-4: Most abundant proteins in the protein corona of SPIONs in dependence of preparation method. Values were calculated from the molar masses of each protein identified by LC-MS for three biological and two technical replicates. Shown are only those proteins which constitute for at least 1% of the protein corona after either magnetic separation or centrifugation. Percentages of the proteins determined for human plasma are shown for comparison.

Protein	Magnetic	Centrifugation	Plasma
Fibrinogen gamma chain	22.40%	19.06%	0.54%
Clusterin	14.60%	17.61%	0.14%
Fibrinogen beta chain	13.87%	11.84%	0.31%
Fibrinogen alpha chain	9.47%	7.45%	0.31%
Kininogen-1	4.04%	2.73%	0.19%
Vitronectin	3.16%	5.02%	0.15%
Alpha-2-HS-glycoprotein	2.98%	3.93%	0.50%
Ig kappa chain C region	2.51%	2.54%	9.18%
Vitamin D-binding protein	2.01%	2.37%	0.28%
Apolipoprotein A-I	1.51%	1.43%	0.38%
Ig mu chain C region	1.46%	1.31%	0.49%
Serum albumin	1.33%	1.26%	58.75%
Ig gamma-1 chain C region	1.32%	1.27%	9.37%
Transthyretin	1.23%	1.21%	0.40%
Hemopexin	1.10%	1.15%	1.16%
Zinc finger protein basonuclin-2	0.93%	1.44%	0.00%

4.6.3 FROM SOFT TO HARD CORONA

Having established that magnetic separation is a reliable method for the preparation of the hard corona, in a next step the procedure was exploited to investigate the alteration of the protein composition during preparation. It was anticipated that in this way the development of the protein corona from soft to hard corona could be monitored. With each washing step the loosely bound proteins belonging to the soft corona are consecutively removed thus leaving behind only strongly binding proteins at the NP surface.

Figure 4-43 confirms the reduction of proteins which can be reconstituted from the SPIONs after each washing step. As expected, the amount of protein decreases continuously during the procedure. A very high protein amount was quantified for the NP-protein complexes removed from the surrounding incubation medium by magnetic separation without being washed in PBS (0 washing cycles). In the polyacrylamide gel in Figure 4-43b this sample demonstrates a strong blurred albumin band which is also detected in the pure plasma sample. With each washing step the albumin fraction is reduced and the progressing enrichment of the three fibrinogen subunits at 47, 56, and 63 kDa becomes more and more apparent.

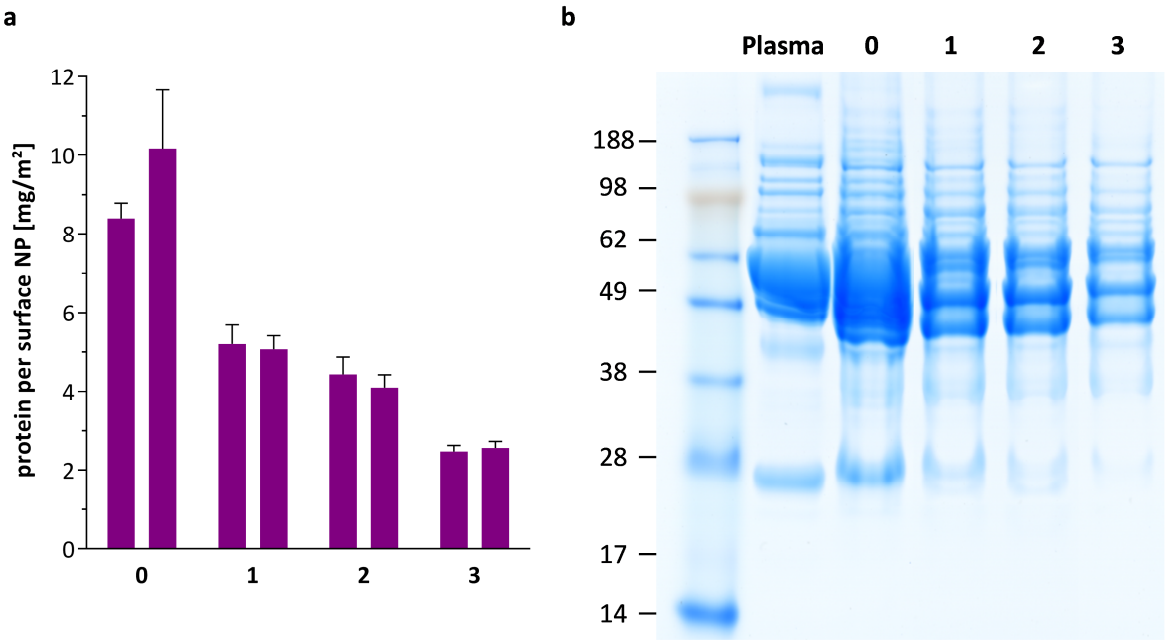

Figure 4-43: Development of the protein corona of SPIONs during preparation.
The NPs were incubated with human plasma (0.05 m²/ml) for 1 h at 37 °C. The NP-protein complexes were then separated from the plasma by a strong magnet (0). Increasing numbers of washing cycles (1 to 3) in PBS were performed to remove loosely bound proteins. Proteins were desorbed with 7 M urea, 2 M thiourea and 4% CHAPS. (a) Quantification of adsorbed proteins with Pierce660nm Assay in mg protein per NP surface area (m²) Values are expressed as mean ± SD of triplicates. (b) SDS-PAGE analysis of the samples visualises protein corona composition. For clarity only one sample for each step is shown and human plasma was loaded in the left lane.

The samples produced during hard corona preparation were further analysed by proteomic mass spectrometry. Figure 4-44 depicts single proteins which are either enriched (a) or reduced (b) in the protein corona of SPIONs in comparison to their abundance in human plasma.

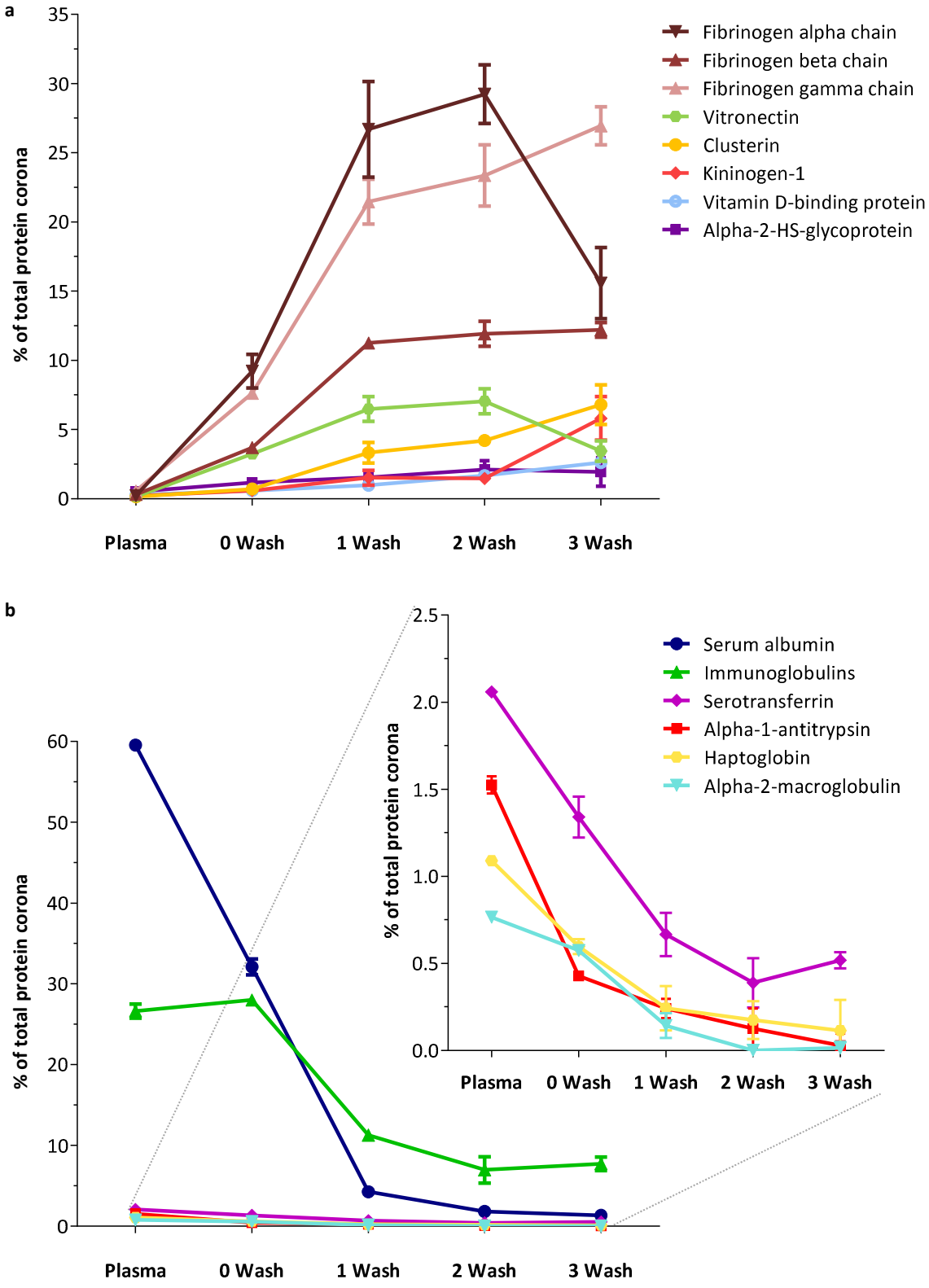

Figure 4-44: Developing abundances of single proteins on SPIONs during preparation of hard corona with increasing number of washing steps.

Values were calculated from the molar masses of each protein identified by LC-MS for two biological and three technical replicates (mean ± SD). (a) Proteins which are enriched in the hard corona of SPIONs and therefore concentrated during hard corona preparation with each washing step. (b) Proteins which are abundant in human plasma and removed from the SPION surface with each washing cycle.

The strong enrichment of fibrinogen in the hard corona is developed during the washing procedure. The normal concentration of fibrinogen in blood is between 1.5 and 4 g/l[212] which equals 2-6% for the heparin plasma used for NP incubation. The quantities determined by LC-MS for the three fibrinogen subunits only add up to a 1.1% share in plasma, but the low fibrinogen level can be explained by a removal of fibrinogen containing cryo-precipitates[212] during centrifugation previous to NP incubation. In the "soft corona" of SPIONs, directly after incubation (0 wash), fibrinogen has a share of 20.5% of the corona proteome. This percentage rises during the first two washing cycles to 59% and 65%. The percentage increase indicates the removal of soft corona proteins leading to a proportional enrichment of fibrinogen. After the third washing step the percentage is found to be slightly reduced to 55% caused by a mild detachment of the fibrinogen alpha chain.

Further proteins which accumulate on the SPION surface during the procedure are vitronectin, clusterin, kininogen-1, vitamin D-binding protein and alpha-2-HS-glycoprotein - matching those proteins identified as highly abundant in the previous section. Although some minor changes in the composition are detected during the last washing cycle, the assembly of the protein corona seems rather stable already after the first purification step.

This observation is also confirmed for the proteins dissociating during the hard corona preparation (Figure 4-44b). Most prominent is the displacement of serum albumin. In humans, albumin is the most abundant plasma protein, accounting for 55-60% of the plasma proteins[22,213] which is also the percentage identified with LC-MS in this study. While there is a lot of albumin still present in the corona before washing, it is drastically reduced with each washing step. It is yet found as the most frequent protein in the soft corona with a 32.1% share, but already after one washing step, it is reduced below 5% and levels off at 1 to 2 % in the hard corona.

Immunoglobulins constitute about 7% of the total proteins identified in the hard corona of SPIONs after two or three washing cycles. Hence, they belong to the same group of dissociating proteins during corona preparation as albumin. In plasma a 26.7% immunoglobulin share was identified resulting in a concentration of 17.5 mg/ml which is

in accordance with published values of normal immunoglobulin levels.[214,215] The proportion of immunoglobulins determined for the soft corona is in the same range with a minor enrichment of antibodies adsorbing to the SPION surface.

Other proteins which were generally reduced by the successive purification cycles are serotransferrin, alpha-1-antitrypsin, haptoglobin and alpha-2-macroglobulin – all proteins belonging to the ten most abundant proteins in the plasma proteome.[216]

4.6.4 DISCUSSION

To date, centrifugation is the most conventional method for isolating NP-protein complexes from the rest of plasma and loosely bound proteins. The present study takes advantage of the magnetic feature of SPIONs and compares centrifugation with magnetic isolation for protein corona preparation.

For both separation techniques a similar amount of associated proteins and almost the same protein pattern was determined. With LC-MS fibrinogen and clusterin were identified as the proteins with the highest share in the protein corona and no significant difference in their percentage was found when comparing the two preparation methods. The centrifugation steps required for a thorough isolation of particle-associated proteins are rather time consuming. Thus, future studies could benefit from the verification of the reliability of the convenient magnetic separation as an alternative to centrifugation.

Aggarwal *et al*. raised some concerns about the centrifugation method as high molecular weight and protein agglomerates might sediment during centrifugation and hence be falsely identified as protein corona proteins.[51] The comparison proves that under these conditions this is not the case - at least not if the incubation medium is previously cleared of protein aggregates by centrifugation.

In a former report, Thode *et al.* have also compared the two preparation methods and additionally gel filtration and membrane-based static microfiltration by 2D-SDS-PAGE. They also concluded that the adsorption pattern obtained after centrifugation and magnetic separation are comparable and acknowledged the two methods superior to

both filtration techniques.[126] Furthermore, they also identified fibrinogen as the major protein corona component on polystyrene particles with an iron oxide core.

The protein corona formed around SPIONs was the subject of several other studies.[53,217,218] The protein compositions reported vary substantially across the studies which emphasises the dependence on particle size, coating and initial surface charge for protein adsorption. Nevertheless, for negatively charged SPIONs, fibrinogen was always determined as a major component of the PC.

Fibrinogen is a protein which has been associated with a wide range of particles of seemingly disparate molecular composition.[11] In accordance with the Vroman effect fibrinogen is often described as a quickly dissociating protein,[11] with a maximum at an intermediate incubation time.[219] However, for ultrasmall superparamagnetic iron oxide (USPIO) particles an increasing amount of fibrinogen was observed with prolonged incubation times or increasing plasma concentrations besides a displacement of albumin by fibrinogen.[37] For the SPIONs analysed here more than half of the hard corona shaped after 1 h incubation in plasma was constituted of the three fibrinogen subunits.

Many studies exploiting the magnetic features of SPIONs use the MACS system for magnetic isolation of NP-protein complexes.[49,126,217] This methods allows definition of protein binding affinities by applying various molarities of protein washing solutions.[49] On the other hand, irreversible protein aggregation within the column can occur. Therefore, magnetic isolation without a MACS column was preferred for this study.

The second part of the chapter covers the development of the hard corona during sample preparation. With each washing cycle loosely associated proteins are removed from the SPION surface. Highly abundant plasma proteins as albumin and immunoglobulins but also serotransferrin, alpha-1-antitrypsin, haptoglobin and alpha-2-macroglobulin are consecutively removed during hard corona preparation. They are washed out with PBS, which indicates that these proteins have only a low affinity for the SPION surface and are probably part of the soft corona. Albumin, the most abundant protein in human plasma and therefore, according to Vroman expected to be one of the first proteins adsorbing to the nanoparticles surface, is only present in a significant amount before the first washing step.

On the other hand, the SPIONs could maintain some specific proteins as fibrinogen, even after extensive washing, which shows that these proteins have the highest affinities to the surface. Fibrinogen is more and more enriched during the purification of the hard corona. Furthermore, vitronectin, clusterin and kininogen-1 were identified as hard corona proteins whose percentage is continuously increased.

Most importantly, it was shown that already after the first washing step, the protein corona seems to be rather stable with only slight changes during the next two purification cycles. This illustrates the consistency of the preparation method with no further purification necessary and the importance of the first washing step to remove loosely bound albumin and immunoglobulins.

5 SUMMARY AND CONCLUSION

Polymeric nanocarriers offer a high potential for medical applications and are of particular interest as drug delivery vehicles in cancer treatment. The possibility of a precise adjustment of nanocarriers´ properties enables the development of specialised vectors. As more nanocarriers are developed it becomes readily evident that our knowledge of the molecular mechanisms of nanoparticle-cell interactions is limited.

Adsorption of proteins from physiological fluids to nanocarriers, leads to the formation of a protein shell, which defines their biological identity and causes considerable challenges. Hence, there is an urgent need to understand the influence of this protein corona on nanocarriers´ interactions with cells.

This study attempts to contribute to a better understanding of the protein corona formation around nanocarriers as it is of great importance for the further assessment of biological effects. In all chapters of this study, the composition of the hard protein corona formed around distinct polymeric nanocarriers was determined by label-free quantitative liquid chromatography mass spectrometry and different aspects of the protein adsorption are further evaluated. It is of course important to keep in mind, that the hard corona prepared *in vitro* can vary significantly from the protein composition present *in vivo*. All experimental preparation methods to date influence the composition, which makes predication of NP behaviour *in vivo* more difficult. Nevertheless, the method presented here allows detection of differences in the corona composition as a function of surface modifications. The complexity of the protein corona makes it difficult to predict its impact on physiological responses. Breaking it down to individual proteins enables the identification of specific proteins responsible for the biological fate of the nanocarriers.

First, the impact of surface functionalisation was described for distinct polystyrene nanoparticles. In general, a high enrichment of apolipoproteins was identified in the protein corona of all PS-NPs. A methodology to dissect the biological influence of individual corona proteins on cellular uptake was demonstrated. By correlating the adsorption of individual proteins with the internalisation of the nanoparticles into cells, single proteins were determined as important factors. To validate the correlation data,

nanoparticles were coated with the identified proteins and the uptake in hMSCs was measured. A major impact on cellular uptake was determined for apolipoprotein A4 and C3, reducing the nanoparticle internalisation to a minimum level. In contrast, coating the nanoparticles with apolipoprotein H doubled the uptake compared to nanoparticles with a full serum protein corona. The results demonstrate that in a mixed protein corona, which is formed as a consequence of the NPs physicochemical properties, specific proteins are more likely to be involved in cell interactions.

Next it was shown that a similar protein corona pattern can be connected to similar aggregation behaviour and biodistribution of PS-NPs. Complement C1 is proposed as a candidate to induce NP aggregation as it was found to be specifically enriched on PS-SDS, a particle building large aggregates when incubated in serum. The most promising *in vivo* distribution was detected for PS-LUT-NH_2 with a more pronounced lung allocation in addition to a strong liver accumulation observed for all NPs. This NP was also the only one not forming any aggregates. Again apolipoproteins were identified as the major class on these nanoparticles which could potentially trigger uptake by liver and lung macrophages via a scavenger receptor mediated uptake.

Nanocarriers applied *in vivo* are rapidly removed from the bloodstream by phagocytic cells of the mononuclear phagocyte system (MPS). Attachment of IgG, complement factors or other opsonins to the nanocarriers´ surface assist their identification by the immune system. Despite many efforts, the modification of nanocarriers with protein repellent polymers as PEG has not achieved a complete prevention of protein adsorption. Poly(ethyl ethylene phosphate) (PEEP) could function as a biodegradable alternative to PEG and was investigated regarding its protein repellent properties. Functionalisation of polystyrene nanoparticles with PEEP resulted in a reduced protein adsorption and an impaired uptake by macrophages.

It was shown that stealth nanocarriers either functionalised with PEG or PEEP were internalised by macrophages when no proteins are present and therefore opsonisation cannot have occurred. One major finding of this work was the identification of clusterin as a highly abundant protein in the protein corona of stealth nanocarriers, with its highest enrichment on PPEylated surfaces. Further, pre-coating of the PPEylated nanocarrier with

clusterin reduced the macrophage uptake, providing evidence for a dysopsonising function of clusterin concerning internalisation into macrophages.

Polysaccharides have also been reviewed with respect to their protein repulsive capabilities and could substitute PEG as a natural protein repulsive polymer. Nanocapsules synthesised from hydroxyethyl starch (HES) are promising tools for the transport of hydrophilic cargo and were analysed regarding their protein corona. It was demonstrated that the affinity of plasma proteins to HES nanocapsules is significantly lower than for PS-NPs. Furthermore, functionalisation of HES nanocapsules with mannose, galactose and DEC-205 does not cause an increased protein adsorption and only has a minimal influence on the protein pattern. These findings are a prerequisite for a successful targeting of dendritic cells because only if the targeting moieties are not covered by proteins a selective binding can be achieved.

An important aspect of this work is the emphasis on a thoughtful selection of the protein source used for *in vitro* protein corona preparation and uptake studies. Serum and plasma concentrations applied in cell culture affected the internalisation of nanoparticles into different cell types considerably with a strong reduction of uptake at concentrations as low as 0.5%. A major impact on protein corona composition and uptake of PS-NPs into HeLa cells and macrophages was determined for distinct protein sources as FBS, human serum and human plasma. A strong uptake of nanoparticles coated with FBS was observed for both cell lines, while human serum and human citrate plasma impairs NP internalisation. The most exciting finding was the opposing uptake of particles incubated in human heparin plasma. While the particles were internalised by macrophages, no uptake was observed for HeLa cells. Further experiments proved that heparin is responsible for this effect but the mechanism still need to be resolved.

Finally, using superparamagnetic iron oxide nanoparticles (SPION) the most common protein corona preparation technique using several centrifugation steps is compared with a more comfortable magnetic separation. The protein coronas obtained with the two methods are almost identical which proves the reliability of the convenient magnetic separation as well as the good reproducibly of the preparation methods. Furthermore, the evolution of the hard corona during sample preparation is monitored. With each washing

step loosely associated proteins as albumin are consecutively removed from the nanoparticles´ surface, while plasma proteins specifically adsorbing to the SPION surface as fibrinogen are enriched during the purification. Already after one washing cycle a stable corona is formed with only slight changes in protein pattern observed after the second and third preparation step.

Overall, this study emphasises the importance of protein corona analysis for a better understanding of nanoparticle behaviour *in vivo*. The current analysis demonstrates the potential of a combination of protein corona analysis with *in vitro* cell studies for predicting *in vivo* performance of nanoparticles especially regarding interaction with cells of the immune system. Furthermore it was shown that the stealth effect is dependent on proteins which could be exploited for the further development of novel protein repellent surfaces.

Adjusting the nanoparticles´ chemical surface characteristics and hence the particular protein corona might enable a controlled targeted delivery by exploiting the forming protein corona for a directed cellular uptake. The individual adsorption of defined proteins could function as an alternative to targeting with antibodies as nanoparticles with surface-adsorbed proteins could potentially trigger receptor-mediated endocytosis to enter cells. A firm understanding of the nanoparticle-corona complex is a prerequisite for future developments in nanomedicine.

6 REFERENCES

1 Davis, M.E.; Chen, Z. and Shin, D.M., *Nanoparticle therapeutics: an emerging treatment modality for cancer*. Nat Rev Drug Discov, 2008. **7** (9): 771-782.

2 Rahman, M.; Laurent, S.; Tawil, N.; Yahia, L. and Mahmoudi, M. *Protein-Nanoparticle-Interactions, The Bio-Nano Interface*. Vol. 15 (Springer-Verlag, 2013).

3 Mitragotri, S.; Burke, P.A. and Langer, R., *Overcoming the challenges in administering biopharmaceuticals: formulation and delivery strategies*. Nat Rev Drug Discov, 2014. **13** (9): 655-672.

4 Morachis, J.M.; Mahmoud, E.A. and Almutairi, A., *Physical and chemical strategies for therapeutic delivery by using polymeric nanoparticles*. Pharmacol Rev, 2012. **64** (3): 505-519.

5 Zhang, Z.; Jia, J.; Lai, Y.; Ma, Y.; Weng, J. and Sun, L., *Conjugating folic acid to gold nanoparticles through glutathione for targeting and detecting cancer cells*. Bioorganic & Medicinal Chemistry, 2010. **18** (15): 5528-5534.

6 van Vlerken, L.E. and Amiji, M.M., *Multi-functional polymeric nanoparticles for tumour-targeted drug delivery*. Expert Opinion on Drug Delivery, 2006. **3** (2): 205-216.

7 Bicho, A.; Peca, I.N.; Roque, A.C. and Cardoso, M.M., *Anti-CD8 conjugated nanoparticles to target mammalian cells expressing CD8*. Int J Pharm, 2010. **399** (1-2): 80-86.

8 Von Hoff, D.D.; Ervin, T.; Arena, F.P.; Chiorean, E.G.; Infante, J.; Moore, M.; Seay, T.; Tjulandin, S.A.; Ma, W.W.; Saleh, M.N.; Harris, M.; Reni, M.; Dowden, S.; Laheru, D.; Bahary, N.; Ramanathan, R.K.; Tabernero, J.; Hidalgo, M.; Goldstein, D.; Van Cutsem, E.; Wei, X.; Iglesias, J. and Renschler, M.F., *Increased survival in pancreatic cancer with nab-paclitaxel plus gemcitabine*. N Engl J Med, 2013. **369** (18): 1691-1703.

9 Barenholz, Y., *Doxil(R)--the first FDA-approved nano-drug: lessons learned*. J Control Release, 2012. **160** (2): 117-134.

10 Walczyk, D.; Bombelli, F.B.; Monopoli, M.P.; Lynch, I. and Dawson, K.A., *What the cell "sees" in bionanoscience*. J Am Chem Soc, 2010. **132** (16): 5761-5768.

11 Cedervall, T.; Lynch, I.; Lindman, S.; Berggard, T.; Thulin, E.; Nilsson, H.; Dawson, K.A. and Linse, S., *Understanding the nanoparticle-protein corona using methods to quantify exchange rates and affinities of proteins for nanoparticles*. Proc Natl Acad Sci U S A, 2007. **104** (7): 2050-2055.

12 Tenzer, S.; Docter, D.; Kuharev, J.; Musyanovych, A.; Fetz, V.; Hecht, R.; Schlenk, F.; Fischer, D.; Kiouptsi, K.; Reinhardt, C.; Landfester, K.; Schild, H.; Maskos, M.; Knauer, S.K. and Stauber, R.H., *Rapid formation of plasma protein corona critically affects nanoparticle pathophysiology*. Nat Nanotechnol, 2013. **8** (10): 772-781.

13 Walkey, C.D. and Chan, W.C., *Understanding and controlling the interaction of nanomaterials with proteins in a physiological environment*. Chem Soc Rev, 2012. **41** (7): 2780-2799.

14 Hellstrand, E.; Lynch, I.; Andersson, A.; Drakenberg, T.; Dahlback, B.; Dawson, K.A.; Linse, S. and Cedervall, T., *Complete high-density lipoproteins in nanoparticle corona*. FEBS J, 2009. **276** (12): 3372-3381.

15 Lundqvist, M.; Stigler, J.; Elia, G.; Lynch, I.; Cedervall, T. and Dawson, K.A., *Nanoparticle size and surface properties determine the protein corona with possible implications for biological impacts*. Proc Natl Acad Sci U S A, 2008. **105** (38): 14265-14270.

16 Monopoli, M.P.; Walczyk, D.; Campbell, A.; Elia, G.; Lynch, I.; Bombelli, F.B. and Dawson, K.A., *Physical-chemical aspects of protein corona: relevance to in vitro and in vivo biological impacts of nanoparticles*. J Am Chem Soc, 2011. **133** (8): 2525-2534.

17 Mortensen, N.P.; Hurst, G.B.; Wang, W.; Foster, C.M.; Nallathamby, P.D. and Retterer, S.T., *Dynamic development of the protein corona on silica nanoparticles: composition and role in toxicity*. Nanoscale, 2013. **5** (14): 6372-6380.

18 Casals, E.; Pfaller, T.; Duschl, A.; Oostingh, G.J. and Puntes, V., *Time Evolution of the Nanoparticle Protein Corona*. ACS Nano, 2010. **4** (7): 3623-3632.

19 Deng, Z.J.; Mortimer, G.; Schiller, T.; Musumeci, A.; Martin, D. and Minchin, R.F., *Differential plasma protein binding to metal oxide nanoparticles*. Nanotechnology, 2009. **20** (45): 455101.

20 Barran-Berdon, A.L.; Pozzi, D.; Caracciolo, G.; Capriotti, A.L.; Caruso, G.; Cavaliere, C.; Riccioli, A.; Palchetti, S. and Lagana, A., *Time evolution of nanoparticle-protein corona in human plasma: relevance for targeted drug delivery*. Langmuir, 2013. **29** (21): 6485-6494.

21 Muthusamy, B.; Hanumanthu, G.; Suresh, S.; Rekha, B.; Srinivas, D.; Karthick, L.; Vrushabendra, B.M.; Sharma, S.; Mishra, G.; Chatterjee, P.; Mangala, K.S.; Shivashankar, H.N.; Chandrika, K.N.; Deshpande, N.; Suresh, M.; Kannabiran, N.; Niranjan, V.; Nalli, A.; Prasad, T.S.K.; Arun, K.S.; Reddy, R.; Chandran, S.; Jadhav, T.; Julie, D.; Mahesh, M.; John, S.L.; Palvankar, K.; Sudhir, D.; Bala, P.; Rashmi, N.S.; Vishnupriya, G.; Dhar, K.; Reshma, S.; Chaerkady, R.; Gandhi, T.K.B.; Harsha, H.C.; Mohan, S.S.; Deshpande, K.S.; Sarker, M. and Pandey, A., *Plasma Proteome Database as a resource for proteomics research*. PROTEOMICS, 2005. **5** (13): 3531-3536.

22 Anderson, N.L. and Anderson, N.G., *The human plasma proteome: history, character, and diagnostic prospects*. Mol Cell Proteomics, 2002. **1** (11): 845-867.

23 Cedervall, T.; Lynch, I.; Foy, M.; Berggad, T.; Donnelly, S.C.; Cagney, G.; Linse, S. and Dawson, K.A., *Detailed identification of plasma proteins adsorbed on copolymer nanoparticles*. Angewandte Chemie-International Edition, 2007. **46** (30): 5754-5756.

24 Tenzer, S.; Docter, D.; Rosfa, S.; Wlodarski, A.; Kuharev, J.; Rekik, A.; Knauer, S.K.; Bantz, C.; Nawroth, T.; Bier, C.; Sirirattanapan, J.; Mann, W.; Treuel, L.; Zellner, R.; Maskos, M.; Schild, H. and Stauber, R.H., *Nanoparticle Size Is a Critical Physicochemical Determinant of the Human Blood Plasma Corona: A Comprehensive Quantitative Proteomic Analysis*. ACS Nano, 2011. **5** (9): 7155-7167.

25 Diederichs, J.E., *Plasma protein adsorption patterns on liposomes: Establishment of analytical procedure*. ELECTROPHORESIS, 1996. **17** (3): 607-611.

26 Monopoli, M.P.; Aberg, C.; Salvati, A. and Dawson, K.A., *Biomolecular coronas provide the biological identity of nanosized materials*. Nat Nano, 2012. **7** (12): 779-786.

27 Lynch, I. and Dawson, K.A., *Protein-nanoparticle interactions*. Nano Today, 2008. **3** (1–2): 40-47.

28 Kim, H.R.; Andrieux, K.; Delomenie, C.; Chacun, H.; Appel, M.; Desmaele, D.; Taran, F.; Georgin, D.; Couvreur, P. and Taverna, M., *Analysis of plasma protein adsorption onto PEGylated nanoparticles by complementary methods: 2-DE, CE and Protein Lab-on-chip system*. Electrophoresis, 2007. **28** (13): 2252-2261.

29 Dell'Orco, D.; Lundqvist, M.; Oslakovic, C.; Cedervall, T. and Linse, S., *Modeling the Time Evolution of the Nanoparticle-Protein Corona in a Body Fluid*. PLoS ONE, 2010. **5** (6): e10949.

30 Walkey, C.D.; Olsen, J.B.; Guo, H.; Emili, A. and Chan, W.C., *Nanoparticle size and surface chemistry determine serum protein adsorption and macrophage uptake*. J Am Chem Soc, 2012. **134** (4): 2139-2147.

31 Nagayama, S.; Ogawara, K.; Fukuoka, Y.; Higaki, K. and Kimura, T., *Time-dependent changes in opsonin amount associated on nanoparticles alter their hepatic uptake characteristics*. Int J Pharm, 2007. **342** (1-2): 215-221.

32 Allemann, E.; Gravel, P.; Leroux, J.C.; Balant, L. and Gurny, R., *Kinetics of blood component adsorption on poly(D,L-lactic acid) nanoparticles: evidence of complement C3 component involvement*. J Biomed Mater Res, 1997. **37** (2): 229-234.

33 Vroman, L., *Effect of absorbed proteins on the wettability of hydrophilic and hydrophobic solids*. Nature, 1962. **196**: 476-477.

34 Vroman, L.; Adams, A.L.; Fischer, G.C. and Munoz, P.C., *Interaction of high molecular weight kininogen, factor XII, and fibrinogen in plasma at interfaces*. Blood, 1980. **55** (1): 156-159.

35 Blunk, T.; Luck, M.; Calvor, A.; Hochstrasser, D.F.; Sanchez, J.C.; Muller, B.W. and Muller, R.H., *Kinetics of plasma protein adsorption on model particles for controlled drug delivery and drug targeting*. European Journal of Pharmaceutics and Biopharmaceutics, 1996. **42** (4): 262-268.

36 Goppert, T.M. and Muller, R.H., *Adsorption kinetics of plasma proteins on solid lipid nanoparticles for drug targeting*. Int J Pharm, 2005. **302** (1-2): 172-186.

37 Jansch, M.; Stumpf, P.; Graf, C.; Rühl, E. and Müller, R.H., *Adsorption kinetics of plasma proteins on ultrasmall superparamagnetic iron oxide (USPIO) nanoparticles*. International Journal of Pharmaceutics, 2012. **428** (1–2): 125-133.

38 Harnisch, S. and Müller, R.H., *Adsorption kinetics of plasma proteins on oil-in-water emulsions for parenteral nutrition*. European Journal of Pharmaceutics and Biopharmaceutics, 2000. **49** (1): 41-46.

39 Dobrovolskaia, M.A.; Neun, B.W.; Man, S.; Ye, X.; Hansen, M.; Patri, A.K.; Crist, R.M. and McNeil, S.E., *Protein corona composition does not accurately predict hematocompatibility of colloidal gold nanoparticles*. Nanomedicine: Nanotechnology, Biology and Medicine, 2014. **10** (7): 1453-1463.

40 Lundqvist, M.; Stigler, J.; Cedervall, T.; Berggard, T.; Flanagan, M.B.; Lynch, I.; Elia, G. and Dawson, K., *The Evolution of the Protein Corona around Nanoparticles: A Test Study*. ACS Nano, 2011. **5** (9): 7503-7509.

41 Hofmann, D.; Tenzer, S.; Bannwarth, M.B.; Messerschmidt, C.; Glaser, S.-F.; Schild, H.; Landfester, K. and Mailänder, V., *Mass Spectrometry and Imaging Analysis of Nanoparticle-Containing Vesicles Provide a Mechanistic Insight into Cellular Trafficking*. ACS Nano, 2014. **8** (10): 10077-10088.

42 Schaffler, M.; Semmler-Behnke, M.; Sarioglu, H.; Takenaka, S.; Wenk, A.; Schleh, C.; Hauck, S.M.; Johnston, B.D. and Kreyling, W.G., *Serum protein identification and quantification of the corona of 5, 15 and 80 nm gold nanoparticles*. Nanotechnology, 2013. **24** (26): 265103.

43 Saie, A.A.; Ray, M.; Mahmoudi, M. and Rotello, V.M., *Engineering the nanoparticle-protein interface for cancer therapeutics*. Cancer Treat Res, 2015. **166**: 245-273.

44 Yang, S.-T.; Liu, Y.; Wang, Y.-W. and Cao, A., *Biosafety and Bioapplication of Nanomaterials by Designing Protein–Nanoparticle Interactions*. Small, 2013. **9** (9-10): 1635-1653.

45 Ehrenberg, M.S.; Friedman, A.E.; Finkelstein, J.N.; Oberdorster, G. and McGrath, J.L., *The influence of protein adsorption on nanoparticle association with cultured endothelial cells*. Biomaterials, 2009. **30** (4): 603-610.

46 Gessner, A.; Waicz, R.; Lieske, A.; Paulke, B.; Mader, K. and Muller, R.H., *Nanoparticles with decreasing surface hydrophobicities: influence on plasma protein adsorption*. Int J Pharm, 2000. **196** (2): 245-249.

47 Wolfram, J.; Yang, Y.; Shen, J.; Moten, A.; Chen, C.; Shen, H.; Ferrari, M. and Zhao, Y., *The nano-plasma interface: Implications of the protein corona*. Colloids and Surfaces B: Biointerfaces, 2014. **124** (0): 17-24.

48 Alexis, F.; Pridgen, E.; Molnar, L.K. and Farokhzad, O.C., *Factors Affecting the Clearance and Biodistribution of Polymeric Nanoparticles*. Molecular Pharmaceutics, 2008. **5** (4): 505-515.

49 Mahmoudi, M.; Lynch, I.; Ejtehadi, M.R.; Monopoli, M.P.; Bombelli, F.B. and Laurent, S., *Protein-nanoparticle interactions: opportunities and challenges*. Chem Rev, 2011. **111** (9): 5610-5637.

50 Fleischer, C.C. and Payne, C.K., *Nanoparticle surface charge mediates the cellular receptors used by protein-nanoparticle complexes*. J Phys Chem B, 2012. **116** (30): 8901-8907.

51 Aggarwal, P.; Hall, J.B.; McLeland, C.B.; Dobrovolskaia, M.A. and McNeil, S.E., *Nanoparticle interaction with plasma proteins as it relates to particle biodistribution, biocompatibility and therapeutic efficacy*. Advanced drug delivery reviews, 2009. **61** (6): 428-437.

52 Gessner, A.; Lieske, A.; Paulke, B.-R. and Müller, R.H., *Functional groups on polystyrene model nanoparticles: Influence on protein adsorption*. Journal of Biomedical Materials Research Part A, 2003. **65A** (3): 319-326.

53 Sakulkhu, U.; Mahmoudi, M.; Maurizi, L.; Salaklang, J. and Hofmann, H., *Protein Corona Composition of Superparamagnetic Iron Oxide Nanoparticles with Various Physico-Chemical Properties and Coatings*. Sci. Rep., 2014. **4**.

54 Gasser, M.; Rothen-Rutishauser, B.; Krug, H.; Gehr, P.; Nelle, M.; Yan, B. and Wick, P., *The adsorption of biomolecules to multi-walled carbon nanotubes is influenced by both pulmonary surfactant lipids and surface chemistry*. Journal of Nanobiotechnology, 2010. **8** (1): 31.

55 Laurent, S.; Burtea, C.; Thirifays, C.; Rezaee, F. and Mahmoudi, M., *Significance of cell "observer" and protein source in nanobiosciences*. J Colloid Interface Sci, 2013. **392**: 431-445.

56 Hajipour, M.J.; Laurent, S.; Aghaie, A.; Rezaee, F. and Mahmoudi, M., *Personalized protein coronas: a "key" factor at the nanobiointerface*. Biomaterials Science, 2014. **2** (9): 1210-1221.

57 Ghavami, M.; Saffar, S.; Abd Emamy, B.; Peirovi, A.; Shokrgozar, M.A.; Serpooshan, V. and Mahmoudi, M., *Plasma concentration gradient influences the protein corona decoration on nanoparticles*. RSC Advances, 2013. **3** (4): 1119-1126.

58 Mahmoudi, M.; Abdelmonem, A.M.; Behzadi, S.; Clement, J.H.; Dutz, S.; Ejtehadi, M.R.; Hartmann, R.; Kantner, K.; Linne, U.; Maffre, P.; Metzler, S.; Moghadam, M.K.; Pfeiffer, C.; Rezaei, M.; Ruiz-Lozano, P.; Serpooshan, V.; Shokrgozar, M.A.; Nienhaus, G.U. and Parak, W.J., *Temperature: The "Ignored" Factor at the NanoBio Interface*. ACS Nano, 2013. **7** (8): 6555-6562.

59 Amoozgar, Z. and Yeo, Y., *Recent advances in stealth coating of nanoparticle drug delivery systems*. Wiley Interdiscip Rev Nanomed Nanobiotechnol, 2012. **4** (2): 219-233.

60 Abuchowski, A.; McCoy, J.R.; Palczuk, N.C.; van Es, T. and Davis, F.F., *Effect of covalent attachment of polyethylene glycol on immunogenicity and circulating life of bovine liver catalase*. J Biol Chem, 1977. **252** (11): 3582-3586.

61 Reddy, K.R.; Wright, T.L.; Pockros, P.J.; Shiffman, M.; Everson, G.; Reindollar, R.; Fried, M.W.; Purdum, P.P.; Jensen, D.; Smith, C.; Lee, W.M.; Boyer, T.D.; Lin, A.; Pedder, S. and DePamphilis, J., *Efficacy and safety of pegylated (40-kd) interferon α-2a compared with interferon α-2a in noncirrhotic patients with chronic hepatitis C*. Hepatology, 2001. **33** (2): 433-438.

62 Gref, R.; Luck, M.; Quellec, P.; Marchand, M.; Dellacherie, E.; Harnisch, S.; Blunk, T. and Muller, R.H., *'Stealth' corona-core nanoparticles surface modified by polyethylene glycol (PEG): influences of the corona (PEG chain length and surface density) and of the core composition on phagocytic uptake and plasma protein adsorption*. Colloids Surf B Biointerfaces, 2000. **18** (3-4): 301-313.

63 Essa, S.; Rabanel, J.M. and Hildgen, P., *Characterization of rhodamine loaded PEG-g-PLA nanoparticles (NPs): effect of poly(ethylene glycol) grafting density*. Int J Pharm, 2011. **411** (1-2): 178-187.

64 Ebrahimnejad, P.; Dinarvand, R.; Jafari, M.R.; Tabasi, S.A. and Atyabi, F., *Characterization, blood profile and biodistribution properties of surface modified PLGA nanoparticles of SN-38*. Int J Pharm, 2011. **406** (1-2): 122-127.

65 Klibanov, A.L.; Maruyama, K.; Torchilin, V.P. and Huang, L., *Amphipathic polyethyleneglycols effectively prolong the circulation time of liposomes*. FEBS Lett, 1990. **268** (1): 235-237.

66 Allen, T.M.; Hansen, C.B. and de Menezes, D.E.L., *Pharmacokinetics of long-circulating liposomes*. Advanced Drug Delivery Reviews, 1995. **16** (2–3): 267-284.

67 Jeon, S.I.; Lee, J.H.; Andrade, J.D. and De Gennes, P.G., *Protein—surface interactions in the presence of polyethylene oxide: I. Simplified theory*. Journal of Colloid and Interface Science, 1991. **142** (1): 149-158.

68 Vonarbourg, A.; Passirani, C.; Saulnier, P. and Benoit, J.P., *Parameters influencing the stealthiness of colloidal drug delivery systems*. Biomaterials, 2006. **27** (24): 4356-4373.

69 Bergström, K.; Holmberg, K.; Safranj, A.; Hoffman, A.S.; Edgell, M.J.; Kozlowski, A.; Hovanes, B.A. and Harris, J.M., *Reduction of fibrinogen adsorption on PEG-coated polystyrene surfaces*. Journal of Biomedical Materials Research, 1992. **26** (6): 779-790.

70 Niidome, T.; Yamagata, M.; Okamoto, Y.; Akiyama, Y.; Takahashi, H.; Kawano, T.; Katayama, Y. and Niidome, Y., *PEG-modified gold nanorods with a stealth character for in vivo applications*. J Control Release, 2006. **114** (3): 343-347.

71 Ishida, T.; Ichihara, M.; Wang, X.; Yamamoto, K.; Kimura, J.; Majima, E. and Kiwada, H., *Injection of PEGylated liposomes in rats elicits PEG-specific IgM, which is responsible for rapid elimination of a second dose of PEGylated liposomes*. J Control Release, 2006. **112** (1): 15-25.

72 Ishida, T. and Kiwada, H., *Anti-polyethyleneglycol antibody response to PEGylated substances*. Biol Pharm Bull, 2013. **36** (6): 889-891.

73 Shah, S.; Prematta, T.; Adkinson, N.F. and Ishmael, F.T., *Hypersensitivity to polyethylene glycols*. J Clin Pharmacol, 2013. **53** (3): 352-355.

74 Bertrand, N. and Leroux, J.C., *The journey of a drug-carrier in the body: an anatomo-physiological perspective*. J Control Release, 2012. **161** (2): 152-163.

75 Brandes, N.; Welzel, P.B.; Werner, C. and Kroh, L.W., *Adsorption-induced conformational changes of proteins onto ceramic particles: Differential scanning calorimetry and FTIR analysis*. Journal of Colloid and Interface Science, 2006. **299** (1): 56-69.

76 Treuel, L. and Nienhaus, G., *Toward a molecular understanding of nanoparticle–protein interactions*. Biophys Rev, 2012. **4** (2): 137-147.

77 Vertegel, A.A.; Siegel, R.W. and Dordick, J.S., *Silica nanoparticle size influences the structure and enzymatic activity of adsorbed lysozyme*. Langmuir, 2004. **20** (16): 6800-6807.

78 Lynch, I.; Dawson, K.A. and Linse, S., *Detecting cryptic epitopes created by nanoparticles*. Sci STKE, 2006. **2006** (327): pe14.

79 Nel, A.E.; Madler, L.; Velegol, D.; Xia, T.; Hoek, E.M.V.; Somasundaran, P.; Klaessig, F.; Castranova, V. and Thompson, M., *Understanding biophysicochemical interactions at the nano-bio interface*. Nat Mater, 2009. **8** (7): 543-557.

80 Mirshafiee, V.; Mahmoudi, M.; Lou, K.; Cheng, J. and Kraft, M.L., *Protein corona significantly reduces active targeting yield*. Chem Commun (Camb), 2013. **49** (25): 2557-2559.

81 Salvati, A.; Pitek, A.S.; Monopoli, M.P.; Prapainop, K.; Bombelli, F.B.; Hristov, D.R.; Kelly, P.M.; Aberg, C.; Mahon, E. and Dawson, K.A., *Transferrin-functionalized nanoparticles lose their targeting capabilities when a biomolecule corona adsorbs on the surface*. Nat Nano, 2013. **8** (2): 137-143.

82 Wang, G.; Papasani, M.R.; Cheguru, P.; Hrdlicka, P.J. and Hill, R.A., *Gold-peptide nanoconjugate cellular uptake is modulated by serum proteins*. Nanomedicine, 2012. **8** (6): 822-832.

83 Patel, P.C.; Giljohann, D.A.; Daniel, W.L.; Zheng, D.; Prigodich, A.E. and Mirkin, C.A., *Scavenger receptors mediate cellular uptake of polyvalent oligonucleotide-functionalized gold nanoparticles*. Bioconjug Chem, 2010. **21** (12): 2250-2256.

84 Jiang, X.; Weise, S.; Hafner, M.; Rocker, C.; Zhang, F.; Parak, W.J. and Nienhaus, G.U., *Quantitative analysis of the protein corona on FePt nanoparticles formed by transferrin binding*. J R Soc Interface, 2010. **7 Suppl 1**: S5-S13.

85 Lesniak, A.; Fenaroli, F.; Monopoli, M.P.; Aberg, C.; Dawson, K.A. and Salvati, A., *Effects of the presence or absence of a protein corona on silica nanoparticle uptake and impact on cells*. ACS Nano, 2012. **6** (7): 5845-5857.

86 Lesniak, A.; Salvati, A.; Santos-Martinez, M.J.; Radomski, M.W.; Dawson, K.A. and Aberg, C., *Nanoparticle adhesion to the cell membrane and its effect on nanoparticle uptake efficiency*. J Am Chem Soc, 2013. **135** (4): 1438-1444.

87 Lunov, O.; Syrovets, T.; Loos, C.; Beil, J.; Delacher, M.; Tron, K.; Nienhaus, G.U.; Musyanovych, A.; Mailander, V.; Landfester, K. and Simmet, T., *Differential uptake of functionalized polystyrene nanoparticles by human macrophages and a monocytic cell line*. ACS Nano, 2011. **5** (3): 1657-1669.

88 Brun, E. and Sicard-Roselli, C., *Could nanoparticle corona characterization help for biological consequence prediction?* Cancer Nanotechnol, 2014. **5** (1): 7.

89 Peng, Q.; Zhang, S.; Yang, Q.; Zhang, T.; Wei, X.Q.; Jiang, L.; Zhang, C.L.; Chen, Q.M.; Zhang, Z.R. and Lin, Y.F., *Preformed albumin corona, a protective coating for nanoparticles based drug delivery system*. Biomaterials, 2013. **34** (33): 8521-8530.

90 Ponka, P. and Lok, C.N., *The transferrin receptor: role in health and disease*. Int J Biochem Cell Biol, 1999. **31** (10): 1111-1137.

91 Schnitzer, J.E., *gp60 is an albumin-binding glycoprotein expressed by continuous endothelium involved in albumin transcytosis*. Am J Physiol, 1992. **262** (1 Pt 2): H246-254.

92 Kim, H.R.; Gil, S.; Andrieux, K.; Nicolas, V.; Appel, M.; Chacun, H.; Desmaele, D.; Taran, F.; Georgin, D. and Couvreur, P., *Low-density lipoprotein receptor-mediated endocytosis of PEGylated nanoparticles in rat brain endothelial cells*. Cell Mol Life Sci, 2007. **64** (3): 356-364.

93 Zannis, V.I.; Chroni, A. and Krieger, M., *Role of apoA-I, ABCA1, LCAT, and SR-BI in the biogenesis of HDL*. J Mol Med (Berl), 2006. **84** (4): 276-294.

94 Kim, H.R.; Andrieux, K.; Gil, S.; Taverna, M.; Chacun, H.; Desmaele, D.; Taran, F.; Georgin, D. and Couvreur, P., *Translocation of poly(ethylene glycol-co-hexadecyl)cyanoacrylate nanoparticles into rat brain endothelial cells: Role of apolipoproteins in receptor-mediated endocytosis*. Biomacromolecules, 2007. **8** (3): 793-799.

95 Kreuter, J., *Nanoparticulate systems for brain delivery of drugs*. Advanced Drug Delivery Reviews, 2012. **64** (0): 213-222.

96 Kreuter, J.; Hekmatara, T.; Dreis, S.; Vogel, T.; Gelperina, S. and Langer, K., *Covalent attachment of apolipoprotein A-I and apolipoprotein B-100 to albumin nanoparticles enables drug transport into the brain*. J Control Release, 2007. **118** (1): 54-58.

97 Michaelis, K.; Hoffmann, M.M.; Dreis, S.; Herbert, E.; Alyautdin, R.N.; Michaelis, M.; Kreuter, J. and Langer, K., *Covalent Linkage of Apolipoprotein E to Albumin Nanoparticles Strongly Enhances Drug Transport into the Brain*. Journal of Pharmacology and Experimental Therapeutics, 2006. **317** (3): 1246-1253.

98 Zensi, A.; Begley, D.; Pontikis, C.; Legros, C.; Mihoreanu, L.; Wagner, S.; Büchel, C.; von Briesen, H. and Kreuter, J., *Albumin nanoparticles targeted with Apo E enter the CNS by transcytosis and are delivered to neurones*. Journal of Controlled Release, 2009. **137** (1): 78-86.

99 Bisgaier, C.L.; Siebenkas, M.V. and Williams, K.J., *Effects of apolipoproteins A-IV and A-I on the uptake of phospholipid liposomes by hepatocytes*. J Biol Chem, 1989. **264** (2): 862-866.

100 Rensen, P.C.; van Dijk, M.C.; Havenaar, E.C.; Bijsterbosch, M.K.; Kruijt, J.K. and van Berkel, T.J., *Selective liver targeting of antivirals by recombinant chylomicrons--a new therapeutic approach to hepatitis B*. Nat Med, 1995. **1** (3): 221-225.

101 Nagayama, S.; Ogawara, K.i.; Minato, K.; Fukuoka, Y.; Takakura, Y.; Hashida, M.; Higaki, K. and Kimura, T., *Fetuin mediates hepatic uptake of negatively charged nanoparticles via scavenger receptor*. International Journal of Pharmaceutics, 2007. **329** (1-2): 192-198.

102 Cifuentes-Rius, A.; de Puig, H.; Kah, J.C.Y.; Borros, S. and Hamad-Schifferli, K., *Optimizing the Properties of the Protein Corona Surrounding Nanoparticles for Tuning Payload Release*. ACS Nano, 2013. **7** (11): 10066-10074.

103 Kah, J.C.; Chen, J.; Zubieta, A. and Hamad-Schifferli, K., *Exploiting the protein corona around gold nanorods for loading and triggered release*. ACS Nano, 2012. **6** (8): 6730-6740.

104 Walkey, C.D.; Olsen, J.B.; Song, F.Y.; Liu, R.; Guo, H.B.; Olsen, D.W.H.; Cohen, Y.; Emili, A. and Chan, W.C.W., *Protein Corona Fingerprinting Predicts the Cellular Interaction of Gold and Silver Nanoparticles*. ACS Nano, 2014. **8** (3): 2439-2455.

105 Royer, C.A., *Probing Protein Folding and Conformational Transitions with Fluorescence*. Chemical Reviews, 2006. **106** (5): 1769-1784.

106 Shang, L.; Wang, Y.; Jiang, J. and Dong, S., *pH-Dependent Protein Conformational Changes in Albumin:Gold Nanoparticle Bioconjugates: A Spectroscopic Study*. Langmuir, 2007. **23** (5): 2714-2721.

107 Rocker, C.; Potzl, M.; Zhang, F.; Parak, W.J. and Nienhaus, G.U., *A quantitative fluorescence study of protein monolayer formation on colloidal nanoparticles*. Nat Nano, 2009. **4** (9): 577-580.

108 Baier, G.; Costa, C.; Zeller, A.; Baumann, D.; Sayer, C.; Araujo, P.H.H.; Mailänder, V.; Musyanovych, A. and Landfester, K., *BSA Adsorption on Differently Charged Polystyrene Nanoparticles using Isothermal Titration Calorimetry and the Influence on Cellular Uptake*. Macromolecular Bioscience, 2011. **11** (5): 628-638.

109 Winzen, S.; Schoettler, S.; Baier, G.; Rosenauer, C.; Mailaender, V.; Landfester, K. and Mohr, K., *Complementary analysis of the hard and soft protein corona: sample preparation critically effects corona composition*. Nanoscale, 2015. **7** (7): 2992-3001.

110 Cheng, Y.; Wang, M.; Borghs, G. and Chen, H., *Gold Nanoparticle Dimers for Plasmon Sensing*. Langmuir, 2011. **27** (12): 7884-7891.

111 Linse, S.; Cabaleiro-Lago, C.; Xue, W.-F.; Lynch, I.; Lindman, S.; Thulin, E.; Radford, S.E. and Dawson, K.A., *Nucleation of protein fibrillation by nanoparticles*. Proceedings of the National Academy of Sciences, 2007. **104** (21): 8691-8696.

112 Pitek, A.S.; O'Connell, D.; Mahon, E.; Monopoli, M.P.; Baldelli Bombelli, F. and Dawson, K.A., *Transferrin Coated Nanoparticles: Study of the Bionano Interface in Human Plasma*. PLoS ONE, 2012. **7** (7): e40685.

113 Delfino, I. and Cannistraro, S., *Optical investigation of the electron transfer protein azurin-gold nanoparticle system*. Biophys Chem, 2009. **139** (1): 1-7.

114 Bhattacharya, J.; Choudhuri, U.; Siwach, O.; Sen, P. and Dasgupta, A.K., *Interaction of hemoglobin and copper nanoparticles: implications in hemoglobinopathy*. Nanomedicine: Nanotechnology, Biology and Medicine, 2006. **2** (3): 191-199.

115 Deng, Z.J.; Liang, M.; Monteiro, M.; Toth, I. and Minchin, R.F., *Nanoparticle-induced unfolding of fibrinogen promotes Mac-1 receptor activation and inflammation*. Nat Nano, 2011. **6** (1): 39-44.

116 Lacerda, S.H.D.P.; Park, J.J.; Meuse, C.; Pristinski, D.; Becker, M.L.; Karim, A. and Douglas, J.F., *Interaction of Gold Nanoparticles with Common Human Blood Proteins*. ACS Nano, 2010. **4** (1): 365-379.

117 Chittur, K.K., *FTIR/ATR for protein adsorption to biomaterial surfaces*. Biomaterials, 1998. **19** (4-5): 357-369.

118 Wang, T.; Bai, J.; Jiang, X. and Nienhaus, G.U., *Cellular uptake of nanoparticles by membrane penetration: a study combining confocal microscopy with FTIR spectroelectrochemistry*. ACS Nano, 2012. **6** (2): 1251-1259.

119 Shao, M.; Lu, L.; Wang, H.; Luo, S. and Ma, D., *Microfabrication of a new sensor based on silver and silicon nanomaterials, and its application to the enrichment and detection of bovine serum albumin via surface-enhanced Raman scattering*. Microchim Acta, 2009. **164** (1-2): 157-160.

120 Shen, X.C.; Liou, X.Y.; Ye, L.P.; Liang, H. and Wang, Z.Y., *Spectroscopic studies on the interaction between human hemoglobin and CdS quantum dots*. J Colloid Interface Sci, 2007. **311** (2): 400-406.

121 Xu, L.-J.; Zong, C.; Zheng, X.-S.; Hu, P.; Feng, J.-M. and Ren, B., *Label-Free Detection of Native Proteins by Surface-Enhanced Raman Spectroscopy Using Iodide-Modified Nanoparticles*. Analytical Chemistry, 2014. **86** (4): 2238-2245.

122 Klein, J., *Probing the interactions of proteins and nanoparticles*. Proc Natl Acad Sci U S A, 2007. **104** (7): 2029-2030.

123 Capriotti, A.; Caracciolo, G.; Cavaliere, C.; Colapicchioni, V.; Piovesana, S.; Pozzi, D. and Laganà, A., *Analytical Methods for Characterizing the Nanoparticle–Protein Corona*. Chromatographia, 2014. **77** (11-12): 755-769.

124 Mahmoudi, M.; Shokrgozar, M.A.; Sardari, S.; Moghadam, M.K.; Vali, H.; Laurent, S. and Stroeve, P., *Irreversible changes in protein conformation due to interaction with superparamagnetic iron oxide nanoparticles*. Nanoscale, 2011. **3** (3): 1127-1138.

125 Mahmoudi, M.; Sant, S.; Wang, B.; Laurent, S. and Sen, T., *Superparamagnetic iron oxide nanoparticles (SPIONs): Development, surface modification and applications in chemotherapy*. Advanced Drug Delivery Reviews, 2011. **63** (1–2): 24-46.

126 Thode, K.; Luck, M.; Semmler, W.; Muller, R.H. and Kresse, M., *Determination of plasma protein adsorption on magnetic iron oxides: sample preparation*. Pharm Res, 1997. **14** (7): 905-910.

127 Kotman, N., *Nanopartikel-Protein-Interaktionen.* PhD Thesis, Max Planck Institute for Polymer Research, Johannes Gutenberg-Universität Mainz, 2013.

128 Ritz, S.; Schöttler, S.; Kotman, N.; Baier, G.; Musyanovych, A.; Kuharev, J.; Landfester, K.; Schild, H.; Jahn, O.; Tenzer, S. and Mailänder, V., *Protein Corona of Nanoparticles: Distinct Proteins Regulate the Cellular Uptake*. Biomacromolecules, 2015. **16** (4): 1311-1321.

129 Neuhoff, V.; Stamm, R. and Eibl, H., *Clear background and highly sensitive protein staining with Coomassie Blue dyes in polyacrylamide gels: A systematic analysis*. ELECTROPHORESIS, 1985. **6** (9): 427-448.

130 Smejkal, G.B., *The Coomassie chronicles: past, present and future perspectives in polyacrylamide gel staining*. Expert Rev Proteomics, 2004. **1** (4): 381-387.

131 Patton, W.F., *Detection technologies in proteome analysis*. Journal of Chromatography B, 2002. **771** (1–2): 3-31.

132 Sasse, J. and Gallagher, S.R., *Staining proteins in gels*. Curr Protoc Immunol, 2004. **Chapter 8**: Unit 8 9.

133 Gessner, A.; Lieske, A.; Paulke, B.R. and Müller, R.H., *Influence of surface charge density on protein adsorption on polymeric nanoparticles: analysis by two-dimensional electrophoresis*. European Journal of Pharmaceutics and Biopharmaceutics, 2002. **54** (2): 165-170.

134 Lemarchand, C.; Gref, R.; Passirani, C.; Garcion, E.; Petri, B.; Muller, R.; Costantini, D. and Couvreur, P., *Influence of polysaccharide coating on the interactions of nanoparticles with biological systems*. Biomaterials, 2006. **27** (1): 108-118.

135 Dobrovolskaia, M.A.; Patri, A.K.; Zheng, J.; Clogston, J.D.; Ayub, N.; Aggarwal, P.; Neun, B.W.; Hall, J.B. and McNeil, S.E., *Interaction of colloidal gold nanoparticles with human blood: effects on particle size and analysis of plasma protein binding profiles*. Nanomedicine: Nanotechnology, Biology and Medicine, 2009. **5** (2): 106-117.

136 Burkhart, J.M.; Schumbrutzki, C.; Wortelkamp, S.; Sickmann, A. and Zahedi, R.P., *Systematic and quantitative comparison of digest efficiency and specificity reveals the impact of trypsin quality on MS-based proteomics*. Journal of Proteomics, 2012. **75** (4): 1454-1462.

137 Karas, M.; Bahr, U. and Dülcks, T., *Nano-electrospray ionization mass spectrometry: addressing analytical problems beyond routine*. Fresenius J Anal Chem, 2000. **366** (6-7): 669-676.

138 Waters Corporation, USA, 2015. .

139 Zhu, W.; Smith, J.W. and Huang, C.-M., *Mass Spectrometry-Based Label-Free Quantitative Proteomics*. Journal of Biomedicine and Biotechnology, 2010. **2010**: 6.

140 Bantscheff, M.; Schirle, M.; Sweetman, G.; Rick, J. and Kuster, B., *Quantitative mass spectrometry in proteomics: a critical review*. Anal Bioanal Chem, 2007. **389** (4): 1017-1031.

141 Silva, J.C.; Gorenstein, M.V.; Li, G.Z.; Vissers, J.P. and Geromanos, S.J., *Absolute quantification of proteins by LCMSE: a virtue of parallel MS acquisition*. Mol Cell Proteomics, 2006. **5** (1): 144-156.

142 Patzig, J.; Jahn, O.; Tenzer, S.; Wichert, S.P.; de Monasterio-Schrader, P.; Rosfa, S.; Kuharev, J.; Yan, K.; Bormuth, I.; Bremer, J.; Aguzzi, A.; Orfaniotou, F.; Hesse, D.; Schwab, M.H.; Mobius, W.; Nave, K.A. and Werner, H.B., *Quantitative and integrative proteome analysis of peripheral nerve myelin identifies novel myelin proteins and candidate neuropathy loci*. J Neurosci, 2011. **31** (45): 16369-16386.

143 Bradshaw, R.A.; Burlingame, A.L.; Carr, S. and Aebersold, R., *Reporting protein identification data: the next generation of guidelines*. Mol Cell Proteomics, 2006. **5** (5): 787-788.

144 Freichels, H.; Wagner, M.; Okwieka, P.; Meyer, R.G.; Mailander, V.; Landfester, K. and Musyanovych, A., *(Oligo)mannose functionalized hydroxyethyl starch nanocapsules: en route to drug delivery systems with targeting properties*. Journal of Materials Chemistry B, 2013. **1** (34): 4338-4348.

145 Loos, C.; Syrovets, T.; Musyanovych, A.; Mailander, V.; Landfester, K.; Nienhaus, G.U. and Simmet, T., *Functionalized polystyrene nanoparticles as a platform for studying bio-nano interactions*. Beilstein J Nanotechnol, 2014. **5**: 2403-2412.

146 Landfester, K., *Synthesis of colloidal particles in miniemulsions*. Annual Review of Materials Research, 2006. **36** (1): 231-279.

147 Alkilany, A.M.; Nagaria, P.K.; Hexel, C.R.; Shaw, T.J.; Murphy, C.J. and Wyatt, M.D., *Cellular uptake and cytotoxicity of gold nanorods: molecular origin of cytotoxicity and surface effects*. Small, 2009. **5** (6): 701-708.

148 Wessel, D. and Flügge, U.I., *A method for the quantitative recovery of protein in dilute solution in the presence of detergents and lipids*. Analytical Biochemistry, 1984. **138** (1): 141-143.

149 Thiagarajan, P.; Le, A. and Benedict, C.R., *Beta(2)-glycoprotein I promotes the binding of anionic phospholipid vesicles by macrophages*. Arterioscler Thromb Vasc Biol, 1999. **19** (11): 2807-2811.

150 Chonn, A.; Semple, S.C. and Cullis, P.R., *Beta 2 glycoprotein I is a major protein associated with very rapidly cleared liposomes in vivo, suggesting a significant role in the immune clearance of "non-self" particles*. J Biol Chem, 1995. **270** (43): 25845-25849.

151 Miyakis, S.; Giannakopoulos, B. and Krilis, S.A., *Beta 2 glycoprotein I--function in health and disease*. Thromb Res, 2004. **114** (5-6): 335-346.

152 Sheng, Y.; Sali, A.; Herzog, H.; Lahnstein, J. and Krilis, S.A., *Site-directed mutagenesis of recombinant human beta 2-glycoprotein I identifies a cluster of lysine residues that are critical for phospholipid binding and anti-cardiolipin antibody activity*. J Immunol, 1996. **157** (8): 3744-3751.

153 Mohr, K.; Sommer, M.; Baier, G.; Schöttler, S.; Okwieka, P.; Tenzer, S.; Landfester, K.; Mailänder, V.; Schmidt, M. and Meyer, R.G., *Aggregation Behavior of Polystyrene-Nanoparticles in Human Blood Serum and its Impact on the in vivo Distribution in Mice*. J Nanomed Nanotechnol 2014. **5** (2): 193.

154 Adjei, I.M.; Peetla, C. and Labhasetwar, V., *Heterogeneity in nanoparticles influences biodistribution and targeting*. Nanomedicine (Lond), 2014. **9** (2): 267-278.

155 Kodama, T.; Doi, T.; Suzuki, H.; Takahashi, K.; Wada, Y. and Gordon, S., *Collagenous macrophage scavenger receptors*. Curr Opin Lipidol, 1996. **7** (5): 287-291.

156 Krieger, M. and Herz, J., *Structures and functions of multiligand lipoprotein receptors: macrophage scavenger receptors and LDL receptor-related protein (LRP)*. Annu Rev Biochem, 1994. **63**: 601-637.

157 Laskin, D.L.; Weinberger, B. and Laskin, J.D., *Functional heterogeneity in liver and lung macrophages*. J Leukoc Biol, 2001. **70** (2): 163-170.

158 Neyen, C.; Pluddemann, A.; Mukhopadhyay, S.; Maniati, E.; Bossard, M.; Gordon, S. and Hagemann, T., *Macrophage scavenger receptor a promotes tumor progression in murine models of ovarian and pancreatic cancer*. J Immunol, 2013. **190** (7): 3798-3805.

159 Hirsjarvi, S.; Dufort, S.; Gravier, J.; Texier, I.; Yan, Q.; Bibette, J.; Sancey, L.; Josserand, V.; Passirani, C.; Benoit, J.P. and Coll, J.L., *Influence of size, surface coating and fine chemical composition on the in vitro reactivity and in vivo biodistribution of lipid nanocapsules versus lipid nanoemulsions in cancer models*. Nanomedicine, 2013. **9** (3): 375-387.

160 Doshi, N. and Mitragotri, S., *Macrophages recognize size and shape of their targets*. PLoS One, 2010. **5** (4): e10051.

161 Champion, J.A.; Walker, A. and Mitragotri, S., *Role of particle size in phagocytosis of polymeric microspheres*. Pharm Res, 2008. **25** (8): 1815-1821.

162 Helmy, K.Y.; Katschke, K.J., Jr.; Gorgani, N.N.; Kljavin, N.M.; Elliott, J.M.; Diehl, L.; Scales, S.J.; Ghilardi, N. and van Lookeren Campagne, M., *CRIg: a macrophage complement receptor required for phagocytosis of circulating pathogens*. Cell, 2006. **124** (5): 915-927.

163 Bhanumathy, C.D.; Tang, Y.; Monga, S.P.; Katuri, V.; Cox, J.A.; Mishra, B. and Mishra, L., *Itih-4, a serine protease inhibitor regulated in interleukin-6-dependent liver formation: role in liver development and regeneration*. Dev Dyn, 2002. **223** (1): 59-69.

164 Becker, G., *The "Stealth Effect" of Poly(phosphoester)s.* Diploma Thesis, Max Planck Institute for Polymer Research, Johannes Gutenberg-Universität Mainz, 2013.

165 Shannan, B.; Seifert, M.; Leskov, K.; Willis, J.; Boothman, D.; Tilgen, W. and Reichrath, J., *Challenge and promise: roles for clusterin in pathogenesis, progression and therapy of cancer*. Cell Death Differ, 2005. **13** (1): 12-19.

166 Jenne, D.E. and Tschopp, J., *Clusterin: the intriguing guises of a widely expressed glycoprotein*. Trends Biochem Sci, 1992. **17** (4): 154-159.

167 Gelissen, I.C.; Hochgrebe, T.; Wilson, M.R.; Easterbrook-Smith, S.B.; Jessup, W.; Dean, R.T. and Brown, A.J., *Apolipoprotein J (clusterin) induces cholesterol export from macrophage-foam cells: a potential anti-atherogenic function?* Biochem J, 1998. **331 (Pt 1)**: 231-237.

168 Thiele, L.; Diederichs, J.E.; Reszka, R.; Merkle, H.P. and Walter, E., *Competitive adsorption of serum proteins at microparticles affects phagocytosis by dendritic cells*. Biomaterials, 2003. **24** (8): 1409-1418.

169 Silajdzic, E.; Minthon, L.; Bjorkqvist, M. and Hansson, O., *No diagnostic value of plasma clusterin in Alzheimer's disease*. PLoS One, 2012. **7** (11): e50237.

170 Poon, S.; Easterbrook-Smith, S.B.; Rybchyn, M.S.; Carver, J.A. and Wilson, M.R., *Clusterin is an ATP-independent chaperone with very broad substrate specificity that stabilizes stressed proteins in a folding-competent state*. Biochemistry, 2000. **39** (51): 15953-15960.

171 Holzapfel, V.; Musyanovych, A.; Landfester, K.; Lorenz, M.R. and Mailänder, V., *Preparation of Fluorescent Carboxyl and Amino Functionalized Polystyrene Particles by Miniemulsion Polymerization as Markers for Cells*. Macromolecular Chemistry and Physics, 2005. **206** (24): 2440-2449.

172 Fichter, M.; Baier, G.; Dedters, M.; Pretsch, L.; Pietrzak-Nguyen, A.; Landfester, K. and Gehring, S., *Nanocapsules generated out of a polymeric dexamethasone shell suppress the inflammatory response of liver macrophages*. Nanomedicine: Nanotechnology, Biology and Medicine, **9** (8): 1223-1234.

173 Baier, G.; Baumann, D.; Siebert, J.M.; Musyanovych, A.; Mailander, V. and Landfester, K., *Suppressing unspecific cell uptake for targeted delivery using hydroxyethyl starch nanocapsules*. Biomacromolecules, 2012. **13** (9): 2704-2715.

174 Kang, B.; Okwieka, P.; Schöttler, S.; Seifert, O.; Kontermann, R.E.; Pfizenmaier, K.; Musyanovych, A.; Meyer, R.; Diken, M.; Sahin, U.; Mailänder, V.; Wurm, F.R. and Landfester, K., *Tailoring the stealth properties of biocompatible polysaccharide nanocontainers*. Biomaterials, 2015. **49** (0): 125-134.

175 Besheer, A.; Vogel, J.; Glanz, D.; Kressler, J.; Groth, T. and Mäder, K., *Characterization of PLGA Nanospheres Stabilized with Amphiphilic Polymers: Hydrophobically Modified Hydroxyethyl Starch vs Pluronics*. Molecular Pharmaceutics, 2009. **6** (2): 407-415.

176 Kang, B.; Okwieka, P.; Schöttler, S.; Winzen, S.; Langhanki, J.; Mohr, K.; Opatz, T.; Mailander, V.; Landfester, K. and Wurm, F.R., *Carbohydrate-Based Nanocarriers Exhibiting Specific Cell Targeting with Minimum Influence from the Protein Corona*. Angew Chem Int Ed Engl, 2015. n/a-n/a.

177 Van Kooyk, Y., *C-type lectins on dendritic cells: key modulators for the induction of immune responses*. Biochem Soc Trans, 2008. **36** (Pt 6): 1478-1481.

178 Guo, M.; Gong, S.; Maric, S.; Misulovin, Z.; Pack, M.; Mahnke, K.; Nussenzweig, M.C. and Steinman, R.M., *A monoclonal antibody to the DEC-205 endocytosis receptor on human dendritic cells*. Human Immunology, 2000. **61** (8): 729-738.

179 Chevallet, M.; Luche, S. and Rabilloud, T., *Silver staining of proteins in polyacrylamide gels*. Nature Protocols, 2006. **1** (4): 1852-1858.

180 Timpl, R.; Sasaki, T.; Kostka, G. and Chu, M.-L., *Fibulins: a versatile family of extracellular matrix proteins*. Nat Rev Mol Cell Biol, 2003. **4** (6): 479-489.

181 Okwieka, P., *In vivo targeting von humanen dendritischen Zellen mit Hilfe von polymeren Nanocarriern.* PhD Thesis, Universitätsmedizin der Johannes Gutenberg-Universität Mainz, Johannes Gutenberg-Universität Mainz, 2015.

182 McKee, P.A.; Rogers, L.A.; Marler, E. and Hill, R.L., *The subunit polypeptides of human fibrinogen*. Arch Biochem Biophys, 1966. **116** (1): 271-279.

183 BD Diagnostics, *Preanalytical Systems - Product Catalogue*, 2009/10.

184 Baumann, D.; Hofmann, D.; Nullmeier, S.; Panther, P.; Dietze, C.; Musyanovych, A.; Ritz, S.; Landfester, K. and Mailander, V., *Complex encounters: nanoparticles in whole blood and their uptake into different types of white blood cells*. Nanomedicine (Lond), 2013. **8** (5): 699-713.

185 Shriver, Z.; Capila, I.; Venkataraman, G. and Sasisekharan, R., *Heparin and Heparan Sulfate: Analyzing Structure and Microheterogeneity*. Handbook of experimental pharmacology, 2012. (207): 159-176.

186 Mousa, S.A. and Petersen, L.J., *Anti-cancer properties of low-molecular-weight heparin: preclinical evidence*. Thromb Haemost, 2009. **102** (2): 258-267.

187 Linhardt, R.J., *2003 Claude S. Hudson Award address in carbohydrate chemistry. Heparin: structure and activity*. J Med Chem, 2003. **46** (13): 2551-2564.

188 Harush-Frenkel, O.; Debotton, N.; Benita, S. and Altschuler, Y., *Targeting of nanoparticles to the clathrin-mediated endocytic pathway*. Biochemical and Biophysical Research Communications, 2007. **353** (1): 26-32.

189 Gratton, S.E.A.; Ropp, P.A.; Pohlhaus, P.D.; Luft, J.C.; Madden, V.J.; Napier, M.E. and DeSimone, J.M., *The effect of particle design on cellular internalization pathways*. Proceedings of the National Academy of Sciences of the United States of America, 2008. **105** (33): 11613-11618.

190 Verma, A. and Stellacci, F., *Effect of Surface Properties on Nanoparticle–Cell Interactions*. Small, 2010. **6** (1): 12-21.

191 Ekre, H.P.; Naparstek, Y.; Lider, O.; Hyden, P.; Hagermark, O.; Nilsson, T.; Vlodavsky, I. and Cohen, I., *Anti-inflammatory effects of heparin and its derivatives: inhibition of complement and of lymphocyte migration*. Adv Exp Med Biol, 1992. **313**: 329-340.

192 Lappegard, K.T.; Fung, M.; Bergseth, G.; Riesenfeld, J.; Lambris, J.D.; Videm, V. and Mollnes, T.E., *Effect of complement inhibition and heparin coating on artificial surface-induced leukocyte and platelet activation*. Ann Thorac Surg, 2004. **77** (3): 932-941.

193 Passirani, C.; Barratt, G.; Devissaguet, J.P. and Labarre, D., *Interactions of nanoparticles bearing heparin or dextran covalently bound to poly(methyl methacrylate) with the complement system*. Life Sci, 1998. **62** (8): 775-785.

194 Socha, M.; Lamprecht, A.; El Ghazouani, F.; Emond, E.; Maincent, P.; Barre, J.; Hoffman, M. and Ubrich, N., *Increase in the vascular residence time of propranolol-loaded nanoparticles coated with heparin*. J Nanosci Nanotechnol, 2008. **8** (5): 2369-2376.

195 Passirani, C.; Barratt, G.; Devissaguet, J.P. and Labarre, D., *Long-circulating nanoparticles bearing heparin or dextran covalently bound to poly(methyl methacrylate)*. Pharm Res, 1998. **15** (7): 1046-1050.

196 Socha, M.; Bartecki, P.; Passirani, C.; Sapin, A.; Damge, C.; Lecompte, T.; Barre, J.; El Ghazouani, F. and Maincent, P., *Stealth nanoparticles coated with heparin as peptide or protein carriers*. J Drug Target, 2009. **17** (8): 575-585.

197 Jaulin, N.; Appel, M.; Passirani, C.; Barratt, G. and Labarre, D., *Reduction of the uptake by a macrophagic cell line of nanoparticles bearing heparin or dextran covalently bound to poly(methyl methacrylate)*. J Drug Target, 2000. **8** (3): 165-172.

198 Baier, G.; Winzen, S.; Messerschmidt, C.; Frank, D.; Fichter, M.; Gehring, S.; Mailänder, V. and Landfester, K., *Heparin-Based Nanocapsules as Potential Drug Delivery Systems*. Macromolecular Bioscience, 2015. n/a-n/a.

199 Chung, Y.-I.; Kim, J.C.; Kim, Y.H.; Tae, G.; Lee, S.-Y.; Kim, K. and Kwon, I.C., *The effect of surface functionalization of PLGA nanoparticles by heparin- or chitosan-conjugated Pluronic on tumor targeting*. Journal of Controlled Release, 2010. **143** (3): 374-382.

200 Kuo, C.C. and Grayston, T., *Interaction of Chlamydia trachomatis organisms and HeLa 229 cells*. Infect Immun, 1976. **13** (4): 1103-1109.

201 Zhang, J.P. and Stephens, R.S., *Mechanism of C. trachomatis attachment to eukaryotic host cells*. Cell, 1992. **69** (5): 861-869.

202 Gutierrez-Martin, C.B.; Ojcius, D.M.; Hsia, R.; Hellio, R.; Bavoil, P.M. and Dautry-Varsat, A., *Heparin-mediated inhibition of Chlamydia psittaci adherence to HeLa cells*. Microb Pathog, 1997. **22** (1): 47-57.

203 Stephens, R.S.; Fawaz, F.S.; Kennedy, K.A.; Koshiyama, K.; Nichols, B.; van Ooij, C. and Engel, J.N., *Eukaryotic Cell Uptake of Heparin-Coated Microspheres: a Model of Host Cell Invasion by Chlamydia trachomatis*. Infection and Immunity, 2000. **68** (3): 1080-1085.

204 Bleiberg, I.; MacGregor, I. and Aronson, M., *Heparin receptors on mouse macrophages*. Thrombosis Research, 1983. **29** (1): 53-61.

205 Falcone, D.J., *Heparin stimulation of plasminogen activator secretion by macrophage-like cell line RAW264.7: role of the scavenger receptor*. J Cell Physiol, 1989. **140** (2): 219-226.

206 Stehle, G.; Friedrich, E.A.; Sinn, H.; Wunder, A.; Harenberg, J.; Dempfle, C.E.; Maier-Borst, W. and Heene, D.L., *Hepatic uptake of a modified low molecular weight heparin in rats*. The Journal of Clinical Investigation, 1992. **90** (5): 2110-2116.

207 Lindstedt, K.A.; Kokkonen, J.O. and Kovanen, P.T., *Soluble heparin proteoglycans released from stimulated mast cells induce uptake of low density lipoproteins by macrophages via scavenger receptor-mediated phagocytosis*. J Lipid Res, 1992. **33** (1): 65-75.

208 Bannwarth, M.B.; Kazer, S.W.; Ulrich, S.; Glasser, G.; Crespy, D. and Landfester, K., *Well-Defined Nanofibers with Tunable Morphology from Spherical Colloidal Building Blocks*. Angewandte Chemie International Edition, 2013. **52** (38): 10107-10111.

209 Bannwarth, M.B.; Ebert, S.; Lauck, M.; Ziener, U.; Tomcin, S.; Jakob, G.; Munnemann, K.; Mailander, V.; Musyanovych, A. and Landfester, K., *Tailor-made nanocontainers for combined magnetic-field-induced release and MRI*. Macromol Biosci, 2014. **14** (9): 1205-1214.

210 Plouffe, B.D.; Murthy, S.K. and Lewis, L.H., *Fundamentals and application of magnetic particles in cell isolation and enrichment: a review*. Reports on Progress in Physics, 2015. **78** (1): 016601.

211 Polyak, B. and Friedman, G., *Magnetic targeting for site-specific drug delivery: Applications and clinical potential*. Expert Opinion on Drug Delivery, 2009. **6** (1): 53-70.

212 Mackie, I.J.; Kitchen, S.; Machin, S.J. and Lowe, G.D., *Guidelines on fibrinogen assays*. Br J Haematol, 2003. **121** (3): 396-404.

213 Nicholson, J.P.; Wolmarans, M.R. and Park, G.R., *The role of albumin in critical illness*. British Journal of Anaesthesia, 2000. **85** (4): 599-610.

214 Stiehm, E.R. and Fudenberg, H.H., *SERUM LEVELS OF IMMUNE GLOBULINS IN HEALTH AND DISEASE: A SURVEY*. Pediatrics, 1966. **37** (5): 715-727.

215 Gonzalez-Quintela, A.; Alende, R.; Gude, F.; Campos, J.; Rey, J.; Meijide, L.M.; Fernandez-Merino, C. and Vidal, C., *Serum levels of immunoglobulins (IgG, IgA, IgM) in a general adult population and their relationship with alcohol consumption, smoking and common metabolic abnormalities*. Clinical and Experimental Immunology, 2008. **151** (1): 42-50.

216 Tirumalai, R.S.; Chan, K.C.; Prieto, D.A.; Issaq, H.J.; Conrads, T.P. and Veenstra, T.D., *Characterization of the low molecular weight human serum proteome*. Mol Cell Proteomics, 2003. **2** (10): 1096-1103.

217 Sakulkhu, U.; Maurizi, L.; Mahmoudi, M.; Motazacker, M.; Vries, M.; Gramoun, A.; Ollivier Beuzelin, M.-G.; Vallee, J.-P.; Rezaee, F. and Hofmann, H., *Ex situ evaluation of the composition of protein corona of intravenously injected superparamagnetic nanoparticles in rats*. Nanoscale, 2014. **6** (19): 11439-11450.

218 Jedlovszky-Hajdú, A.; Bombelli, F.B.; Monopoli, M.P.; Tombácz, E. and Dawson, K.A., *Surface Coatings Shape the Protein Corona of SPIONs with Relevance to Their Application in Vivo*. Langmuir, 2012. **28** (42): 14983-14991.

219 Vilaseca, P.; Dawson, K.A. and Franzese, G., *Understanding and modulating the competitive surface-adsorption of proteins through coarse-grained molecular dynamics simulations*. Soft Matter, 2013. **9** (29): 6978-6985.

7 APPENDIX

7.1 ABBREVIATIONS

Table 7-1: List of abbreviations

Abbreviation	Name
2D-GE	Two-dimensional gel electrophoresis
7-AAD	7-Aminoactinomycin D
AA	Acrylic acid
AEMH	Aminoethyl methacrylate hydrochloride
ALBU	Serum albumin
ANT3	Antithrombin III
APOA1	Apolipoprotein A-I
APOA4	Apolipoprotein A-IV
APOB	Apolipoprotein B-100
APOC2	Apolipoprotein C-II
APOC3	Apolipoprotein C-III
APOD	Apolipoprotein D
APOH	Apolipoprotein H/Beta 2 glycoprotein
APOM	Apolipoprotein M
BNC2	Basonuclin 2
BSA	Bovine Serum Albumin
C12-PET	12-Methacrylamidododecylphosphonic acid
C1QA	Complement C1q subcomponent subunit A
C1QB	Complement C1q subcomponent subunit B
C1QC	Complement C1q subcomponent subunit C
C1R	Complement C1r subcomponent
C1S	Complement C1s subcomponent
C4BPA	C4b binding protein alpha chain
C4BPB	C4b binding protein beta chain
CD	circular dichroism
CFAH	Complement factor H
CHAPS	3-[(3-Cholamidopropyl)dimethylammonio]-1-propanesulfonate
CLSM	Confocal laser scanning microscopy
CLUS	Clusterin
CO3	Complement component C3
CO4A	Complement component 4A
CO4B	Complement component 4B
CO6	Complement component C6
CO8A	Complement component C8 alpha chain
CO8G	Complement component C8 gamma chain
CTMA-Cl	Cetyl trimethyl ammonium chloride
CXCL7	Platelet basic protein
DC	Dendritic cell
DCS	Differential centrifugal sedimentation
DLS	Dynamic light scattering
DMEM	Dulbecco's Modified Eagle Medium
DMSO	Dimethyl sulfoxide
DTT	Dithiothreitol

EPR	Enhanced permeability and retention
ESI	Electrospray ionisation
F13B	Coagulation factor XIII B chain
FA12	Coagulation factor XII
FA5	Coagulation factor V
FBS	Foetal bovine serum
FDA	Food and drug administration
FETUA	Alpha 2 HS glycoprotein
FHR1	Complement factor H related protein 1
FHR2	Complement factor H related protein 2
Gal	Galactose
GELS	Gelsolin
HABP2	Hyaluronan binding protein 2
HDL	High densitiy lipoprotein
HeLa	Human cervix carcinoma cells
HEP2	Heparin cofactor 2
HES	Hydroxyethyl starch
HMSC	Human mesenchymal stem cells
HRG	Histidine rich glycoprotein
HSA	Human serum albumin
IAA	Iodoacetamide
IC1	Plasma protease C1 inhibitor
IEF	Isoelectric focusing
IgG	Immunoglobulin G
IGHG1	Ig gamma 1 chain C region
IGHG2	Ig gamma 2 chain C region
IGHG3	Ig gamma 3 chain C region
ITC	Isothermal titration calorimetry
ITIH4	Inter alpha trypsin inhibitor heavy chain
KLKB1	Plasma kallikrein
KNG1	Kininogen 1
LAT50	Lutensol AT50
LC-MS	Liquid-chromatography mass-spectrometry
LDL	Low densitiy lipoprotein
LUT	Lutensol AT50
LV102	Ig lambda chain V I region
MALDI-TOF	Matrix-assisted laser desorption/ionisation
Man	Mannose
MPS	Mononuclear phagocyte system
MS	Mass spectrometry
NC	Nanocapsule
NP	Nanoparticle
PAGE	Polyacrylamide gel electrophoresis
PBS	Phosphate-buffered saline
PC	Protein corona
PEEP	Poly(ethyl ethylene phosphate)
PEG	Poly(ethylene glycol)
PLF4	Platelet factor 4
PLGA	Poly(lactic-co-glycolic acid)
PLTP	Phospholipid transfer protein

PROS	Vitamin K dependent protein S
PS	Polystyrene
RAW264.7	Mouse macrophage-like cell line
RES	Reticuloendothelial system
RPMI	Roswell Park Memorial Institute medium
SAA4	Serum amyloid A 4 protein
SDS	Sodium dodecyl sulphate
SEC	Size exclusion chromatography
SEM	Scanning electron microscope
SPION	Superparamagnetic nanoparticles
SPR	Surface plasmon resonance
SR-B1	Scavenger receptor class B type 1
SSNa	Sodium 4-styrene sulfonate
TEM	Transmission electron microscopy
THRB	Prothrombin
VTDB	Vitamin D binding protein
VTNC	Vitronectin

7.2 COMPLETE LISTS OF PROTEINS IDENTIFIED BY LC-MS ANALYSIS

Table 7-2: List of corona proteins identified by LC-MS for the PS-NPs discussed in 4.1.
Relative abundance of each protein indicated as average of parts per million (ppm) calculated from the three technical replicates. Proteins are ordered alphabetically.

Protein name	PS-COOH	PS-NH_2	PS-SO_3	PS-PO_3	PS-PO_3-Lut	PS-PO_3-SDS
Actin, cytoplasmic 1	471.4	1576.2	400.1	392.9	578.4	527.5
Actin, gamma-enteric	213.6	1096.6	111.4	239.8	278.3	278.4
Alpha-1-acid glycoprotein		372.0		104.3		
Alpha-1-acid glycoprotein 2		220.5				
Alpha-1-antichymotrypsin		292.1		233.7		
Alpha-1-antitrypsin	3595.0	2680.6	4649.4	1789.3	2398.1	1889.2
Alpha-1B-glycoprotein		415.1		370.3		418.9
Alpha-1-microglobulin	460.2	453.0		709.0	327.5	658.5
Alpha-2-antiplasmin	727.3	584.2		931.7	270.0	975.7
Alpha-2-HS-glycoprotein	356.5	631.0		1909.8	217.8	2225.7
Alpha-2-macroglobulin	1718.3	5472.1	1210.9		659.0	1019.1
Angiotensinogen		398.4		319.3		381.8
Antithrombin-III	39433.1	5838.2	1955.6	18299.2	18577.5	21211.5
Apolipoprotein A-I	220232.2	85387.8	301967.2	89194.8	132857.1	75341.3
Apolipoprotein A-II	672.1	4728.3	4039.5	575.9	1478.2	430.3
Apolipoprotein A-IV	9797.5	78516.4	76589.2	9415.5	26634.5	7505.5
Apolipoprotein A-V	219.2	232.1		194.3	152.8	200.1
Apolipoprotein B-100	9092.8	39241.8	25178.3	4735.9	4243.3	3436.5
Apolipoprotein C-I	2703.2	1406.8	2838.5	1981.0	3670.6	1672.3
Apolipoprotein C-II	69.3	896.4	394.0	199.3	384.3	119.3
Apolipoprotein C-III	2032.2	16468.8	4992.1	4898.5	9916.1	2593.0
Apolipoprotein C-IV	153.4	188.1	228.0		53.0	

Apolipoprotein D	1172.7	2559.5	2351.0	404.6	2206.9	314.1
Apolipoprotein E	18354.4	8195.3	7964.4	5821.6	8024.3	4951.7
Apolipoprotein F	315.7	744.6	996.1	185.6	196.2	
Apolipoprotein L1		511.6	429.7	656.4	175.3	259.8
Apolipoprotein M	115.8	738.1	444.9		65.7	
Beta-2-glycoprotein 1	49718.9	669.6	1375.2	112198.9	146328.2	75359.3
Beta-actin-like protein 2	137.9	83.8	100.2	94.8	40.1	143.6
C4b-binding protein alpha chain	4087.7	2043.0	1049.5	15004.9	907.5	18081.7
C4b-binding protein beta chain	169.3	146.9		753.5		826.7
CD5 antigen-like	446.7	801.5	287.8	442.3	199.3	431.4
Clusterin	165887.1	166996.4	174578.6	109050.3	190072.5	154367.9
Coagulation factor IX	313.5	250.3		1861.4	4188.0	1839.0
Coagulation factor V	5865.1	3225.4	2494.5	5048.1	3971.2	4561.5
Coagulation factor VII	5494.3	187.7		6091.2	6453.5	3649.6
Coagulation factor X	543.9			715.1	1234.9	645.0
Coagulation factor XI	843.7	2036.5	537.3	721.9	1114.5	411.7
Coagulation factor XII		202.7		1325.6		3869.0
Coagulation factor XIII B chain		188.4		3016.7		3136.4
Cofilin-1		167.5			90.5	93.9
Complement C1q subcomponent subunit A	144.8	158.9		136.8		253.8
Complement C1q subcomponent subunit B	209.6	212.3		143.1		223.2
Complement C1q subcomponent subunit C	336.0	329.1		156.9		454.2
Complement C1r subcomponent	1961.0	1977.4	658.6	6014.8	4532.3	6121.1
Complement C1s subcomponent	1482.6	1513.7	551.8	4360.3	3199.6	4271.6
Complement C2		202.1		2062.2		1836.8
Complement C3	39211.6	121983.3	91583.8	57795.6	45162.9	71399.8
Complement C4 A	10966.7	10097.6	7502.2	8866.6	2003.0	6551.4
Complement C4 B	14852.3	14276.3	7017.6	13671.8	2875.2	7747.0
Complement C5	4659.2	4672.2	5253.4	2549.2	2184.0	4317.1
Complement component C6	892.3	2236.8	1431.6	3017.8	589.5	3698.9
Complement component C7	723.1	1670.3	1117.3	2625.0	521.4	2515.2
Complement component C8 alpha chain	1613.1	1042.6	2027.2	1222.3	859.3	805.1
Complement component C8 beta chain	2271.4	779.3	1091.3	1089.8	2263.4	890.7
Complement component C8 gamma chain	196.0	382.5	192.0	320.1	108.0	202.5
Complement component C9	2409.6	4659.2	5380.8	9344.4	3099.0	8333.2
Complement factor B	457.5	931.2		3610.7		3881.9
Complement factor H	7713.9	5908.5	2368.7	60792.6	5084.3	56342.5
Complement factor H-related protein 1	710.1	522.0	236.4	2709.5	317.9	2012.8
Complement factor H-related protein 2	245.2	234.2		1501.1	104.9	1184.4
Complement factor H-related protein 5	968.1	1391.6	324.5	2235.9	1092.2	1986.8
Erythrocyte band 7 integral membrane protein	210.9	295.6		425.3	540.1	333.5
Extracellular matrix protein 1		167.3		747.2	272.1	890.0
Fetuin-B				487.9		464.4
Fibrinogen alpha chain	527.0	1413.3		1002.9	3567.4	1067.8
Fibrinogen beta chain	665.0	728.4		348.5	1920.8	630.1
Fibrinogen gamma chain		966.0		408.4	2856.5	667.1

Fibronectin	3121.4	5513.0	1970.0	4073.2	8016.9	3789.7
Fibulin-1		307.8		1206.5		404.9
Gelsolin	1715.8	955.8		22715.3	1215.6	20720.1
Glutathione peroxidase 3		136.2			90.5	
Glyceraldehyde-3-phosphate dehydrogenase		355.8				
Haptoglobin	640.1	2607.9	653.6	624.7	229.3	898.0
Haptoglobin-related protein	371.1	653.4	281.6	484.1	213.1	513.3
Haemoglobin subunit alpha	464.6	5536.3	431.2	260.1	1067.5	593.5
Haemoglobin subunit beta	1121.5	5637.2	1344.3	585.3	3380.9	1689.1
Haemoglobin subunit delta	457.2	188.1	633.1	262.7	139.8	100.9
Hemoxin	470.0	1628.7		3579.5	268.4	3382.8
Heparin cofactor 2	1555.7	585.8		1091.4	519.2	1572.1
Histidine-rich glycoprotein	8175.6	360.7		1401.1	2744.2	2150.7
Hyaluronan-binding protein 2	731.3	1259.5	462.3	1289.5	265.5	1338.0
Ig alpha-1 chain C region	1011.7	2123.4	819.0	3330.5	728.8	2678.9
Ig alpha-2 chain C region	410.6	310.0	315.4	1187.7	272.8	964.6
Ig gamma-1 chain C region	7531.3	18608.6	6564.0	18811.2	5537.5	16057.4
Ig gamma-2 chain C region	11533.3	11055.3	1426.2	5536.0	929.5	4689.0
Ig gamma-3 chain C region	600.0	1424.9	1614.8	3167.8	561.6	3190.0
Ig gamma-4 chain C region	465.3	1213.2	830.6	1838.9	797.5	1260.0
Ig heavy chain V-II region NEWM		35.7		112.2		98.7
Ig heavy chain V-III region BRO	679.4	398.8	168.9	309.3	91.9	338.5
Ig heavy chain V-III region BUT	55.0	95.4		89.0	15.1	88.5
Ig heavy chain V-III region GAL	511.8	151.2		119.3		118.8
Ig heavy chain V-III region TUR	66.4	65.0	38.8	49.0	38.5	103.1
Ig heavy chain V-III region VH26	145.0	354.2	96.6	296.0	65.1	271.2
Ig heavy chain V-III region WEA	170.1	112.0		90.8	15.4	90.2
Ig kappa chain C region	4254.8	4794.1	1098.9	6646.3	937.8	5889.0
Ig kappa chain V-I region EU	95.1	124.8		126.4	16.5	107.5
Ig kappa chain V-I region WEA	159.7	58.6		336.0	56.3	256.6
Ig kappa chain V-I region Wes	81.8	57.5		63.0	16.2	49.3
Ig kappa chain V-II region TEW	124.4	265.7	113.3	293.9	52.8	227.5
Ig kappa chain V-III region VG Fragment	53.1	88.8	84.8	168.4		149.9
Ig kappa chain V-III region WOL	263.3	270.4	89.1	391.0	71.4	334.9
Ig kappa chain V-IV region Len	112.2	218.4		196.8	59.6	172.7
Ig lambda chain V-I region HA	159.5	261.1	103.3	153.6	86.8	126.2
Ig lambda chain V-III region LOI	133.4	111.5		223.2		215.1
Ig lambda chain V-III region SH		46.3		67.5		61.1
Ig lambda-2 chain C regions	1764.7	2558.3	1919.4	2052.4	1239.0	1809.2
Ig mu chain C region	5769.2	10162.2	5737.6	5346.3	2567.5	5623.4
Ig mu heavy chain disease protein	872.6	3548.1	2438.1	2329.8	1104.9	2389.3
Immunoglobulin J chain	167.2	288.0	149.8	161.8	73.6	140.1
Immunoglobulin lambda-like polypeptide 5	558.9	1416.8	1357.5	1375.0	132.8	1221.6
Integrin alpha-IIb	786.1	1166.6	930.2		419.0	
Inter-alpha-trypsin inhibitor heavy chain H1		1135.4		1775.1	333.8	1885.0
Inter-alpha-trypsin inhibitor heavy chain H2	1112.6	2640.9	2121.8	2886.6	1241.4	2363.5
Inter-alpha-trypsin inhibitor heavy chain H4	42391.2	1508.0	1292.5	73795.9	32456.0	66978.4
Keratin, type I cytoskeletal 10	1710.6	730.7	1349.8	1355.4	675.7	1542.9
Keratin, type I cytoskeletal 13	258.7	189.2	353.5	137.6	152.2	221.3

Keratin, type I cytoskeletal 14	446.6	543.4	362.9	313.3	174.4	237.7
Keratin, type I cytoskeletal 15	1922.6	24.9	165.6	2992.0	2471.0	2171.0
Keratin, type I cytoskeletal 16	130.6	24.6	473.7	101.7	138.6	314.8
Keratin, type I cytoskeletal 17	42.2	24.4	66.0	30.9	24.4	91.7
Keratin, type I cytoskeletal 24	265.8	34.6	149.1	256.0	260.2	302.3
Keratin, type I cytoskeletal 9	1840.5	454.5	1553.0	1088.1	909.6	1196.5
Keratin, type II cytoskeletal 1	3913.8	1461.2	3720.6	3588.5	1791.1	3619.1
Keratin, type II cytoskeletal 1b	875.7	156.9	749.5	501.9	355.0	516.3
Keratin, type II cytoskeletal 2 epidermal	1984.9	759.6	1859.4	1041.7	1067.8	930.1
Keratin, type II cytoskeletal 5	348.5	67.8	239.6	193.2	84.0	431.0
Keratin, type II cytoskeletal 6B	247.9	103.8	212.8	380.6	254.6	165.4
Keratin, type II cytoskeletal 75	256.1	74.1	146.7	133.2	80.6	141.2
Keratinocyte differentiation-associated protein	77.8	73.5		67.8	62.1	65.4
Kininogen-1	8737.7	827.4		23341.4	2636.0	28904.3
Lipopolysaccharide-binding protein	2438.7	1183.3	978.6	3026.9	3108.9	2876.7
Lumican		260.3			197.1	
Monocyte differentiation antigen CD14	171.4	132.9		622.7		357.3
N-acetylmuramoyl-L-alanine amidase		229.2		358.0		282.9
Phosphatidylinitol-glycan-specific phospholipase D		312.3		472.5		430.2
Phospholipid transfer protein	457.5	939.0	559.1	303.8	334.3	
Pigment epithelium-derived factor				478.9	154.7	336.4
Plasma kallikrein	2601.0	288.8		1512.2	788.5	4102.1
Plasma protease C1 inhibitor	1650.4	1647.1	736.0	4669.3	3971.3	6759.3
Plasma serine protease inhibitor	961.8	366.3		715.5	156.7	856.9
Plasminogen	1796.7	572.8	3115.9	3288.4	1023.1	5160.1
Platelet basic protein	93.8	48.5		875.6	101.2	670.0
Platelet factor 4	1628.9	102.6	100.3	2776.0	1809.4	2372.4
POTE ankyrin domain family member F	1875.1	1690.1	6001.6	1103.2	1136.2	1239.3
POTE ankyrin domain family member J	184.7	992.7	3462.3	409.8	485.9	569.7
Pregnancy zone protein	479.7	1059.0			333.2	
Profilin 1		94.5		100.5	81.5	120.2
Properdin	2035.6	6196.3	2929.2	1540.1	1269.3	827.9
Protein Z-dependent protease inhibitor	388.3	164.7		400.0	265.0	298.2
Proteoglycan 4	1132.4			777.2		1291.3
Prothrombin	56024.3	19426.7	3046.4	31232.7	49161.8	47771.8
Secreted phosphoprotein 24		160.0		192.3	119.4	143.9
Selenoprotein P	527.6	135.0		809.7	291.9	889.2
Serotransferrin	1194.5	5228.5	740.9	2422.6	422.1	2316.7
Serum albumin	27532.7	133201.4	20327.6	27247.5	12280.1	12760.6
Serum amyloid A protein	291.7	125.8	288.9	284.8	281.2	226.5
Serum amyloid A-4 protein	1504.9	386.1	1298.5	164.2	125.0	158.2
Serum amyloid P-component	461.8	244.7	322.5	2006.7	313.6	590.0
Serum paraoxonase/arylesterase 1	400.5	879.2	801.1	212.9	162.3	
Sex hormone-binding globulin		125.1		240.4		
Talin-1		3193.1			1107.4	1188.7

Tetranectin		73.3		607.8		523.8
Thrombospondin-1		339.8		2526.0	667.5	2111.7
Transthyretin	305.1	472.5	632.4	485.9	592.9	510.7
Vitamin D-binding protein	305.1	654.4		2342.2	243.6	3200.9
Vitamin K-dependent protein S	569.7	505.4		2698.5		2250.7
Vitronectin	40161.4	36343.3	6444.7	44813.4	42903.7	59062.1
Zinc finger protein basonuclin-2	21427.9	19630.8	26940.9	16093.4	30423.7	19589.9

Table 7-3: List of corona proteins identified by LC-MS for the PS-NPs discussed 4.2.

Relative abundance of each protein indicated as average of parts per million (ppm) calculated from two biological and two technical replicates. Proteins are ordered alphabetically.

Protein name	PS-SDS	PS-LUT	PS-LUT-COOH	PS-LUT-NH_2
14 3 3 protein zeta delta	57.0	72.5	127.6	58.3
Actin cytoplasmic 2	993.6	794.9	2386.0	500.2
Actin gamma enteric smooth muscle	187.5	313.6	721.2	287.3
Alpha 1 antitrypsin	1391.2	887.0	704.0	954.4
Alpha 2 antiplasmin	1528.5	209.0	616.8	219.6
Alpha 2 HS glycoprotein	4471.6	52.6	117.1	71.6
Alpha 2 macroglobulin	1462.5	607.8	1008.9	590.7
Angiotensinogen	823.4	95.4	56.5	94.2
Antithrombin III	30448.0	74124.6	35604.8	93294.0
Apolipoprotein A I	235786.4	227458.6	114162.7	237502.9
Apolipoprotein A II	1343.6	1335.4	141.4	1228.5
Apolipoprotein A IV	11344.7	18807.4	8389.7	25238.7
Apolipoprotein A V	226.2	298.9	302.0	284.0
Apolipoprotein B 100	8372.0	24640.3	9699.3	19913.8
Apolipoprotein C I	2418.3	4694.1	3366.2	3985.1
Apolipoprotein C II	332.3	483.9	66.9	418.4
Apolipoprotein C III	10885.0	6598.1	1189.3	5438.0
Apolipoprotein C IV	167.4	605.1	591.0	621.7
Apolipoprotein D	467.3	1867.8	944.3	1784.3
Apolipoprotein E	8013.8	14165.6	20008.2	13802.9
Apolipoprotein F	410.6	511.8	145.6	518.7
Apolipoprotein L1	397.2	220.2	64.0	244.8
Apolipoprotein M	67.8	410.6	41.3	501.7
Band 3 anion transport protein	379.4	189.1	1455.8	149.7
Beta 2 glycoprotein 1	8853.0	516.2	55119.2	598.5
Beta actin like protein 2	269.9	124.7	252.1	95.9
C4b binding protein alpha chain	14031.7	1364.8	1399.3	1164.3
C4b binding protein beta chain	462.7	42.8	62.2	30.2
Carboxypeptidase B2	180.4	159.8	579.6	158.1
Cathelicidin antimicrobial peptide	64.5	158.7	222.3	155.5
CD5 antigen like	374.1	185.2	294.3	175.6

Clusterin	123826.1	312179.0	75782.4	309914.3
Coagulation factor IX	278.0		559.9	22.5
Coagulation factor V	4572.8	3900.6	15963.7	3363.9
Coagulation factor XI	453.9	129.6	3366.2	90.8
Coagulation factor XII	3297.0	444.6	251.8	334.9
Coagulation factor XIII B chain	1741.0		115.2	
Cofilin 1	108.7	61.6	180.5	63.1
Complement C1q subcomponent subunit A	336.6	66.0	136.0	67.1
Complement C1q subcomponent subunit B	997.5	161.3	226.3	98.9
Complement C1q subcomponent subunit C	1019.0	165.8	276.5	97.7
Complement C1r subcomponent	4570.1	898.0	917.0	884.6
Complement C1s subcomponent	4718.9	811.9	931.3	981.8
Complement C3	62219.0	129018.2	112489.5	110396.6
Complement C4 A	9688.2	12314.9	7378.2	12161.6
Complement C4 B	27985.4	29150.1	19495.2	25784.3
Complement C5	4309.2	7111.0	12830.9	6246.4
Complement component C6	1871.1	3156.1	1954.9	2579.7
Complement component C7	3270.2	3890.1	2716.9	4302.2
Complement component C8 alpha chain	1210.2	1718.8	1094.2	1703.3
Complement component C8 beta chain	675.9	1118.4	439.3	1115.7
Complement component C8 gamma chain	224.0	634.5	445.2	605.1
Complement component C9	5929.9	9814.0	6080.5	9391.2
Complement factor B	4068.8	134.1	448.9	130.9
Complement factor H	12996.5	2994.0	11457.4	2710.1
Complement factor H related protein 1	721.3	274.0	2591.9	282.9
Complement factor H related protein 2	512.2	51.6	237.7	49.2
Complement factor H related protein 5	2088.5	1318.4	3872.7	1263.3
Erythrocyte band 7 integral membrane protein	108.1	77.1	280.2	62.6
Extracellular matrix protein 1	379.0		77.2	
Fibrinogen alpha chain	916.7	267.5	1438.3	223.5
Fibrinogen beta chain	454.0	222.1	1026.1	179.0
Fibrinogen gamma chain	675.7	130.2	800.1	73.9
Fibronectin	4574.1	778.4	2718.9	353.9
Gelsolin	14517.6	268.3	3418.9	242.3
Glutathione peroxidase 3	257.2	69.3	258.6	71.4
Glyceraldehyde 3 phosphate dehydrogenase	360.9	473.6	464.1	535.6
Haptoglobin	916.2	181.7	249.0	205.9
Haptoglobin related protein	800.9	349.1	279.3	402.9
Haemoglobin subunit alpha	3105.9	3564.9	3451.8	3445.9
Haemoglobin subunit beta	2564.7	3580.6	3049.4	3476.8
Haemoglobin subunit delta	90.7	123.5	131.7	114.0
Haemoglobin subunit gamma 2	314.5	739.2	3.9	759.2
Hemopexin	9312.1	85.5	199.0	71.1
Heparin cofactor 2	2391.8	146.6	1012.6	150.7
Histidine protein methyltransferase 1 homolog	563.4	590.0	204.1	1253.5
Histidine rich glycoprotein	2436.4	181.6	6999.6	283.0
Hyaluronan binding protein 2	532.8		491.6	

Ig alpha 1 chain C region	5483.0	491.5	465.4	477.0
Ig alpha 2 chain C region	302.4	116.1	92.9	125.7
Ig delta chain C region	347.8	38.6	96.5	33.1
Ig gamma 1 chain C region	50797.6	21081.6	12700.8	18112.0
Ig gamma 2 chain C region	12581.3	1627.4	1871.5	1567.8
Ig gamma 3 chain C region	6727.9	433.4	2192.2	373.5
Ig gamma 4 chain C region	3416.4	127.4	200.7	191.2
Ig heavy chain V III region BRO	482.1	71.6	80.4	52.9
Ig heavy chain V III region VH26	733.6	51.8	72.7	51.4
Ig heavy chain V III region WEA	7.5	29.3	35.9	29.9
Ig kappa chain C region	10795.2	518.0	718.0	490.6
Ig kappa chain V I region WEA	278.7	25.7	28.2	27.1
Ig kappa chain V II region TEW	221.2	63.8	53.3	68.3
Ig kappa chain V III region SIE	491.7	56.1	55.0	49.0
Ig kappa chain V III region VG Fragment	149.6	9.5	17.8	7.4
Ig kappa chain V IV region Len	185.8	20.9	50.0	23.3
Ig lambda 2 chain C regions	3485.9	2804.7	1678.9	2929.8
Ig lambda chain V I region HA	143.1	378.6	277.8	326.6
Ig mu chain C region	5189.7	3143.5	2943.5	3045.1
Ig mu heavy chain disease protein	2738.5	949.5	1955.7	685.6
Immunoglobulin J chain	104.0	51.3	42.0	42.5
Immunoglobulin lambda like polypeptide 5	1929.1	164.0	179.0	127.3
Insulin like growth factor binding protein 4			177.4	
Insulin like growth factor binding protein complex acid labile subunit	200.7	305.1	181.7	314.2
Integrin beta 3	141.3	144.2	414.9	129.1
Inter alpha trypsin inhibitor heavy chain H1	2065.4	96.7	154.0	110.7
Inter alpha trypsin inhibitor heavy chain H2	3738.7	519.1	383.3	621.8
Inter alpha trypsin inhibitor heavy chain H4	30438.0	1109.0	115577.3	1245.5
Keratinocyte differentiation associated protein	105.4	88.9	126.9	99.2
Kininogen 1	13607.9	100.3	36916.0	146.0
Lactotransferrin			465.0	
Lipopolysaccharide binding protein	1730.1	293.2	6537.0	309.9
Lumican	121.4	25.8	252.3	38.8
Monocyte differentiation antigen CD14	275.8			18.4
Multimerin 1	793.0	157.3	2344.1	110.2
Myosin Vb	813.5	900.1	1034.8	760.4
N acetylmuramoyl L alanine amidase	729.4	81.0	114.8	74.0
Phospholipid transfer protein	103.8	1153.4	77.8	1027.1
Plasma kallikrein	1135.6	218.7	4237.1	148.7
Plasma protease C1 inhibitor	3496.3	555.1	1274.9	567.3
Plasma serine protease inhibitor	268.3	120.5	1731.9	102.6
Plasminogen	2534.3	477.0	1755.0	433.4
Platelet basic protein	375.3	10.8	199.3	11.1
Platelet factor 4	342.8	110.3	4387.0	168.0
Platelet factor 4 variant	159.0	46.1	262.0	74.0
POTE ankyrin domain family member J	541.2	495.1	1155.8	388.8

Properdin	2537.1	7783.2	1981.0	7530.4
Protein AMBP	546.9	70.1	292.9	76.1
Proteoglycan 4	1356.7	86.5	2172.3	97.4
Prothrombin	20295.5	7302.7	106745.4	8102.5
Ras related protein Rap 1b	31.6	47.2	76.5	59.1
Selenoprotein P	209.6	36.4	802.3	50.8
Serotransferrin	5992.9	216.5	364.3	173.7
Serum albumin	58939.3	8087.2	8268.6	8959.2
Serum amyloid A 4 protein	152.6	528.6	581.5	560.3
Serum amyloid A protein	161.9	26.0	112.0	33.8
Serum amyloid P component	277.9	60.1	441.9	59.4
Serum paraoxonase arylesterase 1	274.3	311.3	232.2	324.8
Transthyretin	547.1	904.1	389.2	778.2
Vitamin D binding protein	6556.4	64.7	258.5	75.0
Vitamin K dependent protein S	1762.5	340.1	386.3	391.8
Vitronectin	42865.6	8482.1	88502.3	10897.3

Table 7-4: List of corona proteins identified by LC-MS for the PS-NPs discussed in 4.3.

Average amount of each protein in fmol was calculated from the three biological and two technical replicates. Proteins are ordered alphabetically.

Protein name	PS-NH_2	PS-PEG-44	PS-PEG-110	PS-PEEP-49	PS-PEEP-92
28S ribosomal protein S18b, mitochondrial	0.000	0.000	0.000	0.000	0.013
Actin, aortic smooth muscle	0.000	0.036	0.000	0.000	0.000
Actin, cytoplasmic 1	0.000	0.214	0.114	0.102	0.281
Acyl-CoA-binding domain-containing protein 7	0.000	0.000	0.000	0.008	0.000
Alcohol dehydrogenase [NADP(+)]	0.000	0.012	0.000	0.000	0.000
Alpha-1-antitrypsin	1.115	0.370	0.110	0.543	0.429
Alpha-2-macroglobulin	0.604	0.000	0.021	0.000	0.000
Alpha-synuclein	0.000	0.000	0.000	0.000	0.027
Antithrombin-III	0.239	0.040	0.052	0.000	0.000
AP-4 complex subunit beta-1	0.000	0.000	0.508	0.000	0.000
Apolipoprotein A-I	4.250	35.227	18.290	4.672	1.575
Apolipoprotein A-II	0.000	0.817	0.079	1.295	1.748
Apolipoprotein A-IV	1.319	3.930	1.547	8.790	6.917
Apolipoprotein A-V	0.000	0.017	0.000	0.092	0.061
Apolipoprotein B-100	0.000	0.230	0.061	0.338	0.166
Apolipoprotein C-II	0.000	0.568	0.351	2.038	1.913
Apolipoprotein C-III	4.818	10.942	6.752	8.391	5.873
Apolipoprotein C-IV	0.000	0.226	0.000	0.751	0.768
Apolipoprotein D	0.000	0.067	0.078	7.098	7.391
Apolipoprotein E	0.656	2.716	1.017	2.317	1.568
Apolipoprotein L1	0.000	0.033	0.000	0.431	1.304

Apolipoprotein M	0.000	0.000	0.000	0.045	0.076
Arfaptin-1	0.000	0.000	0.000	0.000	0.229
Arf-GAP with GTPase, ANK repeat and PH domain-containing protein 11	0.000	0.250	0.000	0.000	0.000
Baculoviral IAP repeat-containing protein 5	0.000	0.000	0.000	0.024	0.000
Beta-2-glycoprotein 1	3.380	0.438	0.133	0.361	0.193
Beta-actin-like protein 2	0.000	0.000	0.000	0.000	0.000
Beta-crystallin A2	0.000	0.000	0.000	0.000	0.000
BTB/POZ domain-containing adapter for CUL3-mediated RhoA degradation protein 2	0.000	0.000	0.000	0.289	0.399
BTB/POZ domain-containing protein KCTD16	1.285	0.000	0.000	0.000	0.000
C4b-binding protein alpha chain	0.442	0.227	0.176	0.648	0.336
Calcium-binding protein 5	0.000	0.005	0.000	0.000	0.000
Calcyphosin	0.000	0.000	0.000	0.110	0.000
Carbohydrate sulfotransferase 12	0.000	0.015	0.000	0.000	0.000
Cathelicidin antimicrobial peptide	0.000	0.000	0.000	0.029	0.000
CD5 antigen-like	0.028	0.143	0.178	0.204	0.209
Clusterin	15.141	169.912	77.886	376.107	357.968
Coagulation factor XIII A chain	0.024	0.000	0.000	0.000	0.000
Coagulation factor XIII B chain	0.316	0.000	0.000	0.000	0.000
Coiled-coil domain-containing protein 97	0.000	0.061	0.000	0.000	0.000
Complement C1q subcomponent subunit A	0.168	1.524	0.300	1.665	2.977
Complement C1q subcomponent subunit B	1.625	4.762	1.587	5.977	8.182
Complement C1q subcomponent subunit C	1.724	4.981	1.166	4.738	7.876
Complement C1r subcomponent	1.025	1.808	1.126	2.628	2.706
Complement C1s subcomponent	0.996	1.393	0.949	2.186	2.113
Complement C3	1.507	1.852	1.488	1.823	1.622
Complement C4-A	0.000	0.174	0.082	0.312	0.281
Complement C4-B	0.000	0.139	0.143	0.246	0.263
Complement component C6	0.000	0.000	0.000	0.154	0.000
Complement component C7	0.000	0.000	0.000	0.017	0.000
Complement component C8 beta chain	0.000	0.000	0.000	0.000	0.015
Complement component C8 gamma chain	0.000	0.007	0.000	0.024	0.030
Complement component C9	0.000	0.214	0.088	0.210	0.184
Complement factor H	1.505	0.193	0.112	0.291	0.370
Cytosolic Fe-S cluster assembly factor NARFL	0.000	0.039	0.000	0.019	0.000
DC-STAMP domain-containing protein 2	0.000	0.011	0.000	0.000	0.000
Dual specificity protein phosphatase 3	0.000	0.000	0.000	0.023	0.000
Endothelial cell-specific molecule 1	0.000	0.000	0.000	0.029	0.000
Enoyl-CoA delta isomerase 2, mitochondrial	0.000	0.000	0.000	0.032	0.000
Epsilon-sarcoglycan	0.000	0.000	0.105	0.140	0.000
Extracellular matrix protein 1	0.000	0.093	0.047	0.176	0.166
Fibrinogen alpha chain	40.655	3.855	1.861	0.522	0.461
Fibrinogen beta chain	73.861	6.422	2.979	0.807	0.596
Fibrinogen gamma chain	73.735	6.103	3.075	0.947	0.771
Fibronectin	2.645	6.351	4.113	9.531	11.099
Ficolin-1	0.000	0.000	0.000	0.025	0.022
Gelsolin	0.129	0.012	0.000	0.000	0.000

General transcription factor 3C polypeptide 4	0.000	0.000	0.000	0.012	0.000
Glucokinase	0.000	0.000	0.000	0.007	0.000
Glutamate-rich protein 5	0.000	0.009	0.000	0.000	0.000
Golgin subfamily A member 1	0.000	0.000	0.007	0.000	0.000
GRB2-related adapter protein	1.377	0.000	0.000	0.000	0.000
Haptoglobin	0.249	0.000	0.000	0.000	0.000
Haptoglobin-related protein	0.024	0.103	0.089	0.125	0.087
Heat shock protein beta-7	0.000	0.000	0.000	0.011	0.000
Hemopexin	0.411	0.000	0.000	0.000	0.000
Histidine-rich glycoprotein	0.033	0.000	0.007	0.000	0.000
Homeodomain-only protein	0.514	0.000	0.000	0.000	0.000
Hyaluronan synthase 3	0.121	0.000	0.000	0.000	0.000
Hyaluronan-binding protein 2	1.021	0.000	0.000	0.000	0.000
Hyaluronidase-1	0.000	0.000	0.000	0.000	0.058
Ig alpha-1 chain C region	1.664	0.775	0.543	0.775	0.851
Ig alpha-2 chain C region	0.020	0.033	0.023	0.000	0.077
Ig gamma-1 chain C region	13.840	2.662	1.890	2.583	2.554
Ig gamma-2 chain C region	3.529	2.426	1.662	0.587	0.568
Ig gamma-3 chain C region	1.206	0.642	0.520	1.100	1.100
Ig gamma-4 chain C region	0.924	0.057	0.000	0.010	0.000
Ig heavy chain V-II region ARH-77	0.000	0.077	0.000	0.000	0.000
Ig heavy chain V-III region BRO	0.230	0.321	0.321	0.204	0.291
Ig heavy chain V-III region BUT	0.017	0.026	0.024	0.021	0.020
Ig heavy chain V-III region GAL	0.000	0.043	0.027	0.000	0.000
Ig heavy chain V-III region TIL	0.053	0.000	0.000	0.000	0.000
Ig kappa chain C region	12.582	5.084	3.928	5.575	5.030
Ig kappa chain V-I region AG	0.059	0.000	0.000	0.000	0.021
Ig kappa chain V-II region TEW	0.000	0.055	0.248	0.185	0.174
Ig kappa chain V-III region CLL	0.000	0.030	0.011	0.024	0.013
Ig kappa chain V-III region HIC	0.000	0.533	0.248	0.000	0.006
Ig kappa chain V-III region SIE	0.333	0.624	0.644	0.460	0.426
Ig lambda-3 chain C regions	0.000	0.000	0.000	0.000	0.386
Ig mu chain C region	2.881	2.825	3.078	5.933	6.469
Ig mu heavy chain disease protein	0.000	0.355	0.425	0.498	0.000
Immunoglobulin J chain	0.000	0.035	0.138	0.096	0.065
Immunoglobulin lambda-like polypeptide 5	0.000	0.000	0.000	0.000	0.386
Immunoglobulin-like domain-containing receptor 1	0.000	0.000	0.000	0.017	0.000
Indian hedgehog protein	0.000	0.000	0.000	0.000	0.022
Insulin-like growth factor-binding protein complex acid labile subunit	0.015	0.084	0.005	0.506	0.503
Integrin alpha-E	0.000	0.000	0.000	0.000	0.015
Inter-alpha-trypsin inhibitor heavy chain H2	0.000	0.058	0.102	0.000	0.000
Inter-alpha-trypsin inhibitor heavy chain H4	0.637	0.132	0.030	0.098	0.027
Iron-sulfur cluster assembly enzyme ISCU, mitochondrial	0.000	0.000	0.000	0.000	0.028
Keratin, type I cytoskeletal 10	0.000	0.029	0.012	0.012	0.017
Keratin, type I cytoskeletal 9	0.000	0.020	0.055	0.050	0.000
Keratin, type II cytoskeletal 1	0.000	0.236	0.182	0.347	0.069

Keratin, type II cytoskeletal 1b	0.000	0.021	0.017	0.035	0.000
Keratin, type II cytoskeletal 2 epidermal	0.000	0.000	0.035	0.028	0.000
Keratin, type II cytoskeletal 6B	0.000	0.000	0.016	0.000	0.000
Kininogen-1	0.265	0.000	0.000	0.000	0.000
Lipopolysaccharide-binding protein	0.045	0.009	0.000	0.000	0.000
L-lactate dehydrogenase C chain	0.000	0.000	0.284	0.000	0.000
Lumican	0.000	0.162	0.076	0.000	0.000
Neurexin-1	0.000	0.000	0.000	0.009	0.000
Nuclear receptor ROR-beta	0.000	0.000	0.000	0.030	0.000
Nuclear receptor-interacting protein 1	0.000	0.000	0.000	0.007	0.000
Nucleosome assembly protein 1-like 4	0.000	0.000	0.000	0.079	0.000
NudC domain-containing protein 2	0.000	0.106	0.000	0.000	0.000
Phospholipid transfer protein	0.000	0.445	0.095	0.854	0.862
Plasma protease C1 inhibitor	0.000	0.039	0.131	0.140	0.127
Plasminogen	0.839	0.000	0.000	0.000	0.000
POTE ankyrin domain family member E	0.000	0.022	0.000	0.000	0.024
POTE ankyrin domain family member F	0.000	0.023	0.000	0.000	0.000
Probable histone-lysine N-methyltransferase PRDM7	0.000	0.248	0.000	0.000	0.011
Probable ribonuclease 11	0.000	0.000	0.000	0.000	0.135
Proenkephalin-B	0.000	0.005	0.000	0.000	0.000
Profilin-1	0.000	0.008	0.000	0.000	0.000
Proline-, glutamic acid- and leucine-rich protein 1	0.000	0.000	0.000	0.000	1.288
Properdin	0.000	0.406	0.235	0.384	0.423
Protein AMBP	0.032	0.023	0.000	0.000	0.000
Protein FAM177A1	0.000	0.013	0.034	0.000	0.000
Protein FAM194B	0.000	0.007	0.000	0.000	0.000
Protein PAT1 homolog 1	0.000	0.000	0.000	0.000	0.014
Prothrombin	0.096	0.000	0.000	0.000	0.000
Ras-related protein Rap-1A	0.000	0.000	0.000	0.009	0.000
RING finger protein 219	0.000	0.429	0.000	0.000	1.921
RING finger protein 39	0.000	0.000	0.000	0.021	0.000
Runt-related transcription factor 2	0.000	0.018	0.000	0.000	0.000
Serine/threonine-protein phosphatase 4 regulatory subunit 2	0.000	0.000	0.006	0.000	0.000
Serotransferrin	0.484	0.000	0.006	0.000	0.000
Serum albumin	129.947	5.532	0.638	0.433	0.369
Serum amyloid A-1 protein	0.268	0.124	0.058	0.048	0.023
Serum amyloid A-4 protein	0.000	0.046	0.000	0.854	0.784
Serum amyloid P-component	0.434	0.000	0.006	8.590	0.023
Serum paraoxonase/arylesterase 1	0.000	0.014	0.000	0.216	0.197
Sex hormone-binding globulin	0.000	0.007	0.000	0.096	0.069
Signal-regulatory protein delta	0.000	0.000	0.022	0.000	0.000
Sodium-dependent neutral amino acid transporter B(0)AT2	0.000	0.000	0.011	0.000	0.000
Sperm-associated antigen 4 protein	0.000	0.000	0.000	0.000	0.023
Sperm-associated antigen 6	0.000	0.000	0.000	0.000	0.174
T-cell receptor gamma chain V region PT-gamma-1/2	0.000	0.000	0.000	0.000	0.030
TNF receptor-associated factor 3	0.000	0.000	0.010	0.000	0.000

Trafficking protein particle complex subunit 3-like protein	0.000	0.000	0.000	0.040	0.000
Transcription elongation factor A protein-like 4	0.000	0.000	0.023	0.000	0.000
Transthyretin	1.352	0.499	0.473	0.106	0.000
Tripartite motif-containing protein 52	0.066	0.064	0.000	0.154	0.070
Tsukushin	0.000	0.033	0.008	0.113	0.174
Tubulin polymerization-promoting protein family member 2	0.000	0.000	0.000	0.000	0.057
Tyrosine-protein phosphatase non-receptor type 1	0.000	0.000	0.010	0.000	0.000
Vitamin D-binding protein	1.046	0.077	0.000	0.000	0.000
Vitronectin	49.525	11.663	5.849	7.359	4.004
Zinc finger protein 280A	0.000	0.000	0.026	0.000	0.000
Zinc finger protein 594	0.000	1.462	0.000	1.150	2.737
Zinc finger protein basonuclin-2	0.000	0.578	0.061	2.706	2.178

Table 7-5: List of corona proteins identified by LC-MS for the HES-NCs discussed in 4.4.
Average amount of each protein in fmol was calculated from three technical replicates. Proteins are ordered alphabetically.

Protein name	HES	HES-PEG	HES-PEG-Man	HES-PEG-DEC-205	HES-PEG-Gal
Actin, cytoplasmic 1	0.007	0.086	0.024	0.039	0.037
Afamin	0.000	0.003	0.004	0.006	0.000
A-kinase anchor protein 8	0.891	0.745	2.317	2.116	1.321
Alpha-1-acid glycoprotein 1	0.013	0.038	0.009	0.016	0.027
Alpha-1-acid glycoprotein 2	0.000	0.005	0.001	0.002	0.013
Alpha-1-antichymotrypsin	0.087	0.843	0.044	0.113	0.076
Alpha-1-antitrypsin	0.065	0.178	0.168	0.231	0.179
Alpha-1B-glycoprotein	0.015	0.036	0.045	0.109	0.037
Alpha-2-antiplasmin	0.029	0.137	0.033	0.046	0.069
Alpha-2-HS-glycoprotein	0.026	0.454	0.384	0.256	0.152
Alpha-2-macroglobulin	3.958	4.086	6.360	6.120	2.545
Alpha-amylase 1	0.845	0.793	0.666	0.973	0.533
Angiotensinogen	0.186	0.251	0.068	0.075	0.058
Ankyrin repeat and SAM domain-containing protein 3	3.986	0.789	4.065	2.164	1.751
Antithrombin-III	0.027	0.183	0.053	0.072	0.095
Apolipoprotein A-I	10.466	34.405	22.544	16.621	18.233
Apolipoprotein A-II	0.004	0.076	0.034	0.178	0.344
Apolipoprotein A-IV	7.182	18.112	12.413	9.032	11.588
Apolipoprotein A-V	0.091	1.199	0.422	0.246	0.461
Apolipoprotein B-100	0.742	0.822	0.176	0.576	0.411
Apolipoprotein C-III	0.001	0.062	0.081	0.001	0.858
Apolipoprotein D	1.995	1.141	1.494	1.406	1.127

Apolipoprotein E	5.239	9.733	2.056	2.173	1.222
Apolipoprotein L1	0.159	2.328	0.147	0.118	0.132
Apolipoprotein(a)	0.215	0.500	0.152	0.321	0.089
Beta-2-glycoprotein 1	0.000	0.004	0.005	0.004	0.005
C4b-binding protein alpha chain	1.407	1.022	1.386	1.579	1.127
Calpain-8	0.000	0.000	0.063	0.000	0.105
Carboxyl-terminal PDZ ligand of neuronal nitric oxide synthase protein	4.687	2.054	4.864	4.047	1.729
CD5 antigen-like	0.300	0.986	0.320	0.523	0.396
Ceruloplasmin	0.023	0.048	0.077	0.032	0.069
Cholesteryl ester transfer protein	0.020	0.079	0.218	0.052	0.198
Claspin	0.001	0.645	0.078	0.025	0.132
Clusterin	401.316	80.399	363.364	348.300	280.986
Coenzyme Q-binding protein COQ10 homolog A, mitochondrial	0.048	0.044	0.044	0.090	0.041
Coiled-coil domain-containing protein 27	0.048	0.179	0.108	0.076	0.120
Complement C1q subcomponent subunit A	0.441	7.489	4.044	1.052	4.087
Complement C1q subcomponent subunit B	15.984	47.069	8.881	11.545	11.507
Complement C1q subcomponent subunit C	21.682	31.307	7.697	10.393	7.087
Complement C1r subcomponent	3.193	7.823	2.509	3.362	2.720
Complement C1s subcomponent	1.893	6.822	1.744	1.579	2.182
Complement C3	18.335	12.901	7.127	9.451	6.101
Complement C4-A	0.117	0.055	0.065	0.071	0.036
Complement C4-B	0.760	0.358	0.420	0.462	0.233
Complement C5	0.744	0.496	0.691	0.791	0.446
Complement component C6	1.006	1.597	12.601	2.929	6.977
Complement component C7	3.132	3.273	2.779	1.945	2.115
Complement component C8 alpha chain	0.334	0.658	0.060	0.124	0.072
Complement component C8 beta chain	0.133	0.338	1.146	0.331	0.884
Complement component C8 gamma chain	0.524	0.912	1.888	1.361	2.707
Complement component C9	1.313	1.227	0.919	1.165	0.730
Complement factor B	1.328	0.795	0.411	0.791	0.269
Complement factor H	3.222	3.259	2.455	2.513	1.891
Cytoplasmic dynein 1 heavy chain 1	0.121	0.243	0.174	0.202	0.147
Dipeptidase 3	0.245	0.548	1.627	0.602	2.542
Diphthamide biosynthesis protein 2	0.784	0.304	1.485	1.038	0.412
Doublecortin domain-containing protein 2	0.035	0.863	0.009	0.064	0.098
Extracellular matrix protein 1	0.193	0.625	0.071	0.112	0.211
F-actin-capping protein subunit alpha-2	0.204	0.271	0.194	0.256	0.171
Fibrinogen alpha chain	0.348	0.787	2.129	1.011	0.914
Fibrinogen beta chain	0.476	1.040	4.088	0.864	1.377
Fibrinogen gamma chain	0.311	1.327	2.035	1.250	1.230
Fibronectin	6.485	9.512	1.960	3.234	2.654
Fibulin-1	69.427	10.780	52.311	49.769	31.752
Ficolin-2	0.114	0.311	0.484	0.352	0.490
Fidgetin-like protein 1	0.162	0.470	0.113	0.246	0.168
Folliculin-interacting protein 1	0.018	0.129	0.012	0.030	0.051
Gelsolin	0.002	0.011	0.033	0.055	0.028

Glutathione peroxidase 3	5.010	1.750	2.317	2.352	1.097
Haptoglobin	1.406	0.415	1.378	0.490	0.478
Haptoglobin-related protein	0.347	0.347	0.419	0.240	0.240
Hemopexin	0.463	0.118	0.192	0.177	0.158
Heparin cofactor 2	0.012	0.022	0.011	0.007	0.006
Histidine-rich glycoprotein	0.276	0.085	0.375	0.399	0.306
Histone-lysine N-methyltransferase EZH2	0.150	0.415	0.119	0.269	0.273
Hyaluronan mediated motility receptor	0.628	0.734	0.376	0.929	0.809
Hyaluronan-binding protein 2	0.160	1.102	0.527	0.453	0.414
Hyaluronidase-1	0.016	0.103	0.005	0.004	0.035
Ig alpha-1 chain C region	0.802	2.718	0.944	1.670	1.187
Ig alpha-2 chain C region	0.028	0.046	0.088	0.043	0.099
Ig gamma-1 chain C region	4.818	3.309	3.118	3.245	2.804
Ig gamma-2 chain C region	1.239	1.565	1.803	2.137	1.746
Ig gamma-3 chain C region	0.428	1.868	0.610	0.786	0.692
Ig gamma-4 chain C region	0.402	0.237	0.572	0.898	0.214
Ig heavy chain V-III region BRO	1.050	0.976	0.598	0.986	0.476
Ig heavy chain V-III region GAL	0.661	0.477	0.350	0.381	0.492
Ig heavy chain V-III region TUR	0.155	0.395	0.257	5.049	0.390
Ig heavy chain V-III region VH26	0.247	0.535	0.332	0.266	0.376
Ig heavy chain V-III region WEA	0.009	0.008	0.006	0.006	0.004
Ig kappa chain C region	5.245	8.241	3.895	6.363	3.520
Ig kappa chain V-I region AG	0.003	0.023	0.016	0.017	0.023
Ig kappa chain V-I region EU	0.002	0.000	0.000	0.000	0.000
Ig kappa chain V-II region TEW	0.058	0.113	0.056	0.076	0.047
Ig kappa chain V-III region GOL	0.586	0.557	0.439	0.492	0.398
Ig kappa chain V-III region NG9 (Fragment)	0.082	0.100	0.093	0.136	0.058
Ig kappa chain V-III region SIE	0.146	0.138	0.109	0.122	0.099
Ig lambda-2 chain C regions	1.344	0.751	0.444	1.402	0.468
Ig mu chain C region	10.616	10.458	3.934	5.874	3.763
Ig mu heavy chain disease protein	3.205	4.726	3.513	1.918	3.354
Immunoglobulin J chain	0.335	0.653	0.416	0.503	0.323
Immunoglobulin lambda-like polypeptide 5	0.576	0.345	0.210	0.617	0.210
Inhibin beta E chain	0.288	0.096	0.389	0.901	0.758
Insulin-like growth factor-binding protein complex acid labile subunit	0.035	0.149	0.066	0.127	0.126
Intelectin-1	0.281	0.402	0.441	0.413	0.495
Inter-alpha-trypsin inhibitor heavy chain H1	0.001	0.024	0.028	0.033	0.028
Inter-alpha-trypsin inhibitor heavy chain H2	0.184	0.040	0.038	0.037	0.036
Inter-alpha-trypsin inhibitor heavy chain H4	1.255	0.280	0.972	1.078	0.662
Interferon regulatory factor 6	0.023	0.072	0.008	0.031	0.036
Keratin, type I cytoskeletal 10	0.016	0.192	0.164	0.255	0.047
Keratin, type I cytoskeletal 9	0.254	0.435	2.169	0.248	2.458
Keratin, type II cytoskeletal 1	1.365	3.147	0.690	1.112	0.692
Keratin, type II cytoskeletal 2 epidermal	0.004	0.119	0.073	0.080	0.017
Kinesin light chain 1	0.534	0.190	0.426	0.301	0.273
Kininogen-1	27.661	12.187	10.512	20.192	21.499

Lipopolysaccharide-binding protein	0.004	0.020	0.563	0.359	0.317
Lipoprotein lipase	0.126	0.079	0.219	0.197	0.260
Long-chain-fatty-acid--CoA ligase ACSBG1	0.001	0.392	0.101	0.026	0.061
Microfibril-associated glycoprotein 4	0.004	0.023	0.022	0.005	0.092
Mitogen-activated protein kinase kinase kinase 14	0.002	0.017	0.023	0.002	0.011
Nitric oxide synthase, inducible	0.660	0.267	0.849	0.923	1.041
Osteopontin	0.000	0.000	0.001	0.000	0.028
Pancreatic alpha-amylase	0.147	0.140	0.085	0.115	0.076
Phosphatidate phosphatase PPAPDC1B	0.001	0.833	0.094	0.154	0.129
Plasma protease C1 inhibitor	0.050	0.264	0.087	0.110	0.177
Plasminogen	0.069	0.068	0.319	0.039	0.158
Polymerase delta-interacting protein 2	0.323	2.172	0.280	0.377	0.305
Pregnancy zone protein	0.081	0.106	0.048	0.060	0.062
Properdin	4.974	3.444	1.756	2.439	1.527
Protein AATF	0.023	0.225	0.026	0.040	0.063
Protein AMBP	0.028	0.010	0.064	0.087	0.031
Protein jagged-1	0.019	0.021	0.034	0.040	0.024
Prothrombin	0.009	0.021	0.001	0.013	0.012
Rab11 family-interacting protein 4	0.001	0.010	0.196	0.084	0.047
Ras-related protein Rab-15	0.003	0.355	0.145	0.003	0.114
Regulator of microtubule dynamics protein 3	0.594	1.646	0.168	0.239	0.374
RING finger protein 219	9.496	2.294	7.837	6.961	5.704
RING finger protein 32	0.532	0.348	0.795	1.043	0.669
Serotransferrin	0.299	0.363	0.244	0.262	0.201
Serum albumin	0.549	0.926	1.721	1.963	1.012
Serum amyloid A-1 protein	0.010	0.153	0.425	0.489	0.732
Serum amyloid A-4 protein	0.289	0.505	0.200	0.476	0.475
Serum amyloid P-component	0.220	0.226	0.095	0.129	0.117
Serum paraoxonase/arylesterase 1	0.298	0.281	0.305	0.251	0.313
SKI family transcriptional corepressor 2	0.027	0.155	0.264	0.220	0.260
Transcription elongation factor A protein-like 4	0.086	0.002	0.124	0.102	0.064
Transthyretin	0.893	0.437	15.573	5.518	10.657
Triggering receptor expressed on myeloid cells 1	0.025	0.205	0.015	0.056	0.049
Tripartite motif-containing protein 35	0.344	0.525	1.749	1.270	1.341
Tsukushin	0.001	0.181	0.117	0.013	0.253
Tuftelin-interacting protein 11	0.769	0.113	0.314	0.580	0.411
U3 small nucleolar RNA-associated protein 15 homolog	1.057	1.393	1.554	1.334	0.866
Vimentin	0.815	1.244	0.589	0.853	0.457
Vitamin D-binding protein	0.067	0.071	0.024	0.097	0.042
Vitronectin	4.260	3.342	16.376	14.343	10.913
Zinc finger CCCH domain-containing protein 7B	3.497	1.080	1.710	2.235	0.647
Zinc finger protein basonuclin-2	14.233	2.181	4.025	10.413	4.753

Table 7-6: List of proteins identified in the protein corona (PC) of PS-NH_2 formed in human serum (HS), human heparin plasma (HHP) and human citrate plasma (HCP) and analysis of the respective media by LC-MS as discussed in 4.5.

Average amount of each protein in fmol was calculated from three biological and three technical replicates. Proteins are ordered alphabetically.

Protein name	PC HS	HS	PC HHP	HHP	PC HCP	HCP
Afamin	0.000	0.043	0.000	0.050	0.000	0.110
AKT-interacting protein	0.000	0.000	0.000	0.000	0.000	0.047
Alpha-1,6-mannosyl-glycoprotein 2-beta-N-acetylglucosaminyltransferase	0.000	0.220	0.000	0.000	0.000	0.000
Alpha-1-acid glycoprotein 1	0.000	3.378	0.000	2.091	0.000	2.108
Alpha-1-acid glycoprotein 2	0.000	1.206	0.000	0.926	0.000	0.908
Alpha-1-antichymotrypsin	0.000	0.941	0.000	0.746	0.000	0.781
Alpha-1-antitrypsin	0.711	6.505	0.169	6.201	0.060	5.027
Alpha-1B-glycoprotein	0.000	1.202	0.000	0.915	0.000	0.785
Alpha-2-antiplasmin	0.131	0.000	0.000	0.104	0.016	0.094
Alpha-2-HS-glycoprotein	0.000	1.810	0.000	1.731	0.000	1.698
Alpha-2-macroglobulin	0.000	4.645	0.000	3.773	0.000	3.442
Alpha-ketoglutarate-dependent dioxygenase FTO	0.000	0.000	0.000	0.000	0.172	0.000
Angiotensinogen	0.000	0.343	0.000	0.390	0.000	0.046
Antithrombin-III	0.556	0.294	0.000	0.422	0.000	0.400
Apolipoprotein A-I	4.977	1.443	1.273	1.144	0.278	1.032
Apolipoprotein A-IV	1.120	0.507	0.601	0.000	0.435	0.222
Apolipoprotein B-100	0.000	1.126	0.000	0.756	0.000	0.529
Apolipoprotein C-III	1.113	0.000	0.590	0.000	0.639	0.000
Apolipoprotein E	0.848	0.000	0.273	0.000	0.085	0.000
Beta-2-glycoprotein 1	0.041	1.217	0.467	1.000	0.021	0.958
BTB/POZ domain-containing protein KCTD12	0.000	0.000	0.000	0.000	0.000	3.330
BTB/POZ domain-containing protein KCTD16	0.000	0.000	0.000	0.000	0.000	4.365
C4b-binding protein alpha chain	0.409	0.530	0.000	0.470	2.244	0.462
Calmodulin-like protein 5	0.000	0.161	0.000	0.000	0.000	0.000
Carboxypeptidase B2	0.211	0.000	0.000	0.000	0.000	0.000
Casein kinase II subunit alpha'	0.000	0.000	0.000	0.715	0.000	1.273
CD5 antigen-like	0.000	0.262	0.000	0.110	0.000	0.244
Centromere protein I	0.000	0.000	0.000	0.000	0.120	0.000
Ceruloplasmin	0.000	1.263	0.000	0.946	0.000	0.817
Cleavage stimulation factor subunit 1	0.000	0.000	0.000	0.000	0.000	0.044
Clusterin	44.530	0.780	17.213	0.824	16.939	0.470
Coagulation factor IX	0.000	0.000	0.000	0.000	0.141	0.000
Coagulation factor VII	0.000	0.000	0.000	0.000	0.060	0.000
Coiled-coil domain-containing protein 78	0.000	0.591	0.000	0.000	0.000	0.000
Cold shock domain-containing protein E1	0.000	0.000	0.000	0.000	0.024	0.000

Complement C1q subcomponent subunit C	0.000	0.000	0.000	0.047	0.000	0.000
Complement C1r subcomponent	0.016	0.000	0.000	0.000	0.000	0.000
Complement C3	2.135	2.737	1.499	2.387	0.153	2.462
Complement C4-A	0.399	1.399	0.000	0.291	0.270	0.888
Complement C4-B	0.000	0.000	0.000	0.372	0.052	0.504
Complement C5	0.028	0.000	0.000	0.000	0.000	0.000
Complement component C6	0.033	0.000	0.000	0.000	0.000	0.000
Complement component C7	0.051	0.000	0.000	0.000	0.000	0.000
Complement component C8 gamma chain	0.013	0.000	0.000	0.000	0.000	0.000
Complement component C9	0.547	0.000	0.019	0.000	0.000	0.000
Complement factor B	0.214	0.700	0.000	0.533	0.000	0.457
Complement factor H	0.000	1.914	0.000	1.377	0.000	0.847
Corticosteroid-binding globulin	0.000	0.000	0.000	0.107	0.000	0.000
Cytoplasmic protein NCK2	0.000	0.000	0.000	0.108	0.000	0.000
Death domain-associated protein 6	0.000	0.000	0.000	0.000	0.028	0.000
Developmentally-regulated GTP-binding protein 2	0.000	0.000	0.000	0.027	0.000	0.000
E3 UFM1-protein ligase 1	0.000	0.000	0.000	0.277	0.000	0.000
Emerin	0.000	0.000	0.000	0.000	0.000	0.190
Fibrinogen alpha chain	0.000	0.000	10.599	0.913	23.713	2.371
Fibrinogen beta chain	0.000	0.000	14.900	1.095	34.716	2.727
Fibrinogen gamma chain	0.021	0.000	25.459	2.123	61.457	5.236
Fibronectin	0.000	0.151	0.000	0.000	0.000	0.726
Forkhead box protein K2	0.000	0.000	0.000	0.000	0.060	0.000
Formimidoyltransferase-cyclodeaminase	0.028	0.000	0.027	0.000	0.000	0.000
Formiminotransferase N-terminal subdomain-containing protein	0.000	0.031	0.000	0.000	0.000	0.000
Fractalkine	0.000	0.000	0.498	0.000	0.000	0.000
Gap junction delta-2 protein	0.000	3.746	0.000	0.000	0.000	0.000
Gelsolin	0.218	0.177	0.020	0.240	0.319	0.195
Glucose 1,6-bisphosphate synthase	0.372	0.000	0.000	0.000	0.000	0.000
Glutamate carboxypeptidase 2	0.000	0.000	0.013	0.000	0.000	0.000
Glutathione S-transferase Mu 2	0.000	3.925	0.000	4.500	0.000	0.000
Glyceraldehyde-3-phosphate dehydrogenase	0.074	0.000	0.000	0.000	0.000	0.000
Golgin subfamily A member 6-like protein 2	0.000	0.000	0.000	0.000	0.059	0.000
GRB2-related adapter protein	0.000	0.000	0.025	0.000	0.000	0.000
Guanine nucleotide-binding protein subunit alpha-13	0.030	0.000	0.000	0.000	0.000	0.000
Haptoglobin	0.000	6.750	0.000	4.856	0.000	8.631
Haptoglobin-related protein	0.000	0.545	0.000	0.576	0.000	0.615
Hemopexin	0.077	6.600	0.000	5.357	0.093	4.666
Heparin cofactor 2	0.023	0.043	0.000	0.054	0.000	0.044
High mobility group nucleosome-binding domain-containing protein 5	0.000	0.000	0.000	0.000	0.026	0.000
Histidine-rich glycoprotein	0.000	0.287	0.000	0.322	0.000	0.261
Hyaluronan-binding protein 2	0.026	0.000	0.428	0.000	0.643	0.000
Ig alpha-1 chain C region	0.064	5.022	0.000	4.502	0.515	2.894
Ig alpha-2 chain C region	0.017	2.122	0.000	0.916	0.000	0.976

Ig delta chain C region	0.000	0.030	0.000	0.000	0.000	0.094
Ig gamma-1 chain C region	1.602	88.140	1.070	51.325	2.001	68.753
Ig gamma-2 chain C region	0.606	11.927	0.249	8.582	0.158	3.886
Ig gamma-3 chain C region	0.000	2.678	0.000	2.288	1.385	2.037
Ig gamma-4 chain C region	0.000	4.060	0.000	5.184	0.111	28.456
Ig heavy chain V-III region BRO	0.000	1.129	0.000	1.403	0.000	0.896
Ig heavy chain V-III region TUR	0.000	0.374	0.000	0.033	0.000	0.000
Ig heavy chain V-III region VH26	0.000	0.489	0.000	0.483	0.000	0.392
Ig kappa chain C region	1.325	35.586	1.144	34.656	3.447	43.482
Ig kappa chain V-I region AG	0.000	1.606	0.000	1.309	0.000	2.638
Ig kappa chain V-I region EU	0.000	0.000	0.000	0.149	0.000	0.000
Ig kappa chain V-I region Wes	0.000	0.000	0.000	0.000	0.000	0.060
Ig kappa chain V-II region Cum	0.000	0.000	0.000	0.000	0.000	0.111
Ig kappa chain V-II region RPMI 6410	0.000	0.000	0.000	0.033	0.000	0.000
Ig kappa chain V-II region TEW	0.000	1.572	0.000	1.220	0.000	0.588
Ig kappa chain V-III region NG9 (Fragment)	0.000	0.111	0.000	0.000	0.000	0.242
Ig kappa chain V-III region SIE	0.034	1.692	0.000	1.598	0.119	2.382
Ig kappa chain V-III region VG (Fragment)	0.000	0.338	0.000	0.278	0.000	0.152
Ig kappa chain V-IV region Len	0.000	0.822	0.000	0.694	0.000	0.710
Ig mu chain C region	1.010	3.676	0.973	2.042	1.397	2.735
Ig mu heavy chain disease protein	0.000	0.000	0.000	0.269	0.000	0.000
Immunoglobulin J chain	0.000	0.051	0.000	0.000	0.000	0.000
Immunoglobulin lambda-like polypeptide 5	0.000	5.412	0.000	4.120	0.000	2.075
Insulin-like growth factor-binding protein complex acid labile subunit	0.000	0.000	0.000	0.040	0.000	0.000
Inter-alpha-trypsin inhibitor heavy chain H1	0.000	3.269	0.000	0.518	0.000	0.347
Inter-alpha-trypsin inhibitor heavy chain H2	0.022	0.923	0.000	0.797	0.000	0.604
Inter-alpha-trypsin inhibitor heavy chain H4	1.455	0.905	0.335	0.483	0.000	0.636
Interleukin-7	0.000	0.000	0.000	0.000	0.000	0.044
Isthmin-1	0.000	0.000	0.000	0.053	0.000	0.000
Kelch-like protein 28	0.000	0.000	0.000	0.000	0.038	0.000
Keratin, type I cuticular Ha1	0.069	0.000	0.000	0.000	0.000	0.000
Keratin, type I cytoskeletal 10	0.000	0.000	0.000	0.000	0.015	0.000
Keratin, type I cytoskeletal 9	0.000	0.000	0.063	0.000	0.021	0.000
Keratin, type II cytoskeletal 1	0.000	0.000	0.120	0.000	0.359	0.000
Kininogen-1	1.856	1.054	0.181	0.872	0.018	0.644
Kv channel-interacting protein 2	0.000	0.000	0.000	0.000	0.000	0.084
Lipopolysaccharide-binding protein	0.157	0.000	0.000	0.000	0.000	0.000
Lumican	0.351	0.000	0.000	0.000	0.000	0.000
Lysophospholipid acyltransferase LPCAT4	0.000	0.000	0.000	0.000	0.000	0.069
MAGE-like protein 2	0.000	0.000	0.000	0.000	0.000	0.034
Mitochondrial import receptor subunit TOM40B	0.000	0.000	0.000	0.000	0.114	0.000
M-phase inducer phosphatase 3	0.000	0.000	0.000	0.000	0.000	0.057
N(G),N(G)-dimethylarginine dimethylaminohydrolase 1	0.000	0.000	0.000	0.000	0.000	0.034
Nicotinamide phosphoribosyltransferase	0.000	0.000	0.000	0.053	0.000	0.000
Nuclear distribution protein nudE-like 1	0.000	0.000	0.000	0.000	0.000	0.061

Paladin	0.000	0.000	0.036	0.000	0.000	0.000
Plasma protease C1 inhibitor	0.000	0.514	0.000	0.502	0.000	0.154
Plasminogen	0.000	1.139	0.000	0.876	0.000	0.711
Pregnancy zone protein	0.000	0.483	0.000	0.179	0.000	0.337
Properdin	0.660	0.000	0.096	0.000	0.000	0.000
Protein AMBP	0.000	0.427	0.000	0.372	0.000	0.173
Protein FAM208B	0.000	0.000	0.135	0.000	0.000	0.000
Protein kinase C and casein kinase substrate in neurons protein 3	0.029	0.000	0.000	0.140	0.000	0.000
Protein LBH	0.000	0.000	0.000	0.018	0.000	0.000
Protein Njmu-R1	0.000	1.834	0.150	3.240	0.099	1.630
Prothrombin	5.944	0.756	0.000	0.718	0.028	0.593
Rab11 family-interacting protein 5	0.000	0.000	0.000	0.000	0.000	0.041
Regulatory solute carrier protein family 1 member 1	0.000	0.132	0.000	0.000	0.000	0.095
Retinol-binding protein 4	0.000	0.400	0.000	0.311	0.000	0.237
Secreted phosphoprotein 24	0.000	0.000	0.000	0.000	0.135	0.000
Serine/threonine-protein kinase 35	0.000	0.000	0.000	0.000	0.052	0.000
Serotransferrin	0.000	15.333	0.000	10.316	0.000	9.833
Serum albumin	138.419	293.477	110.376	278.527	122.492	200.502
Serum amyloid A-1 protein	0.097	0.000	0.052	0.000	0.024	0.000
Serum amyloid P-component	0.000	0.074	0.000	0.000	0.000	0.000
Serum paraoxonase/arylesterase 1	0.000	0.240	0.000	0.273	0.000	0.096
Sine oculis-binding protein homolog	0.016	0.000	0.000	0.000	0.000	0.000
Tether containing UBX domain for GLUT4	0.000	0.000	0.000	0.000	0.154	0.000
Thyroxine-binding globulin	0.000	0.000	0.000	0.035	0.000	0.000
TNF receptor-associated factor 1	0.000	0.000	0.000	0.000	0.000	0.230
Transcription initiation factor TFIID subunit 5	0.000	0.000	0.000	0.000	0.044	0.000
Transcription termination factor 1	0.000	0.000	0.000	0.000	0.320	0.000
Transforming acidic coiled-coil-containing protein 1	0.000	0.000	0.000	0.000	0.041	0.000
Transmembrane protein 44	0.000	0.000	0.000	0.000	0.130	0.000
Transthyretin	0.982	3.334	1.663	2.372	0.817	2.436
Trinucleotide repeat-containing gene 6A protein	0.000	0.000	0.000	0.000	0.049	0.000
Tripartite motif-containing protein 35	0.000	0.000	0.000	0.000	0.000	0.058
Tubulin beta-4A chain	0.000	0.075	0.000	0.000	0.000	0.000
UPF0585 protein C16orf13	0.000	0.068	0.000	0.000	0.000	0.000
UV-stimulated scaffold protein A	0.000	0.000	0.043	0.000	0.000	0.000
Vitamin D-binding protein	0.912	1.380	0.644	1.196	0.696	0.872
Vitamin K-dependent protein C	0.000	0.000	0.000	0.000	0.335	0.000
Vitamin K-dependent protein S	0.000	0.000	0.000	0.000	0.680	0.000
Vitronectin	22.801	1.100	45.002	0.845	32.703	0.712
Xaa-Pro aminopeptidase 1	0.000	0.000	0.029	0.000	0.000	0.000
Zinc finger protein basonuclin-2	0.663	0.000	0.000	0.000	0.000	0.000
Zinc-alpha-2-glycoprotein	0.000	0.531	0.000	0.370	0.000	0.229

Table 7-7: List of proteins identified in the protein corona (PC) of PS-NH_2 formed in foetal bovine serum (FBS) and analysis of the respective media by LC-MS as discussed in 4.5.

Average amount of each protein in fmol was calculated from three biological and three technical replicates. Proteins are ordered alphabetically.

Protein name	PC FBS	FBS
60S ribosomal protein L9 (Fragment)	0.015	0.000
Actin, alpha cardiac muscle 1	0.010	0.054
Adenosylhomocysteinase	0.139	0.000
Adenylyl cyclase-associated protein	0.087	0.000
Adiponectin	0.000	0.298
ADP-ribosylation factor 2	0.047	0.000
A-kinase anchor protein 10	0.062	0.000
ALB protein	45.136	184.662
Alcohol dehydrogenase class-3	0.502	0.000
Alpha-1-acid glycoprotein	0.000	3.195
Alpha-1-antiproteinase	4.506	49.951
Alpha-1B-glycoprotein	0.000	1.897
Alpha-2-antiplasmin	0.316	2.308
Alpha-2-macroglobulin	1.617	5.841
Alpha-2-macroglobulin variant 5	0.070	0.217
Alpha-fetoprotein	1.476	15.196
Angiotensinogen	0.501	0.738
Antithrombin-III	3.718	0.543
Apolipoprotein A-I	3.341	0.000
Apolipoprotein A-II	0.077	0.000
Apolipoprotein D	0.024	0.000
Apolipoprotein E	1.060	0.000
Argininosuccinate synthase	0.226	0.000
Beta-2-glycoprotein 1	0.258	2.099
C4b-binding protein alpha chain	3.838	0.000
Calponin-2 (Fragment)	0.260	0.000
Carboxypeptidase B2	0.016	0.000
CCDC101 protein	0.102	0.000
Clusterin	6.927	0.000
Coagulation factor V	0.382	0.000
Coagulation factor XIII A chain (Fragment)	0.022	0.000
Cofilin 1 (Non-muscle)	0.383	0.000
Complement C3	0.562	1.099
Complement C4 (Fragments)	0.043	0.080
Complement factor B	0.173	0.500
Complement factor H	0.000	0.126
Creatine kinase B-type	0.112	0.000
Cytochrome P450, family 2, subfamily J, polypeptide 2	0.000	0.057
D-3-phosphoglycerate dehydrogenase	0.019	0.000

Dihydropyrimidinase-related protein 2	0.000	0.047
DNA-directed RNA polymerase III subunit RPC4	0.034	0.000
Dual specificity protein phosphatase 6	0.021	0.000
E3 ubiquitin-protein ligase RNF8	0.013	0.000
EH domain-containing protein 1	0.071	0.000
Endopin 2B	0.366	1.120
Endopin 2C	0.000	0.681
Exocyst complex component 6B	0.011	0.000
Fermitin family homolog 3	0.133	0.000
Fetuin-B	0.679	4.652
Fibrinogen alpha chain	0.416	0.000
Fibrinogen beta chain	0.018	0.000
Fibronectin	0.074	0.000
Fibulin-1	0.000	0.368
Galactokinase	0.042	0.000
Gelsolin	0.091	0.173
Glutathione peroxidase	0.215	0.000
Glyceraldehyde-3-phosphate dehydrogenase	3.629	0.000
Heat shock protein beta-1	0.308	0.000
Heat shock protein HSP 90-beta	0.156	0.000
Heat shock-related 70 kDa protein 2	0.017	0.000
Haemoglobin foetal subunit beta	8.745	0.835
Haemoglobin subunit alpha	10.942	0.117
Haemoglobin subunit beta	0.000	0.033
Hemopexin	0.070	1.649
Herpesvirus entry mediator C (Fragment)	0.060	0.000
Hormone-sensitive lipase	0.028	0.000
Hyaluronan-binding protein 2	0.217	0.000
Inter-alpha-trypsin inhibitor heavy chain H3	0.000	0.345
Inter-alpha-trypsin inhibitor heavy chain H4	0.845	1.241
ITIH2 protein	0.079	2.326
Keratin, type II cytoskeletal 5	0.014	0.000
Keratin, type II cytoskeletal 7	0.097	0.000
Kininogen-1	0.708	1.746
Lactotransferrin	0.000	0.033
L-lactate dehydrogenase A chain	0.025	0.000
Lon protease homolog, mitochondrial	0.324	0.000
Lumican	0.013	0.000
MHC class I antigen (Fragment)	0.000	0.106
Microtubule-associated protein RP/EB family member 2	0.039	0.000
Mitochondrial brown fat uncoupling protein 1 (Fragment)	0.552	0.000
MYH3 protein	0.062	0.000
NAD-dependent protein deacetylase sirtuin-4	0.000	1.169
Nucleoporin SEH1	0.012	0.000
Nucleosome assembly protein 1-like 1	0.018	0.000
OLFM3 protein	0.000	0.049
Oncoprotein-induced transcript 3 protein	0.105	0.000

Outer dense fiber protein 2-like	0.476	0.000
Pantetheinase	0.000	0.226
Periostin variant 9	0.363	0.000
Pigment epithelium-derived factor	0.000	0.393
Plakophilin-1	0.049	0.000
Plasma serine protease inhibitor	0.097	0.139
Plasmalemma vesicle associated protein	2.232	0.000
Plasminogen	0.085	0.278
Protein AMBP	0.000	0.979
Prothrombin	23.940	0.514
Pyruvate kinase	0.178	0.000
Rab GTPase-binding effector protein 2	0.030	0.000
Ras-related C3 botulinum toxin substrate 2	0.010	0.000
Ras-related protein Rap-1b	0.459	0.000
Reticulon-3	0.108	0.000
Retinol-binding protein 4	0.000	0.078
Ribonuclease P/MRP protein subunit POP5	0.013	0.000
Serotransferrin	0.293	2.545
Serotransferrin	0.000	13.905
Serotransferrin-like	0.000	0.061
Serpin A3-1	0.006	1.134
Serpin H1	0.014	0.000
Serum albumin	33.000	153.215
Short-chain specific acyl-CoA dehydrogenase, mitochondrial	0.025	0.000
Spermine synthase (Fragment)	0.000	6.663
STK24 protein	0.032	0.000
Tenascin C	0.353	0.000
Thyroxine-binding globulin	0.000	0.323
Transgelin-2	0.384	0.000
Transketolase	0.016	0.000
Transthyretin	0.227	1.617
Tubulin alpha-1D chain	0.046	0.000
Tubulin beta-4B chain	0.030	0.000
Tyrosine-protein kinase receptor	0.012	0.000
UDP-glucose 6-dehydrogenase	0.010	0.000
Vitamin D-binding protein	1.805	0.000
Vitamin D-binding protein	0.606	1.498
WC1	0.133	0.000

8 ZUSAMMENFASSUNG

Das Interesse an polymeren Nanocarriern für medizinische Anwendungen hat sich im letzten Jahrzehnt stetig gesteigert und eine entsprechend große Anzahl an verschiedenen Nanopartikeln wurde hergestellt. Vor allem als Wirkstoffträger zur gezielten Verabreichung von Medikamenten könnten Nanocarrier zahlreiche Schwierigkeiten in der Krebstherapie überwinden.

Ihr erfolgreicher Einsatz wird jedoch durch unzureichendes Wissen über die Wechselwirkungen der Nanocarrier mit ihrer biologischen Umgebung beeinträchtigt. Die schnelle Bedeckung intravenös injizierter Nanocarrier mit Blutproteinen erschwert die Vorhersage von Zellinteraktionen, Biodistribution und Toxizität. Die Bildung dieser komplexen Proteincorona ist sowohl von den Oberflächenmerkmalen der Nanopartikel als auch von der biologischen Umgebung stark abhängig und verändert die Eigenschaften der Nanopartikel dramatisch.

Diese Studie entschlüsselt die Zusammensetzung der Proteincorona auf verschiedenen polymeren Nanocarriern durch markierungsfreie quantitative Flüssigchromatographie-gekoppelte Massenspektrometrie. Durch Korrelation der relativen Häufigkeiten der identifizierten Proteine mit der zellulären Aufnahme von Nanopartikeln können Proteine bestimmt werden die möglicherweise eine Schlüsselrolle bei der Aufnahme spielen. Der Einfluss von Apolipoproteinen, einer der häufigsten Proteinklassen in der Corona, kann teilweise aufgeklärt werden. Durch die Beschichtung von Polystyrol-Nanopartikeln mit einzelnen Proteinen kann der Einfluss auf die Zellinteraktion aufgedeckt werden. Es wird gezeigt, dass Apolipoproteine A4 und C3 die zelluläre Aufnahme verringern, während APOH die Internalisierung in Zellen erhöht.

Bisher sind alle Ansätze die Proteinadsorption auf Nanopartikeln durch Modifikationen wie Polyethylenglykol (PEG) vollständig zu verhindern gescheitert. Mit Hydroxyethylstärke (HES) und Poly-(ethylen-ethylphosphat) (PEEP) werden innovative, biologisch abbaubare „Stealth“ Materialien vorgestellt und hinsichtlich ihrer Proteinadsorption und der Fähigkeit, sich der Zellaufnahme zu entziehen, analysiert. Es wird gezeigt, dass der Tarnkappeneffekt („Stealth Effect“) von Polyethylenglykol (PEG) und PEEP von der

Proteinadsorption abhängig zu sein scheint. Zusätzlich wird Clusterin wird als entscheidender Faktor für diesen Mechanismus identifiziert.

Weiterhin werden zwei verschiedene Techniken für die Präparation der Proteincorona verglichen und die Zuverlässigkeit der magnetischen Separation als geeignete Alternative zur Zentrifugation bestätigt. Die Entwicklung der Corona während der Präparation wird überprüft und spezifische Proteine die sich mit jedem Waschschritt an- bzw. abreichern, werden identifiziert.

Schließlich, wird die Bedeutung der Proteinquelle, welche für die *in vitro* Analyse der Proteincorona verwendet wird, hervorgehoben. Es werden wesentliche Unterschiede in der Zusammensetzung der Coronas, die sich in Serum und Plasma ausbilden, bestimmt. Ein starker Einfluss von Heparin, welches als Antikoagulans für die Plasmaerzeugung verwendet wird, wird detektiert. Während Heparin die Aufnahme in Makrophagen verstärkt, verhindert es die Internalisierung in HeLa-Zellen. Der starke Einfluss der Proteinquelle auf die Bildung der Corona und die Auswirkung auf die Interaktion mit verschiedenen Zelltypen sind Faktoren die häufig wenig beachtet werden, für eine aussagekräftige Analyse jedoch berücksichtigt werden sollten.

9 ACKNOWLEDGEMENTS

10 CURRICULUM VITAE

11 PUBLICATIONS

Schöttler, S.; Klein, K.; Landfester, K. and Mailänder, V., *Protein source and choice of anticoagulant decisively affect nanoparticle protein corona and cellular uptake*. [Accepted in Nanoscale]

Schöttler, S.; Becker, G.; Winzen, S.; Steinbach, T.; Mohr, K.; Landfester, K.; Mailänder, V. and Wurm, F., *The influence of poly(phosphoester)s on the protein corona provides a different perspective on the stealth effect*. [Acdepted in Nature Nanotechnology]

Ritz, S.*; **Schöttler, S**.*; Kotman, N.*; Baier, G.; Musyanovych, A.; Kuharev, J.; Landfester, K.; Schild, H.; Jahn, O.; Tenzer, S. and Mailänder, V., *Protein Corona of Nanoparticles: Disctinct Proteins regulate the Cellular Uptake*. Biomacromolecules, **2015**. 16 (4): p. 1311-1321. (*shared first authorship)

Kang, B.; Okwieka, P.; **Schöttler, S**.; Winzen, S.; Langhanki, J.; Mohr, K.; Opatz, T.; Mailänder, V.; Wurm, F.R. and Landfester, K., *Carbohydrate-based nanocarriers with specific cell targeting and minimum influence by protein corona*. Angewandte Chemie, **2015**. DOI: 10.1002/anie.201502398.

Kang, B.; Okwieka, P.; **Schöttler, S**.; Seifert, O.; Kontermann, R.E.; Pfizenmaier, K.; Musyanovych, A.; Meyer, R.; Diken, M.; Sahin, U.; Mailänder, V.; Wurm, F.R. and Landfester, K., *Tailoring the stealth properties of biocompatible polysaccharide nanocontainers*. Biomaterials, **2015**. 49(0): p. 125-134.

Winzen, S.; **Schöttler, S**.; Baier, G.; Rosenauer, C.; Mailaender, V.; Landfester, K. and Mohr, K., *Complementary analysis of the hard and soft protein corona: sample preparation critically effects corona composition*. Nanoscale, **2015**. 7(7): p. 2992-3001.

Mohr, K.; Sommer, M.; Baier, G.; **Schöttler, S**.; Okwieka, P.; Tenzer, S.; Landfester, K.; Mailander, V.; Schmidt, M. and Meyer, R.G., *Aggregation Behavior of Polystyrene-Nanoparticles in Human Blood Serum and its Impact on the in vivo Distribution in Mice*. J Nanomed Nanotechnol, **2014**. 5(2): p. 193.

Paven, M.; Papadopoulos, P.; **Schöttler, S**.; Deng, X.; Mailänder, V.; Vollmer, D. and Butt, H.-J., *Super liquid-repellent gas membranes for carbon dioxide capture and heart–lung machines*. Nat Commun, **2013**. 4.

Weller, D.; Medina-Oliva, A.; Claus, H.; Gietzen, S.; Mohr, K.; Reuter, A.; Schäffel, D.; **Schöttler, S.;** Koynov, K.; Bros, M.; Grabbe, S.; Fischer, K. and Schmidt, M., *Solution Properties and Potential Biological Applications of Zwitterionic Poly(ε-N-methacryloyl-l-lysine).* Macromolecules*,* **2013**. 46(21): p. 8519-8527.

12 DECLARATION

This dissertation was carried out from June 1st, 2012 to June 12th, 2015 at the Max Planck Institute for Polymer Research.

I hereby declare that I wrote the dissertation submitted without any unauthorised external assistance and used only sources acknowledged in the work. All textual passages which are appropriated verbatim or paraphrased from published and unpublished texts as well as all information obtained from oral sources are duly indicated and listed in accordance with bibliographical rules. In carrying out this research, I complied with the rules of standard scientific practice as formulated in the statutes of Johannes Gutenberg-University Mainz to insure standard scientific practice.

Mainz, 12.06.2015

Susanne Schöttler